Thesis submitted to fulfill the requirements for the degree of Doctor in Health Sciences

VIB-UGENT CENTER FOR MEDICAL BIOTECHNOLOGY

UNIVERSITEIT GENT

YCRL CYTOKINE RECEPTOR LAB

Protein-protein interaction mapping to study the role of RNF41 in intracellular trafficking

Delphine Masschaele

Protein-protein interaction mapping to study the role of RNF41 in intracellular trafficking

Delphine Masschaele

Protein-protein interaction mapping to study the role of RNF41 in intracellular trafficking

Delphine Masschaele

Promotor: Prof. Dr. Jan Tavernier

Thesis submitted to fulfill the requirements for the degree of Doctor in Health Sciences.

Faculty of Medicine and Health Sciences

Academic Year 2017-2018

Promotor: Prof. Dr. Jan Tavernier
Department of Biochemistry, Faculty of Medicine and Health Sciences, Ghent University, Belgium
Center for Medical Biotechnology, VIB

Chair
Prof. Dr. Frank Speleman
Center for Medical Genetics, Ghent University and Hospital
Cancer Research Institute Ghent

Members of the examination committee
Prof. Dr. Sarah Gerlo
Department of Biochemistry, Faculty of Medicine and Health Sciences, Ghent University, Belgium
Center for Medical Biotechnology, VIB

Prof. Dr. Jan Gettemans
Department of Biochemistry, Faculty of Medicine and Health Sciences, Ghent University, Belgium

Prof. Dr. Roosmarijn Vandenbroucke
Department of Biomedical molecular biology, Faculty of Science, Ghent University, Belgium
Center for Inflammation Research, VIB

Dr. Ragna Sannerud
Department of Neuroscience, Faculty of Medecine, KU Leuven, Belgium
Center for Brain & Disease Research, VIB , Laboratory of Membrane Trafficking

Dr. Ignace Lasters
CTO Complix, Belgium

Prof. Dr. Erich Wanker
Max Delbrück Center for Molecular Medicine, Germany

Table of contents

List of abbreviations

ABPN: A4-amino-2-(butyrylamino)phenyl (2E,4E,6E,8E)- 3,7-dimethyl-9-(2,6,6-trimethyl-1-cyclohexenyl)- 2,4,6,8-nonatetraenoate

AD: activation domain

ADAM: a disintegrin and metalloproteinase

AgRP: agouti-related protein

AMPK: AMP-activated protein kinase

AMSH: associated molecule with the SH3 domain of STAM

AP: adaptor protein

AP2S1: Adaptor related Protein complex 2 Sigma 1 subunit

AP-MS: affinity-purification-mass spectrometry

APP: amyloid precursor protein

AR: androgen receptor

ARE: androgen response element

ARF: ADP ribosylation factor

ARL: ARF-like

ATG: autophagy-related protein

BAR: Bin-Amphiphysin-Rvs

BiFC: Bimolecular fluorescence complementation

BioID: proximity-dependent biotin identification

BIR: baculoviral IAP repeat

BRUCE: BIR repeat containing ubiquitin-conjugating enzyme

C/EBPβ: CCAAT/Enhancer-binding protein β

CATCHR: complexes associated with tethering containing helical rods

CBP: calmodulin binding peptide

CC: coiled-coil

CCP: clathrin-coated pit

CCV: clathrin-coated vesicles

CDC42: Cell division control protein 42

CHMP: charged multivesicular body protein

CI-M6PR: cation-independent M6PR

CLEC16A: C-type lectin domain family 16, member A

CLICs: clathrin-independent carriers

CMA: chaperone-mediated autophagy

CME: clathrin-mediated endocytosis

COG: conserved oligomeric Golgi complex

COP: coat protein complex

CORVET: class C core vacuole/endosome tethering

CTxB: Cholera toxin B subunit

CXCR4: chemokine receptor 4

DBD: DNA binding domain

DFCP1: Double FYVE-containing protein 1

DHFR: dihydrofolate reductase

DIABLO: Direct IAP-Binding protein with Low pI

DOR: δ- opioid receptor

DUB: deubiquitinating enzyme

DVL: Dishevelled

EARP: endosome-associated recycling protein

ECM: extracellular matrix

EE: early endosome

EGFR: Epidermal growth factor receptor

EHD: Eps15 homology domain

EPOR: Erythropoietin receptor

EpsinR: Epsin related protein

ER: endoplasmic reticulum

ERAD: ER-associated degradation

ERC: endocytic recycling compartment

ERGIC: ER- to- Golgi intermediate compartment

ESCRT: endosomal sorting complexes required for transport

FEME: fast endophilin-mediated endocytosis

FlnA: Filamin A

FLRF: fetal liver RING finger

FYVE: Fab1, YOTB, Vac1 and EEA1

GAP: GTPase Activating Protein

GARP: Golgi-associated retrograde protein

GBM: glioblastoma multiforme

GDF: GDP Dissociating Factor

GDI: GDP Dissociating Inhibitor

GDP: guanosine 5'-diphosphate

GEEC: GPI-anchored protein enriched compartment

GEF: Guanine Nucleotide Exchange Factor

GGA: Golgi-localized, γ-ear containing, ADP-ribosylation factor-binding protein

GLUE: GRAM-like ubiquitin-binding in EAP45

GLUT1: glucose transporter 1

GM-CSF: granulocyte-macrophage colony-stimulating factor

GPCR: G-protein coupled receptor

GPI: glycosylphosphatidylinositol

GRAF: GTPase regulator associated with focal adhesion kinase

GTP: guanosine 5'-triphosphate

GTPase: guanosine 5′-triphosphatases

HBx: hepatitis B virus encoded X protein

HDAC6: histone deacetylase 6

HECT: homologous to the E6AP carboxyl terminus

HOPS: homotypic fusion and vacuole protein sorting

HPLC: high-performance liquid chromatography

HPV16: human papillomavirus 16

HRS: hepatocyte growth factor receptor tyrosine kinase substrate

HSC: hematopoietic stem cells

HSC70: heat shock protein 70

huORF: human open reading frame

IAP: inhibitor of apoptosis proteins

IFN-β: interferon-β

IGF-1R: insulin-like growth factor-1 receptor

IL-2Rβ: interleukin 2 receptor β

ILVs: intraluminal vesicles

IRF3: interferon regulatory factor-3

JAK: Janus kinase

JIP: c-Jun N-terminal interacting kinase

KISS: KInase Substrate Sensor

KITENIN: KAI1 C-terminal interacting tetraspanin

LAMP1: lysosomal-associated membrane protein 1

LBPA: phospholipid lysobisphosphatidic acid

LDLR: low-density lipoprotein receptor

LE: late endosome

LIFR: Leukaemia inhibitory factor receptor

LPS: lipopolysaccharide

LR: leptin receptor

M6PR: mannose-6-phosphate receptor

MAGEL2: melanoma antigen L2

MALS: Multi-angle light scattering

MaMTH: mammalian membrane two-hybrid

MAPPIT: MAmmalian Protein-Protein Interaction Trap

MHC: major histocompatibility complex

MTC: multisubunit tethering complex

mTORC1: mammalian target of rapamycin complex 1

MVBs: multivesicular bodies

MYTH: membrane-based Y2H

NDN: necdin

NPY: neuropeptide Y

NRDP1: neuregulin receptor degradation protein-1

NRZ: NAG, RINT-1, ZW10

NSF: N-ethylmaleimide-sensitive fusion protein

N-WASP: neuronal Wiskott-Aldrich syndrome protein

OPTN: optineurin

PA: phosphatidic acid

PAK1: p21-activated kinase 1

PAR2: protease-activated receptor 2

PAS: pre-autophagosomal structure

PCa: Prostate cancer

PCA: protein complementation assay

PH: pleckstrin homology

PI(3)P: phosphatidylinositol (3)-phosphate

PI(3,4,5)P3: phosphatidylinositol (3,4,5)-trisphosphate

PI(4,5)P2: phosphatidylinositol (4,5)-bisphosphate

PI3K: phosphatidylinositol-3-kinase

PIP: phosphatidylinositol phospholipid

PIP5K: phosphatidylinositol-4-phosphate 5-kinase

PKC: protein kinase C

PLD: phospholipase D

PM: plasma membrane

POMC: pro-opiomelanocortin

PPI: protein-protein interaction

PTM: post-translational modification

PWS: Prader-Willi syndrome

PX: phox homology

RAC1: Ras-related C3 botulinum toxin substrate 1

RARα: retinoic acid receptor

RBR: RING-between-RING

RE: recycling endosome

RHOA: Ras homolog gene family member A

RING: Really Interesting New Gene

RTK: receptor tyrosine kinase

RTN4A: Reticulon 4A

SEC: Size exclusion chromatography

SILAC: stable-isotope labelling with amino acids in cell culture

SM: Sec1/Munc18-like

SMAC: second mitochondria-derived activator of caspases

SNAP: soluble NSF attachment protein

SNARE: soluble N-ethylmaleimide-sensitive factor attachment protein receptor

SNX: sorting nexin

STAM: Signal transducing adapter molecule

STAT: signal transducers and activators of transcription

STX: syntaxin

STxB: Shiga toxin B subunit

SV40: simian virus 40

TACE: TNFα converting enzyme

TAP: tandem affinity purification

TBK1: TANK-binding kinase 1

TCR: T cell antigen receptor

TEV: tobacco etch virus

TfR: transferrin receptor

TGFβR: transforming growth factor β receptor

TGN: trans-Golgi network

TIP47: tail-interacting protein of 47 kD

TLR: Toll-like receptor

TRAPP: transport protein particle

TSG101: Tumor susceptibility gene 101

TYK2: tyrosine kinase 2

Ubl: ubiquitin-like protein

UEV: ubiquitin E2 variant

UIM: ubiquitin-interacting motif

ULK: Unc-51 like autophagy activating kinase

UPL: Ubl-specific proteases

USP8: Ubiquitin-specific protease 8

UVRAG: UV radiation resistance associated gene

VAMP: Vesicle-associated membrane protein

VANGL: Vang-like protein

VLPs: virus-like particles

VPS52: vacuolar protein sorting 52

VSV-G: vesicular stomatitis virus G

VTI1A: Vesicle transport through interaction with T-SNAREs 1A

WIPI2: WD repeat domain phosphoinositide-interacting protein 2

Y2H: Yeast Two-Hybrid

Y3H: Yeast three-hybrid

Summary

Intracellular trafficking of proteins and lipids is essential for maintaining cellular homeostasis. The biosynthetic pathway delivers newly synthesized proteins to their final destination either inside or outside the cell, while the endocytic pathway controls the transport of molecules that enter the cell. These pathways are interconnected as they share intracellular compartments and protein machinery. Coat proteins, small G proteins from the RAB and ARF family, tethering complexes and SNARE proteins all work together to balance targeting, retention and retrieval mechanisms necessary to maintain a steady state within these intracellular compartments. Defects in these highly regulated processes often lie at the basis of pathologies such as neurodegenerative, inflammatory and cardiovascular diseases and several cancers. Furthermore, the trafficking machinery is often hijacked by viruses and bacteria to gain access into the living cells. Therefore, it is of great interest to acquire knowledge about intracellular transport and proteins that regulate these trafficking steps, especially since it also offers opportunities to be used as a delivery system for therapeutic molecules. Our lab previously identified RNF41 as a key regulator of basal cytokine receptor trafficking. This E3 ligase blocks lysosomal sorting and simultaneously enhances ectodomain shedding of JAK2-associated cytokine receptors such as the leptin, IL-6 and LIF receptor by ubiquitinating and destabilizing the deubiquitinase USP8. In this way, RNF41 indirectly destabilizes the ESCRT-0 complex which results in the rerouting of these cytokine receptors from the lysosomal degradation pathway towards compartments for ectodomain shedding. To further elucidate the role of RNF41 in intracellular trafficking we used a strategy where we expand the characterization of RNF41 based on the function of newly identified RNF41 interaction partners. An initial array MAPPIT screen led to the identification of VPS52 as a novel RNF41 interaction partner. VPS52 is a subunit of two distinct tethering complexes GARP and EARP, which are respectively involved in retrograde cargo transport from the endosomes to the Golgi network and cargo recycling to the plasma membrane. We show that RNF41 ubiquitinates and relocates VPS52 away from its subcellular location. It thereby affects EARP function resulting in defective transferrin recycling. We next performed additional RNF41 screens using Virotrap, BioID and AP-MS and combined them with data from previously performed microarray MAPPIT and Y2H screens in order to build an RNF41 interactome network. This allowed us to identify highly confidential interaction partners of RNF41 and highlights its possible implication in certain functional clusters. As such, we reveal a role for AP2S1, the sigma subunit of the clathrin-mediated endocytosis adaptor protein AP-2, in leptin and LIF receptor signaling and show that RNF41 stabilizes and relocates AP2S1. Finally, further characterization of immunofluorescent detected RNF41-positive structures exposed a role for RNF41 in autophagy. We show that RNF41 is necessary to maintain the levels of the autophagy receptor p62 and phosphorylated TBK1. Additional detected interactions between RNF41 and autophagy related proteins Beclin1, ATG14, WIPI2 and ATG5 indicated that RNF41 functions in autophagosome biogenesis of the selective autophagy pathway aggrephagy. Collectively, our findings of possible functions of RNF41 in recycling, endocytosis and autophagy further establish the importance of RNF41 intracellular trafficking. Moreover, RNF41 has been implicated in several disorders like Parkinson's disease, cardiomyopathies and cancer, which resemble pathologies associated with dysfunctional intracellular trafficking. Our characterization of the interactions between RNF41 and proteins involved in intracellular trafficking, and the elucidation of how these interactions relate to these processes could therefore provide new insights for the development of novel therapeutics.

Samenvatting

Intracellulair transport van eiwitten en vetten is essentieel voor het behoud van homeostase binnenin de cel. De secretorische route levert nieuw gevormde eiwitten naar hun uiteindelijke bestemming binnen of buiten de cel, terwijl de endocytische route het vervoer van moleculen regelt die binnen komen in de cel. Deze twee routes zijn gelinkt aan elkaar aangezien ze hiervoor dezelfde eiwitten en sommige dezelfde intracellulaire compartimenten kunnen gebruiken. Coat eiwitten, kleine G eiwitten van de RAB en ARF familie, tethering complexen en SNARE eiwitten werken samen om vesikels met een bepaalde cargo naar het juiste compartiment te sturen, terug te brengen of de cargo ter plaatse te houden en bewaren op deze manier het dynamisch evenwicht binnenin deze intracellulaire compartimenten. Afwijkingen in deze sterk gereguleerde processen liggen vaak aan de basis van verscheidene kankers, en van neurodegeneratieve, inflammatoire en cardiovasculaire ziektebeelden. Daarbovenop kunnen deze transportroutes gekaapt worden door verscheidene virussen en bacteriën die zo hun weg banen in de cel. Kennis over intracellulair transport en de eiwitten die deze stappen reguleren is daarvoor van groot belang, zeker aangezien deze ook gebruikt kunnen worden als toedieningsweg voor therapeutische moleculen. Onze onderzoeksgroep identificeerde RNF41, een E3 ligase, als een belangrijke regulator van het intracellulair transport van JAK2-geassocieerde type I cytokine receptoren zoals de leptine, LIF en IL-6 receptor. Via ubiquitinatie en redistributie van het de-ubiquitinerend enzyme USP8 zorgt RNF41 voor een indirecte destabilisatie van het ESCRT-0 complex. Dit leidt tot de her-oriëntatie van deze receptoren bestemd voor lysosomale degradatie naar cellulaire compartimenten waar ectodomain shedding plaatsvindt. Om de rol van RNF41 in intracellulair transport uitgebreider te bestuderen gebruikten we een methode waarbij we RNF41 verder karakteriseren op basis van de functie van nieuw geïdentificeerde RNF41 interactiepartners. Een initiële array MAPPIT screen leidde tot de identificatie van VPS52 als een nieuwe interactiepartner van RNF41. VPS52 is een subunit van het GARP en EARP complex, die respectievelijk betrokken zijn in retrograad cargo transport van endosomen naar het Golgi netwerk en in recyclering van cargo terug naar het plasma membraan. We tonen aan dat RNF41 ubiquitinatie en relocalizatie van VPS52 veroorzaakt, waarbij VPS52 op een andere locatie terecht komt in de cel en op deze manier leidt tot een verstoorde EARP-gemedieerde transferrine recyclering. Om het interactienetwerk van RNF41 verder uit te bouwen werd gebruik gemaakt van verschillende methodes zoals Bio-ID, Virotrap en AP-MS om bijkomstige RNF41 screens uit te voeren. Deze resultaten werd gecombineerd met data van reeds uitgevoerde microarray MAPPIT en Y2H screens om zo verder het RNF41 interactoom uit te bouwen. Dit liet ons toe om met sterke zekerheid RNF41 interactiepartners te identificeren en een mogelijke rol van RNF41 in bepaalde functionele clusters op te lichten. Op deze manier ontdekten we een rol voor AP2S1, het sigma subunit van het clathrine-gemedieerde endocytose adaptor eiwit AP-2, in leptine en LIF receptor signalering. Daarnaast toonden we aan dat RNF41 AP2S1 kan stabiliseren en relocalizeren. Tot slot onthulden we een rol voor RNF41 in autofagie via de karakterisering van de RNF41-positieve structuren gedetecteerd met immunofluorescentie. We toonden aan dat RNF41 belangrijk is om de niveaus van de autofagie receptor p62 en gefosforyleerd TBK1 te behouden. Dit, samen met gedetecteerde interacties tussen RNF41 en de autofagie-gerelateerde eiwitten Beclin1, ATG14, WIPI2 en ATG5, wijst erop dat RNF41 een rol speelt in de vorming van autofagosomen betrokken in de selectieve autofagie route genaamd aggrefagie. Alles samen wijzen onze bevindingen op een mogelijke rol van RNF41 in recyclering, endocytose en autofagie, wat verder het belang van RNF41 in intracellulair transport bevestigt. Bovendien is RNF41 betrokken in verschillende stoornissen zoals de ziekte van Parkinson,

cardiomyopathie en kanker, ziektebeelden die tevens geassocieerd zijn met verstoord intracellulair transport. Onze karakterisering van de interacties tussen RNF41 en eiwitten betrokken in intracellulair transport, samen met de opheldering hoe deze interacties betrokken zijn tot de processen in intracellulair transport, kan mogelijks leiden tot bijkomende inzichten voor de ontwikkeling van nieuwe therapeutica.

Introduction

1. Intracellular trafficking

1.1. Bidirectional vesicle transport

"What goes up, must come down"…, similar to this quote regarding the law of gravity, one could say "what goes out, must come back in" to define the law of intracellular trafficking. It is essential for tissue and organ functioning that eukaryotic cells communicate with their environment by releasing lipids and proteins outside the cell and by compensatory uptake of material. This forward flow of cargo counterbalanced by the retrograde movement of material is executed by the secretory and endocytic pathways. The secretory pathway delivers newly synthesized lipids, secretory and membrane proteins via the ER (endoplasmic reticulum) and the Golgi complex to the cell surface, the extracellular space or the appropriate intracellular compartment, while the endocytic pathway internalizes material from the extracellular environment and cell surface and sorts cargo via the EEs (early endosomes) into the correct intracellular compartment. The cargo is either destined for degradation in the lysosomes or gets recycled back to the PM (plasma membrane) via the RE (recycling endosomes). Next to this, material also traffics between the different internal compartments that constitute the cell (Figure 1). These cellular compartments are characterized by distinct lipid and protein compositions, which maintain their integrity and functionality by bidirectional fluxes that retrieve transport machinery components and proteins back to their original compartment. Bidirectional traffic is defined by a tightly regulated process of vesicular transport, where membrane-enclosed vesicles bud from a donor compartment and fuse with an acceptor compartment, a process that takes only seconds. This is coordinated by a series of consecutive steps, where cargo selection and vesicle budding, mediated by protein coats, is followed by motor protein (kinesin, dynein and myosin)-driven transportation along microtubules or actin to reach their destination compartment. Here, vesicles interact with the target membrane with the help of tethering complexes and small GTPases (guanosine 5′-triphosphatases) that determine the specificity of vesicle targeting, resulting in membrane fusion with the aid of SNARE (soluble N-ethylmaleimide-sensitive factor attachment protein receptor) proteins (Figure 2; [1–3]).
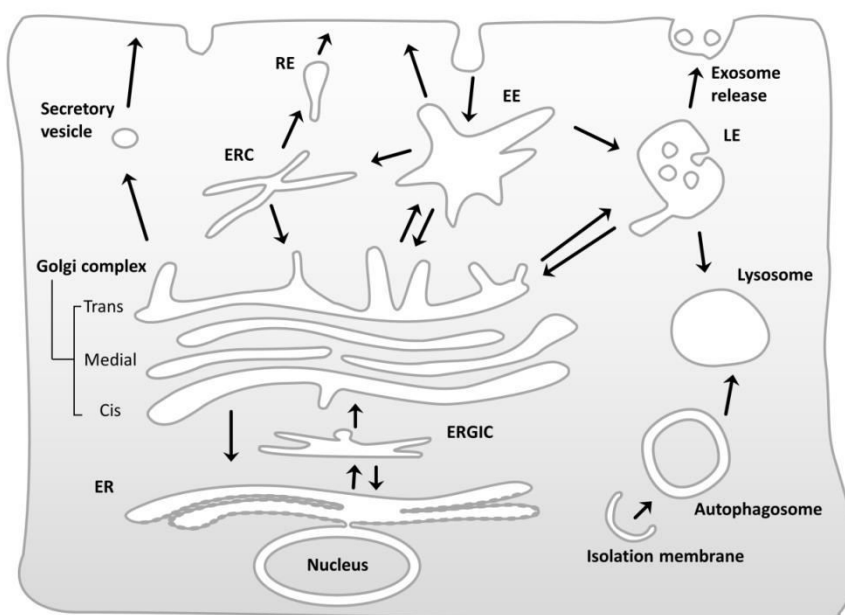
Figure 1: Overview of intracellular transport pathways. The arrows represent transport steps between the compartments of the secretory, endocytic and lysosomal pathways. EE (early endosome); LE (late endosome), RE (recycling endosome); ERC (endocytic recycling compartment); ER (endoplasmatic reticulum); ERGIC (ER-Golgi intermediate compartment). Figure adapted from [4]*.*
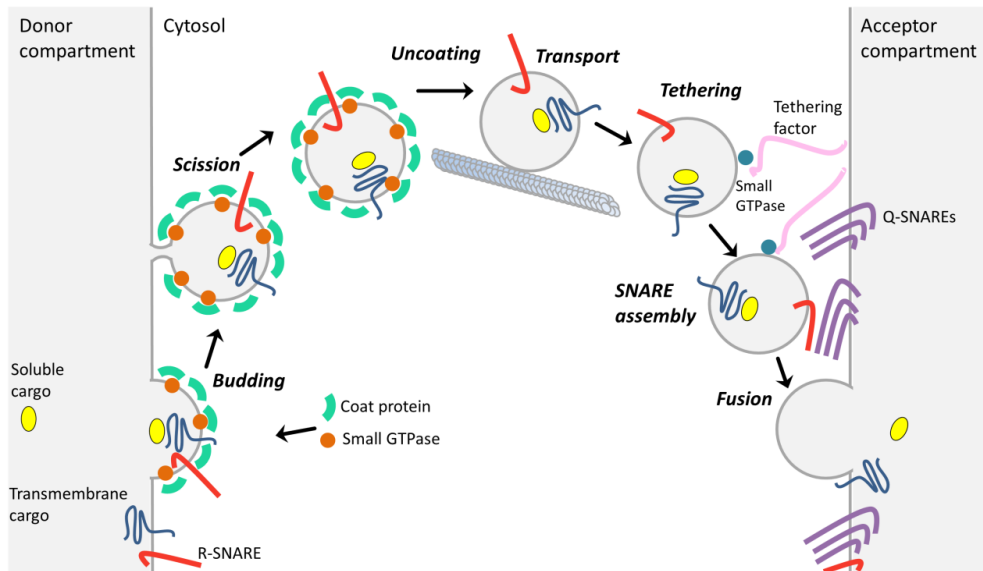

Figure 2: General mechanism of intracellular vesicular budding and fusion. Vesicles (transport carriers) bud from the donor membrane, a process mediated by small GTPases (guanosine 5'-triphosphatases) and coat proteins. These coat proteins are also involved in the sorting of cargo into vesicles. After scission, mediated by coats or accessory proteins, vesicles uncoat (note: uncoating may take place in cytosol, prior to tethering; or at the target membrane after tethering; or after fusion [5]*) and are transported along the cytoskeleton components to reach the acceptor membrane. Small GTPases recruit tethering factors that assist the R (arginine)-SNAREs (soluble N-ethylmaleimide-sensitive factor attachment protein receptors) on vesicles to pair with specific Q (glutamine)-SNAREs on acceptor membrane (see 1.1.4), resulting in fusion of the vesicle with the proper acceptor membrane and cargo release in the acceptor compartment. Figure adapted from* [2]*.*

1.1.1 Coats

Electron microscopy studies first identified transport vesicles surrounded by an electron-dense coat. These small vesicles, with a 60-100nm diameter, were located at the cell surface and in intracellular compartments [6]. Three types of coated vesicles have been identified so far, CCV (clathrin-coated vesicles), COPI (coat protein complex I) and COPII-coated vesicles (summarized in Table 1 and Figure 3; note: all proteins described in this thesis are human, unless otherwise specified). These coat components are necessary for the induction of membrane curvature, the recruitment of cargo, vesicle budding and the final uncoating steps.
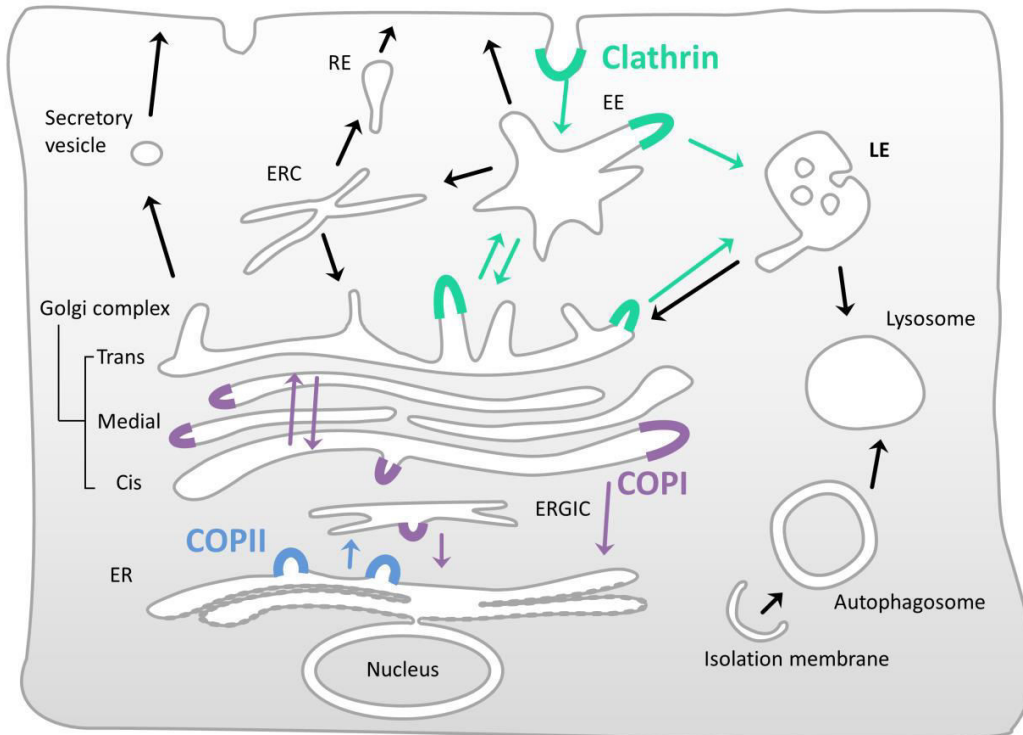
Figure 3: Coats involved in intracellular trafficking steps. Involvement of Clathrin (green), COPI (Coat protein complex I, purple) and COPII (Coat protein complex II, blue) is depicted on the figure. Clathrin coats contain different adaptor and accessory proteins at different locations. The roles of clathrin at plasma membrane in endocytosis and of COPII vesicles at ER export are well-known. Uncertainty remains about the exact function of clathrin at the TGN, recycling and late endosomes and secretory vesicles, and of COPI at the ERGIC (ER-to-Golgi intermediate compartment) and Golgi complex. EE (early endosome); LE (late endosome), RE (recycling endosome); ERC (endocytic recycling compartment); ER (endoplasmatic reticulum); ERGIC (ER-Golgi intermediate compartment). Figure adapted from [4]*.*

CCVs bud from the PM, TGN (trans-Golgi network) and endosomes [7]. Clathrin exists as a three-legged structure called a triskelion, composed of three heavy chains and three light chains (Figure 4). These clathrin triskelions polymerize into a polyhedral coat surrounding membrane vesicles [8]. The clathrin coat acts as a scaffold and is recruited to different membranes by specific AP (adaptor protein) complexes that are also responsible for cargo binding. Five different AP complexes (AP-1, -2, -3, -4 and -5) have been identified, of which AP-1 and AP-2 sort cargo proteins into CCVs [9]. Both AP-1 and AP-2 are heterotetramers, consisting of two large subunits (γ and β1 in AP-1; α and β2 in AP-2), a medium subunit (μ1 in AP-1; μ2 in AP-2) and a small subunit (σ1 in AP-1; σ2 in AP-2). AP-1 is located at the TGN and endosomes, and mediates bidirectional transport between these organelles, while AP-2, located at the PM, plays a role in clathrin-dependent endocytosis (Figure 4, [10,11]). GGA (Golgi-localized, γ-ear containing, ADP-ribosylation factor-binding proteins) and HRS (hepatocyte growth factor receptor tyrosine kinase substrate) are two alternative clathrin adaptors that also function in clathrin-mediated vesicle budding. The monomeric GGA adaptor regulates the sorting of cargo from the TGN to endosomes and lysosomes, sometimes simultaneously with AP-1 [12], whereas dimeric HRS sorts ubiquitinated cargo from the EEs to the LEs (late endosomes) [13]. Both AP-1 and GGAs are recruited to membranes via the RAS superfamily of ARF (ADP ribosylation factor) small GTPases (Figure 4). The ARFs regulate the assembly and disassembly of the coats by

respectively switching between an active (GTP (guanosine 5'-triphosphate) bound) and inactive (GDP (guanosine 5'-diphosphate) bound) state. Conversely, AP-2 and HRS directly interact with phosphatidylinositol (4,5)-bisphosphate (PI(4,5)P2) and phosphatidylinositol (3)-phosphate (PI(3)P) present in the cell membrane [14,15].

COPI and COPII can be considered as multisubunit protein complexes, where the COPI coatomer is a complex of seven proteins divided into two subcomplexes, the F-subcomplex: β, γ, δ, ζ and the B-subcomplex: α, β', ε. These COPI coat components have sequence homology to the clathrin AP-2 and AP-2 adaptor proteins [14]. COPI vesicles traffic from the Golgi to the ER and between Golgi cisternae and are, similar to the clathrin adaptors AP-1 and GGAs, recruited to membranes via ARF1. On the other hand, COPII coats are composed of four proteins that form the SEC13-SEC31 and SEC23-SEC24 subcomplexes, of which the latter is responsible for cargo recruitment. COPII vesicular traffic from the ER to the Golgi and COPII membrane recruitment depend on the ARF-related protein SAR1 (Figure 4).
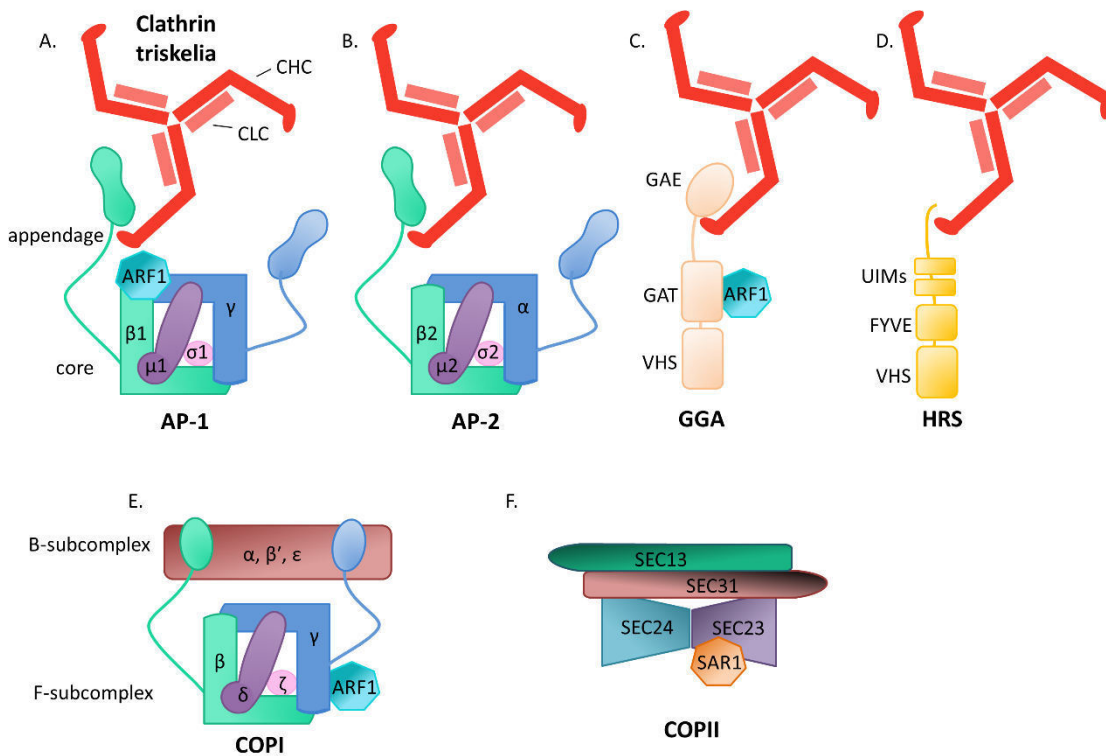
Figure 4: Schematic representation of the different coat proteins. A and B: Clathrin triskelion with CHC (clathrin heavy chain) and CLC (clathrin light chain) interacts with the appendage domain of the β1 or β2 subunit of adaptor protein AP-1 or AP-2. C: Clathrin interacts with the hinge and GAE (γ-adaptin ear) domains of the GGA (for Golgi-localized, γ-ear-containing, ADP-ribosylation factor-binding protein) adaptor protein. D: Clathrin interacts with a clathrin-box motif in HRS (hepatocyte growth factor-regulated tyrosine kinase substrate). E: Structure of the COPI (coat protein complex I) coat protein, the structure of the F-subcomplex (β, γ, δ, ζ) is based on the model of AP-1 and -2 because of the homology of their subunits, while the arrangement of the B-subcomplex (α, β', ε) has not been elucidated yet. F: Structure of the COPII (coat protein complex II) coat protein. The small G proteins ARF1 and SAR1 are shown next to the coat proteins that they regulate. GAT (GGAs and TOM1 (target of Myb 1)); VHS (VPS27, HRS and STAM); UIMs (ubiquitin- interacting motifs); FYVE (FAB1, YOTB, VAC1 and EEA1). Figure adapted from [14].

COPI, COPII and the clathrin adaptors recognize different motifs present in the cytosolic domain of transmembrane cargo proteins. AP-1 and AP-2 adaptors bind the acidic dileucine motif [D/E]XXXL[L/I] and the tyrosine-based motif' Yxxϕ (where ϕ indicates a hydrophobic residue) [16]. GGAs bind to cargo proteins with a DXXLL motif, while HRS directly interacts with ubiquitinated cargo via its UIM (ubiquitin-interacting motif) domain. COPI-coated vesicles capture proteins carrying the "KKXX", "KXKXX" or "FFXXRRXX" motif and COPII-coated vesicles recognize the di-acidic motif DXE [2,17,18].

After coat formation, vesicles bud by scission of the neck, thereby detaching the forming vesicle from the donor membrane. For COPI and COPII coated vesicles this process is induced by coat polymerization, whereas CCVs depend on the action of amphiphysin that recruits the GTPase dynamin followed by endophilin to induce membrane deformation and scission. In the final uncoating step, the coat components are released prior to membrane fusion, although recent data suggest that coats appear to be involved in the tethering step, and thus may remain attached much longer than previously assumed [5]. These cytosolic coat proteins are then recycled for the next round of vesicle budding. Also here, the uncoating mechanisms for COPI and COPII coats differs from CCVs. For COPI and COPII this requires GTP hydrolysis of ARF1 and SAR1 respectively, while the ATPase HSC70 (heat shock protein 70) and auxilin work together to drive clathrin coat disassembly [10,14,17].

Table 1: Overview of the different coat proteins and their properties.

Coats	Subunits	Recruitment to membrane via GTPase	Location	Function	Motif
Clathrin-AP-1	γ , β1, μ1, σ1	ARF1 (via γ and β1 subunit)	TGN/endosomes	bidirectional sorting of proteins between TGN and endosomes	the σ1 subunit recognizes the "[DE]XXXL[LI]" motif and the μ1 subunit recognizes the Yxxϕ motif present in cargo
Clathrin-AP-2	α, β2, μ2, σ2	PI(4,5)P2 (via α and μ2 subunit)	plasma membrane	sorting of proteins from plasma membrane to early endosomes	the σ2 subunit recognizes the "[DE]XXXL[LI]" motif and the μ2 subunit recognizes the Yxxϕ motif present in cargo
Clathrin-GGA	GGA	ARF1 (via GAT domain)	TGN/endosomes	sorting of proteins from TGN to endosomes and lysosomes	VHS domain recognizes "DXXLL" motif in present in cargo
Clathrin-HRS	HRS	PI(3)P (via FYVE domain)	endosomes	sorting of proteins from early to late endosomes	UIM domain recognizes ubiquitinated cargo
COPI	F-subcomplex: β, γ, δ, ζ; B-subcomplex: α, β', ε	ARF1 (via γ subunit)	Golgi/ER	sorting of proteins from the Golgi to the ER and between Golgi cisternae	the γ subunit recognizes cargo with "KKXX", "KXKXX" or "FFXXRRXX"motif

COPII	SEC13-SEC31 subcomplex and SEC23-SEC24 subcomplex	SAR1 (via SEC23)	ER	sorting of proteins from the ER to the Golgi	SEC24 recognizes the "DXE" motif present in cargo

AP-1/2 (adaptor protein-1/2); ARF1 (ADP ribosylation factor 1); PI(4,5)P2 (phosphatidylinositol (4,5)-bisphosphate); PI(3)P (phosphatidylinositol (3)-phosphate); GGA (Golgi-localized, γ-ear-containing, ADP-ribosylation factor-binding protein); HRS (hepatocyte growth factor-regulated tyrosine kinase substrate); ER (endoplasmic reticulum); TGN (trans-Golgi network); COPI/II (coat protein complex I/II); GAT (GGAs and TOM1 (target of Myb 1)); VHS (VPS27, HRS and STAM); FYVE (FAB1, YOTB, VAC1 and EEA1);UIMs (ubiquitin-interacting motifs). Table adapted from [14,17].

1.1.2   RAB GTPases

RAB proteins are small (21–25 kDa) GTPases that belong to the RAS superfamily. Approximately 70 RAB proteins have been identified in humans, of which nearly 50 are involved in intracellular trafficking [19]. These RAB GTPases have been implicated in the regulation of vesicle formation, transportation along the cytoskeleton, docking and fusion through the recruitment of effector proteins. The importance of RABs is reflected by various diseases such as to Charcot-Marie-Tooth Type 2B and Carpenter syndrome [20,21], due to mutations in RAB proteins, while altered expression of RAB genes is associated with diseases such as cancer and Alzheimer's disease [22,23]. RAB proteins function as molecular switches, and cycle between the cytosolic GDP-bound inactive and membrane-anchored GTP-bound active form. The cytosolic inactive RABs bind to GDI (GDP Dissociating Inhibitors) and membrane binding depends on the GDF (GDP Dissociating Factor) that catalyzes the dissociation of GDI from RAB proteins, allowing insertion into the membrane. Here, GEFs (Guanine Nucleotide Exchange Factors) catalyze GDP dissociation, allowing GTP binding and activation of RABs, resulting in their interaction with different effectors. RABs are converted back to their inactive GDP-bound state by GTP hydrolysis, mediated by GAPs (GTPase Activating Proteins). These inactive RABs are then removed from the membrane by GDI, reforming the cytosolic RAB-GDI complex [24,25]. Reversible membrane association of RABs is achieved by the attachment of a geranylgeranyl (20-C) group, rendering the protein hydrophobic ([26], Figure 5).
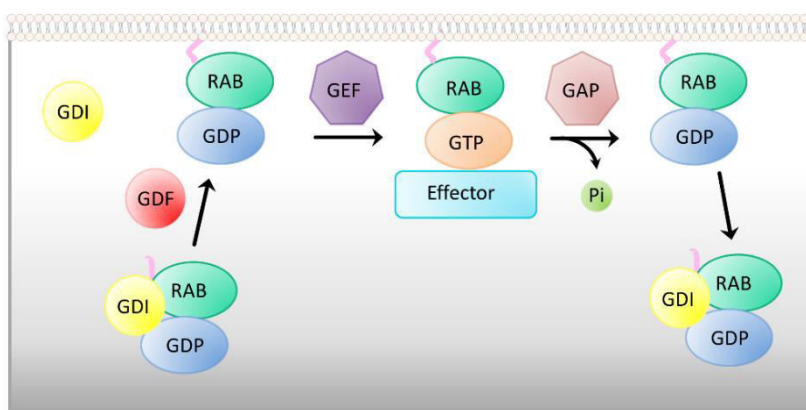
Figure 5: RAB GTPase (guanosine 5'-triphosphatase) cycle. Cytosolic inactive GDP (guanosine 5'-diphosphate)-bound RABs are associated with GDI (GDP Dissociating Inhibitor). GDF (GDP Dissociating Factor) mediates the displacement of GDI, allowing GDP-RABs to insert into the membrane via its geranylgeranyl group (pink). GEFs (Guanine Nucleotide Exchange Factors) catalyze the exchange of GDP for GTP (guanosine 5'-triphosphate), resulting in RAB activation and interaction with its effector. GAPs (GTPase Activating Proteins) convert the

active GTP-bound RABs back to the GDP-bound inactive form via GTP hydrolysis, thereby releasing Pi (inorganic phosphate). The inactive RABs are removed from the membrane by GDI that maintains GDP-RABs in the cytoplasm ready for the next cycle. Figure adapted from [25]*.*

RAB proteins localize to the membranes of transport vesicles and other membrane bound organelles from where they control a specific trafficking step. Since RAB proteins accumulate at these distinct compartments, they are often used as markers for different organelles [27] and discrimination between endosomes is based on the different RAB populations and lipid composition of the membrane. Each step in intracellular trafficking is mediated by a different RAB protein, although some RABs can act at multiple stages of the secretory and endocytic pathway. The most generic RABs relevant to this thesis are described below and their function and effectors are listed in Table 2 and depicted in Figure 6 [19,24,28,29]. RAB5, the EE marker regulates traffic from the PM to the EE [30] whereas the LE marker RAB7 is involved in early-to-late endosome and LE to Golgi transport [31]. RAB4 and RAB11 are typically involved in recycling, where RAB4 mediates fast recycling from EEs to the PM, while RAB11 regulates slow recycling through the REs [32–34]. RAB9, located on LE mediates traffic towards the TGN [35], while RAB14, found at both TGN and EE, controls EE to Golgi transport [36]. Conversely, Golgi-localized RAB6 regulates Golgi to endosome transport [37], and additionally, RAB6 also functions in the secretory pathway by mediating intra-Golgi transport [38]. Similarly, next to the RE, RAB11 also associates with the Golgi and regulates transport from EEs to the TGN [39] and from the TGN to the PM [40]. In this way, RAB11 connects the endocytic and secretory pathway. Moreover, RAB11, in addition to RAB35 and RAB27, has been shown to play a role in exosome biogenesis and secretion. Other important secretory RABs are the ER-localized RAB1 and RAB2 that regulate ER to Golgi transport [41].
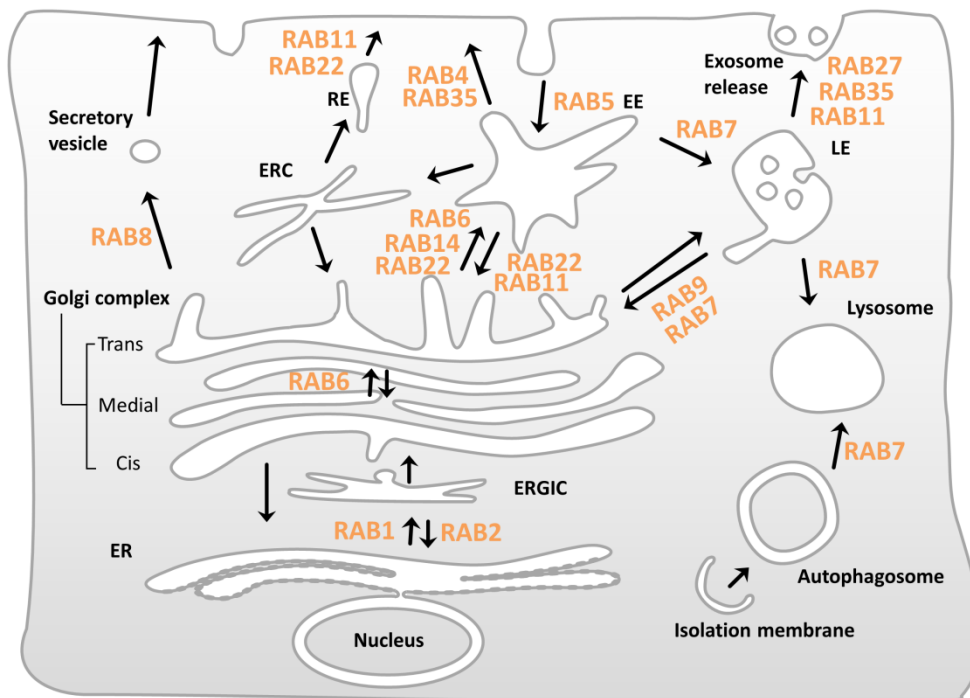

Figure 6: Location and function of RAB GTPases relevant for this thesis. For details regarding function, we refer to Table 2 and text. EE (early endosome); LE (late endosome), RE (recycling endosome); ERC (endocytic recycling compartment); ER (endoplasmatic reticulum); ERGIC (ER-Golgi intermediate compartment). Figure adapted from [25,28]*.*

Table 2: Overview of the most typical RABs involved in intracellular trafficking.

RABs	Location	Trafficking function	Effectors
RAB1	ER/Golgi	ER–Golgi transport	p115 (tethering factor)
RAB2	ER/Golgi	ER–Golgi transport	p115 and Golgin45 (coiled-coil Golgi protein)
RAB4	EE	recycling EE to PM	Rabaptin-4/Rabaptin-5 (required for protein sorting and recycling)
RAB5	EE, CCV	endocytosis and EE fusion	EEA1 and CORVET (tethering factors)/ p150 and VPS34 (PI3K class III subunits)
RAB6	Golgi	intra-Golgi transport; Golgi to PM, endosomes and ER transport	VPS52 (subunit of tethering factor GARP)
RAB7	LE	EE-LE transport; LE-Golgi transport	HOPS (tethering factor)/ VPS35 (retromer subunit)
RAB8	TGN	secretory vesicle transport to PM	exocyst (tethering factor)
RAB9	LE	LE-Golgi transport	TIP47 (Cargo adaptor, involved in sorting CI-M6PR to TGN)
RAB11	TGN/RE	recycling RE to PM; EE-TGN and TGN-PM transport; exosome secretion	Myosin 5B (motor protein); RAB11-FIPs (family interacting proteins; facilitate vesicle recycling)
RAB14	EE/Golgi	trafficking between Golgi and EE	KIF16B (motor protein)
RAB22	EE/TGN; RE	EE-TGN transport; recycling RE to PM	EEA1
RAB27	LE, lysosome	LE/lysosome to PM transport; exosome secretion	granuphilin-a/b and exophilin-5 (involved in exosome secretion)
RAB35	EE	recycling EE to PM; exosome secretion	FSCN1 (fascin homolog 1, actin-bundling protein)

EE (early endosome); LE (late endosome), RE (recycling endosome); ERC (endocytic recycling compartment); ER (endoplasmatic reticulum); PM (plasma membrane); CCV (clathrin-coated vesicles); CORVET (class C core vacuole/endosome tethering); HOPS (homotypic fusion and vacuole protein sorting); TIP47 (tail-interacting protein of 47 kD). Table adapted from [19,24,29].

1.1.3 Tethering complexes

Tethering factors are extended proteins or protein complexes that function in the initial docking or 'bridging' of transport vesicles to the target membrane prior to fusion. This is accomplished by recognizing and binding specific determinants on these vesicles. Vesicle tethering is a highly regulated process involving interaction with RABs, SNAREs and coat proteins. These interactions also specify the location of tethering factors, where they can act alone or with other tethering factors in one trafficking event or participate in more events. Loss of tethering factors often results in a block of membrane transport and impaired organization and identity of compartments pointing to their role as essential mediators of intracellular transport [42]. Tethering factors can be divided in two, highly conserved classes: the long coiled-coil proteins and the MTCs (multisubunit tethering complexes). The coiled-coil tethers are large hydrophilic homodimeric proteins comprising two globular heads connected by a long coiled-coil domain. These large tethers can form a bridge over a distance of up to 200nm [43]. Coiled-coil tethers such as p115, p230, GM130, GCC88 and GCC185 are mostly present at the Golgi, although some, like EEA1, are present at endosomes (overview in Table 3). The MTCs can be subdivided into CATCHR (complexes associated with tethering containing helical rods) and non-CATCHR complexes, based on their structural and sequence similarities. The COG (conserved oligomeric Golgi complex), NRZ (NAG, RINT-1, ZW10); DslI in yeast), GARP (Golgi-

associated retrograde protein), EARP (endosome-associated recycling protein) and the exocyst complex belong to the CATCHR family, while TRAPPI (transport protein particle I), TRAPPII, TRAPIII, HOPS (homotypic fusion and vacuole protein sorting) and CORVET (class C core vacuole/endosome tethering) make up the non-CATCHR family [4] (overview in Table 3 and Figure 7 and 8). Each member of the MTC consists of 3 to 10 subunits, resulting in an overall molecular weight of 250 to 800kDa. In contrast to the coiled-coil tethers, these MTCs can only bridge over a distance of up to 30nm [43]. Accordingly, coiled-coil tethers are considered to play a role in the initial, highly dynamic stages of tethering due to their ability to form transient, reversible and low-affinity interactions [44]. Conversely, MTCs that capture targets at short distances, possibly interact simultaneously with different transport components through their multiple subunits, and could therefore couple vesicular tethering, docking and fusion events. The discovery that the coiled-coil p115 tether directly interacts with the COG complex suggested that coiled-coil tethers and MTCs likely cooperate during these steps [45].
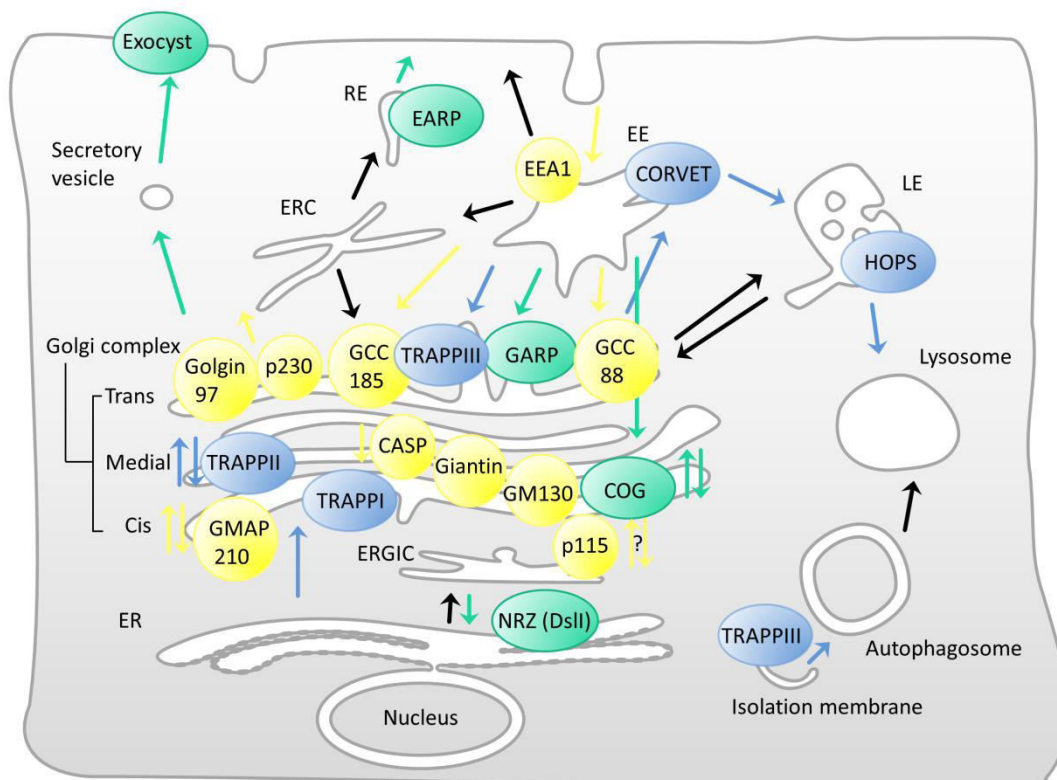
Figure 7: Schematic overview of the subcellular location of the different tethering complexes. Coiled-coil tethers are indicated in yellow, multisubunit tethering complexes of the CATCHR (complexes associated with tethering containing helical rods) family in green, and of the non-CATCHR family in blue. For details regarding function, we refer to Table 3 and text. EE (early endosome); LE (late endosome); RE (recycling endosome); ERC (endocytic recycling compartment); ER (endoplasmic reticulum); ERGIC (ER-Golgi intermediate compartment); CORVET (class C core vacuole/endosome tethering); HOPS (homotypic fusion and vacuole protein sorting); COG (conserved oligomeric Golgi complex); NRZ (NAG, RINT-1, ZW10), GARP (Golgi-associated retrograde protein), EARP (endosome-associated recycling protein); TRAPP (transport protein particle). Figure adapted from [4,42].

Figure 8: Schematic representation of coiled-coil tethers and multisubunit tethering complexes of the CATCHR (complexes associated with tethering containing helical rods) and non-CATCHR family. The coiled-coil tethers consist of a long coiled-coil domain that associate with the Golgi membrane through interactions with other Golgi-localized proteins via two globular heads (e.g. p230, GCC185, GCC85, Golgin97), or through carboxy-terminal transmembrane domains (e.g. Giantin and CASP). CATCHR family teth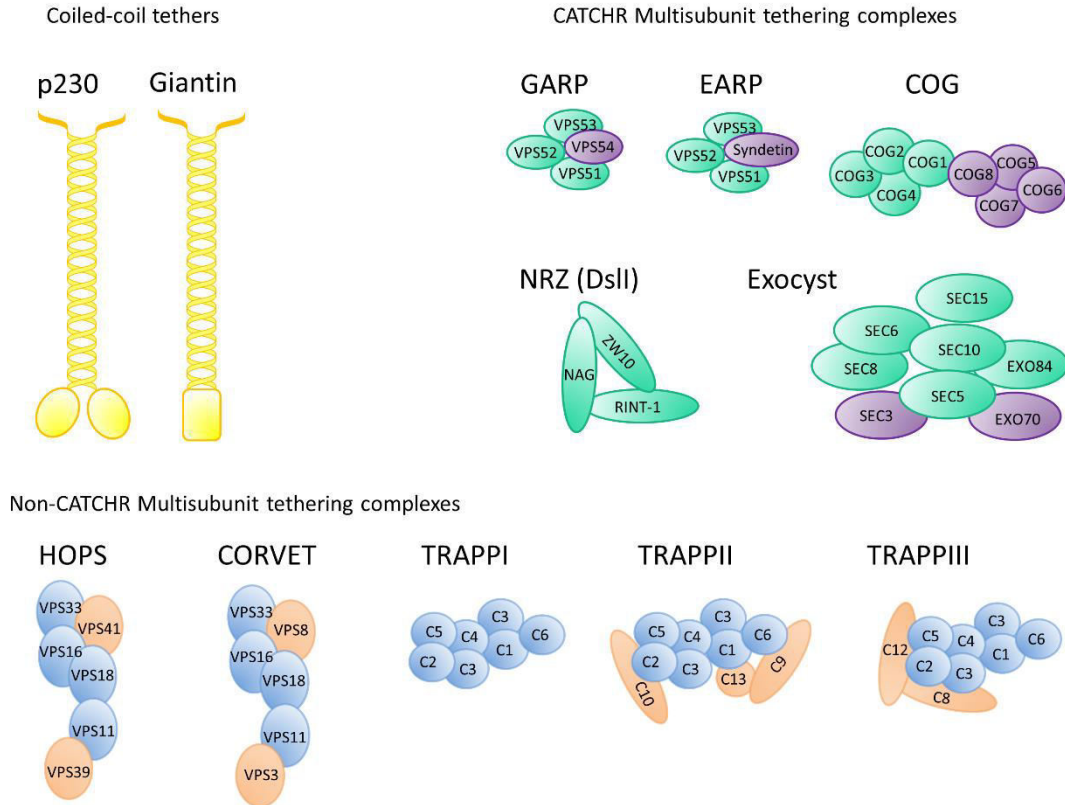ering factors: eight subunits of the COG (conserved oligomeric Golgi complex) complex are organized in two structurally and functionally distinct lobes (green and purple). The GARP (Golgi-associated retrograde protein) and EARP (endosome-associated recycling protein) complexes share VPS51, VPS52 and VPS53 (green), while VPS54 and syndetin (purple) are specific for the GARP and EARP complex respectively. The Exocyst subunits SEC3 and EXO70 (purple) interact with the plasma membrane, while SEC15 (green) interacts with the vesicle through vesicle-localized RAB8. Non-CATCHR family tethering factors: VPS33, VPS16, VPS18 and VPS11 (blue) are the common subunits of the HOPS (homotypic fusion and vacuole protein sorting) and CORVET (class C core vacuole/endosome tethering) complex, while VPS41 and VPS39 (orange) represent HOPS specific subunits, and VPS8 and VPS3 (orange) CORVET specific subunits. The core subunits of the TRAPP (transport protein particle) complexes (TRAPPC1-6) are indicated in blue, and the TRAPPII (C9, C10, C13) and TRAPPIII (C8, C12) specific subunits are indicated in orange. For more details about the function we refer to Table 4 and text. Figure adapted from [42,46,47].

As previously mentioned, tethering factors are RAB effectors, and activated GTP-bound RABs facilitate the recruitment of tethers to specific locations. The exocyst complex consisting of SEC3, SEC5, SEC6, SEC8, SEC10, SEC15, EXO70 and EXO84 mediates the transport of secretory vesicles from the TGN and RE to the PM. It binds to the RAB GTPase RAB8 on secretory vesicles via its subunit SEC15, and to the Rho GTPases RHOA (Ras homolog gene family member A), RAC1 (Ras-related C3 botulinum toxin substrate 1) and CDC42 (Cell division control protein 42) at the PM via SEC3 [48–50].

The RAB1 effector COG consists of 8 subunits, COG1-8, and acts as a tether for intra-Golgi transport next to regulating retrograde transport from endosomes to Golgi [51]. VPS51, 52, 53 and VPS54 compose the GARP complex, which is recruited by RAB6 through its VPS52 interaction and functions in retrograde traffic from the endosomes to the TGN [37,52]. The GARP subunit VPS54 is replaced by Syndetin to form another complex called EARP. Although VPS52 is a mutual subunit of both the GARP and EARP complex, there is no evidence that RAB6 recruits the EARP complex, moreover, the EARP complex was shown to colocalize with RAB4, RAB5 and RAB11, making these possible candidates for EARP recruitment [53]. HOPS and CORVET were respectively shown to be RAB7 and RAB5 effectors. HOPS regulates the endolysosomal pathway, while CORVET functions upstream of HOPS and mediates TGN to EE transport. HOPS and CORVET share four subunits, VPS11, VPS16, VPS18 and VPS33. The other subunits (VPS39 and 41 for HOPS and VPS3 and 8 for CORVET) are responsible for changing the RAB-interacting specificity from RAB7 (HOPS) to RAB5 (CORVET) [54]. In certain cases, tethering factors can function both as an effector and activator of RAB proteins. This is the case for the HOPS complex, where VPS39 functions as GEF and promotes RAB7-GDP to RAB7-GTP conversion [55]. TRAPPI and TRAPPII were also identified as GEFs, where the shared subunits TRAPPC1, TRAPPC3, TRAPPC4 and TRAPPC5 are necessary for RAB1 GEF activity [56–58]. Two additional subunits (TRAPPC2 and TRAPPC6) further compose TRAPPI, which functions as a tether in ER to Golgi transport, while five additional subunits (TRAPPC2, TRAPPC6, TRAPPC13, TRAPPC9 and TRAPPC10) are found in the TRAPPII complex that mediates intra-Golgi transport and endosome to Golgi transport [4,59,60].

As stated before, vesicles can retain protein coats at least through the initiation of tethering since many tethers were found to interact with coat proteins. COG3 of the COG complex and the coiled coil tether p115 showed specific interactions with the β COPI subunit [61,62], while the TRAPPC10 subunit of TRAPPII interacted with the γ COPI subunit [58]. The ER-localized NRZ/DslI complex regulates the retrograde transport of COPI vesicles from the Golgi to the ER. In yeast, the Dsl1 subunit interacts with both the α and δ COPI subunit [63], while the mammalian Dls1 homolog, ZW10, lacks this binding site and additionally requires UVRAG1 (UV radiation resistance associated gene 1) for this COPI interaction [64,65]. Furthermore, the TRAPPI tether directly binds to SEC23 of COPII vesicles via its TRAPPC3 subunit [56,66].

Tethering factors further couple the process of vesicle recognition to the process of membrane fusion by physically interacting with SNAREs. Moreover, some tethers, like p115 are able to induce SNARE-mediated membrane fusion by promoting SNARE complex formation. p115 couples COPI vesicles to the Golgi membrane by sequentially linking GM130 to Giantin, followed the induction of GOSR1-STX5 (syntaxin 5) SNARE complex assembly [67]. The GARP complex also directly interacts with a SNARE protein. The VPS51 subunit binds to the N-terminal Habc domain of the STX6 (Tlg1p in yeast) SNARE present on the Golgi membrane. It has been suggested that this VPS51 interaction results in the release of the autoinhibition caused by closed conformation, where the N-terminal domain interacts with the C-terminal SNARE motif of STX6 (see 1.1.4; [52,68]). The HOPS complex has also been shown to interact with the SNARE STX8 (Vam7 in yeast) and as such plays a role in initiating SNARE complex assembly [69]. Furthermore, COG and NRZ complexes interact with intra-Golgi SNAREs like SEC22, GOSR1, STX5 and YKT6, and with ER-localized SNAREs like USE1 and BNIP1 respectively [70,71].

Table 3: Overview of the different tethering factors and their properties.

Group	Sub-group	Tethering factor	Subunits	Location	Function	GTPase	SNAREs	Coat
Coiled-coil:	/	p115	/	ERGIC	COPI vesicles to golgi tethering; transport of newly synthesized cargo	RAB1	STX5, GOSR1	COPI
		GM130	/	Golgi	involved in p115-dependent tethering	RAB1	STX5	COPI
		Giantin	/	Golgi	involved in p115-dependent tethering	RAB1	STX5	COPI
		CASP	/	Golgi	retrograde transport in Golgi	?	?	?
		GMAP210	/	Golgi	intra-Golgi trafficking	ARF1	?	?
		GCC185	/	TGN	Endosome-TGN transport	RAB9	?	?
		GCC88	/	TGN	Endosome-TGN transport	ARL1/3	SEC22b, GOSR1	?
		p230	/	TGN	anterograde transport from TGN	ARL1/3	?	?
		Golgin97	/	TGN	anterograde transport from TGN	ARL1/3	STX16	?
		EEA1	/	EE	vesicle docking and fusion at EE	RAB5	STX13	?
MTC:	CATCHR:	COG	COG1, COG2, COG3, COG4, COG5, COG6, COG7, COG8	Golgi	Intra-golgi transport; Endosome-Golgi retrograde transport	RAB1	SEC22b, GOSR1; STX5, YKT6	COPI
		NRZ (DslI in yeast)	ZW10, NAG, RINT-1 (Dsl1, Dsl3, Tip20 in yeast)	ER	Golgi-ER retrograde transport	RAB1?	USE1, BNIP1	COPI
		GARP	VPS51, VPS52, VPS53, VPS54	TGN	endosome to TGN retrograde transport	RAB6	STX6	?
		EARP	VPS51, VPS52, VPS53, Syndetin	RE/EE	endosome to PM recycling	?	?	
		Exocyst	SEC3, SEC5, SEC6, SEC8, SEC10, SEC15, EXO70, EXO84	PM	secretory vesicle transport from RE and Golgi to PM	RAB8, CDC42, RHOA, RAC1, ARF6	STX1; VAMP2; SNAP-23	?
	non-CATCHR:	TRAPPI	TRAPPC1-6 (Bet3A, Bet3B, Bet5,	Golgi	Tethering COPII vesicles from ER to Golgi	RAB1	?	COPII

			Trs20, Trs23, Trs31, Trs33 in yeast)				
		TRAPPII	TRAPPC1-6 + TRAPPC13, TRAPPC9, TRAPPC10 (Trs65, Trs120, Trs130 in yeast)	Golgi	Intra-golgi transport; endosome-Golgi retrograde transport	RAB1, RAB11	?	COPI
		TRAPPIII	TRAPPC1-6 + TRAPPC12, TRAPPC8 (Trs85 in yeast)	phagophore	endosome-TGN retrograde transport; autophagy	RAB1	?	?
		HOPS	VPS11, VPS16, VPS18, VPS33, VPS39, VPS41	endosome	endolysosomal fusion	RAB7	STX7, STX8, VTI1B, VAMP7	AP-3 sub-unit
		CORVET	VPS3, VPS8, VPS11, VPS16, VPS18, VPS33	endosome	functions upstream of HOPS, endosome fusion; TGN-EE transport	RAB5	?	?

COPI/II (coat protein complex I/II); MTC (multisubunit tethering complex); CATCHR (complexes associated with tethering containing helical rods); EE (early endosome); RE (recycling endosome); ERC (endocytic recycling compartment); ER (endoplasmatic reticulum); CORVET (class C core vacuole/endosome tethering); HOPS (homotypic fusion and vacuole protein sorting); COG (conserved oligomeric Golgi complex); NRZ (NAG, RINT-1, ZW10), GARP (Golgi-associated retrograde protein), EARP (endosome-associated recycling protein); ARF (ADP ribosylation factor); ARL (ARF-like); RHOA (Ras homolog gene family member A); RAC1 (Ras-related C3 botulinum toxin substrate 1); CDC42 (Cell division control protein 42); TRAPP (transport protein particle); VTI1B (Vesicle transport through interaction with T-SNAREs 1B); STX (syntaxin); VAMP (Vesicle-associated membrane protein); AP-3 (adaptor protein-3). Table Adapted from [5,42,43].

1.1.4 SNAREs

Membrane fusion requires the interaction between SNARE proteins associated with the two opposing membranes. Originally, SNAREs were classified as v-(vesicle) or t-(target membrane) SNAREs, based on their subcellular localization [72]. However, this classification is confusing when homotypic fusion between two organelle membranes or vesicles takes place and many SNAREs are found on both vesicles and target membranes. Therefore, a new nomenclature was introduced depending on a single key residue that is either arginine (R-SNAREs) or glutamine (Q-SNAREs) [73]. Membrane fusion usually requires four SNAREs and this complex generally consist of one R-SNARE and three Q-SNAREs. The R-SNARE often originates from the vesicle, while the Q-SNAREs are mostly present on the target organelle [74]. The SNAREs assemble into a trans-SNARE complex, also called

SNAREpin, which bridges the two opposing membranes resulting in membrane fusion. A single SNARE can be assembled into more than one trans-SNARE complex and can regulate multiple fusion events, also, several SNARE complexes can be formed but not all will functionally drive membrane fusion [75].

SNAREs typically contain an evolutionary conserved 60 to 70 amino acid SNARE motif which consists of heptad repeats that have the ability to form coiled-coils (Figure 9). This motif allows assembly into a tight four-helix bundle in the trans-SNARE complex and is connected by a short linker to a hydrophobic transmembrane domain at its C-terminus. Of the 38 identified SNAREs in humans, seven (SNAP-23, SNAP-25, SNAP-29, SNAP47, STX9/19, STX11 and YKT6) do not contain this transmembrane domain and instead associate with membranes via different lipid modifications such as palmitoylation and prenylation [47]. In contrast to the conserved SNARE motifs, SNAREs contain different types of independently folded N-terminal domains [76]. Some SNAREs have an N-terminal Habc domain that reversibly associates with the SNARE motif on the same SNARE thereby forming a closed conformation and preventing the SNARE from assembling into the SNARE complex [77]. These N-terminal regions can also interact with SM (SEC1/Munc18-like) proteins, a small family of soluble proteins essential for fusion [78]. SM proteins stimulate specific SNARE pairing and considerably accelerate the rate of SNARE-mediated fusion [79,80]. Next to SM proteins, tethering factors also influence trans-SNARE complex formation. Their ability to interact with both SNAREs and SM proteins through their different subunits, either simultaneously or sequentially contributes to the spatial and temporal regulation of trans-SNARE assembly and to its stability [47,67,81]. The tethering factors GARP and COG, both involved in endosome to TGN transport, were found to regulate the assembly of the same SNARE complex: STX6-STX16-VTI1A (Vesicle transport through interaction with T-SNAREs 1A)-VAMP4 (Vesicle-associated membrane protein 4) (see Figure 10; [52,82–84]). It is currently unclear why these and other tethers have overlapping functions. Binding affinity between tethers and SNAREs or PTMs (post-translational modifications) might additionally influence and regulate SNARE assembly [47].

Figure 9: Schematic presentation of different SNAREs (soluble N-ethylmaleimide-sensitive factor attachment protein receptor). Most SNAREs contain one SNARE motif, while SNAP-23, SNAP-25, SNAP-29 and SNAP-47 contain two SNARE motifs. These latter SNAREs, together with STX (syntaxin) 9/19, STX11 and YKT6, also lack a C-terminal TM (transmembrane domain), but associate with membranes via palmitoylation and/or prenylation. Many SNAREs contain an N-terminal regulatory region comprising a Habc domain, with or without a short N-

terminal peptide that can interact with SM (SEC1/Munc18-like) proteins. VAMP4 (Vesicle-associated membrane protein 4) contains an N-terminal motif that can interact with the TGN. VTI1A/B (Vesicle transport through interaction with T-SNAREs 1A/B). Figure adapted from [47].
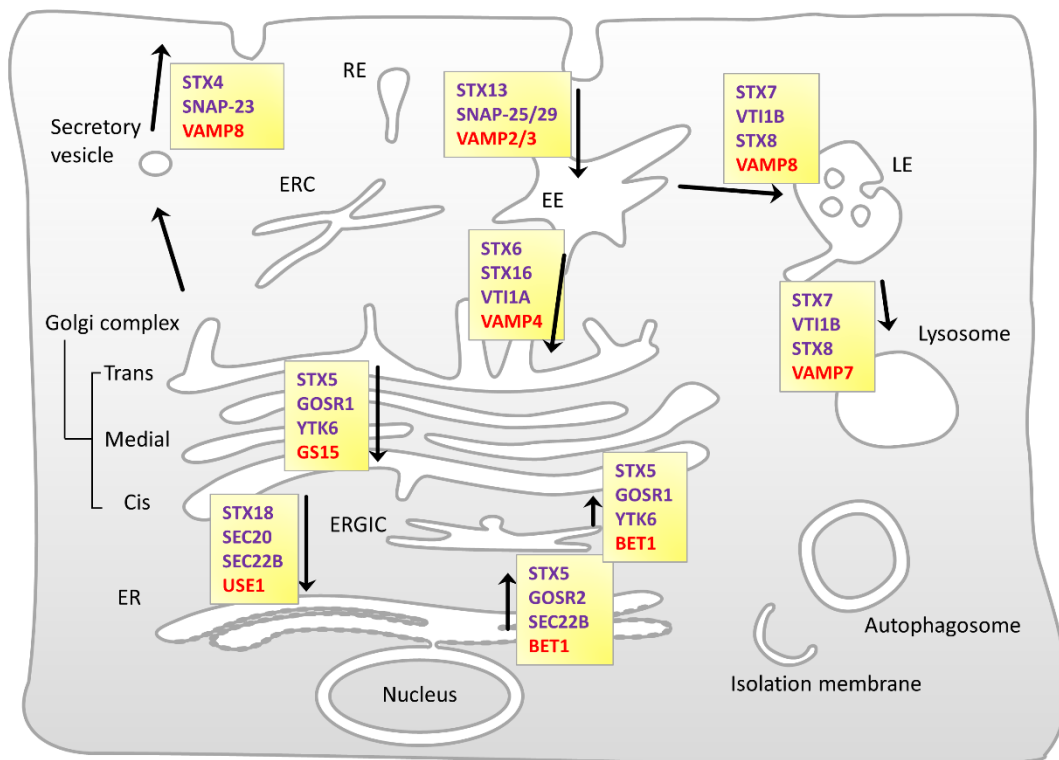
Figure 10: Overview of known mammalian SNARE complexes in intracellular trafficking. R (arginine)-SNAREs (soluble N-ethylmaleimide-sensitive factor attachment protein receptors) are indicated in red, Q (glutamine)-SNAREs in purple. EE (early endosome); LE (late endosome); RE (recycling endosome); ERC (endocytic recycling compartment); ER (endoplasmatic reticulum); ERGIC (ER-Golgi intermediate compartment); STX (syntaxin); VAMP (Vesicle-associated membrane protein). Figure adapted from [47].

SNARE assembly is an ordered process of continuous coiling that starts at the N-terminus of the SNARE motif and proceeds in a 'zipper-like' fashion towards their C-terminal membrane anchors. In this way the SNAREs form a tight, stable four-helix bundle which attaches the membranes together thereby generating energy to initiate fusion [85]. Tightening of the rigid linkers between the transmembrane domain and SNARE motifs transmits enough energy onto the membranes to overcome the repulsive electrostatic forces between them, which further bends the membranes and disrupts the lipid bilayer thereby forming a fusion stalk. This is followed by hemifusion, a state where the lipids of the proximal membrane leaflets interact, and eventually leads to the breakdown of the distal membrane leaflets, resulting the opening of the fusion pore (see Figure 11, [86,87]). Although other fusion models exist, this 'stalk hypothesis' was experimentally verified and is the most generally assumed model [88]. Finally, after fusion, SNARE complexes convert from a trans- to a cis-configuration, where all the SNAREs in the complex reside together in the resulting fused membrane. This cis-SNARE complex is disassembled by the actions of the ATPase NSF (N-ethylmaleimide-sensitive fusion protein) and its cofactor SNAP (soluble NSF attachment protein), resulting in the recycling of SNAREs for subsequent rounds of fusion [72].
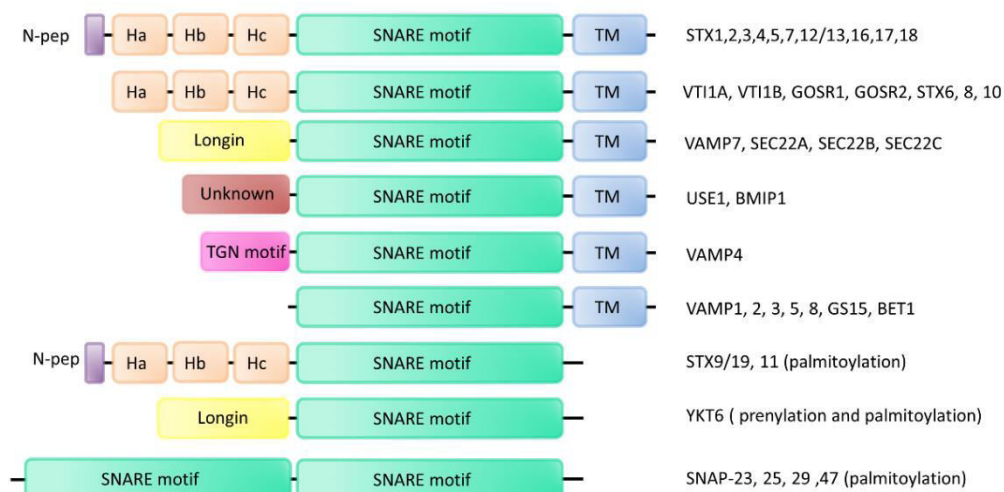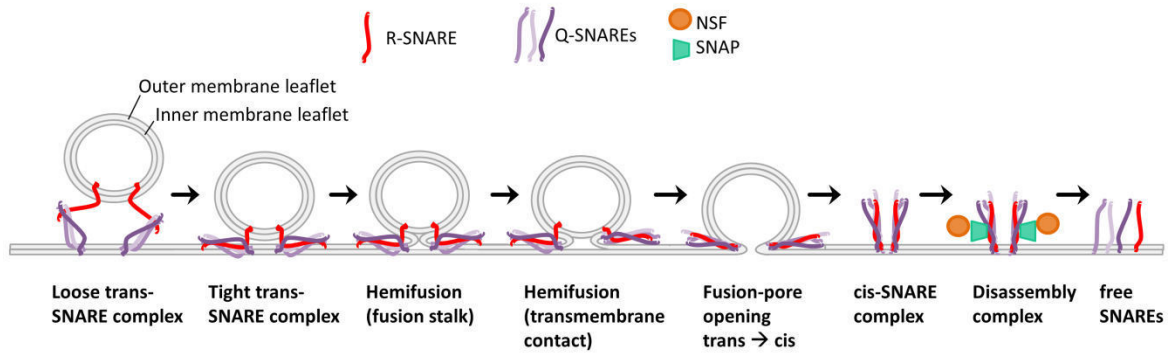
Figure 11: Schematic representation of SNARE (soluble N-ethylmaleimide-sensitive factor attachment protein receptor) assembly and stalk hypothesis. The vesicular R (arginine)-SNARE interacts with three Q (glutamine)-SNAREs on the acceptor membrane through the N-terminal end of the SNARE motifs, forming a four-helical trans-complex. This trans-complex progresses from a loose state, where only the N-terminal portions of the SNARE motifs are 'zipped up', into a tight state, where the zipping process towards the C-terminal membrane anchors is almost completed. This tightening transmits energy onto the membranes resulting in disruption of the outer membrane lipid bilayer thereby forming a fusion stalk. This is known as hemifusion, a state in which the outer membrane leaflets are already continuous, but no connection has formed. Hemifusion proceeds with interaction of the lipids from the inner membrane leaflet thereby disrupting them, resulting in the opening of a fusion pore. During fusion the trans-complex relaxes into a cis-configuration. These cis-complexes are disassembled by NSF (N-ethylmaleimide-sensitive fusion protein) and SNAP (soluble NSF attachment protein) proteins. Figure adapted from [88]*.*

1.2 Ubiquitination

Correct intracellular sorting of proteins also depends on ubiquitination, one of the most common PTMs. Direct ubiquitination, interaction with sorting factors that contain ubiquitin binding domains or deubiquitinating events regulate the itineraries of cargo and affect their localization, trafficking and abundance. Ubiquitin is a highly conserved 76 amino acid protein, characterized by a core β-grasp fold consisting of two α-helices and five β-sheets in a ββαββαβ arrangement. It is ubiquitously expressed in all eukaryotes and attaches covalently to a target protein during ubiquitination. Ubiquitination is a three-step process involving the actions of an activating (E1), conjugating (E2) and ligating (E3) enzyme (see Figure 12). During the initial step, ubiquitin is activated by the E1 enzyme in an ATP-dependent manner, resulting in a thioester bond between the C-terminal glycine of ubiquitin and the active site cysteine residue in the E1. Secondly, ubiquitin is transferred from the E1 to the cysteine residue of an E2 enzyme via a trans(thio)esterification reaction. Finally, an E3 ligase mediates the transfer of ubiquitin from the charged E2 to a lysine residue in the substrate resulting in an isopeptide bond between the carboxyl-terminal glycine in ubiquitin and the ε-amino group of lysine residues in the substrate [89]. To date, there are only few E1 enzymes identified in humans compared to the amount of E2 enzymes (~40) and E3 ligases (>600) of which the latter and largest group provides substrate specificity in the ubiquitination process [90]. E3 ligases can be classified in three types depending on the presence of characteristic domains and on the mechanism of ubiquitin transfer to the substrate proteins. The HECT (homologous to the E6AP carboxyl terminus) E3 ligases contain the HECT domain and catalyze ubiquitin transfer to the substrate protein in a two-step process. They first couple ubiquitin onto the catalytic cysteine in their HECT domain followed by

transfer to the substrate [91]. The RBR (RING-between-RING) E3 ligases similarly mediate ubiquitin transfer through this two-step reaction [92]. A third group, the RING (Really Interesting New Gene) E3 ligases comprise the largest family of E3 enzymes and have a characteristic RING domain that mediates the direct transfer of ubiquitin to the substrate. These E3 ligases thus act as a scaffold, binding both the E2 enzyme and the substrate protein [93].
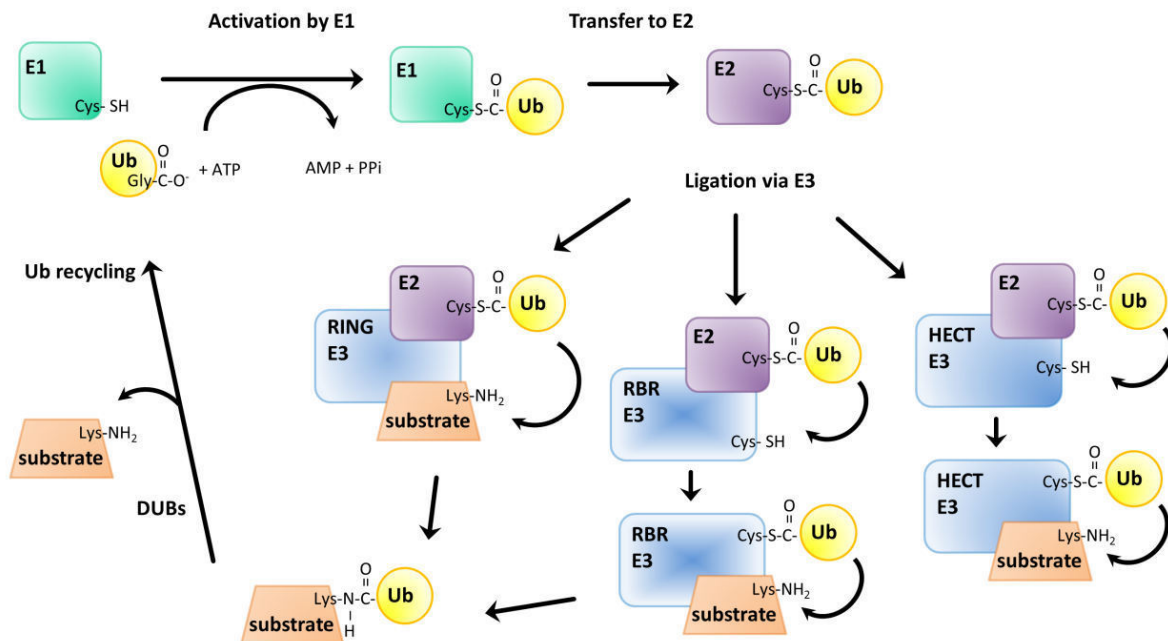

Figure 12: The ubiquitination cascade. The glycine residue at the C-terminus of ubiquitin is adenylated by E1, followed by attack of a cysteine side chain in E1, resulting in an E1-ubiquitin thioester intermediate. The activated ubiquitin is subsequently transferred to a cysteine residue in the active site of an E2 via a trans(thio)esterification reaction. Finally, an E3 ubiquitin ligase catalyzes the transfer of ubiquitin to the target substrate. RING E3s simultaneously bind the Ubl-E2 thioester complex and the substrate, and mediate the transfer of ubiquitin directly from the E2 to the lysine on the substrate. HECT E3s first transfer ubiquitin to a catalytic cysteine in the HECT E3 via trans(thio)esterification, followed by the transfer of the ubiquitin to the lysine on the substrate. The RBR E3s function like the HECT E3s and bind the Ubl-E2 thioester complex via their RING domain, followed by transfer of ubiquitin to a catalytic cysteine in their RING2 domain before transfer to the substate. In a last step, DUBs can remove ubiquitin from the substrate, thereby enabling recycling of ubiquitin. Figure adapted from [94].

Substrates can undergo monoubiquitination or polyubiquitination at one or more lysine residues. Ubiquitin itself has seven lysine residues (K6, K11, K27, K29, K33, K48 and K63), and all of these, also including the amino-terminal methionine of ubiquitin, can be used to assemble polyubiquitin chains of variable lengths [95]. Different chain linkages can lead to different functional outcomes. The most common are K48- and K63-polyubiquitin chains, with well characterized cellular functions. K48-linkages typically lead to proteasomal degradation, while K63 chains play a role in cell signaling, endocytosis and DNA damage repair [96]. The third most abundant linkage type, K11 chains, regulates both degradative and non-degradative pathways and has been implicated in different signaling pathways [97]. Not much is known for the other linkage types.

The formation of poly-ubiquitin chains can occur on the same lysine residue (homotypic chain linkages) or it can be a combination of different lysine linkages, resulting in mixed or branched

structures (heterotypic chain linkages). Next to this, ubiquitin itself can also undergo PTMs like phosphorylation, acetylation and SUMOylation, which further contributes to the complexity of the ubiquitin code and the fate of the different substrates [98–100]. Moreover, ubiquitin can be removed from substrates through the action of roughly 90 identified DUBs (deubiquitinating enzymes), which strictly control the ubiquitination process [101]. Altogether, ubiquitin constitutes a sorting tag which has extensive functions in the regulation of protein degradation, the ERAD (ER-associated degradation) pathway, DNA repair, endocytosis, apoptosis and autophagy (see 1.6; [90,100]).

Additionally, the ubiquitin β-grasp fold was found to be conserved in other proteins called Ubls (ubiquitin-like proteins), although they share little sequence identity [102]. These Ubls, including SUMO, NEDD8, ISG15, ATG8 (autophagy-related protein 8), ATG12, FUB1, FAT10, URM1, and UFM1, modify proteins by using a cascade reaction similar to that of the ubiquitin conjugation system. E1, E2 and E3 enzymes specific to each Ubl are utilized to covalent link the Ubl to a lysine in its substrate. Next to this, the Ubls also require isopeptidases, or UPLs (Ubl-specific proteases), that have a dual function. One the one hand they process Ubl precursors by removing the C-terminal residues thereby exposing the Gly-Gly motif necessary for conjugation. On the other hand, analogous to DUBs for ubiquitin, they remove Ubls from their modified targets [94]. The Ubl-modified proteins are involved in cellular functions such as DNA replication and repair, intracellular trafficking, cell cycle progression, immune response, autophagy and apoptosis [103].

1.3 The secretory pathway

As mentioned before, the biosynthetic secretory pathway transports soluble and transmembrane proteins and lipids through a series of organelles and delivers them to their proper destination, either in or outside the cell. Soluble proteins can be secreted in a constitutive manner or in a regulated way, upon different neural or hormonal stimuli. The secretory organelles, consisting of the rough ER, ER exit sites, ERGIC (ER- to Golgi intermediate compartment) and the Golgi complex each have a distinct organization and structure and provide a proper environment for protein folding and protein modification, which includes the addition of sugars and lipids [104–106]. Proteins require an ER signal sequence, generally at the N-terminus, to enter the ER during or after translation. Here, proteins are subjected to quality control by molecular chaperones that ensure proper folding and assembly [107]. Misfolded and excess proteins are ubiquitinated and targeted to the ERAD pathway that delivers the ubiquitinated proteins via retrotranslocation back to the cytosol resulting in proteasomal degradation [108]. Properly folded proteins are packaged in COPII-coated vesicles and leave the ER at the ER exit sites followed by transportation to the cis Golgi cisternae. The Golgi complex is defined by cis-, medial- and trans-cisternae, each containing different protein-modifying enzymes. To date, there are three different models explaining cargo movement between these Golgi cisternae and future experiments are needed to reach a consensus. The vesicular transport model stated that COPI-coated vesicles bud from a donor compartment and fuse with an acceptor compartment. In this way they are involved in the anterograde and retrograde transport of cargo and resident proteins (glycosylation enzymes), respectively, between the Golgi cisternae. In contrast, the cisternal maturation model suggests that the Golgi is a dynamic organelle in which Golgi cisternae mature with the cargo inside by fusing with retrograde vesicles coming from more mature cisternae and by producing retrograde vesicles that fuse with younger cisternae. The cargo progresses as a

result of maturation of an earlier compartment into a later one. Finally, the rapid partitioning model assumes that the Golgi cisternae are continuous, in which cargo as well as resident proteins and lipids travel bidirectionally between the different cisternae [109,110]. In the last step of the secretory pathway, the secretory vesicles, usually CCVs, detach from the trans-Golgi and fuse with the PM, EE or LE to deliver their proteins and lipid cargo.

The cells can also secrete proteins via other, unconventional pathways involving vesicles such as apoptotic bodies (50-500nm), released by cells undergoing apoptosis; microvesicles (>100nm) budding directly from the plasma membrane and exosomes (~30-100nm), derived from the intraluminal vesicles in the LE. Although both contain miRNA and mRNA, microvesicles and exosomes vary in their protein composition, morphology and density ([111,112]; exosomes are further discussed in 1.5.1).

1.4 The endocytic pathway

Cells internalize macromolecules and membrane proteins such as receptors, channels and transporters from the PM during endocytosis. In this way, endocytosis regulates many processes ranging from nutrient uptake, antigen presentation, receptor signaling and downregulation, to fundamental cellular programs including polarization, migration, differentiation, adhesion and mitosis [113]. On the downside, many pathogens and toxins hijack the endocytic pathway to gain access into the cell [114,115]. Next to the well-known clathrin dependent endocytic pathway, many other clathrin-independent routes exist including the caveolae-dependent, ARF6-dependent, Flotillin-dependent, CLIC/GEEC (clathrin-independent carriers/GPI-anchored protein enriched compartments), IL2Rβ (interleukin 2 receptor β) and FEME (fast endophilin-mediated endocytosis) pathway, phagocytosis and macropinocytosis (Overview in Table 4 and Figure 13).
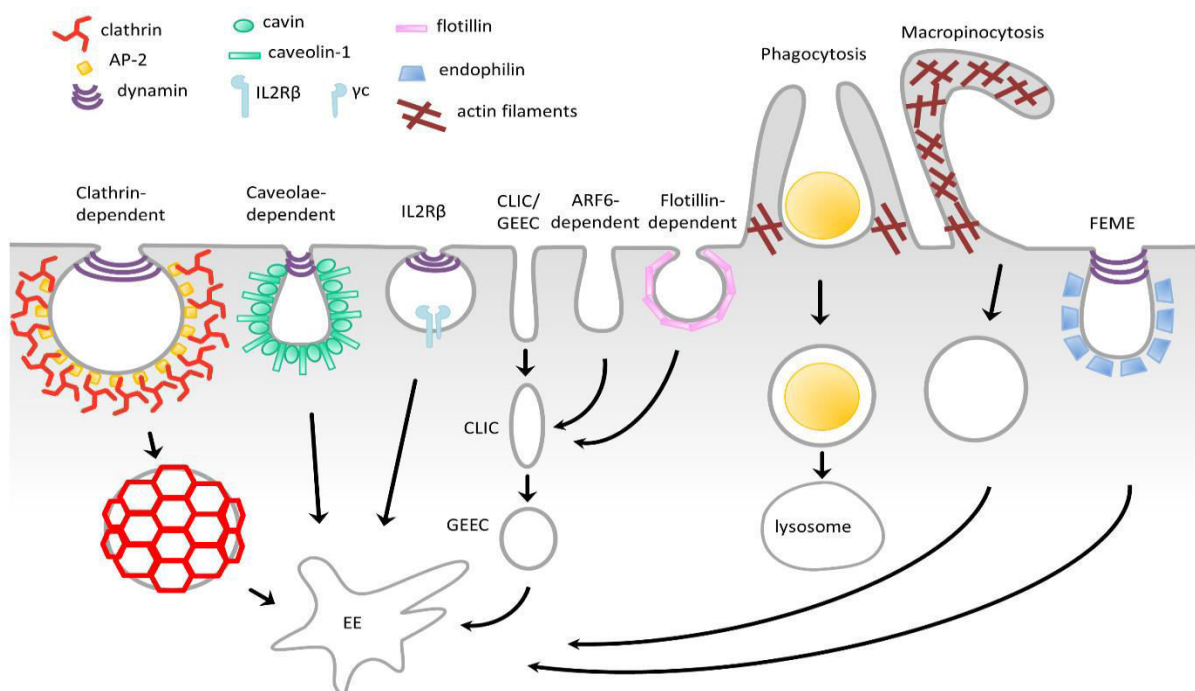
1.4.1 Clathrin-dependent endocytosis

CME (clathrin-mediated endocytosis) is the best characterized endocytic pathway. In this pathway, adaptor protein AP-2 is recruited to the PI(4,5)P2 enriched regions of the PM with the help of other scaffolding proteins such as FCHO, EPS15 and intersectin, and selects cargo by recognizing distinct sorting signals present in their cytoplasmic tail [119]. AP-2 simultaneously binds cargo and clathrin, thereby coupling cargo capture with clathrin coat assembly [119–121]. The clathrin triskelions polymerize into hexagons and pentagons to form the clathrin coat around the growing pit. Maturation of the resulting CCP (clathrin coated pit) is driven by clathrin polymerization and other BAR (Bin-Amphiphysin-Rvs) domain-containing proteins such as amphiphysin, endophilin, and sorting nexin 9, which are known to generate membrane curvature [122]. These latter proteins subsequently recruit dynamin resulting in membrane scission and release of the CCV into the cell, followed by HSC70- and auxilin-mediated uncoating and fusion with the EE (see 1.1.1; [123,124]). Next to AP-2, other cargo-specific adaptors such as β-arrestin, AP180, epsin, HIP1 and NUMB are involved in CME. These adaptors recognize alternative motifs, including ubiquitinated and phosphorylated cargo, and are able to bind AP-2 and as such recruit different receptors to the AP-2 hub [124,125]. This diversity of adaptor proteins reflects the broad range of cargo such as RTKs (receptor tyrosine kinases), GPCR (G-protein coupled receptors), LDLR (low-density lipoprotein receptor) and the TfR (transferrin receptor) undergoing CME. There seems to be a redundancy in the sorting of cargo in CCP/CCV, as in the absence of one adaptor, other adaptors with lower-affinity interaction for the cargo are able to recruit the CME machinery. CCV have been shown to contain more than one type of cargo, however, it is not clear whether sorting of cargo already occurs in CCV or in sorting endosomes. Since multiple receptors are endocytosed in the same cell, it is possible that the specific adaptor proteins recognizing different motifs are responsible for clustering cargo into distinct CCP/CCV, ensuring cargo-dependent vesicle trafficking towards their appropriate intracellular destination [123].

1.4.2 Clathrin-independent endocytosis

Next to CME, several other clathrin-independent endocytic pathways exist, involving different protein machinery. Caveolae-mediated endocytosis is the second best studied endocytic pathway, in which caveolae represent specialized lipid rafts, enriched in cholesterol and sphingolipids that form flask- or omega-shaped invaginations of the PM [126]. Similarly to CME, dynamin is required to pinch off caveolae. The main structural component of caveolae is caveolin-1, a small integral membrane protein capable of binding cholesterol and fatty acids. Caveolin-1 assembles with cavins, which are cytosolic coat proteins, to form caveolae [127]. As caveolin-1 binds fatty acids, it is able to endocytose GPI (glycosylphosphatidylinositol)-linked proteins, glycosphingolipid GM1 together with its ligand CTxB (Cholera toxin B subunit) and ganglioside receptors for SV40 (simian virus 40) virions

[128–130]. Several kinases and phosphatases have been shown to regulate caveolae-dependent endocytosis, but the specific coordination is still unclear. In addition to its role in endocytosis, caveolae regulate lipid metabolism and play a role in sensing cell surface tension. Furthermore, caveolae may act as signaling platforms since many signaling proteins have been found to associate with and were regulated by caveolae [131].

Another dynamin-dependent, cholesterol sensitive endocytic pathway is the IL-2Rβ (interleukin 2 receptor β) route [132]. IL2 activates a PI(3,4,5)P3 signaling cascade that in turn sequentially activates the GTPases RHOA and RAC1 [133]. The downstream RAC1 target PAK1 (p21-activated kinase 1) subsequently phosphorylates cortactin and promotes its interaction with N-WASP (neuronal Wiskott-Aldrich syndrome protein) which assemble into a complex that mediates actin polymerization during endocytosis [134]. Next to the IL-2R, this pathway also internalizes several other receptor complexes that contain the common cytokine receptor gamma chain via these small non-coated invaginations [135].

Besides caveolin-dependent endocytosis, GPI-linked proteins are also endocytosed via a dynamin-independent route which is mediated by non-coated tubulovesicular carriers called CLICs (clathrin-independent carriers). These CLICs are directly derived from the PM and mature into tubular early endocytic compartments called GEECs (GPI-anchored protein enriched compartments). Apart from GPI-linked proteins, this CLIC/GEEC pathway also accommodates the endocytosis of CTxB as well as the constitutive uptake of bulk fluid and membrane [123,136]. The CLIC/GEEC pathway is controlled by the cholesterol-sensitive GTPase CDC42. Cycling between the GTP-bound active and GDP-bound inactive state of CDC42 is required for the recruitment of the actin polymerization machinery. The regulation of CDC42 itself is achieved by the concerted actions of the GTPases ARF1 and two GAPs, GRAF1 and GRAF2 [137–139].

An alternate dynamin-independent pathway relying on the cycling state of a GTPase is the ARF6-dependent endocytic pathway [140]. A wide variety of cargo have been identified for this pathway including GLUT1 (glucose transporter 1), MHC (major histocompatibility complex) I and II proteins, and GPI-anchored proteins CD55 and CD59 [141–144]. ARF6 activates PIP5K (phosphatidylinositol-4-phosphate 5-kinase) to produce PI(4,5)P2, thereby stimulating actin polymerization. In most cases, activated ARF6 is not required for endocytosis but instead regulates the recycling from this pathway through the activation of PLD (phospholipase D) which generates PA (phosphatidic acid) [145–147]. Since CME also requires PI(4,5)P2, ARF6 can also affect CME [148]. The ARF6-dependent and CLIC/GEEC pathways seem to internalize similar cargo and although they are considered as separate pathways, it is possible that these entry routes share a similar mechanism, but this however, remains uncertain [117,123].

Flotillin proteins are found in distinct membrane microdomains and their homology to caveolin1 implies an analogous manner of PM lipid ordering to that found in caveolae [149]. This flotillin-dependent endocytic pathway represents another dynamin-independent route that internalizes CTxB, GPI-linked CD59 and cell surface proteoglycans [149–151]. Flotillin can act as a pathway upstream of CLIC/GEEC as it was also found to be concentrated in the membranes of early CLIC/GEEC intermediates [139].

In contrast to the small-scale endocytic processes, macropinocytosis and phagocytosis represent two large-scale clathrin-independent internalization routes, where the former is responsible for fluid uptake and the latter internalizes large particles. These pathways are triggered by and dependent on actin-mediated remodeling of the PM. Macrophages, monocytes and neutrophils are well-known phagocytic cells that depend on small GTPases for the uptake of particles. CDC42, RHOA and RAC1 are necessary to form extensions around the particle and recruit N-WASP and actin to further induce phagocytosis [152]. Amphiphysin 1, a BAR domain containing protein usually associated with CME, also appears to be important for phagocytosis [153]. On the other hand, macropinocytosis requires the kinase PAK1 to bind and activate the GTPase RAC1. Next to this, macropinoctosis also depends on the actions of PI3K (Phosphatidylinositol-3-kinase), SRC and RAS [154–156]. Cortactin and dynamin together with several kinases and adhesion molecules are implied in the formation of membrane ruffles giving rise to macropinosomes and evidence shows that the EGF receptor can also be internalized via this pathway [157,158].

Since CME is relatively slow in internalizing proteins, the cell is in need of some fast endocytic pathways to respond to certain physiological stimuli. Next to macropinocytosis, FEME represents a process that rapidly removes receptors and proteins from the cell surface in a not-constitutively active way. In the FEME pathway, the BAR-containing protein endophilin mediates membrane deformation. The resulting tubulovesicular structures lack clathrin, but depend on dynamin and actin polymerization to induce membrane scission. FEME further relies on Rac and Rho GTPases, and the PI3K and PAK1 kinases [159]. Endophilin directly or indirectly associates with many activated GPCRs and RTKs leading to their rapid internalization, also Shiga and Cholera toxins were found to hijack this pathway [160].

Table 4: Overview of the different endocytic pathways.

Endocytic pathway	Morphology	Coat or coat like	Dynamin-dependent	Small GTPase involved	Cargoes	Other associated/ regulatory proteins
clathrin-mediated	vesicular; 150-200nm	clathrin	yes	RAB5, ARF6 implicated	RTKs, GPCRs, TfR, LDLR, toxins, pathogens	AP-2, epsin, EPS15, actin, synaptojanin, amphiphysin, endophilin
caveolae-dependent	vesicular/ tubulovesicular; 50-120nm	caveolin-1, cavin	yes	unclear (caveolins may regulate CDC42 activity)	CTxB, SV40, GPI-linked proteins, TGF-βR, IGF-1R	SRC, PKC, actin (many singaling proteins localize to these sites)
IL2Rβ	vesicular; 50-100nm	none	yes	RHOA, RAC1	IL-2Rβ, γc-cytokine receptor	PAK1, PAK2, N-WASP, cortactin
CLIC/GEEC	tubular/ ring-like	none	no	CDC42, ARF1	fluid phase markers, bulk membrane, CtxB, GPI-linked proteins	actin, GRAF1, GRAF2 and other GRAFs

ARF6-dependent	vesicular/ tubular	none	no	ARF6	MHCI, MHCII, CD55, CD59, GLUT1	unclear
flotillin-dependent	vesicular	flotillin-1 and 2	no	unclear	CTxB, CD59, proteoglycans	unclear
phagocytosis	cargo-shaped; > 500nm	none	no	ARF6, CDC42, RAC1, RHOA (depending on type)	pathogens, apoptotic cells	actin, PI3K, amphiphysin, Rho kinase, adhesion proteins, WASP
macro-pinocytosis	ruffled; 0.2-10µm	none	in some cases	ARF6, CDC42, RAC1, RAB5	fluid phase markers, RTKs	actin, cortactin, PAK1, PI3K, RAS, SRC, HDAC6
FEME	tubulovesicular; < 1µm	endophilin	yes	RHOA, RAC1	RTKs, GPCRs, toxins	actin, PI3K

IL2Rβ (interleukin 2 receptor β); CLIC/GEEC (clathrin-independent carriers/GPI-anchored protein enriched compartments); ARF6 (ADP ribosylation factor 6); FEME (fast endophilin-mediated endocytosis); RTKs (receptor tyrosine kinases); GPRC (G-protein coupled receptor); TfR (transferrin receptor); LDLR (low-density lipoprotein receptor); AP-2 (adaptor protein-2); CTxB (Cholera toxin B subunit); SV40 (simian virus 40); GPI (glycosylphosphatidylinositol); TGFβR (transforming growth factor β receptor); IGF-1R (insulin-like growth factor-1 receptor); N-WASP (neural Wiskott-Aldrich syndrome protein); RAC1 (Ras-related C3 botulinum toxin substrate 1); RHOA (Ras homolog gene family member A); GRAF1/2 (GTPase regulator associated with focal adhesion kinase-1/2); MHC I/II (major histocompatibility complex I/II); GLUT1 (glucose transporter 1); PI3K (phosphatidylinositol-3-kinase); PKC (protein kinase C); IL-2Rβ (interleukin 2 receptor β); γc (γ common chain); HDAC6 (histone deacetylase 6). CDC42 (Cell division control protein 42). Table adapted from [113,123].

1.4.3 Endocytosis and signaling

Endocytosis regulates signaling by internalizing and trafficking receptors and their associated signaling molecules. Vice versa, the activation of receptors or downstream effectors can also stimulate receptor endocytosis. Endocytosis controls the number of receptors at the PM available for activation and limits the signaling intensities. Moreover, it also regulates the fate of signaling molecules by routing them towards degradation or recycling pathways. Signaling however is not confined to the PM, and endocytosis can contribute actively to signaling. During this endocytic transport, cargo can undergo several PTMs, including (de)-phosphorylation and ubiquitination, which can influence the signaling cascade [161]. After internalization, cargo's reach the EEs which serve as key sorting stations. These endosomes also function as signaling platforms that regulate signaling complexes containing receptors, signaling enzymes and effectors in a spatial and temporal manner [162,163]. CME and clathrin-independent endocytosis can directly control the biological outcome of signaling. This is exemplified by the EGFR where CME is associated with receptor recycling and sustains signaling while clathrin-independent endocytosis leads to receptor degradation and signal termination [164]. In addition, EGFR signaling is tightly regulated by the concentration of ligand to avoid overstimulation. The EGFR is primarily internalized via CME at low doses of EGF, which results in the recycling of internalized receptors back to the PM to maintain MAPK/ERK signaling necessary for cell proliferation. High doses of EGF trigger EGFR internalization by fast clathrin-independent

pathways which rapidly remove EGFR from the PM and routes them towards the lysosomes for degradation. This protects the cell from excessive EGFR signaling and anti-apoptotic responses which are generally observed during tumorigeneses [165].

1.5 Post-endocytic trafficking

As previously mentioned, after internalization cargo enters the EEs where they are sorted towards the lysosomes for degradation, sent to the TGN via retrograde transport or recycled back to the PM. Cargo traffic and sorting is achieved through a tight spatial and temporal control of early, late and recycling endosomes which all display a unique identity depending on their luminal pH, PIP (phosphatidylinositol phospholipid) composition and RAB GTPase content. However, these endosomes represent a dynamic network in which molecules and cargoes are actively exchanged [118]. Endosomes are enriched in specific PIPs, which originate from phosphatidylinositol, synthesized in the ER and subsequently delivered to the endosomal compartments. Different lipid kinases and phosphatases regulate the reversible (de-)phosphorylation at the 3, 4 and 5 position of the inositol ring [166]. During trafficking, proteins containing FVFE and PX (phox homology) domains primarily bind PI(3)P (phosphatidylinositol (3)-phosphate) present on EEs and ILVs (intraluminal vesicles), while proteins with a PH (pleckstrin homology) domain interacts with either PI(4)P, PI(4,5)P2, PI(3,4)P2 or PI(3,4,5)P3 [167]. PIPs can recruit activators and inactivators of RAB proteins and conversely, PIP kinases and phosphatases have been found to be RAB effectors. In this way, PIPs and RABs closely coordinate membrane identity [19,168].

1.5.1 Lysosomal degradation

As EEs mature into LEs, their lumens acidify through the actions of a v-type vacuolar H+ ATPase which functions as a proton pump [169]. The acidification of EEs, LEs and lysosomes is important for receptor-ligand uncoupling, lysosomal enzyme activity and transport [170]. The switch from EE to LE is also driven by the conversion from RAB5 and PI(3)P to RAB7 and PI(3,5)P2 [171]. This is accompanied by the replacement of the tethering complex CORVET by HOPS along with the concomitant SNARE proteins further determining membrane fusion specificity [172]. Activated signaling receptors and other proteins destined for degradation are sorted into ILVs (intraluminal vesicles), which protrude from the limiting (inner) membrane from endosomes towards the lumen. Vacuolar regions containing ILVs detach, or mature, from the EEs and form MVBs (multivesicular bodies) that eventually fuse with the LEs. The term MVBs is under debate, since some refer to this as transport intermediates between EEs and LEs, while others consider MVBs to be an alternative name for LEs [173]. These LEs function as a second sorting station in the endosomal system. When these LEs fuse with lysosomes they target their cargo for degradation, next to this, LE that fuse with the PM result in the release of ILVs as exosomes (see below, [174]). Moreover, certain cargo like the M6PR (mannose-6-phosphate receptor) undergoes retrograde traffic from the LE back to the TGN [175].

The ESCRT (endosomal sorting complexes required for transport) machinery forms a key mediator for ILV biogenesis and cargo sorting into ILVs. This highly conserved ESCRT machinery comprises five protein complexes; ESCRT-0, -I, -II, -III and the VPS4 ATPase complex, that are sequentially recruited to the membrane (see Figure 14 and Table 5 for ESCRT complexes and their subunits). The sorting of K63-linked polyubiquitinated cargo into ILVs is initiated by PI(3)P, which is generated by the RAB5 effector VPS34, a PI(3)K [176]. The FYVE domain containing HRS subunit of the ESCRT-0 complex is hereby recruited to the EE and binds ubiquitinated cargo. The other ESCRT-0 subunit STAM (Signal

transducing adapter molecule), as well as ESCRT-I subunits TSG101 (Tumor susceptibility gene 101) and ESCRT-II subunit EAP45 also interact with ubiquitinated cargo via their respective ubiquitin binding domains. Next, ESCRT-0 recruits ESCRT-I, which further aids the cargo sorting process and delivers them to the ESCRT-II complex. ESCRT-I together with ESCRT-II is capable of inducing membranes to bud into the lumen and stabilize the bud neck of the growing vesicle. The EAP20 subunit of ESCRT-II interacts with the CHMP6 (charged multivesicular body protein 6) subunit of ESCRT-III and converts it into an active nucleator for ESCRT-III assembly on endosomes. The CHMP4 subunit of ESCRT-III then forms multimeric filaments organized in spirals that bend the endosomal membrane away from the cytoplasm to form invaginated buds. The ESCRT-III complex further recruits the DUBs USP8 (Ubiquitin-specific protease 8) and AMSH (associated molecule with the SH3 domain of STAM), which remove ubiquitin from the cargoes present in the ILVs. Finally, the VPS4 ATPase complex binds and unfolds the ESCRT-III complex which eventually results in ILV budding [177–180]. Additionally, The ESCRT machinery is known to have other functions, ranging from HIV viral budding and autophagy to cytokinesis [181–183].
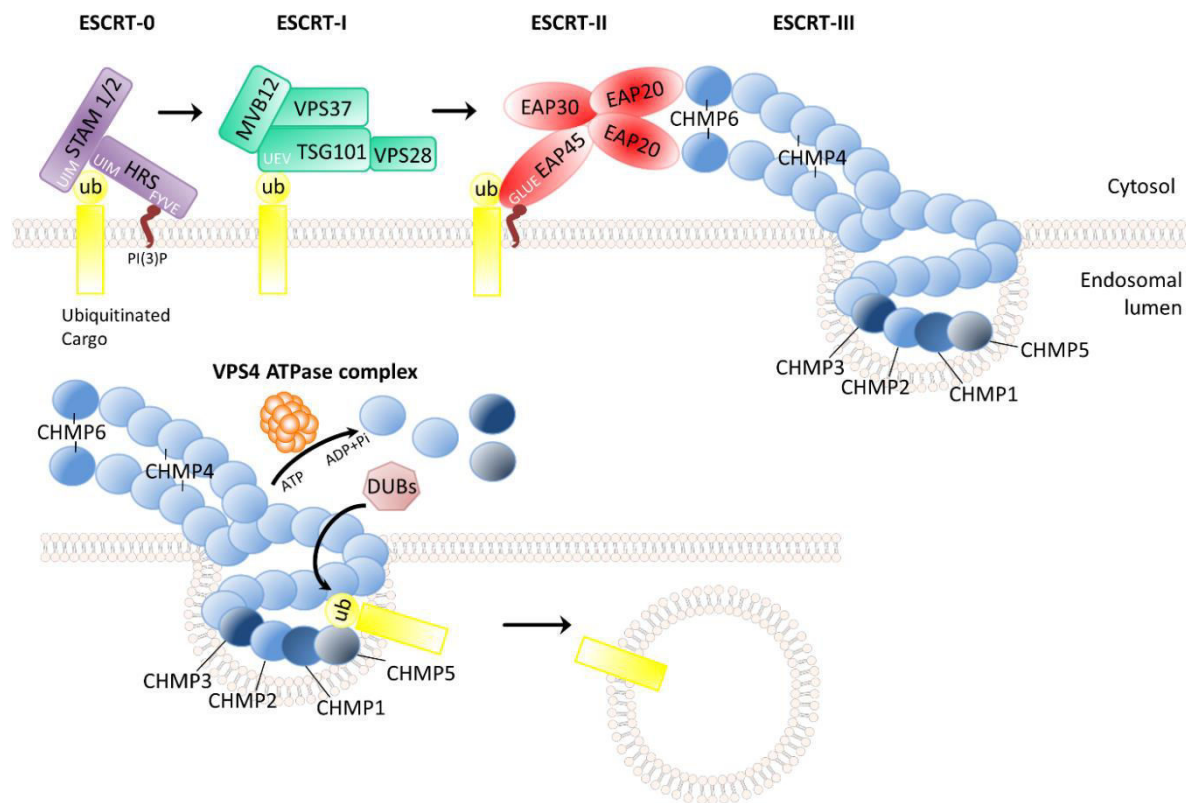
Figure 14: Schematic representation of the ESCRT (endosomal sorting complexes required for transport) machinery involved in ILV (intraluminal vesicle) biogenesis and cargo sorting. The ESCRT-0 subunit HRS (hepatocyte growth factor receptor tyrosine kinase substrate) is recruited to the endosomal membrane via its PI(3)P-binding FYVE (FAB1, YOTB, VAC1 and EEA1) domain. Polyubiquitinated cargo is recognized by the UIM (ubiquitin-interacting motif) domains of HRS and STAM (signal transducing adapter molecule), the second ESCRT-0 subunit. ESCRT-0 recruits ESCRT-I, where TSG101 (Tumor susceptibility gene 101) is also capable of interacting with ubiquitinated cargo via its UEV (ubiquitin E2 variant) domain. Next, the cargo is delivered to the ESCRT-II complex, where the EAP45 subunit interacts with both PI(3)P and ubiquitin via its GLUE (GRAM-like ubiquitin-binding in EAP45) domain. The ESCRT-III complex orchestrates the last steps in the ILV biogenesis. ESCRT-III is recruited via its CHMP6 (charged multivesicular body protein 6) subunit by EAP20, which further activates and initiates ESCRT-III filament assembly by recruiting CHMP4. Together with CHMP1, 2, 3 and 5,

CHMP4 forms membrane-bound filament spirals around the invagination. The ESCRT-III complex also recruits DUBs, like USP8 and AMSH, which deubiquitinate cargo prior to fission and budding. Ultimately, the ESCRT-III complex is disassembled by the VPS4 ATPase complex which also drives membrane constriction and fission. Ub (ubiquitin). Figure adapted from [178]*.*

In contrast to their physical properties and ultrastructure, the molecular distinction between LEs and lysosomes is not clearly delineated. Almost all proteins, including the main membrane constituents LAMP1 (lysosomal-associated membrane protein 1) and LAMP2, are present in both LEs as in lysosomes [171]. LBPA (phospholipid lysobisphosphatidic acid) however, is a specific LE phospholipid and has the intrinsic capacity to deform membranes. Together with the ESCRT-associated protein ALIX, LBPA plays a role during ILV formation within LEs [184–186]. Furthermore, evidence shows that LEs and lysosomes also function as signaling organelles. For instance, membrane contacts between MVB and the ER allows the ER-resident phosphatase PTB1B to dephosphorylate activated EGFR (epidermal growth factor receptor) present in the MVB, and promotes sequestration of EGFR onto the ILVs [187]. Additionally, cholesterol, an essential lipid that plays important roles in membrane composition and other cellular processes such as steroidogenesis and signal transduction, reaches the LEs and lysosomes via the endocytosed LDL receptor. Here, it is released after cholesterylester hydrolysis and is further transported to the PM, ER and mitochondria to fulfill its function [188]. Cholesterol also activates mTORC1 (mammalian target of rapamycin complex 1), present on LE and lysosomes [189]. mTORC1 is a key regulator of cell growth, metabolism and autophagy by functioning as a sensor for nutrients, energy and stress signals (see 1.6; [190]).

As mentioned above, LEs can either fuse with the lysosome for degradation or with the plasma membrane to release exosomes into the extracellular space. Exosomes are secreted in a constitutive or stimulus-dependent way, by various cell types such as hematopoietic, epithelial, neural and tumor cells [111]. As such they mediate intercellular communication in several biological processes which is accomplished through different mechanisms of interaction with their target cells. Exosomes can directly interact with receptors on these target cells thereby activating intracellular signaling pathways. Next to this, exosomes can fuse with the plasma membrane and deliver their content into the cytosol, or they are fully internalized via endocytic pathways [191]. Exosomes generally contain proteins and lipids involved in ILV biogenesis (ALIX, LBPA, TSG101), membrane transport and fusion (RAB GTPase, SNAREs, annexins, and flotillins) and proteins associated with lipid microdomains (integrins and tetraspanins) [111]. Next to this, many exosomes contain MHC I and II molecules thereby modulating the immune response. Exosomes derived from pathogen-infected or tumor cells can act as antigen presenting vesicles and activate T-cells when the MHC peptide directly interacts with its cognate T-cell receptor. On the other hand, exosomes can be engulfed and processed by antigen presenting cells and as such result in T-cell activation [111]. Additionally, exosomes are involved in the pathology of neurodegenerative diseases as they carry cargo such as Aβ, α-synuclein, tau and prions [192]. Most interesting, exosomes also contain mRNA and miRNA, which were found to have a tumor promoting effect [193,194]. These exosomal miRNAs can be used as non-invasive diagnostic biomarkers as they differ in amount and composition between healthy and sick individuals, and are stably present in body fluids such as blood, urine, saliva and cerebrospinal fluid. Moreover, exosomes have distinct surface proteins that reflect their tissue or cell origin. Next to this, exosomes can be exploited as drug delivery vectors to transfer exogenous miRNAs into cells for gene therapy since they are composed of cell membranes and hold great promise to cross the blood-brain barrier [195].

Table 5: Overview ESCRT complex.

Complex	Subunits	Function
ESCRT-0	HRS, STAM1/2	Cargo recognition
ESCRT-I	TSG101, VPS37A/B/C/D, MVB12A/B, VPS28	Upstream adaptor
ESCRT-II	EAP45, EAP30, EAP20	Bridging adaptor
ESCRT-III	CHMP1A/B , CHMP2A/B, CHMP3, CHMP4A/B/C, CHMP5, CHMP6	Membrane remodelling/filament
VPS4 ATPase	VPS4A/B, VTA1	Membrane remodelling/ATPase
ALIX	/	Interacts with ESCRT-I and ESCRT-III. Involved in ILV biogenesis.

ESCRT (endosomal sorting complexes required for transport); HRS (hepatocyte growth factor receptor tyrosine kinase substrate); STAM (signal transducing adapter molecule); TSG101 (Tumor susceptibility gene 101); VPS (vacuolar protein sorting); CHMP (charged multivesicular body protein); ILV (intraluminal vesicle).

1.5.2 Recycling

The recycling pathway is crucial for maintaining cell homeostasis and returns unbound receptors, which underwent low pH-mediated ligand dissociation, back to the cell surface. Cargo can undergo recycling to the PM by a direct route from the EEs, also called fast recycling, or through a slow, indirect route via the REs. Recycling thereby plays a role in various processes such as cytokinesis, cell adhesion and morphogenesis, cell fusion and polarity [196]. The TfR and LDL receptor respectively carrying iron and cholesterol are often seen as classic recycling cargo internalized via CDE that undergo constitutive recycling back to the cell surface, while other cargo, such as signaling receptors, often require specific cytoplasmic sequences for recognition and sorting into REs. The recycling process is mediated by RAB and ARF GTPases and their effectors together with EHD (EPS15 homology domain) proteins which are involved in scaffolding, membrane tubulating and fission processes. The fast recycling route carries cargo such as the TfR and glycosphingolipids back to the PM. This pathway is mediated by RAB4 and RAB35 [32,34]. The slow recycling route traffics cargo from the EE via the ERC (endocytic recycling compartment), from which REs emerge, to the PM. The ERC is a collection of tubular organelles, emanating from the EEs that is often localized centrally, near the microtubule organizing center and Golgi complex and is molecularly characterized by the presence of RAB11 and/or EHD1 [147,196,197]. There are several recycling pathways from the ERC back to the cell surface, all mediated by RAB11. This was seen via the TfR which, next to undergoing fast recycling, was found to be recycled back via RE that were different from tubular RE carrying clathrin-independent endocytosed cargo back to the PM. This latter pathway was additionally found to depend on RAB22 as well as ARF6 and actin [198]. As mentioned above (see 1.4.2), ARF6 activates PLD present on the RE and PIP5K thereby respectively generating PA and PI(4,5)P2. Both products are important for recycling functions and recruit several proteins involved in vesicle formation, fusion and actin polymerization [145,146,199]. ARF6 also promotes recycling of cargo by interacting with and recruiting the exocyst complex [200], and regulates the direction of transport along microtubules by interacting with and controlling JIP (c-Jun N-terminal interacting kinase) 3 and JIP4 binding to motor proteins kinesin and dynein [201]. REs are also implicated in TLR4 and Delta-Notch signaling events. RAB11 was found to be involved in recruiting TLR4 from the ERC to phagosomes thereby controlling IRF3 (interferon regulatory factor-3) activation and IFN-β (interferon-β) production [202]. RAB11-positive REs also recycle activated Delta back to the PM, and in this way regulate the availability of ligand for the Notch receptor [203].

1.5.3   Retrograde transport

Next to the recycling pathway, retrograde transport represents a second major pathway that diverts cargo away from lysosomal degradation. Retrograde trafficking is involved in the retrieval of sorting receptors, processing proteases, SNAREs, lipids and other molecules from the PM or endosomes back to the TGN. Accordingly, the TGN herein represents a major sorting hub that connects the secretory pathway to the endo-lysosomal system. This pathway has a crucial role in development and nutrient homeostasis and aberrant retrograde traffic results in various pathogenesis such as Alzheimer's and Parkinson's disease and lysosomal storage disorders. Similarly to other trafficking routes, the retrograde machinery relies on the cooperation of different GTPases, coat proteins, tethering factors and SNAREs [204]. Two retrograde trafficking pathways emerge from the tubular endosomal network, one that sorts cargo from the EE and/or RE to the TGN and another that transports cargo from the LE to the TGN. The TGN resident protein TGN46 (TGN38 in yeast) and the endopeptidase furin, both cycling between the Golgi, endosomes and PM, use these different pathways and traffic respectively via the EE/RE and the LE back to the Golgi network [205–207]. The former EE/RE pathway is also hijacked by several bacterial and plant toxins such as cholera toxin, Shiga toxin and ricin, to reach the Golgi and ER and eventually the cytosol, where they exert their cytotoxic effects [208,209]. Another well-known protein that utilizes retrograde traffic is the CI-M6PR (cation-independent M6PR) which, at steady state, cycles between the Golgi, PM and LEs. The M6PR binds newly synthesized lysosomal hydrolases that are modified in the Golgi network with a M6P and transports them towards the endosomes where the acidic environment contributes to their release. The hydrolases traffic further to the lysosomes where they accumulate and become active, while the M6PR is retrieved back to the TGN. Abnormal M6PR trafficking results in the secretion of lysosomal hydrolases into the extracellular space and gives rise to dysfunctional lysosomes [210]. This CI-M6PR uses both retrograde traffic pathways to reach the Golgi network, where the EE/RE to Golgi traffic depends on the retromer complex, while the LE to Golgi transport follows a RAB9/TIP47 (tail-interacting protein of 47 kD)-dependent pathway [211–213].

The retromer is a multiprotein complex, whose subunits recognize retrograde cargo, promote sorting into the tubular endosomal network and stimulate microtubule-dependent transport of cargo carriers to the TGN [204,214]. The retromer constitutes two subcomplexes, a cargo selection trimer consisting of VPS26, VPS29 and VPS35, and a dimer of SNX (sorting nexin) proteins, usually a SNX1/2 or SNX5/6 heterodimer or a SNX3 homodimer [215]. SNX proteins contain a PX domain responsible for membrane association via its interaction with PIPs, and a BAR domain that is able to drive, sense and stabilize membrane curvature (see Figure 15, [216]). SNX3 however, does not contain a BAR domain and so far it is unclear how the SNX3-retromer mediates cargo transport. These different SNX-retromers contribute to cargo selectivity as the SNX-BAR retromers sort cargo such as TGN46, M6PR, STxB and SorLA, whereas the SNX3-retromer specifically sorts Wntless [217,218]. Other cargo, like furin does not depend on the retromer for its sorting to the TGN [219]. Next to endosome-to-TGN cargo sorting, the retromer also plays a role in trafficking of cargo from the EE to the PM or RE by associating with different SNX proteins [216]. AP1-clathrin coated vesicles together with adaptor protein EpsinR (Epsin related protein) are the main coat proteins involved in the endosome to TGN trafficking [220]. Upon TGN arrival, tethering factors such as the GARP and COG complex and several golgins capture the incoming transport vesicles and promote SNARE mediated fusion to the TGN membrane [221].
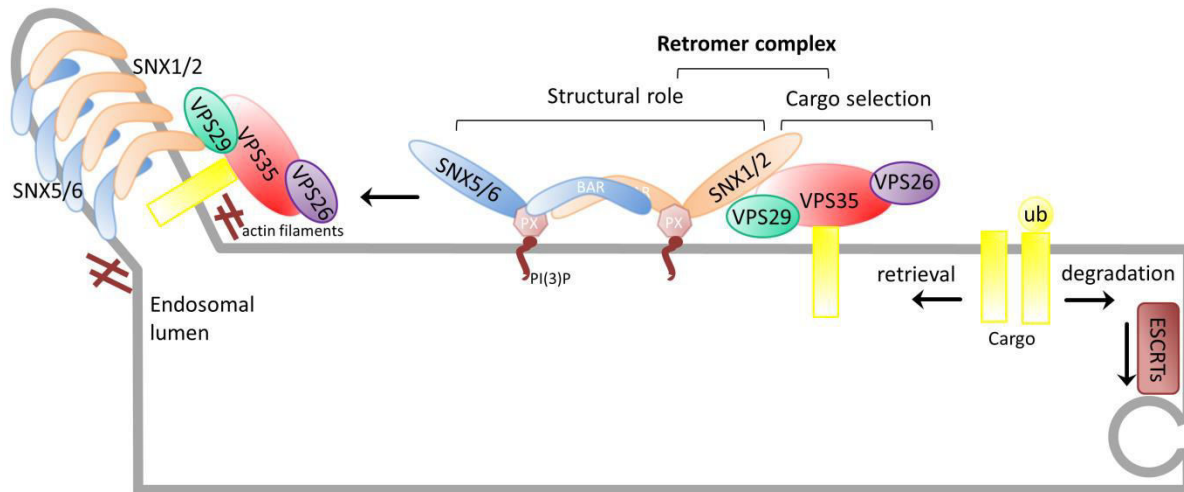
Figure 15: SNX (sorting nexin)- BAR (Bin-Amphiphysin-Rvs)- retromer mediated trafficking. While ubiquitinated cargo is selected for degradation by the ESCRT complex, cargo destined for the TGN (trans-Golgi network), REs (recycling endosomes) or PM (plasma membrane) is recognized by the retromer complex. The core VPS35-VPS29-VPS26 heterotrimer is responsible for cargo selection, where the VPS35 subunit interacts with cargo. The SNX-BAR proteins are characterized by a PX (Phox homology) domain that binds PI(3)P, and a BAR domain. The BAR domain allows the SNX-BARs to form dimers, and the concave surface of the BAR domain bears basic residues that associate with the membrane via electrostatic interactions thereby sensing and driving membrane curvature. The exact composition of the mammalian SNX-BAR subcomplex is still uncertain, although the current view is that it comprises a dimer of SNX1/2 with SNX5/6. Membrane remodeling is further assisted by actin polymerization eventually resulting in the scission of a cargo-enriched tubular transport carrier. Ub (ubiquitin). Figure adapted from [222].

The retromer complex has been implicated in Alzheimer's disease, and mutations of several retromer subunits were found to be associated with the disease [223,224]. APP (amyloid precursor protein) binds the receptor SorLA, which traffics between the TGN, PM and EE via its interaction with the VPS26 subunit of the retromer [225]. Loss of the retromer leads to the accumulation of APP in the endosomes which is sequentially cleaved by the β and γ secretases residing at the same subcellular location, resulting in increased amyloid β production. Furthermore, mutations in VPS35, another subunit of the retromer were found to be associated with Parkinson's disease [226].

1.5.4 Ectodomain shedding

Several membrane-anchored proteins, such as cell adhesion molecules, growth factors, cytokines, and receptors, are known to be released from the cell surface via ectodomain shedding. Ectodomain shedding is a highly regulated and selective process, only occurring for about 2% of the membrane-bound proteins. It rapidly converts membrane proteins into soluble effectors, and concomitantly, reduces the levels of cell surface expression thereby modulating various signaling processes involved in proliferation, differentiation, migration and inflammation with consequences for several diseases [227,228]. Various stimuli are known to induce ectodomain shedding, some of which, like phorbol

esters, globally activate shedding whereas others stimulate shedding of specific ectodomains [229]. Shedding is executed by sheddases, which are members of the ADAM (a disintegrin and metalloproteinase) family [230]. ADAM17 or TACE (TNFα converting enzyme) was the first identified sheddase that, next to TNFα, also mediates ectodomain shedding of several other membrane-bound proteins such as the LR (leptin receptor), IL6R, L-selectin, V-CAM1, ERBB4, APP, TGFα, HB-EGF and many others [231–233]. ADAMs are produced as zymogens that are activated by the serine endopeptidase furin and other proprotein convertases present in the TGN, PM and endosomal compartments which remove their prodomains [234,235]. There is no consensus motif that defines the cleavage site in substrates for the different ADAM proteins, instead substrate recognition depends on the structure of the cleavage region and the distance from the PM [236].

Next to ADAM17, ADAM10 also mediates the shedding of the IL-6R and LR [232,237]. This results in the release of soluble cytokine receptors in the extracellular environment, which can protect circulating cytokines from degradation or glomerular filtration, thereby prolonging their half-life and potentiating signaling. Furthermore, ectodomain shedding enables trans-signaling of cells expressing the signal transducing components of the corresponding soluble receptor. For example, soluble IL-6Rα can bind the gp130 chain thereby allowing IL-6 signaling in IL-6Rα-deficient cells [238]. On the other hand, soluble cytokine receptors can act as antagonists where they function as decoy receptors by capturing and sequestering ligand away from the membrane bound receptors resulting in inhibited signaling [239].

1.6 Autophagy

Autophagy is the process in which toxic aggregates, invading microorganisms and damaged organelles are cleared from the cytoplasm. This highly conserved catabolic process is essential for cell survival, stress responses and homeostatis and involves engulfment by a double-membrane organelle called the autophagosome, which transports the autophagic cargo to the lysosomes for degradation [240]. Autophagy was originally considered to be a non-selective, bulk degradation pathway, induced upon starvation, where the generated metabolites are reused either as sources of energy or building blocks for the synthesis of new molecules. However, it is now clear that autophagy can also be a highly selective process in terms of cargo that can be captured within the autophagosome. Several autophagic cargo receptors such as p62, OPTN (optineurin), NDP52 and NBR1 mediate the selective autophagy of aggregated proteins (aggrephagy), mitochondria (mitophagy), peroxisomes (pexophagy), ribosomes (ribophagy), pathogens (xenophagy) and endoplasmic reticulum (reticulophagy) [241–243]. Next to autophagy, also termed macroautophagy, two other autophagic processes exist, microautophagy and CMA (chaperone-mediated autophagy), which additionally contribute to the delivery of autophagic cargo into lysosomes. In contrast to (macro-) autophagy, CMA and microautophagy do not involve vesicular intermediates. CMA substrates contain a KFERQ-like motif that is recognized by HSC70. HSC70 subsequently delivers the substrate to the lysosomal receptor Lamp2A, which in turn oligomerizes and mediates the translocation of the unfolded substrate into the lysosomal lumen [244]. In microautophagy, cytosolic components are taken up via invaginations of the LEs in a selective or unselective manner, which traps the cytoplasmic material into ILVs. Selective microautophagy requires both the ESCRT system and HSC70 for the uptake of its substrates [245].

Autophagy initiates with the formation of an isolation membrane (or phagophore) followed by membrane nucleation and expansion which eventually leads to the formation of a double-membraned autophagosome. The autophagic machinery mediating these different steps consists of at least 36 ATGs that were originally identified in yeast, but are evolutionary well conserved in mammalian cells. 17 ATGs comprise the core autophagic machinery and can be subdivided into four key functional complexes termed the ULK (Unc-51 like autophagy activating kinase) complex, the class III PI3K complex I and two ubiquitin-like conjugation complexes, ATG12-ATG5-ATG16 and LC3 (or ATG8) (see Figure 16; [246,247]). These ATGs act together with general membrane trafficking components such as coat proteins, SNAREs and RABs to regulate autophagosome biogenesis, maturation and subsequent fusion with the lysosomes [248].

The ULK kinase complex composed of ULK1/2, ATG13, ATG101 and FIP200 is crucial for the induction of autophagy and is in turn positively and negatively regulated by the glucose and amino acid sensing kinases AMPK (AMP-activated protein kinase) and mTORC1 respectively. Under nutrient-rich conditions, this complex is phosphorylated and inhibited by mTORC1, while starvation blocks mTORC1 activity, resulting in the release and recruitment of ULK1/2 to the isolation membrane where it can phosphorylate and activate ATG13 and FIP200 [249,250]. Simultaneously with ULK complex activation, the class III PI3K complex I is activated, which is required for isolation membrane nucleation. This complex consists of Beclin1, VPS34, VPS15 and ATG14. ULK1 phosphorylates Beclin1 and activates the lipid kinase VPS34, which in turn generates PI(3)P on the surface of the isolation membrane resulting in the recruitment of WIPI2 (WD repeat domain phosphoinositide-interacting protein 2) and DFCP1 (Double FYVE-containing protein 1) [251,252]. WIPI2 targets the first ubiquitin-like conjugating complex ATG12-ATG5-ATG16 to the PI(3)P enriched isolation membrane, which is necessary for isolation membrane elongation [253]. In this complex, ATG12 is covalently conjugated to ATG5 via the concerted actions of ATG7 (~E1) and ATG10 (~E2). ATG5 then associates with ATG16 to form the ATG12-ATG5-ATG16 complex. The second ubiquitin-like conjugating system mediates the lipidation of LC3 (ATG8) which results in the conjugation of LC3 to phosphatidylethanolamine, or LC3II [254]. Here, the protease ATG4 cleaves the C-terminus of LC3 thereby exposing a glycine residue. This LC3I is then converted to LC3II with the assistance of ATG7 (~E1), ATG3 (~E2) and the ATG12-ATG5-ATG16 complex which acts as an E3-like enzyme [255]. In contrast to the ATG12-ATG5-ATG16 complex, LC3II remains associated with the mature autophagosome until its degradation in lysosomes [256]. The transmembrane protein ATG9 is another important ATG involved in the elongation of the isolation membrane. ATG9 is located at the TGN, EEs, REs and LEs, and autophagy activation drives the ULK1-mediated trafficking of this membrane-delivering ATG9 to the autophagosomal formation site. This ATG9-dependent lipid delivery together with the LC3 lipidation process allows for further elongation and closure of the autophagosome membranes [257]. The complete autophagosome is transported via microtubules to the LE or lysosomes, where it eventually fuses, forming an amphisome or autolysosome. This fusion involves the class III PI3K complex II, consisting of Beclin1, VPS34, VPS15 and UVRAG (instead of ATG14 in complex I), the ESCRT machinery, RAB7, the HOPS tethering complex and SNARE protein Stx17 [258–260].
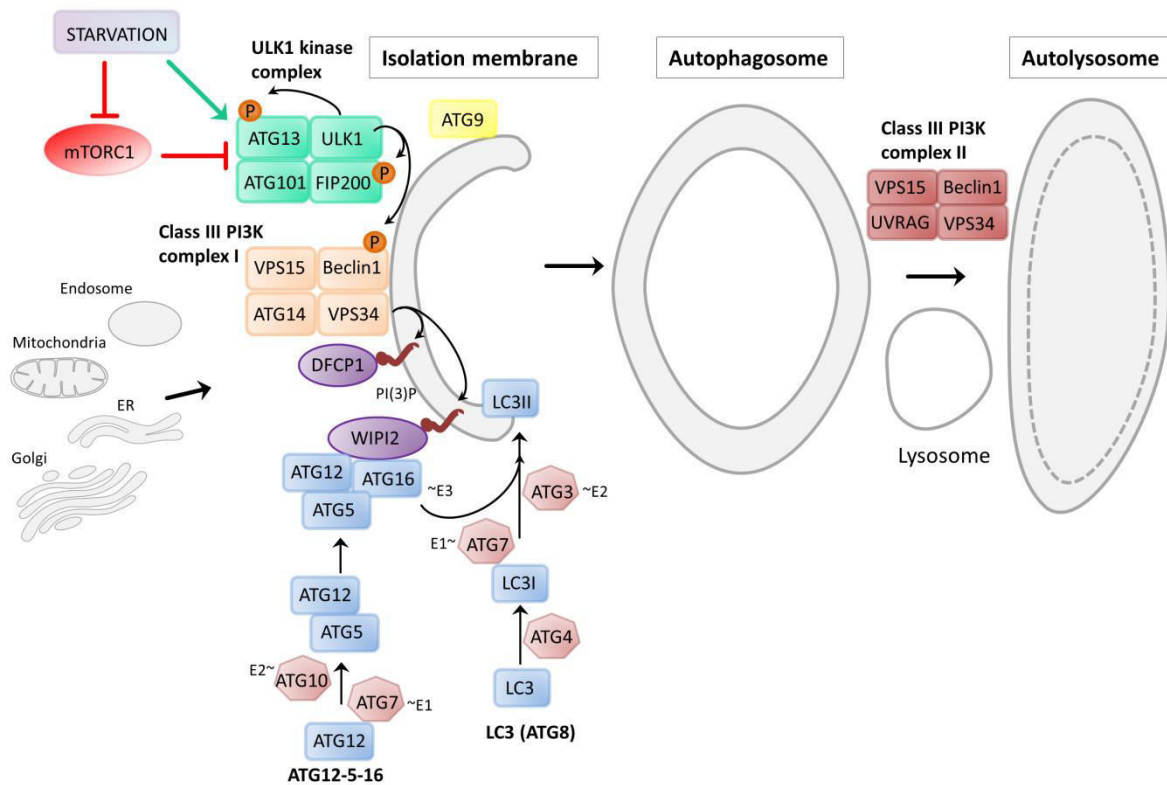
Figure 16: Schematic representation of the autophagy process. The isolation membrane is derived from several organelles including the ER (endoplasmic reticulum), mitochondria, endosomes and the Golgi. Autophagosome formation is initiated by the ULK1 (Unc-51 like autophagy activating kinase 1) kinase complex (ULK1, ATG13, FIP200, ATG101), which is activated upon starvation and inhibited by mTORC1 (mammalian target of rapamycin complex 1). ULK1 phosphorylates and activates the Class III PI3K (phosphatidylinositol-3 kinase) complex I (Beclin1, VPS34, VPS15, ATG14), which generates PI(3)P on the surface of the isolation membrane. This recruits DFCP1 (Double FYVE-containing protein 1) and WIPI2 (WD repeat domain phosphoinositide-interacting protein 2), which in turn recruits the ATG12-ATG5-ATG16 complex. This complex is formed via an ubiquitin-like conjugation system where ATG7 and ATG10 function as E1 and E2 respectively. ATG12-5-16 itself acts as an E3 ligase in the lipidation process of LC3 together with ATG7 (E1) and ATG3 (E2), resulting in anchoring of LC3II in the isolation membrane. ATG9 is also recruited to the isolation membrane and functions together with LC3II in the further elongation and closure of the autophagosome. Finally, the Class III PI3K complex II (Beclin1, VPS34, VPS15, UVRAG (UV radiation resistance associated gene)) is involved in fusion with the lysosome resulting in an autolysosome. Figure adapted from [261,262]*.*

In yeast, the isolation membrane originates from a single PAS (pre-autophagosomal structure), near the vacuole [263]. In multicellular eukaryotes however, the membrane sources for the autophagosome appear to derive from several organelles. Next to the consensus that the ER-mitochondrion interface is the main source for the isolation membrane, various reports indicate that it also receives input from the ER exit sites, ERGIC, Golgi, PM, EEs and REs, although the general assembly remains unclear [260,264]. The formation of the isolation membrane appears to rely on several proteins such as STX17 and RAB1, together with the TRAPPIII tethering complex which interacts with COPII coat proteins [265]. Other endosomal RAB proteins such as RAB4, RAB5, RAB7 and RAB11 are also implicated in autophagy, especially since the endosomes provide membrane input and also fuse with autophagosomes after their closure [260].

2. RNF41

2.1. RNF41, a RING finger ubiquitin ligase

RNF41 (RING (really interesting new gene) finger protein 41) was first discovered in 2001 as FLRF (fetal liver RING finger), a protein differentially expressed in mouse fetal liver and bone marrow hematopoietic stem cells and progenitors [266]. The human ortholog of this 317 amino acid containing protein was later identified as NRDP1 (neuregulin receptor degradation protein-1), due to its interaction with and degradation of ERBB3 and ERBB4 receptors. RNF41 was found to be ubiquitously expressed in human adult tissues, although expression was more pronounced in heart, brain and skeletal muscle. It consists of an N-terminal RING finger domain, followed by two other zinc finger domains, a CC (coiled-coil) domain and a C-terminal substrate binding domain (Figure 17). RING finger proteins represent a large class of E3 ubiquitin ligases involved in many cellular processes such as cell cycle regulation, transcriptional control and apoptosis. They recruit E2 conjugating enzymes via their RING domain and mediate the transfer of ubiquitin to substrates interacting with the substrate binding domain as well as the E3 ligase itself [267]. The Met-Gly sequence at the N-terminus of RNF41 suggests a putative myristoylation site, which could imply membrane anchoring but still needs further experimental validation [268,269]. Over the years it has become clear that RNF41 is involved in a diverse set of cellular processes including signaling of various receptors, intracellular trafficking and apoptosis. Furthermore, its implication in several diseases has been the topic of many studies. This chapter will highlight the functions of RNF41 in these different processes (Figure 18).

Figure 17: Schematic representation of the different domains present in RNF41 (RING finger protein 41). An N-terminal myristoylation site (yellow) is followed by a RING (really interesting new gene) domain, a CC (coiled-coil) domain and a C-terminal substrate binding domain.
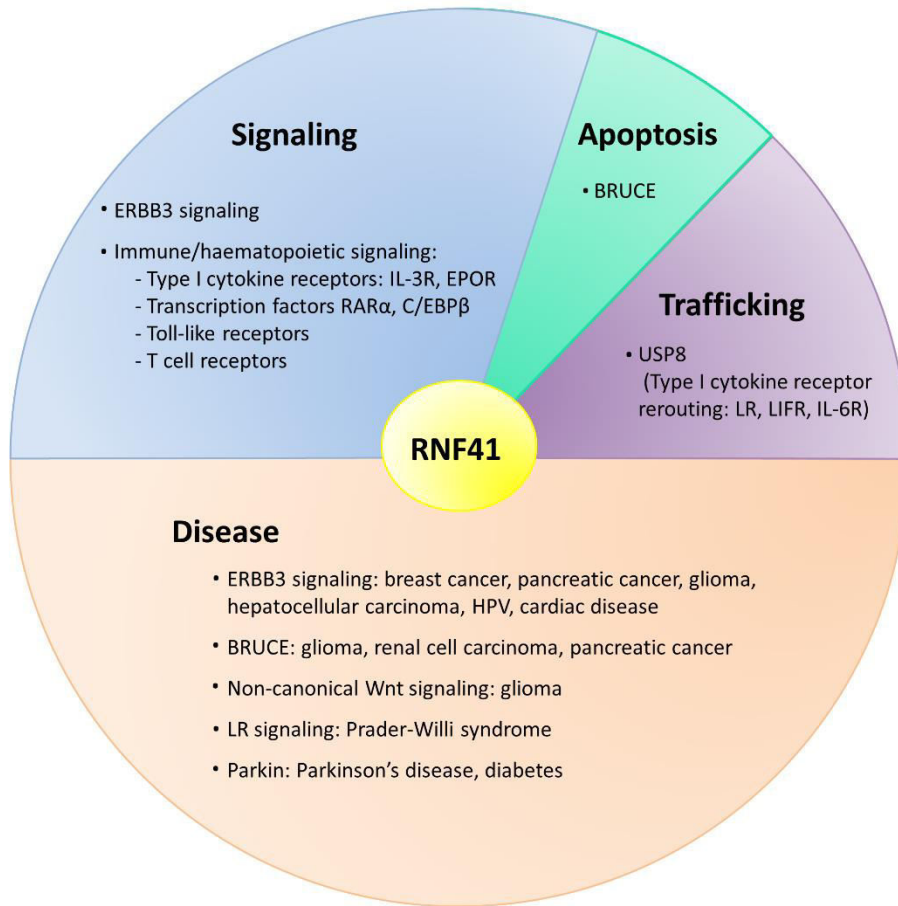
Figure 18: RNF41 (RING finger protein 41) function in cellular processes and disease. This scheme depicts the processes and implicated proteins or diseases regulated by RNF41 that will be highlighted in this chapter. IL-3R (interleukin 3 receptor); EPOR (erythropoietin receptor); RARα (retinoic acid receptor α); C/EBPβ (CCAAT/Enhancer-binding protein β); USP8 (Ubiquitin-specific protease 8); LR (leptin receptor); LIFR (leukaemia inhibitory factor receptor); IL-6R (interleukin 6 receptor); HPV (human papilloma virus); BRUCE (BIR repeat containing ubiquitin-conjugating enzyme).

2.2. Role of RNF41 in signaling

Our lab previously showed that RNF41 attenuates the signaling of several JAK2-associated type I cytokine receptors, including the LR (leptin receptor), LIFR (Leukaemia inhibitory factor receptor), IL-6R (interleukin 6 receptor), IL-3R (interleukin 3 receptor) and EPOR (erythropoietin receptor) [232]. Likewise, RNF41 reduces the signaling of RTKs (receptor tyrosine kinases) ERBB3 and ERBB4, and differentially regulates TLR (Toll-like receptor) signaling. Although it is still unclear how RNF41 downregulates type I cytokine receptor signaling, the mode of action and implications for the other receptors are more elaborated and described below.

2.2.1. ERBB3 signaling

ERBB3 is a member of the epidermal growth factor (EGF) receptor family of RTKs, consisting of four closely related type 1 transmembrane receptors (EGFR, ERBB2, ERBB3 and ERBB4). These receptors

play a role in highly regulated and complex signaling pathways involved in cell proliferation, differentiation and survival, where aberrant signaling generally results in the development of various tumors [270]. In contrast to the other ERBB receptors, ERBB3 lacks intrinsic tyrosine kinase activity and requires heterodimerization with other ERBBs in order to function. ERBB2, which has no direct ligand, is the most potent candidate for this heterodimerization [271].

RNF41 interacts with the ERBB3 receptor via its substrate binding domain and thereby regulates ERBB3 steady state levels through ligand-independent ubiquitination and proteasomal degradation [268,269,272]. RNF41 localized at the ER elicits proteasomal degradation of properly folded ERBB3 receptors via the ERAD pathway [273]. Recently, the factor that regulates this RNF41-mediated ERAD ERBB3 degradation was identified as RTN4A (Reticulon 4A), a structural protein of ER tubules. This protein, upregulated by acute cellular stress, sequesters RNF41 into ER tubules, thereby isolating it from ERBB3 receptors and ERAD ubiquitination machinery located in the rough ER sheets. This allows ERBB3 receptors to mature and traffic to the plasma membrane where they can respond to their ligand [274]. On the other hand, RNF41 present at endosomes is able to down-regulate mature internalized ERBB3 receptors upon ligand stimulation by diverting them away from recycling pathways to lysosomes for degradation [275]. This is accomplished by ligand-induced stabilization of USP8, a DUB known to stabilize RNF41 ([276], see 2.4). Collectively, these studies introduce RNF41 as a key component in the regulation of ERBB3 signaling, thereby preventing excessive signaling. As such, RNF41 was found to be a crucial component in the differentiation process of melanocytes during zebrafish embryogenesis by modulating ERBB3 signaling in neural crest cells [277].

2.2.2. Immune signaling

Screening of cDNA libraries revealed a differential expression of *Rnf41* in mouse fetal liver and bone marrow HSC (hematopoietic stem cells) and progenitors during blood cell development. *Rnf41* is upregulated in mouse fetal liver HSC, but not in progenitors and mature blood cells; whereas in adult mice, *Rnf41* is expressed in a heterogeneous population of bone marrow HSC, downregulated in the progenitor cell population and upregulated again as these progenitors differentiate into mature lymphoid and myeloid cell types [266]. More evidence for the involvement of RNF41 in hematopoiesis was presented by Jing et al, where RNF41 interacted with and downregulated IL-3R, EPOR and RARα (retinoic acid receptor) levels in a ligand independent way. As such, RNF41 attenuated erythroid and myeloid differentiation of mouse cells in response to IL-3, Epo and RA [278]. Additionally, in the presence of IL-4, RNF41 ubiquitinated and activated the transcription factor C/EBPβ (CCAAT/Enhancer-binding protein β). This promoted alternative activation of mouse macrophages (M2), which are known to be essential for anti-parasite immunity and constructive processes like wound healing and tissue repair [279].

RNF41 further influences the innate immune response by controlling TLR signaling in mouse macrophages. By acting both as an adaptor and E3 ligase, RNF41 mediates K48-linked polyubiquitination of MYD88 and K63-linked polyubiquitination of TBK1 (TANK binding kinase 1). This results on the one hand in the attenuation of MYD88-dependent activation of NF-κB and AP-1 and inhibits the production of pro-inflammatory cytokines, suggesting that RNF41 inhibits LPS (lipopolysaccharide)-induced classical activation of macrophages (M1). On the other hand, RNF41 potentiated TRIF-dependent activation of TBK1 and IRF3, thereby promoting the production of type I interferon. In this way, RNF41-transgenic mice are protected against infection with vesicular

stomatitis virus [280]. Similarly, the anti-inflammatory effects of the drug Luteolin in mouse microglial cells can be ascribed to stabilization of RNF41 by upregulation of USP8, thereby suppressing the production of pro-inflammatory cytokines [281]. Also, RNF41 was found to interact with TBK1 in the large yellow croaker, suggesting that RNF41 can regulate TBK1 and immune response in fish [282].

RNF41 is also linked to the adaptive immune response by negatively regulating CD8^{+} T cell activation. RNF41 hereby mediates K33-linked polyubiquitination of ZAP70, a signaling kinase essential for TCR (T cell antigen receptor) signaling, which promotes dephosphorylation of ZAP70 by acidic phosphatase-like proteins STS1 and STS2, resulting in its inactivation and subsequent termination of early TCR signaling. This regulation of TCR signaling has implications in autoimmune diseases, like experimental autoimmune encephalitis, where RNF41 might have pathogenic effects at the initial stage of the disease and protective effects in a later stage of disease progression. Moreover, CD8^{+} cells from mice deficient in *Rnf41* were able to elicit resistance to intracellular *Listeria monocytogenes* infection in liver and spleen and inhibit the growth of B16 melanoma tumors in mice, further confirming that RNF41 deficiency promotes the cytotoxicity of CD8+ T cells [283].

2.3. Role of RNF41 in apoptosis

Apoptosis is a highly regulated process in multicellular organisms resulting in total non-immunogenic cellular disintegration. During this process, apoptotic cells go through sequential steps that include cell shrinkage and blebbing, chromatin condensation, cytoskeletal collapse, nuclear and DNA fragmentation followed by the release of apoptotic bodies that are engulfed by neighboring cells. Cell death can be triggered by a wide variety of stimuli and conditions, both physiological and pathological, but once initiated, apoptosis proceeds through a common pathway [284]. The primary mediators of apoptosis are caspases, cytosolic cysteine proteases that cleave proteins C-terminal of aspartate residues. Through an irreversible cascade of auto- and trans-cleavage steps of different initiator caspases, activated executioner caspases cleave downstream targets resulting in rapid cell death [285]. Apoptosis can be blocked by multiple proteins of which many are known to interfere with caspase function in a direct or indirect way. BCL2, a membrane protein localized to the outer membrane of mitochondria inhibits apoptosis by blocking the efflux of cytochrome c from mitochrondria, which interferes with caspase-9 activation [286,287], while p53 is known to directly bind with and inhibit caspases [288]. Another group of anti-apoptotic proteins is the IAP (inhibitor of apoptosis proteins) family. Members of this family are characterized by the presence of one to three tandem BIR (baculoviral IAP repeat) domains that are able to bind and inhibit specific caspases. In addition to BIR domains, certain IAPs contain a RING-finger domain which allows these IAPs to catalyze ubiquitination and degradation of themselves and other proteins important for apoptosis [289]. BRUCE (BIR repeat containing ubiquitin-conjugating enzyme, also Apollon or BIRC6), is a giant (528 kDa) IAP containing a single N-terminal BIR domain and, unlike other IAPs, a C-terminal E2 motif, which can form thioester bonds with ubiquitin [290]. BRUCE functions as an inhibitor of apoptosis by interacting and inhibiting initiator caspases-8 and -9 and executioner caspases-3, -6 and -7 and by ubiquitinating and degrading the pro-apoptotic mitochondrial protein SMAC/DIABLO (second mitochondria-derived activator of caspases/Direct IAP-Binding protein with Low pI) [291]. Contrary to

other mammalian IAPs, BRUCE is essential for the viability of various cell lines, and *Bruce* deficient mice died at the embryonic or neonatal stage [291,292].

RNF41 interacts with and ubiquitinates BRUCE, resulting in its proteasomal degradation. In response to pro-apoptotic stimuli, this RNF41-mediated degradation of BRUCE causes caspase-3 activation and promotes apoptosis [292]. As such, RNF41 plays an important role in apoptosis of human glioma cells. BRUCE is upregulated in gliomas that are resistant to certain DNA-damaging agents, and antisense oligonucleotides against BRUCE enhance apoptosis induced by these agents [293]. In contrast, RNF41 and (cleaved) caspase-3 expression was found to be relatively lower in human glioma tissues compared to non-tumorous brain tissues. RNF41 overexpression promoted apoptosis in glioma cells by degrading BRUCE and activating caspase-3. This apoptosis was aggravated upon Temozolomide treatment, a drug used for glioma chemotherapy. Contrary, RNF41 depletion inhibited this Temozolomide-induced apoptosis [294]. Similarly, upregulation of RNF41 by LPS in neurons of the cerebral cortex of adult rats enhanced the expression of cleaved caspase-3 and suppressed the levels of BRUCE, suggesting that RNF41 contributes to neuronal apoptosis in a neuroinflammation model [295].

2.4. Role of RNF41 in trafficking via USP8

Spatiotemporal control of protein ubiquitination is regulated by DUBs. The DUB USP8 (or UBPy) was first identified as a protein involved in the control of cell proliferation, where it accumulates in response to growth stimulation and is downregulated upon growth arrest conditions [296]. USP8 is known for its role in endocytic trafficking by deubiquitinating the ESCRT-0 proteins STAM and HRS, and by directly deubiquitinating cargo like RTKs and GPCRs. This differential deubiquitination of either endosomal transport machinery or cargo, together with the type of cargo, decides on the fate of receptors. USP8 deubiquitinates the GPCRs DOR (δ- opioid receptor) and PAR2 (protease-activated receptor 2) and the ion-channel KCa3.1, resulting in receptor degradation by trafficking towards lysosomes [297–299]. Contrary to this, deubiquitination of the RTKs EGFR, Met and ERBB3 by USP8 protects these receptors from lysosomal degradation and assists in the sorting towards recycling endosomes [300–302]. On the other hand, USP8-mediated deubiquitination of the sorting proteins STAM and HRS stabilizes the ESCRT-0 complex and directs the GPCR CXCR4 (chemokine receptor 4) towards lysosomes for further degradation [303]. This deubiquitination of the ESCRT-0 proteins is necessary to maintain endosomal morphology as USP8 depletion results in endosomal swelling and accumulation of ubiquitinated species on these endosomes [304–306].

Next to the N-terminal MIT domain and carboxyl-terminal catalytic domain, responsible for endosomal location and deubiquitinating enzyme activity respectively, USP8 contains a centrally located rhodanese domain [307]. USP8 deubiquitinates and stabilizes RNF41 through interaction via its rhodanese domain [276,308]. Furthermore, our group showed that USP8 itself is a target of RNF41 and interacts with its substrate binding domain [309]. By ubiquitinating and suppressing USP8, RNF41 indirectly destabilizes the ESCRT-0 complex and influences the intracellular trafficking of JAK2-associated type I cytokine receptors. In this way, RNF41 inhibits the lysosomal degradation of the LR, LIFR and the IL-6R and subsequently reroutes them towards compartments for ectodomain shedding, resulting in increased soluble receptors by ADAM proteases [232,309]. Moreover, a recent collaboration with the group of prof. Wevrick (University of Alberta, Canada) revealed that *MAGEL2* (melanoma antigen L2), a candidate gene for the neurodevelopmental disease Prader-Willi, is

responsible for the recruitment of the LR to the sorting endosomes via its interaction with NDN (necdin). MAGEL2 was found to interact with both RNF41 and USP8 where it deubiquitinates and stabilizes RNF41, and destabilizes USP8 and STAM. In this way, the NDN-MAGEL2-RNF41-USP8 complex controls LR cell surface expression and degradation in a ligand-independent way [310]. These data suggest that USP8 targets these type I cytokine receptors for lysosomal degradation the same way as it targets CXCR4 [303].

Direct deubiquitination of ERBB3 by USP8 resulting in blocked lysosomal degradation, as described in Niendorf et al., might also explain the results observed in Cao et al., where RNF41 enhances lysosomal degradation of ERBB3 [275,301]. Since RNF41 ubiquitinates and suppresses USP8 [309], RNF41 might in this way reverse the inhibition of lysosomal degradation, resembling the situation in USP8 depleted cells. This reciprocal RNF41-USP8 regulation also affects BRUCE, where USP8 and RNF41 play a role in cytokinesis by modulating the ubiquitination state of BRUCE. Here, USP8 counteracts the RNF41-mediated BRUCE ubiquitination thereby blocking its proteasomal degradation. Maintaining BRUCE levels appear to be crucial since depletion of BRUCE causes defective abscission in the final stage of cytokinesis and cytokinesis-associated apoptosis [276,311].

2.5. Role of RNF41 in diseases

2.5.1. ERBB3 signaling in cancer

RNF41-mediated modulation of ERBB3 signaling was primarily established in breast cancer cell lines. Overexpression of RNF41 in human breast cancer cells suppresses ERBB3 levels thereby inhibiting cellular growth and motility, while loss of RNF41 promotes breast tumor progression by enhancing ERBB2/ERBB3 signaling. Moreover, RNF41 expression levels in breast cancer patient primary tumors and in mouse mammary tumors were found to inversely correlate with ERBB3 levels [312]. Importantly, these mouse mammary tumors employ post-transcriptional mechanisms to suppress RNF41, since transgenic expression of *RNF41* cDNA could not restore RNF41 levels nor suppress elevated ERBB3 levels [313]. Another study suggested RNF41 as a novel prognostic biomarker for breast cancer, based on 113 primary breast cancer samples. Here, low RNF41 expression implied a decreased overall and disease-free survival of patients [314].

Next to breast cancer, aberrant ERBB3 signaling has been implicated in many other types of cancers [315], and for most of these, RNF41 was found to play a role in the underlying mechanism.

Prostate cancer cells (PCa) rely on signaling through the AR (androgen receptor) and ERBB3 receptor for maintenance and progression. In these androgen-dependent cancer cells, the transcription factor AR induces ERBB3 degradation by upregulating RNF41 transcription [316]. Upregulation of RNF41 by AR can only occur in the presence of nuclear FlnA (Filamin A), which stimulates AR binding to RNF41 ARE (androgen response element) [317]. Drugs like Celexocib that, besides its well-established function as a COX2 inhibitor, upregulate RNF41 and subsequently suppress ERBB3 are of great interest, since ERBB3 signaling leads to constitutive, ligand-independent activation of the AR and renders PCa cells indifferent to androgen withdrawal therapies [318].

In comparison to normal brain tissue, ERBB3 levels are abundant in high-grade glioblastoma multiforme, a malignant tumor of the central nervous system. Also here, depletion of RNF41 was found to dysregulate ERBB3 signaling, contributing to glioma migration and invasion, whereas overexpression of RNF41 inhibited tumor progression [319]. Wu et al, reported an alternatively spliced short variant of RNF41 (NRDP1S), lacking the first 71 amino acids and thus the RING domain, which was expressed in normal human brain tissue and absent in glioma tissues. NRDP1S stabilizes RNF41 resulting in augmented ERBB3 degradation and inhibition of tumor growth. In this way, NRDP1S deficiency could also play an important role in the loss of RNF41 [320]. Another study reported that overexpression of the CC domain of RNF41, which also stabilizes RNF41, resulted in enhanced ERBB3 ubiquitination and degradation [321]. This indicates that both NRDP1S and the CC domain of RNF41 could function as tumor suppressors.

HCC (hepatocellular carcinoma) development is closely linked to hepatitis B infection [322]. Overexpression of ERBB3 has been observed in hepatocellular carcinoma and HBx (hepatitis B virus encoded X protein) was recently found to post-translationally regulate ERBB3 levels [323]. Analogous to breast cancer, prostate cancer and glioma, an inverse correlation between RNF41 and ERBB3 protein levels was found in HBx-induced hepatocellular carcinoma tissues. HBx increased ERBB3 protein expression by destabilizing RNF41, which subsequently promoted the proliferation of HCC cells [324]. Also in pancreatic cancer cells, overexpression of ERBB3 is associated with a decreased cell survival. The retinoic acid derivative ABPN (A4-amino-2-(butyrylamino)phenyl (2E,4E,6E,8E)- 3,7-dimethyl-9-(2,6,6-trimethyl-1-cyclohexenyl)- 2,4,6,8-nonatetraenoate) was found to suppress pancreatic cancer growth by upregulating RNF41 via unknown mechanisms, which causes degradation of ERBB3 and downregulation of the ERBB3 and downstream AKT, MAPK and JNKs signaling pathway [325].

RNF41 also downregulates ERBB3 levels in a HPV16 (human papillomavirus 16)-containing cell line [326]. During viral integration in the cellular genome, the E2 protein, involved in replication of HPV DNA, is lost, which lifts the inhibition of the viral oncogenes E6 and E7. RNF41 was found to interact with the E2 protein of HPV16. By competing for RNF41, E2 upregulated the amount of ERBB3 receptors localizing on the cell membrane which might favor a more stable proliferative effect in epithelia where the viral replication takes part [326].

In contrast to the previously described cancers where ERBB3 appears to be a big culprit, the heart relies on ERBB3 signaling and its downstream RAS/MEK/ERK, PI3K/AKT and STAT3 pathways for cardiac cell survival [327]. Ischemia/reperfusion- and doxorubicin-induced cardiac injury cause an upregulation of RNF41 in mouse heart cells, resulting in increased cardiac apoptosis, autophagy and oxidative stress thereby further promoting cardiac injury and dysfunction. These effects result from an RNF41-mediated inactivation of cardiac ERBB3 and subsequent dysregulation of its downstream signaling pathways. Therefore, targeted therapy to decrease RNF41 expression specifically in the heart may help ameliorate ischemic and doxorubicin-induced cardiac injury [328,329]. Moreover, an *RNF41* polymorphism was recently found to be associated with the risk of congenital heart disease in Chinese Mongolian population, further suggesting that RNF41 plays an important role in heart diseases [330]. Finally, the human and mouse RNF41 sequences contain a potential binding site for Nkx-2.5, a transcription factor that regulates heart development and disease [266].

Next to ERBB3, RNF41 was also found to interact with and suppress ERBB4 [268]. KITENIN (KAI1 C-terminal interacting tetraspanin or VANGL1 (Vang-like protein 1)) can interact with the C-terminal domain of RNF41 and this interaction renders ERBB4 resistant to RNF41-mediated degradation [331]. In CRC (colorectal cancer) tissues, the KITENIN/ERBB4-DVL2 (Dishevelled 2)-c-Jun axis was identified as a novel, EGFR-independent unconventional downstream signal of EGF [332]. EGF stimulated the formation of a KITENIN/ERBB4/RNF41 complex, leading to targeted degradation of DVL2 by RNF41 and resulting into upregulation of c-Jun, thus enhancing CRC cell motility [331]. This implies that the function of RNF41 in colorectal cancer is in strong contrast to the other described cancers, where RNF41 acts as a suppressor via degradation of ERBB3. A clear understanding of the exact mechanism of RNF41 is essential for the development of possible RNF41-targeted anti-cancer strategies.

2.5.2. Dysregulation of BRUCE in cancer

RNF41 appears to be a pro-apoptotic protein by promoting degradation of both BRUCE and ERBB3 [269,292]. In this way, RNF41 contributes to the suppression of several cancers. Loss of RNF41 in human glioma cells augments glioma progression through reduction of apoptosis via upregulated BRUCE levels [294] and via dysregulation of ERBB3 signaling [319]. Likewise, in pancreatic cancer cells, the retinoic acid derivative ABPN downregulated protein levels of both ERBB3 and BRUCE, by upregulating RNF41, thereby suppressing pancreatic cancer cell growth [325]. Additionally, reduced and enhanced protein levels of RNF41 and BRUCE respectively, were detected in renal cell carcinoma tissues compared to normal tissues. Also here, RNF41 affected cell viability and apoptosis via degradation of BRUCE [333], however, ERBB3 was not found to be upregulated in this type of cancer [334].

2.5.3. Loss of cell polarity in cancer

In addition to aberrant signaling of the EGFR family and inhibition of apoptosis, loss of polarity is also commonly observed in cancer cells and RNF41 has been implicated in the regulation of cell polarity in several ways. Phosphorylation of RNF41 by the Ser/Thr kinase Par-1b targets laminin-111 receptors to the basolateral membrane, which facilitate cell anchorage to laminin-111, a major component of the ECM (extracellular matrix). This establishes the cell-ECM contacts required for apical-basal cell polarity in epithelial cells [335]. On the other hand, RNF41 downregulates VANGL-dependent non-canonical Wnt signaling, a pathway necessary for planar cell polarity in neuronal development. By interacting with KITENIN and VANGL2, RNF41 mediates the K63-linked polyubiquitination of DVL, thereby inhibiting its recruitment to activated Frizzled receptors, resulting in suppressed Wnt signaling. This non-canonical Wnt signaling contributes to GBM (glioblastoma multiforme) progression and highlights a role for RNF41 in regulating GBM cell motility and invasiveness [336].

2.5.4. Aberrant LR signaling in Prader-Willi syndrome

LR signaling in the brain is critical for the regulation of energy balance, body weight and glucose homeostasis by the actions of leptin in the arcuate nucleus of the hypothalamus where it inhibits orexigenic AgRP/NPY (agouti-related protein/ neuropeptide Y) neurons and stimulates anorexigenic POMC (pro-opiomelanocortin) neurons [337]. PWS (Prader-Willi syndrome) is a genetic disorder caused by a deletion or disruption of genes, including *MAGEL2* and *NDN*, located on chromosome 15q11-q13 and is characterized by hypotonia, mental retardation, endocrine dysfunction, energy imbalance and obesity [338]. Likewise, mice lacking *Magel2* were found to be obese with endocrine

deficits and exhibit decreased muscle tone. Although these mice have increased levels of leptin they appeared to be insensitive to leptin, even when peripherally administered, suggesting that loss of *Magel2* propagates in PWS through leptin sensing pathways [339]. Moreover, these *Magel2*-null mice were found to have diminished levels of LR and RNF41, and enhanced levels of USP8 and STAM1 [310]. RNF41, USP8 and STAM1 are proteins that regulate LR processing [309], and MAGEL2, which is highly expressed in the arcuate nucleus, stabilizes RNF41 and destabilizes USP8 and STAM1. In this way, MAGEL2 can contribute to the regulation of LR trafficking in POMC neurons [310,340]. The loss of MAGEL2 results in destabilized RNF41 and hampers LR cell surface expression, internalization and degradation, which can explain the leptin-regulated phenotypes like leptin resistance, obesity and glucose dysregulation observed in *Magel2*-null mouse models of PWS [310].

2.5.5. Loss of parkin in Parkinson's disease

Parkinson's disease is a common neurodegenerative disorder characterized by loss of dopaminergic neurons in the substantia nigra and the presence of abnormal protein aggregates called Lewy bodies [341]. Patients develop movement disorders like tremors, rigidity, slowness of movement and experience variable manifestations of dementia. Both genetic defects and environmental factors like oxidative stress are causes of Parkinson's disease. Loss-of-function mutations in the *parkin* gene are the predominant cause of early onset familial Parkinson's disease [342]. Parkin contains two RING domains and functions as an RBR E3 ligase [343]. It hereby ubiquitinates substrates including α-synuclein, Pael receptor, CDCrel-1, tubulin, synphilin-1, synaptotagmin, cyclin E, and p38. Loss of function mutations in *parkin* cause accumulation and aggregation of these substrates, resulting in death of dopaminergic neurons [344].

RNF41 ubiquitinates and degrades parkin, and as such stabilizes its substrate CDCrel-1 [345,346]. Furthermore, RNF41 overexpression enhanced the production of intracellular ROS (reactive oxygen species), while co-expression of parkin reversed this effect [346]. In this way, RNF41 might be involved in the pathogenesis of Parkinson's disease by modulating both parkin stability and the intracellular redox state. Knock out of *parkin* in mice models causes only mild phenotypes, whereas the manifestations in Drosophila are more dramatic and mimic the pathological phenotypes of patients with Parkinson's disease [347]. Overexpression of Drosophila RNF41 in Drosophila dopaminergic neurons provoked several Parkinson's disease-like phenotypes including loss of these dopaminergic neurons and impaired flight ability. Here, RNF41 reduced Drosophila parkin and overexpression of human parkin reversed the observed phenotypes [348]. This suggests that the levels of parkin are important to protect against RNF41-induced toxicity and that RNF41 might be considered a therapeutic target in Parkinson's disease. RNF41 can also contribute to Parkinson's disease by influencing cell growth and apoptosis when cells are exposed to environmental factors, as RNF41 sensitized cells to external oxidative stress inducers like hydrogen peroxide and hydroxynonenal, resulting in apoptosis [349]. Notably, a clinical gene association study failed to show a positive association between the *RNF41* gene and Parkinson's disease development in the Chinese population [350]. However, since the pathogenesis of the disease can be influenced by ethnic background and geographic origin of the patients, perhaps screening for *RNF41* mutations should be performed in other populations.

Parkin is also implicated in regulation of mitochondrial dynamics [347]. Moreover, selective recruitment of parkin to damaged mitochondria promotes mitophagy [351]. Soleimanpour et al.

discovered another protein, CLEC16A (C-type lectin domain family 16, member A), to be involved in the regulation of mitophagy in pancreatic β cells. CLEC16A was found to protect RNF41 from proteasomal degradation by a yet unknown mechanism. Loss of CLEC16A in pancreatic islets of mice significantly reduced RNF41 and increased parkin levels and upregulated early mitophagy. In addition, CLEC16A loss of function impaired autophagosomal-lysosomal trafficking in late mitophagy, causing defects in the clearance of unhealthy mitochondria [352]. As mitochondrial function is imperative for glucose-stimulated insulin release, this dysregulation of glucose homeostasis in pancreatic β cells can lead to diabetes [353]. Thus CLEC16A regulation of the RNF41-parkin interaction can regulate β cell function and prevent diabetes by controlling mitophagy. Furthermore, Pdx1, a transcription factor and master regulator of pancreatic β-cell development, was found to regulate the expression of CLEC16A and to control downstream effects on RNF41, and can in this way direct autophagosome-lysosome fusion during mitophagy [354].

The reciprocal RNF41-USP8 regulation can, next to cytokinesis (see 2.4) also coordinate mitophagy as USP8 was found to remove K6-linked polyubiquitin chains from parkin [355]. This is a crucial step for efficient recruitment of parkin to depolarized mitochondria, suggesting a role for USP8 in promoting parkin-mediated mitophagy and perhaps a function for USP8-RNF41-Parkin as a tripartite protein complex in the regulation of mitophagy.

2.5.6. Drug-mediated regulation of RNF41

Collectively, the described literature suggests that RNF41 may act as a tumor suppressor by maintaining ERBB3 receptors at modest levels. It also functions as a pro-apoptotic protein by targeting BRUCE. Additionally, RNF41 might be considered as therapeutic target for Parkinson's disease since it suppresses the levels of parkin. Knowledge about the exact mode of action of RNF41 is crucial to determine whether to use RNF41 inhibitors or activators as treatment in the different diseases (an overview of RNF41 in diseases is listed in Table 6).

RNF41 is regulated at transcriptional and post-translational levels (see Table 7). RNF41 mRNA and protein levels are upregulated upon LPS stimulation, both in mouse macrophages and in the cerebral cortex of rats [280,295] and by the non-steroidal anti-inflammatory drug Celexocib and the androgen receptor in prostate cancer cells [316,318]. Contrary to this, the microRNA miR-497 binds to RNF41 mRNA and impairs its translation in colorectal cancer cells [356]. Doxorubicin and ABPN, two chemotherapy agents, can respectively upregulate RNF41 protein expression in heart tissue of mouse and in pancreatic cancer cells by currently unknown mechanisms [325,329]. Moreover, the chemotherapeutic drug Lenalidomide inhibits the E3 ligase activity of RNF41 and thus its auto-ubiquitination resulting in increased RNF41 levels in an erythroid progenitor cell line [357]. A summary of these drugs, together with other proteins and PTMs that regulate RNF41 are listed in Table 7.

Table 6: Role of RNF41 in disease.

Disease	RNF41 function	References
Breast cancer	RNF41 suppresses ERBB3. Downregulated RNF41 and upregulated ERBB3 levels in breast cancer cells.	[312–314]
Prostate cancer	RNF41 suppresses ERBB3. The AR upregulates RNF41 transcription and induces ERBB3 degradation.	[316–318]
Glioma	RNF41 suppresses BRUCE. Downregulated RNF41 and upregulated BRUCE levels in human glioma tissues.	[294]
	RNF41 suppresses ERBB3. Downregulated RNF41 and upregulated ERBB3 levels in human glioma tissues.	[319,320]
	RNF41 downregulates non-canonical Wnt signaling, resulting in inhibited glioma progression.	[336]
Pancreatic cancer	RNF41 suppresses ERBB3 and BRUCE. ABPN upregulates RNF41, thereby decreasing ERBB3 and BRUCE resulting in suppressed pancreatic cancer cell growth.	[325]
Cardiac disease	RNF41 suppresses ERBB3. ERBB3 is necessary for cardiac cell survival. Ischemia/reperfusion and doxorubicin upregulate RNF41 in mouse heart, resulting in increased cardiac injury	[328,329]
	Identification of an *RNF41* polymorphism associated with the risk of congenital heart disease in Chinese Mongolian population.	[330]
Hepatocellular carcinoma	RNF41 suppresses ERBB3. Downregulated RNF41 and upregulated ERBB3 levels in HBx-induced hepatocellular carcinoma tissues.	[324]
Colorectal cancer	miR-497 inhibits RNF41 translation. Downregulated RNF41 and upregulated miR-497 in colorectal cancer tissues.	[356]
	RNF41 suppresses DVL2. EGF stimulation leads to the formation of a KITENIN/ERBB4/RNF41 complex, which degrades DVL2, resulting in c-Jun upregulation and enhanced colorectal cancer cell motility.	[331]
Renal cell carcinoma	RNF41 suppresses BRUCE. Downregulated RNF41 and upregulated BRUCE levels in renal cell carcinoma tissues.	[333]
Experimental autoimmune encephalitis (EAE)	RNF41 downregulates CD8 [+]T cell receptor signaling. Upregulation of RNF41 in CD8+ T cells infiltrated into the brain of mice during induction of EAE.	[283]
Parkinson's disease	RNF41 suppresses parkin. RNF41 degrades parkin and stabilizes its substrate CDCrel-1. RNF41 in Drosophila provoked Parkinson's disease-like phenotypes like loss of dopaminergic neurons.	[346,348,349]
Diabetes	CLEC16A stabilizes RNF41. CLEC16A controls β-cell function and prevents diabetes by controlling mitophagy through its actions on RNF41 and parkin	[352,354]
Psychiatric illness	Identification of *RNF41* as candidate gene for anxiety-like behaviors and depression	[358]
Prader-Willi syndrome (PWS)	MAGEL2 stabilizes RNF41. Loss of MAGEL2 destabilizes RNF41 and dysregulates LR trafficking resulting in leptin resistance and obesity in the MAGLE2-null mouse model of PWS	[310]

RNF41 (RING finger protein 41); AR (androgen receptor); BRUCE (BIR repeat containing ubiquitin-conjugating enzyme); APBN (A4-amino-2-(butyrylamino)phenyl (2E,4E,6E,8E)- 3,7-dimethyl-9-(2,6,6-trimethyl-1-cyclohexenyl)- 2,4,6,8-nonatetraenoate); HBx (hepatitis B virus encoded X protein); DVL2 (Dishevelled 2); EGF (Epidermal growth factor); KITENIN (KAI1 C-terminal interacting tetraspanin); CLEC16A (C-type lectin domain family 16, member A); MAGEL2 (melanoma antigen L2).

Table 7: Modes of RNF41 regulation.

Regulator	Type of RNF41 regulation	References
LPS	mRNA and protein upregulation	[280,295]
Androgen receptor	mRNA and protein upregulation	[316,317]
Celexocib	mRNA and protein upregulation	[318]
miR-497	inhibition of translation	[356]
ABPN	upregulation of protein levels	[325]
Doxorubicin	upregulation of protein levels	[329]
Lenalidomide	inhibition of E3 ligase activity resulting in protein stabilization	[357]
RTN4A	sequestration in ER resulting in inhibition of E3 ligase activity and protein stabilization	[274]
CLEC16A	protein stabilization	[352,354]
USP8	protein stabilization	[276]
RNF41	auto-ubiquitination and protein destabilization	[276,321]
HBx	protein destabilization	[324]
Par-1b	PTM: phosphorylation of S254	[335]
?	PTM: S-nitrosylation of C106	[359]

RNF41 (RING finger protein 41); LPS (lipopolysaccharide); APBN (A4-amino-2-(butyrylamino)phenyl (2E,4E,6E,8E)- 3,7-dimethyl-9-(2,6,6-trimethyl-1-cyclohexenyl)- 2,4,6,8-nonatetraenoate); RTN4A (Reticulon 4A); CLEC16A (C-type lectin domain family 16, member A); USP8 (ubiquitin-specific protease 8); HBx (hepatitis B virus encoded X protein);PTM (post-translational modification).

3. Detection of protein-protein interactions

PPIs (protein-protein interactions) constitute the basis of essentially all biological activities including signal transduction, gene regulation and catalytic enzymatic activities in addition to having a structural role in the cell. These PPIs differ based on physical characteristics such as the composition, affinity and whether they represent stable or transient interactions [360]. Consequently, studying these PPIs provides valuable insight into the function of a protein and can facilitate the identification of new drug targets. Moreover, the molecular mechanism of an unidentified protein can be predicted via the so called "guilt-by-association principle", based on the known and established function of an interacting protein. Over the years, various PPI techniques have emerged, contributing to the growing interactome which has been estimated to embody 650,000 interactions [361]. Classical techniques such as Y2H (Yeast Two-Hybrid) [362] and AP-MS (affinity-purification-mass spectrometry) [363] have been complemented with new and improved approaches. These enable the study of PPIs at their subcellular location (e.g. PLA, RET-based approaches [364,365] or in a physiological context, between weak and transient interactions (e.g. MAPPIT, LUMIER, BioID, Virotrap [366–369]), full-length integral membrane proteins (e.g. MaMTH [370]) and post-translationally modified proteins (e.g. protein microarrays [371]). This chapter briefly highlights some important high-throughput approaches subdivided into binary and co-complex techniques (see Figure 19).
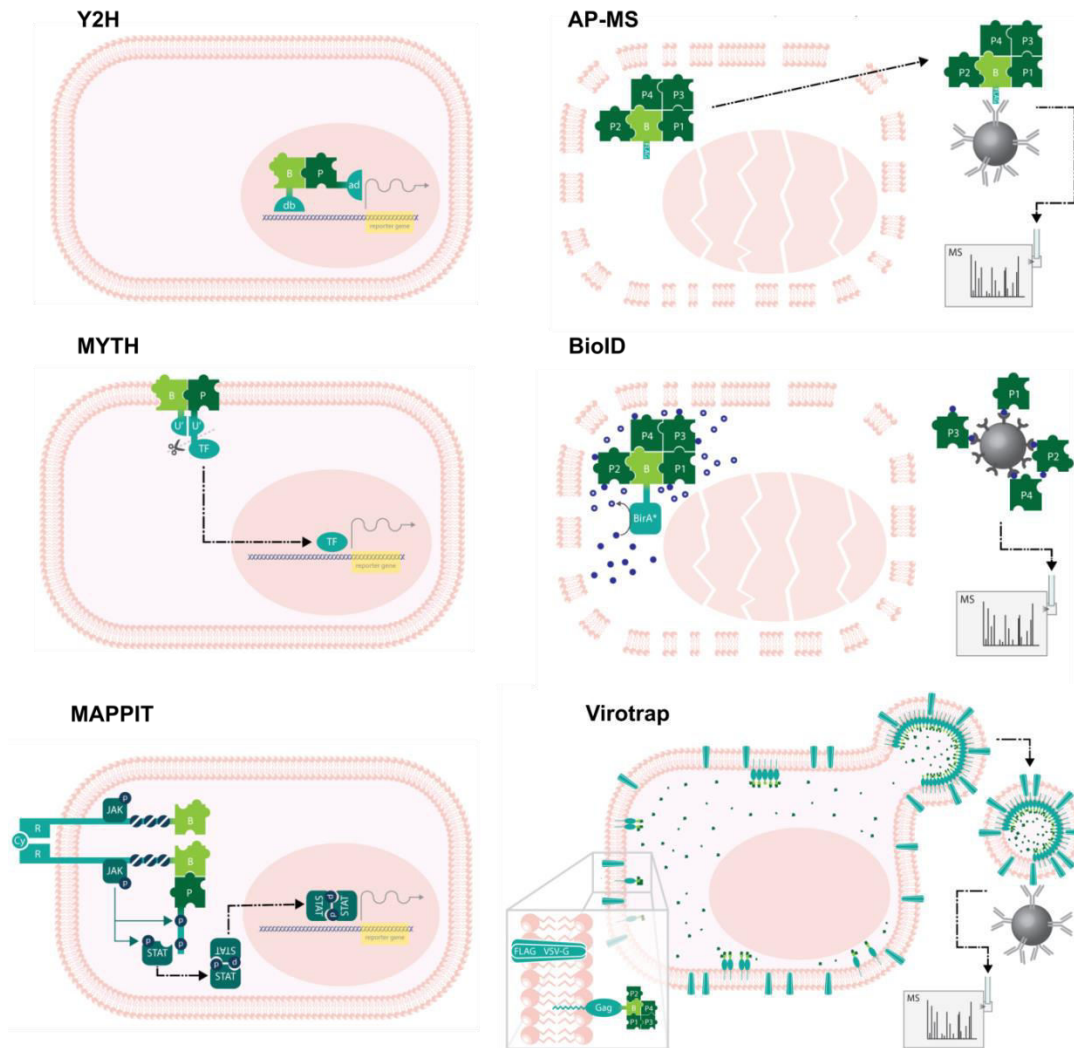
Figure 19: Overview of the different binary and co-complex techniques described in this thesis, see text for details. Y2H (Yeast Two-Hybrid); MYTH (membrane-based Y2H); MAPPIT (Mammalian Protein-Protein Interaction Trap); AP-MS (Affinity Purification-Mass Spectrometry); BioID (Proximity-dependent Biotin Identification); B (bait); P (prey); AD (activating domain); DBD (DNA binding domain); U' (partial ubiquitin); JAK (Janus kinase); STAT (signal transducer and activator of transcription); TF (transcription factor); R (cytokine receptor); Cy (cytokine); VSV-G (vesicular stomatitis virus protein G). Figure adapted from [372].

3.1. Binary techniques

3.1.1. Yeast Two-Hybrid

The classical Y2H method relies on a split transcription factor where the DBD (DNA binding domain) and the AD (activation domain) are fused to a bait or prey protein. Interaction between bait and prey reconstitutes the transcription factor, where the DBD binds the promotor region, while the AD interacts with RNA polymerase II, resulting in the transcription of the reporter gene [362]. This method can be implemented using one prey at a time, or like in the study of Rolland et al., using entire prey protein libraries [373]. Y2H is an efficient, low cost method that requires a limited amount of technology to perform. The eukaryotic environment and well known genome of *S. cerevisiae* allow for easy manipulation. Furthermore, reporter gene expression provides signal amplification which enables the detection of transient and weak PPI interactions. This method

however exhibits a high number of false positives and false negatives. A major limitation is that the interactions take place in the nucleus of yeast cells. This lack of native cellular environment hampers the detection of certain mammalian PPI where the proteins are not able to move to the nucleus or that rely on PTMs, resulting in false negative interactions. Also, Y2H false positives are often the result of interacting proteins that are normally spatially or temporally separated. Additionally, incorrectly folded proteins that bind nonspecifically to many baits or proteins that bind or activate the reporter gene also can give rise to false positives [374].

Multiple alternative Y2H systems have been developed, for example reverse Y2H, which is used to identify mutations or proteins that impair PPIs. Here, bait and prey interaction lead to lethality of yeast cells in selective media, while cells expressing mutant proteins or proteins disrupting the interaction survive [375]. Y3H (Yeast three-hybrid) represents another variant that implements a third factor, for example a bridging protein, modifying enzyme, small molecule or RNA. Co-expression of a modifying enzyme allows for the identification of PTM interactions [376]. Y3H can also be used as drug discovery screening method where a small molecule of interest is linked to an anchor moiety (e.g. methotrexate or dexamethasone), which interacts with a ligand binding domain (e.g. DHFR (dihydrofolate reductase) or glucocorticoid receptor hormone binding domain) coupled to the DBD. Interaction between the small molecule and the target protein fused to the AD results in transcriptional activation of the reporter gene [377,378].

3.1.2. Protein complementation assays

Over the years, many other binary techniques, such as PCAs (protein complementation assays), have been developed to improve on the sensitivity and specificity of the original Y2H procedure. Generally, PCAs are based on the fusion of the bait and prey to a separate fragment of a reporter protein, where bait and prey interaction causes the reassembly of the split fragments ultimately resulting in reporter activity. For example, the split-ubiquitin system, MYTH (membrane-based Y2H), allows for the detection of membrane-bound proteins. Bait and prey, one or both representing an integral membrane protein, are fused to a C-terminal and N-terminal ubiquitin moiety. In addition, the C-terminal moiety is coupled to a tagged DHFR or to a transcription factor. Bait and prey interaction reconstitute the ubiquitin molecule that is recognized by ubiquitin specific proteases which subsequently cleave off the DHFR or transcription factor, allowing detection of tagged DHFR on Western blot or resulting in the activation of a reporter gene [379,380]. MYTH formed the basis for the later developed mammalian variant MaMTH (mammalian membrane two-hybrid) [370]. Other mammalian PCAs include BiFC (Bimolecular fluorescence complementation), where bait-prey interaction complements a split fluorescent protein (e.g. YFP or GFP) that can be readily detected using fluorescence plate readers or microscopy [381]; enzyme complementation assays, where, upon bait-prey interaction, the reconstituted reporter enzyme (e.g. β lactamase, β galactosidase, luciferase or DHFR) results in the enzymatic conversion of a substrate into a detectable end product [382]; and Split-TEV assays, where bait-prey interaction reconstitutes a TEV (tobacco etch virus) protease that cleaves and releases a transcription factor or luciferase enzyme which activates a reporter gene or results in light emission upon luciferin addition, respectively [383]. While the enzyme complementation and Split-TEV assays have higher sensitivity due to their signal amplification ability, BiFC has the added value of providing additional information about the subcellular location where the PPIs occur when visualized with microscopy and allows for the detection of multiple PPIs at the same time.

3.1.3. MAPPIT

MAPPIT (MAmmalian Protein-Protein Interaction Trap) is an in-house developed method to detect PPIs in intact mammalian cells. It is based on the functional complementation of the JAK-STAT (Janus kinases-signal transducers and activators of transcription) signaling pathway of type I cytokine receptors upon bait and prey interaction. In this assay the bait protein is coupled to a signaling-deficient chimeric receptor comprising the extracellular domain of the EPOR and the transmembrane domain and cytoplasmic tail of the LR. The three conserved tyrosine residues in the cytoplasmic tail of the LepR are mutated to phenylalanine, which eliminates STAT3 recruitment (Y1138F) and negative-feedback mechanisms (Y985F and Y1077F). The prey protein is fused to a C-terminal portion of the gp130 (glycoprotein 130) receptor, containing functional STAT3 recruitment sites. Upon ligand binding, bait and prey interaction leads to trans-phosphorylation and activation of the associated JAKs. In turn, JAKs phosphorylate the prey chimera followed by recruitment and activation of STAT3. STAT's dimerize and migrate to the nucleus resulting in transcriptional activation of a luciferase reporter gene [366].

As MAPPIT operates in intact mammalian cells, it provides a natural environment for proteins in the presence of both endogenous cofactors and regulatory proteins enabling proper post-translational modifications and/or PPIs. Furthermore, this context allows analysis of (functional) PPI modulations triggered by exogenously stimuli that, for instance, activate certain signaling pathways or induce a stress response. The signal amplification at multiple levels (substrate and STAT phosphorylation, reporter gene transcription and luciferin conversion) contributes to the sensitivity and robustness of the technology, facilitating the detection of weak and transient interactions. False positive signals are limited due to the physical separation of the interaction zone (cytoplasm) and the read-out zone (nucleus), and the ligand inducible nature of the system. Moreover, MAPPIT proved to be easy scalable and is therefore an excellent tool for high-throughput interactome studies. By using reverse transfection techniques in combination with robotics, ArrayMAPPIT and the highly miniaturized microarrayMAPPIT allow the screening of a large collection of preys, derived from the huORF (human open reading frame) collection, with approximately 15.000 full size ORFs [384,385].

A drawback of MAPPIT is the inevitable membrane anchoring of the bait protein, hindering the study of many PPIs at their native subcellular localization. This problem led to the development of KISS (KInase Substrate Sensor), a MAPPIT-derived method compatible with full-length transmembrane proteins that allows *in situ* analysis of PPIs. This method uses the conventional MAPPIT prey chimera, whereas the bait protein is coupled to a C-terminal, kinase-containing portion of TYK2 (tyrosine kinase 2). Since the Tyk2 kinase domain lacks a subcellular localization signal, localization of the chimeric KISS bait solely relies on the used bait protein (see addendum 1; [386]). MAPPIT further constitutes other interaction tools, including heteromeric MAPPIT and the three-hybrid variant MASPIT. Heteromeric MAPPIT enables the detection of modification-dependent interactions via the extracellular domains of the heteromeric GM-CSF (granulocyte-macrophage colony-stimulating factor) receptor which permit incorporation of modifying enzymes in the trap, while MASPIT allows profiling of small molecule-protein interactions [387,388]. Furthermore, MAPPIT was successfully used in combination with random mutagenesis, resulting in a high-throughput method that allows for extensive mapping of PPI interfaces (see addendum 2; [389–391]).

3.2. Co-complex techniques

3.2.1. AP-MS

The combination of AP-MS represents another classical method for generating interactome maps. This method enables the isolation of multi-protein complexes directly form cell lysates via one or more AP steps. The bait protein of interest is fused to an epitope tag and expressed in the cell. For high-throughput methods this tag is usually a Flag tag or a TAP (tandem affinity purification) tag [392,393]. The Flag tag is purified using an anti-Flag antibody resin and eluted with a large excess of competing Flag peptide. The TAP tag on the other hand, consists of a CBP (calmodulin binding peptide), followed by a TEV protease cleavage site and protein A, and purification of this tag requires multiple steps. First, a matrix coated with IgG is used, which has strong affinity for the protein A moiety in the TAP tag. After TEV cleavage of the tag, the CBP fused protein of interest is immobilized on a calmodulin coated matrix and eventually released using the calcium chelator EGTA. These tags have their own advantages and disadvantages. For instance, Flag-tag purification could detect weaker and more transient PPI compared to the TAP tag, whereas the TAP tag decreases background levels compared to the Flag-tag. After purification the proteins are subjected to proteolytic digestion, usually by trypsin, resulting in a mixture of peptides. These peptides are then separated by HPLC (high-performance liquid chromatography) and ionized prior to identification. The generated data represents the relative abundance of each ionized peptide based on its mass-to-charge ratio, which is used to identify proteins using different search engines [394].

Although originally used in yeast, AP-MS can be performed in all cell types thus providing a physiological relevant background [392,393]. It allows for the identification of PTMs and can detect dynamic changes in the composition of protein complexes by using quantitative methods like SILAC (stable-isotope labelling with amino acids in cell culture) [395]. The biggest limitation of AP-MS is the lysis step in which homogenization generally results in the identification of more false positives. Next to this, the extensive washing steps often disrupt weak and transient interactions, resulting in more false negatives.

3.2.2. BioID

An alternative approach to AP-MS is BioID (proximity-dependent biotin identification), which exploits proximity-dependent in vivo protein biotinylation. In this method the bait protein is fused to a mutated biotin ligase, BirA*, resulting in promiscuous biotinylation [368]. Wild-type BirA catalyzes the reaction in which reactive biotinyl-AMP is formed from biotin and ATP, followed by the attachment of biotinyl-AMP to a specific lysine on a subunit of the acetyl-CoA carboxylase. BirA*, on the other hand, prematurely releases this generated biotinyl-AMP, resulting in the covalent attachment to the lysine residues of nearby proteins [396]. Interaction partners of BirA* fused baits can be enriched by streptavidin affinity purification followed by MS analysis. Since the biotinylation step precedes solubilization, it can detect weak and transient interactions, offering great advantages over regular AP-MS. BioID also provides a native cellular environment, allowing for the detection of indirect and PTM-requiring interactions. In addition, the necessity to add excess biotin to the cell culture medium enables the system with a built-in inducibility, thereby opening up the future possibility of performing pulse–chase type experiments.

This latter advantage also represents a downside of this method, as the permanent addition of biotin to lysines may lead to the loss of charge on these sites and at the same time could inhibit additional secondary modifications, for instance ubiquitination, necessary for the interaction with other proteins. Another limitation of BioID is the fact that the assay may detect adjacent proteins that are not true interactors, the activity radius of BirA* is currently estimated to be within 20-30nm [368]. Also, the fact that BirA* is a large (35kD) fusion protein, may impair normal targeting stability or function of the bait protein of interest. Recently, BioID2 was developed, which deals with some of the limitations arising from classical BioID, as this method uses a substantially smaller BirA* that enhances the labeling of proximate proteins, and requires less biotin supplementation [397].

3.2.3. Virotrap

Virotrap represents another co-purification strategy that relies on the production of VLPs (virus-like particles) to detect PPI and analyze protein complexes. Here, the bait protein of interest is fused to the C-terminus of the Gag protein of HIV. Overexpression of the Gag protein has the inherent potential to produce VLPs and Virotrap hereby allows the entrapment of the Gag-coupled bait together with its interacting partners in these VLPs. Co-expression of Flag-tagged and non-tagged VSV-G (vesicular stomatitis virus G) form trimers on the VLPS surface and enable the purification of the VLPs from the supernatant by using an anti-FLAG coated matrix. After this enrichment step the particles are lysed and the content can be analyzed with MS. This method allows the study of cytosolic complexes and also detects ER and plasma membrane residing proteins. Furthermore, Virotrap is suitable for the detection of small molecule interactors by fusing Gag to DHFR and coupling the small molecule to methotrexate. It can also be used as a binary approach, where labeling of both bait and prey proteins followed by Western blot analysis can validate specific PPIs [369].

The Gag proteins inside the VLP form a scaffold that, due to avidity effects, can increase the sensitivity for interaction partners that otherwise bind with low affinity. Moreover, this method eliminates the need for solubilization and therefore preserves the protein complexes, limits the detection of false positives and enables identification of weak and transient interactions. On the other hand, the VLPs contain a number of non-specific background interactors like structural and serum proteins or proteins that are related to HIV biology. These additional false-positives however, can be extracted using suitable filter strategies. The size of a VLP is approximately 145nm, which also limits the size of the trapped protein complex, although it is currently not known what the maximum amount or size of protein is that fit inside the VLP [398].

References

1 Tokarev AA, Alfonso A & Segev N (2009) Overview of Intracellular Compartments and Trafficking Pathways. .

2 Bonifacino JS & Glick BS (2004) The mechanisms of vesicle budding and fusion. *Cell* **116**, 153–66.

3 Cai H, Reinisch K & Ferro-Novick S (2007) Coats, tethers, Rabs, and SNAREs work together to mediate the intracellular destination of a transport vesicle. *Dev. Cell* **12**, 671–82.

4 Yu I-M & Hughson FM (2010) Tethering factors as organizers of intracellular vesicular traffic. *Annu. Rev. Cell Dev. Biol.* **26**, 137–56.

5 Trahey M & Hay JC (2010) Transport vesicle uncoating: it's later than you think. *F1000 Biol. Rep.* **2**, 47.

6 ROTH TF & PORTER KR (1964) YOLK PROTEIN UPTAKE IN THE OOCYTE OF THE MOSQUITO AEDES AEGYPTI. L. *J. Cell Biol.* **20**, 313–32.

7 Crowther RA & Pearse BM (1981) Assembly and packing of clathrin into coats. *J. Cell Biol.* **91**, 790–7.

8 Kanaseki T & Kadota K (1969) The "vesicle in a baske". A morphological study of the coated vesicle isolated from the nerve endings of the guinea pig brain, with special reference to the mechanism of membrane movements. *J. Cell Biol.* **42**, 202–20.

9 Hirst J, D. Barlow L, Francisco GC, Sahlender DA, Seaman MNJ, Dacks JB & Robinson MS (2011) The Fifth Adaptor Protein Complex. *PLoS Biol.* **9**, e1001170.

10 McMahon HT & Mills IG (2004) COP and clathrin-coated vesicle budding: different pathways, common approaches. *Curr. Opin. Cell Biol.* **16**, 379–91.

11 Park SY & Guo X (2014) Adaptor protein complexes and intracellular transport. *Biosci. Rep.* **34**.

12 Bonifacino JS (2004) The GGA proteins: adaptors on the move. *Nat. Rev. Mol. Cell Biol.* **5**, 23–32.

13 Raiborg C, Bache KG, Gillooly DJ, Madshus IH, Stang E & Stenmark H (2002) HRS sorts ubiquitinated proteins into clathrin-coated microdomains of early endosomes. *Nat. Cell Biol.* **4**, 394–398.

14 Bonifacino JS & Lippincott-Schwartz J (2003) Coat proteins: shaping membrane transport. *Nat. Rev. Mol. Cell Biol.* **4**, 409–414.

15 Robinson MS (2015) Forty Years of Clathrin-coated Vesicles. *Traffic* **16**, 1210–1238.

16 Heilker R, Spiess M & Crottet P (1999) Recognition of sorting signals by clathrin adaptors. *BioEssays* **21**, 558–567.

17 Kirchhausen T (2000) Three ways to make a vesicle. *Nat. Rev. Mol. Cell Biol.* **1**, 187–98.

18 Bonifacino JS & Traub LM (2003) Signals for Sorting of Transmembrane Proteins to Endosomes and Lysosomes. *Annu. Rev. Biochem.* **72**, 395–447.

19 Zerial M & McBride H (2001) Rab proteins as membrane organizers. *Nat. Rev. Mol. Cell Biol.* **2**, 107–117.

20 Meggouh F, Bienfait HME, Weterman MAJ, de Visser M & Baas F (2006) Charcot-Marie-Tooth disease due to a de novo mutation of the RAB7 gene. *Neurology* **67**, 1476–1478.

21 Jenkins D, Seelow D, Jehee FS, Perlyn CA, Alonso LG, Bueno DF, Donnai D, Josifiova D, Mathijssen IMJ, Morton JEV, Helene ?rstavik K, Sweeney E, Wall SA, Marsh JL, N?rnberg P, Rita Passos-Bueno M, Wilkie AOM & Wilkie AOM (2007) RAB23 Mutations in Carpenter Syndrome Imply an Unexpected Role for Hedgehog Signaling in Cranial-Suture Development and Obesity. *Am. J. Hum. Genet.* **80**, 1162–1170.

22 Cheng KW, Lahad JP, Kuo W, Lapuk A, Yamada K, Auersperg N, Liu J, Smith-McCune K, Lu KH, Fishman D, Gray JW & Mills GB (2004) The RAB25 small GTPase determines aggressiveness of ovarian and breast cancers. *Nat. Med.* **10**, 1251–1256.

23 Ginsberg SD, Alldred MJ, Counts SE, Cataldo AM, Neve RL, Jiang Y, Wuu J, Chao M V., Mufson EJ, Nixon RA & Che S (2010) Microarray Analysis of Hippocampal CA1 Neurons Implicates Early Endosomal Dysfunction During Alzheimer's Disease Progression. *Biol. Psychiatry* **68**, 885–893.

24 Bhuin T & Roy JK (2014) Rab proteins: the key regulators of intracellular vesicle transport. *Exp. Cell Res.* **328**, 1–19.

25 Li G & Marlin MC (2015) Rab Family of GTPases. In *Methods in molecular biology (Clifton, N.J.)* pp. 1–15.

26 Andres DA, Seabra MC, Brown MS, Armstrong SA, Smeland TE, Cremers FP & Goldstein JL (1993) cDNA cloning of component A of Rab geranylgeranyl transferase and demonstration of its role as a Rab escort protein. *Cell* **73**, 1091–9.

27 Chavrier P, Gorvel J-P, Stelzer E, Simons K, Gruenberg J & Zerial M (1991) Hypervariable C-termmal domain of rab proteins acts as a targeting signal. *Nature* **353**, 769–772.

28 Stenmark H (2009) Rab GTPases as coordinators of vesicle traffic. *Nat. Rev. Mol. Cell Biol.* **10**, 513–525.

29 Wandinger-Ness A & Zerial M (2014) Rab proteins and the compartmentalization of the endosomal system. *Cold Spring Harb. Perspect. Biol.* **6**, a022616.

30 Bucci C, Parton RG, Mather IH, Stunnenberg H, Simons K, Hoflack B & Zerial M (1992) The small GTPase rab5 functions as a regulatory factor in the early endocytic pathway. *Cell* **70**, 715–28.

31 Feng Y, Press B & Wandinger-Ness A (1995) Rab 7: an important regulator of late endocytic membrane traffic. *J. Cell Biol.* **131**, 1435–52.

32 van der Sluijs P, Hull M, Webster P, Mâle P, Goud B & Mellman I (1992) The small GTP-binding protein rab4 controls an early sorting event on the endocytic pathway. *Cell* **70**, 729–40.

33 Ullrich O, Reinsch S, Urbé S, Zerial M & Parton RG (1996) Rab11 regulates recycling through the pericentriolar recycling endosome. *J. Cell Biol.* **135**, 913–24.

34 Kouranti I, Sachse M, Arouche N, Goud B & Echard A (2006) Rab35 Regulates an Endocytic Recycling Pathway Essential for the Terminal Steps of Cytokinesis. *Curr. Biol.* **16**, 1719–1725.

35 Díaz E, Schimmöller F & Pfeffer SR (1997) A novel Rab9 effector required for endosome-to-TGN transport. *J. Cell Biol.* **138**, 283–90.

36 Junutula JR, De Maziére AM, Peden AA, Ervin KE, Advani RJ, van Dijk SM, Klumperman J & Scheller RH (2004) Rab14 is involved in membrane trafficking between the Golgi complex and endosomes. *Mol. Biol. Cell* **15**, 2218–29.

37 Pérez-Victoria FJ, Mardones GA & Bonifacino JS (2008) Requirement of the human GARP complex for mannose 6-phosphate-receptor-dependent sorting of cathepsin D to lysosomes. *Mol. Biol. Cell* **19**, 2350–62.

38 Martinez O, Schmidt A, Salaméro J, Hoflack B, Roa M & Goud B (1994) The small GTP-binding protein rab6 functions in intra-Golgi transport. *J. Cell Biol.* **127**, 1575–88.

39 Wilcke M, Johannes L, Galli T, Mayau V, Goud B & Salamero J (2000) Rab11 regulates the compartmentalization of early endosomes required for efficient transport from early endosomes to the trans-golgi network. *J. Cell Biol.* **151**, 1207–20.

40 Satoh AK, O'Tousa JE, Ozaki K & Ready DF (2005) Rab11 mediates post-Golgi trafficking of rhodopsin to the photosensitive apical membrane of Drosophila photoreceptors. *Development* **132**, 1487–1497.

41 Tisdale EJ, Bourne JR, Khosravi-Far R, Der CJ & Balch WE (1992) GTP-binding mutants of rab1 and rab2 are potent inhibitors of vesicular transport from the endoplasmic reticulum to the Golgi complex. *J. Cell Biol.* **119**, 749–61.

42 Chia PZC & Gleeson PA (2014) Membrane tethering. *F1000Prime Rep.* **6**, 74.

43 Bröcker C, Engelbrecht-Vandré S & Ungermann C (2010) Multisubunit tethering complexes and their role in membrane fusion. *Curr. Biol.* **20**, R943-52.

44 Gillingham AK & Munro S (2003) Long coiled-coil proteins and membrane traffic. *Biochim. Biophys. Acta* **1641**, 71–85.

45 Sohda M, Misumi Y, Yoshimura S, Nakamura N, Fusano T, Ogata S, Sakisaka S & Ikehara Y (2007) The Interaction of Two Tethering Factors, p115 and COG complex, is Required for Golgi Integrity. *Traffic* **8**, 270–284.

46 Brunet S & Sacher M (2014) Are all multisubunit tethering complexes bona fide tethers? *Traffic* **15**, 1282–7.

47 Hong W & Lev S (2014) Tethering the assembly of SNARE complexes. *Trends Cell Biol.* **24**, 35–43.

48 Munson M & Novick P (2006) The exocyst defrocked, a framework of rods revealed. *Nat. Struct. Mol. Biol.* **13**, 577–581.

49 Sakurai-Yageta M, Recchi C, Le Dez G, Sibarita J-B, Daviet L, Camonis J, D'Souza-Schorey C & Chavrier P (2008) The interaction of IQGAP1 with the exocyst complex is required for tumor cell invasion downstream of Cdc42 and RhoA. *J. Cell Biol.* **181**, 985–998.

50 Jin Y, Sultana A, Gandhi P, Franklin E, Hamamoto S, Khan AR, Munson M, Schekman R & Weisman LS (2011) Myosin V transports secretory vesicles via a Rab GTPase cascade and interaction with the exocyst complex. *Dev. Cell* **21**, 1156–70.

51 Whyte JRC & Munro S (2002) Vesicle tethering complexes in membrane traffic. *J. Cell Sci.* **115**, 2627–2637.

52 Conibear E, Cleck JN & Stevens TH (2003) Vps51p mediates the association of the GARP (Vps52/53/54) complex with the late Golgi t-SNARE Tlg1p. *Mol. Biol. Cell* **14**, 1610–23.

53 Schindler C, Chen Y, Pu J, Guo X & Bonifacino JS (2015) EARP is a multisubunit tethering complex involved in endocytic recycling. *Nat. Cell Biol. 17(5), 639–50.* **17**, 639–50.

54 Peplowska K, Markgraf DF, Ostrowicz CW, Bange G & Ungermann C (2007) The CORVET Tethering Complex Interacts with the Yeast Rab5 Homolog Vps21 and Is Involved in Endo-Lysosomal Biogenesis. *Dev. Cell* **12**, 739–750.

55 Wurmser AE, Sato TK & Emr SD (2000) New component of the vacuolar class C-Vps complex couples nucleotide exchange on the Ypt7 GTPase to SNARE-dependent docking and fusion. *J. Cell Biol.* **151**, 551–62.

56 Sacher M, Barrowman J, Wang W, Horecka J, Zhang Y, Pypaert M & Ferro-Novick S (2001) TRAPP I implicated in the specificity of tethering in ER-to-Golgi transport. *Mol. Cell* **7**, 433–42.

57 Kim Y-G, Raunser S, Munger C, Wagner J, Song Y-L, Cygler M, Walz T, Oh B-H & Sacher M (2006) The Architecture of the Multisubunit TRAPP I Complex Suggests a Model for Vesicle Tethering. *Cell* **127**, 817–830.

58 Yamasaki A, Menon S, Yu S, Barrowman J, Meerloo T, Oorschot V, Klumperman J, Satoh A & Ferro-Novick S (2009) mTrs130 Is a Component of a Mammalian TRAPPII Complex, a Rab1 GEF That Binds to COPI-coated Vesicles. *Mol. Biol. Cell* **20**, 4205–4215.

59 Brunet S & Sacher M (2014) In sickness and in health: the role of TRAPP and associated proteins in disease. *Traffic* **15**, 803–18.

60 Kim JJ, Lipatova Z & Segev N (2016) TRAPP Complexes in Secretion and Autophagy. *Front. cell Dev. Biol.* **4**, 20.

61 Zolov SN & Lupashin V V. (2005) Cog3p depletion blocks vesicle-mediated Golgi retrograde trafficking in HeLa cells. *J. Cell Biol.* **168**, 747–759.

62 Guo Y, Punj V, Sengupta D & Linstedt AD (2008) Coat-Tether Interaction in Golgi Organization. *Mol. Biol. Cell* **19**, 2830–2843.

63 Andag U & Schmitt HD (2003) Dsl1p, an Essential Component of the Golgi-Endoplasmic Reticulum Retrieval System in Yeast, Uses the Same Sequence Motif to Interact with Different Subunits of the COPI Vesicle Coat. *J. Biol. Chem.* **278**, 51722–51734.

64 Spang A (2012) The DSL1 Complex: The Smallest but Not the Least CATCHR. *Traffic* **13**, 908–913.

65 Schröter S, Beckmann S & Schmitt HD (2016) Coat/Tether Interactions—Exception or Rule? *Front. Cell Dev. Biol.* **4**, 44.

66 Zong M, Satoh A, Yu MK, Siu KY, Ng WY, Chan HC, Tanner JA & Yu S (2012) TRAPPC9 mediates the interaction between p150 and COPII vesicles at the target membrane. *PLoS One* **7**, e29995.

67 Shorter J, Beard MB, Seemann J, Dirac-Svejstrup AB & Warren G (2002) Sequential tethering of Golgins and catalysis of SNAREpin assembly by the vesicle-tethering protein p115. *J. Cell Biol.* **157**, 45–62.

68 Siniossoglou S & Pelham HR (2001) An effector of Ypt6p binds the SNARE Tlg1p and mediates selective fusion of vesicles with late Golgi membranes. *EMBO J.* **20**, 5991–8.

69 Stroupe C, Collins KM, Fratti RA & Wickner W (2006) Purification of active HOPS complex reveals its affinities for phosphoinositides and the SNARE Vam7p. *EMBO J.* **25**, 1579–89.

70 Suvorova ES, Duden R & Lupashin V V (2002) The SEC34/SEC35p complex, a Ypt1p effector required for retrograde intra-Golgi trafficking, interacts with Golgi SNAREs and COPI vesicle coat proteins. *J. Cell Biol.* **157**, 631–43.

71 Kraynack BA, Chan A, Rosenthal E, Essid M, Umansky B, Waters MG & Schmitt HD (2005) Dsl1p, Tip20p, and the novel Dsl3(SEC39) protein are required for the stability of the Q/t-SNARE complex at the endoplasmic reticulum in yeast. *Mol. Biol. Cell* **16**, 3963–77.

72 Söllner T, Whiteheart SW, Brunner M, Erdjument-Bromage H, Geromanos S, Tempst P & Rothman JE (1993) SNAP receptors implicated in vesicle targeting and fusion. *Nature* **362**, 318–324.

73 Fasshauer D, Sutton RB, Brunger AT & Jahn R (1998) Conserved structural features of the synaptic fusion complex: SNARE proteins reclassified as Q- and R-SNAREs. *Proc. Natl. Acad. Sci. U. S. A.* **95**, 15781–6.

74 McNew JA, Parlati F, Fukuda R, Johnston RJ, Paz K, Paumet F, Söllner TH & Rothman JE (2000) Compartmental specificity of cellular membrane fusion encoded in SNARE proteins. *Nature* **407**, 153–159.

75 Parlati F, Varlamov O, Paz K, McNew JA, Hurtado D, Söllner TH & Rothman JE (2002) Distinct SNARE complexes mediating membrane fusion in Golgi transport based on combinatorial specificity. *Proc. Natl. Acad. Sci. U. S. A.* **99**, 5424–9.

76 Dietrich LE., Boeddinghaus C, LaGrassa TJ & Ungermann C (2003) Control of eukaryotic membrane fusion by N-terminal domains of SNARE proteins. *Biochim. Biophys. Acta - Mol. Cell Res.* **1641**, 111–119.

77 Dulubova I, Sugita S, Hill S, Hosaka M, Fernandez I, Südhof TC & Rizo J (1999) A conformational switch in syntaxin during exocytosis: role of munc18. *EMBO J.* **18**, 4372–4382.

78 Gallwitz D & Jahn R (2003) The riddle of the SEC1/Munc-18 proteins – new twists added to their interactions with SNAREs. *Trends Biochem. Sci.* **28**, 113–116.

79 Shen J, Tareste DC, Paumet F, Rothman JE & Melia TJ (2007) Selective Activation of Cognate SNAREpins by SEC1/Munc18 Proteins. *Cell* **128**, 183–195.

80 Scott BL, Van Komen JS, Irshad H, Liu S, Wilson KA & McNew JA (2004) SEC1p directly stimulates SNARE-mediated membrane fusion in vitro. *J. Cell Biol.* **167**, 75–85.

81 Laufman O, Kedan A, Hong W & Lev S (2009) Direct interaction between the COG complex and the SM protein, Sly1, is required for Golgi SNARE pairing. *EMBO J.* **28**, 2006–2017.

82 Pérez-Victoria FJ & Bonifacino JS (2009) Dual roles of the mammalian GARP complex in tethering and SNARE complex assembly at the trans-golgi network. *Mol. Cell. Biol.* **29**, 5251–63.

83 Pérez-Victoria FJ, Schindler C, Magadán JG, Mardones GA, Delevoye C, Romao M, Raposo G & Bonifacino JS (2010) Ang2/fat-free is a conserved subunit of the Golgi-associated retrograde protein complex. *Mol. Biol. Cell* **21**, 3386–95.

84 Laufman O, Hong W & Lev S (2013) The COG complex interacts with multiple Golgi SNAREs and enhances fusogenic assembly of SNARE complexes. *J. Cell Sci.* **126**.

85 Lin RC & Scheller RH (1997) Structural organization of the synaptic exocytosis core complex. *Neuron* **19**, 1087–94.

86 Monck JR & Fernandez JM (1996) The fusion pore and mechanisms of biological membrane fusion. *Curr. Opin. Cell Biol.* **8**, 524–33.

87 Chen YA & Scheller RH (2001) SNARE-mediated membrane fusion. *Nat. Rev. Mol. Cell Biol.* **2**, 98–106.

88 Jahn R & Scheller RH (2006) SNAREs - engines for membrane fusion. *Nat. Rev. Mol. Cell Biol.* **7**, 631–643.

89 Hershko A & Ciechanover A (1998) The ubiquitin system. *Annu. Rev. Biochem.* **67**, 425–479.

90 Grabbe C, Husnjak K & Dikic I (2011) The spatial and temporal organization of ubiquitin networks. *Nat. Rev. Mol. Cell Biol.* **12**, 295–307.

91 Rotin D & Kumar S (2009) Physiological functions of the HECT family of ubiquitin ligases. *Nat. Rev. Mol. Cell Biol.* **10**, 398–409.

92 Smit JJ & Sixma TK (2014) RBR E3-ligases at work. *EMBO Rep.* **15**, 142–154.

93 Deshaies RJ & Joazeiro CAP (2009) RING Domain E3 Ubiquitin Ligases. *Annu. Rev. Biochem.* **78**, 399–434.

94 Kerscher O, Felberbaum R & Hochstrasser M (2006) Modification of Proteins by Ubiquitin and Ubiquitin-Like Proteins. *Annu. Rev. Cell Dev. Biol.* **22**, 159–180.

95 Peng J, Schwartz D, Elias JE, Thoreen CC, Cheng D, Marsischky G, Roelofs J, Finley D & Gygi SP (2003) A proteomics approach to understanding protein ubiquitination. *Nat. Biotechnol.* **21**, 921–926.

96 Pickart CM & Fushman D (2004) Polyubiquitin chains: polymeric protein signals. *Curr. Opin. Chem. Biol.* **8**, 610–616.

97 Castañeda CA, Kashyap TR, Nakasone MA, Krueger S & Fushman D (2013) Unique structural, dynamical, and functional properties of k11-linked polyubiquitin chains. *Structure* **21**, 1168–81.

98 Komander D & Rape M (2012) The Ubiquitin Code. *Annu. Rev. Biochem.* **81**, 203–229.

99 Hunter T (2007) The age of crosstalk: phosphorylation, ubiquitination, and beyond. *Mol. Cell* **28**, 730–8.

100 Foot N, Henshall T & Kumar S (2016) Ubiquitination and the Regulation of Membrane Proteins. *Physiol. Rev.* **97**, 253–281.

101 Piper RC, Dikic I & Lukacs GL (2014) Ubiquitin-dependent sorting in endocytosis. *Cold Spring Harb. Perspect. Biol.* **6**, a016808-.

102 Vierstra RD (2012) The Expanding Universe of Ubiquitin and Ubiquitin-Like Modifiers. *PLANT Physiol.* **160**, 2–14.

103 Cajee U-F, Hull R & Ntwasa M (2012) Modification by Ubiquitin-Like Proteins: Significance in Apoptosis and Autophagy Pathways. *Int. J. Mol. Sci.* **13**, 11804–11831.

104 Mellman I & Warren G (2000) The road taken: past and future foundations of membrane traffic. *Cell* **100**, 99–112.

105 Spang A (2009) On vesicle formation and tethering in the ER–Golgi shuttle. *Curr. Opin. Cell Biol.* **21**, 531–536.

106 Farhan H & Rabouille C (2010) Signalling to and from the secretory pathway. *J. Cell Sci.* **124**.

107 Goeckeler JL & Brodsky JL (2010) Molecular chaperones and substrate ubiquitination control the efficiency of endoplasmic reticulum-associated degradation. *Diabetes. Obes. Metab.* **12 Suppl 2**, 32–8.

108 Christianson JC & Ye Y (2014) Cleaning up in the endoplasmic reticulum: ubiquitin in charge. *Nat. Struct. Mol. Biol.* **21**, 325–335.

109 Jackson CL (2009) Mechanisms of transport through the Golgi complex. *J. Cell Sci.* **122**, 443–52.

110 Pelham HR, Rothman JE, McNew J., Westermann B, Gmachl M, Parlati F, Söllner T., Rothman J., Rothman J. & Orci L (2000) The debate about transport in the Golgi--two sides of the same coin? *Cell* **102**, 713–9.

111 Urbanelli L, Magini A, Buratta S, Brozzi A, Sagini K, Polchi A, Tancini B & Emiliani C (2013) Signaling pathways in exosomes biogenesis, secretion and fate. *Genes (Basel).* **4**, 152–70.

112 Raposo G & Stoorvogel W (2013) Extracellular vesicles: Exosomes, microvesicles, and friends. *J. Cell Biol.* **200**, 373–383.

113 Sigismund S, Confalonieri S, Ciliberto A, Polo S, Scita G & Di Fiore PP (2012) Endocytosis and Signaling: Cell Logistics Shape the Eukaryotic Cell Plan. *Physiol. Rev.* **92**, 273–366.

114 Cossart P & Helenius A (2014) Endocytosis of Viruses and Bacteria. *Cold Spring Harb. Perspect. Biol.* **6**, a016972–a016972.

115 Williams JM & Tsai B (2016) Intracellular trafficking of bacterial toxins. *Curr. Opin. Cell Biol.* **41**, 51–56.

116 Lopez S & Arias C (2010) How Viruses Hijack Endocytic Machinery. *Nat. Educ.* **3**, 1–16.

117 Mayor S, Parton RG & Donaldson JG (2014) Clathrin-independent pathways of endocytosis. *Cold Spring Harb. Perspect. Biol.* **6**, a016758.

118 Elkin SR, Lakoduk AM & Schmid SL (2016) Endocytic pathways and endosomal trafficking: a primer. *Wien. Med. Wochenschr.* **166**, 196–204.

119 Cocucci E, Aguet F, Boulant S & Kirchhausen T (2012) The first five seconds in the life of a clathrin-coated pit. *Cell* **150**, 495–507.

120 Jackson LP, Kelly BT, McCoy AJ, Gaffry T, James LC, Collins BM, Höning S, Evans PR & Owen DJ (2010) A large-scale conformational change couples membrane recruitment to cargo binding in the AP2 clathrin adaptor complex. *Cell* **141**, 1220–9.

121 Kelly BT, Graham SC, Liska N, Dannhauser PN, Höning S, Ungewickell EJ & Owen DJ (2014) AP2 controls clathrin polymerization with a membrane-activated switch. *Science (80-.).* **345**, 459–463.

122 Qualmann B, Koch D & Kessels MM (2011) Let's go bananas: revisiting the endocytic BAR code. *EMBO J.* **30**, 3501–3515.

123 Doherty GJ & McMahon HT (2009) Mechanisms of Endocytosis. *Annu. Rev. Biochem.* **78**, 857–902.

124 McMahon HT & Boucrot E (2011) Molecular mechanism and physiological functions of clathrin-mediated endocytosis. *Nat. Rev. Mol. Cell Biol.* **12**, 517–33.

125 Traub LM (2003) Sorting it out: AP-2 and alternate clathrin adaptors in endocytic cargo selection. *J. Cell Biol.* **163**, 203–8.

126 Pelkmans L & Helenius A (2002) Endocytosis via caveolae. *Traffic* **3**, 311–20.

127 Nassar Z & Parat M (2015) Cavin Family: New Players in the Biology of Caveolae. *Int. Rev. Cell Mol. Biol.* **320**, 235–305.

128 Hansen CG & Nichols BJ (2009) Molecular mechanisms of clathrin-independent endocytosis. *J. Cell Sci.* **122**, 1713–1721.

129 Sandvig K, Torgersen ML, Engedal N, Skotland T & Iversen T-G (2010) Protein toxins from plants and bacteria: Probes for intracellular transport and tools in medicine. *FEBS Lett.* **584**, 2626–2634.

130 Mercer J, Schelhaas M & Helenius A (2010) Virus Entry by Endocytosis. *Annu. Rev. Biochem.* **79**, 803–833.

131 Parton RG & del Pozo MA (2013) Caveolae as plasma membrane sensors, protectors and organizers. *Nat. Rev. Mol. Cell Biol.* **14**, 98–112.

132 Lamaze C, Dujeancourt A, Baba T, Lo CG, Benmerah A & Dautry-Varsat A (2001) Interleukin 2 receptors and detergent-resistant membrane domains define a clathrin-independent endocytic pathway. *Mol. Cell* **7**, 661–71.

133 Basquin C, Malarde V, Mellor P, Anderson DH, Meas-Yedid V, Olivo-Marin J-C, Dautry-Varsat A & Sauvonnet N (2013) The signalling factor PI3K is a specific regulator of the clathrin-independent dynamin-dependent endocytosis of IL-2 receptors. *J. Cell Sci.* **126**, 1099–1108.

134 Grassart A, Dujeancourt A, Lazarow PB, Dautry-Varsat A & Sauvonnet N (2008) Clathrin-independent endocytosis used by the IL-2 receptor is regulated by Rac1, Pak1 and Pak2. *EMBO Rep.* **9**, 356–62.

135 Gesbert F, Sauvonnet N & Dautry-Varsat A (2004) Clathrin-Independent Endocytosis and Signalling of Interleukin 2 Receptors. In pp. 119–148. Springer, Berlin, Heidelberg.

136 Sabharanjak S, Sharma P, Parton RG & Mayor S (2002) GPI-anchored proteins are delivered to recycling endosomes via a distinct cdc42-regulated, clathrin-independent pinocytic pathway. *Dev. Cell* **2**, 411–23.

137 Gupta GD, M. G. S, Kumari S, Lakshminarayan R, Dey G & Mayor S (2009) Analysis of Endocytic Pathways in Drosophila Cells Reveals a Conserved Role for GBF1 in Internalization via GEECs. *PLoS One* **4**, e6768.

138 Kumari S & Mayor S (2008) ARF1 is directly involved in dynamin-independent endocytosis. *Nat. Cell Biol.* **10**, 30–41.

139 Lundmark R, Doherty GJ, Howes MT, Cortese K, Vallis Y, Parton RG & McMahon HT (2008) The GTPase-activating protein GRAF1 regulates the CLIC/GEEC endocytic pathway. *Curr. Biol.* **18**, 1802–8.

140 Radhakrishna H & Donaldson JG (1997) ADP-ribosylation factor 6 regulates a novel plasma membrane recycling pathway. *J. Cell Biol.* **139**, 49–61.

141 Eyster CA, Higginson JD, Huebner R, Porat-Shliom N, Weigert R, Wu WW, Shen R-F & Donaldson JG (2009) Discovery of New Cargo Proteins that Enter Cells through Clathrin-Independent Endocytosis. *Traffic* **10**, 590–599.

142 Naslavsky N, Weigert R & Donaldson JG (2004) Characterization of a nonclathrin endocytic pathway: membrane cargo and lipid requirements. *Mol. Biol. Cell* **15**, 3542–52.

143 Blagoveshchenskaya AD, Thomas L, Feliciangeli SF, Hung CH & Thomas G (2002) HIV-1 Nef downregulates MHC-I by a PACS-1- and PI3K-regulated ARF6 endocytic pathway. *Cell* **111**, 853–66.

144 Walseng E, Bakke O & Roche PA (2008) Major Histocompatibility Complex Class II-Peptide Complexes

Internalize Using a Clathrin- and Dynamin-independent Endocytosis Pathway. *J. Biol. Chem.* **283**, 14717–14727.

145 Brown FD, Rozelle AL, Yin HL, Balla T & Donaldson JG (2001) Phosphatidylinositol 4,5-bisphosphate and ARF6-regulated membrane traffic. *J. Cell Biol.* **154**, 1007–1018.

146 Jovanovic OA, Brown FD & Donaldson JG (2006) An effector domain mutant of ARF6 implicates phospholipase D in endosomal membrane recycling. *Mol. Biol. Cell* **17**, 327–35.

147 Grant BD & Donaldson JG (2009) Pathways and mechanisms of endocytic recycling. *Nat. Rev. Mol. Cell Biol.* **10**, 597–608.

148 Naslavsky N, Weigert R & Donaldson JG (2003) Convergence of Non-clathrin- and Clathrin-derived Endosomes Involves ARF6 Inactivation and Changes in Phosphoinositides. *Mol. Biol. Cell* **14**, 417–431.

149 Glebov OO, Bright NA & Nichols BJ (2006) Flotillin-1 defines a clathrin-independent endocytic pathway in mammalian cells. *Nat. Cell Biol.* **8**, 46–54.

150 Frick M, Bright NA, Riento K, Bray A, Merrified C & Nichols BJ (2007) Coassembly of Flotillins Induces Formation of Membrane Microdomains, Membrane Curvature, and Vesicle Budding. *Curr. Biol.* **17**, 1151–1156.

151 Payne CK, Jones SA, Chen C & Zhuang X (2007) Internalization and Trafficking of Cell Surface Proteoglycans and Proteoglycan-Binding Ligands. *Traffic* **8**, 389–401.

152 Chimini G & Chavrier P (2000) Function of Rho family proteins in actin dynamics during phagocytosis and engulfment. *Nat. Cell Biol.* **2**, E191–E196.

153 Yamada H, Ohashi E, Abe T, Kusumi N, Li S-A, Yoshida Y, Watanabe M, Tomizawa K, Kashiwakura Y, Kumon H, Matsui H & Takei K (2007) Amphiphysin 1 is important for actin polymerization during phagocytosis. *Mol. Biol. Cell* **18**, 4669–80.

154 Dharmawardhane S, Schürmann A, Sells MA, Chernoff J, Schmid SL & Bokoch GM (2000) Regulation of macropinocytosis by p21-activated kinase-1. *Mol. Biol. Cell* **11**, 3341–52.

155 Amyere M, Payrastre B, Krause U, Van Der Smissen P, Veithen A & Courtoy PJ (2000) Constitutive macropinocytosis in oncogene-transformed fibroblasts depends on sequential permanent activation of phosphoinositide 3-kinase and phospholipase C. *Mol. Biol. Cell* **11**, 3453–67.

156 Veithen A, Cupers P, Baudhuin P & Courtoy PJ (1996) v-Src induces constitutive macropinocytosis in rat fibroblasts. *J. Cell Sci.* **109 (Pt 8)**, 2005–12.

157 Krueger EW, Orth JD, Cao H & McNiven MA (2003) A Dynamin-Cortactin-Arp2/3 Complex Mediates Actin Reorganization in Growth Factor-stimulated Cells. *Mol. Biol. Cell* **14**, 1085–1096.

158 Orth JD, Krueger EW, Weller SG & McNiven MA (2006) A Novel Endocytic Mechanism of Epidermal Growth Factor Receptor Sequestration and Internalization. *Cancer Res.* **66**, 3603–3610.

159 Boucrot E, Ferreira APA, Almeida-Souza L, Debard S, Vallis Y, Howard G, Bertot L, Sauvonnet N & McMahon HT (2014) Endophilin marks and controls a clathrin-independent endocytic pathway. *Nature* **517**, 460–465.

160 Renard H-F, Simunovic M, Lemière J, Boucrot E, Garcia-Castillo MD, Arumugam S, Chambon V, Lamaze C, Wunder C, Kenworthy AK, Schmidt AA, McMahon HT, Sykes C, Bassereau P & Johannes L (2014) Endophilin-A2 functions in membrane scission in clathrin-independent endocytosis. *Nature* **517**, 493–496.

161 Sorkin A & von Zastrow M (2009) Endocytosis and signalling: intertwining molecular networks. *Nat. Rev. Mol. Cell Biol.* **10**, 609–22.

162 Gould GW & Lippincott-Schwartz J (2009) New roles for endosomes: from vesicular carriers to multi-purpose platforms. *Nat. Rev. Mol. Cell Biol.* **10**, 287–92.

163 Shilo B-Z & Schejter ED (2011) Regulation of developmental intercellular signalling by intracellular trafficking. *EMBO J.* **30**, 3516–3526.

164 Sigismund S, Argenzio E, Tosoni D, Cavallaro E, Polo S & Di Fiore PP (2008) Clathrin-Mediated Internalization Is Essential for Sustained EGFR Signaling but Dispensable for Degradation. *Dev. Cell* **15**, 209–219.

165 Barbieri E, Di Fiore PP & Sigismund S (2016) Endocytic control of signaling at the plasma membrane. *Curr. Opin. Cell Biol.* **39**, 21–27.

166 Di Paolo G & De Camilli P (2006) Phosphoinositides in cell regulation and membrane dynamics. *Nature* **443**, 651–657.

167 Balla T (2005) Inositol-lipid binding motifs: signal integrators through protein-lipid and protein-protein interactions. *J. Cell Sci.* **118**, 2093–2104.

168 Jean S & Kiger AA (2012) Coordination between RAB GTPase and phosphoinositide regulation and functions. *Nat. Rev. Mol. Cell Biol.* **13**, 463–470.

169 Mellman I, Fuchs R & Helenius A (1986) Acidification of the Endocytic and Exocytic Pathways. *Annu. Rev.*

Biochem. **55**, 663–700.

170 Scott CC & Gruenberg J (2011) Ion flux and the function of endosomes and lysosomes: pH is just the start. *BioEssays* **33**, 103–110.

171 Huotari J & Helenius A (2011) Endosome maturation. *EMBO J.* **30**, 3481–500.

172 Spang A (2016) Membrane Tethering Complexes in the Endosomal System. *Front. cell Dev. Biol.* **4**, 35.

173 Gruenberg J & Stenmark H (2004) The biogenesis of multivesicular endosomes. *Nat. Rev. Mol. Cell Biol.* **5**, 317–23.

174 Vlassov A V., Magdaleno S, Setterquist R & Conrad R (2012) Exosomes: Current knowledge of their composition, biological functions, and diagnostic and therapeutic potentials. *Biochim. Biophys. Acta - Gen. Subj.* **1820**, 940–948.

175 Johannes L & Popoff V (2008) Tracing the retrograde route in protein trafficking. *Cell* **135**, 1175–87.

176 Shin H-W, Hayashi M, Christoforidis S, Lacas-Gervais S, Hoepfner S, Wenk MR, Modregger J, Uttenweiler-Joseph S, Wilm M, Nystuen A, Frankel WN, Solimena M, De Camilli P & Zerial M (2005) An enzymatic cascade of Rab5 effectors regulates phosphoinositide turnover in the endocytic pathway. *J. Cell Biol.* **170**, 607–618.

177 Hurley JH & Emr SD (2006) The ESCRT complexes: structure and mechanism of a membrane-trafficking network. *Annu. Rev. Biophys. Biomol. Struct.* **35**, 277–98.

178 Williams RL & Urbé S (2007) The emerging shape of the ESCRT machinery. *Nat. Rev. Mol. Cell Biol.* **8**, 355–68.

179 Schmidt O & Teis D (2012) The ESCRT machinery. *Curr. Biol.* **22**, R116-20.

180 Alfred V & Vaccari T (2016) When membranes need an ESCRT: endosomal sorting and membrane remodelling in health and disease. *Swiss Med. Wkly.* **146**, w14347.

181 Langelier C, von Schwedler UK, Fisher RD, De Domenico I, White PL, Hill CP, Kaplan J, Ward D & Sundquist WI (2006) Human ESCRT-II Complex and Its Role in Human Immunodeficiency Virus Type 1 Release. *J. Virol.* **80**, 9465–9480.

182 Carlton JG & Martin-Serrano J (2007) Parallels Between Cytokinesis and Retroviral Budding: A Role for the ESCRT Machinery. *Science (80-.).* **316**.

183 Rusten TE, Vaccari T, Lindmo K, Rodahl LMW, Nezis IP, Sem-Jacobsen C, Wendler F, Vincent J-P, Brech A, Bilder D & Stenmark H (2007) ESCRTs and Fab1 Regulate Distinct Steps of Autophagy. *Curr. Biol.* **17**, 1817–1825.

184 Kobayashi T, Stang E, Fang KS, de Moerloose P, Parton RG & Gruenberg J (1998) A lipid associated with the antiphospholipid syndrome regulates endosome structure and function. *Nature* **392**, 193–197.

185 Matsuo H, Chevallier J, Mayran N, Le Blanc I, Ferguson C, Fauré J, Blanc NS, Matile S, Dubochet J, Sadoul R, Parton RG, Vilbois F & Gruenberg J (2004) Role of LBPA and Alix in Multivesicular Liposome Formation and Endosome Organization. *Science (80-.).* **303**, 531–534.

186 Bissig C & Gruenberg J (2014) ALIX and the multivesicular endosome: ALIX in Wonderland. *Trends Cell Biol.* **24**, 19–25.

187 Eden ER, White IJ, Tsapara A & Futter CE (2010) Membrane contacts between endosomes and ER provide sites for PTP1B–epidermal growth factor receptor interaction. *Nat. Cell Biol.* **12**, 267–72.

188 Chang T-Y, Chang CCY, Ohgami N & Yamauchi Y (2006) Cholesterol Sensing, Trafficking, and Esterification. *Annu. Rev. Cell Dev. Biol.* **22**, 129–157.

189 Castellano BM, Thelen AM, Moldavski O, Feltes M, van der Welle REN, Mydock-McGrane L, Jiang X, van Eijkeren RJ, Davis OB, Louie SM, Perera RM, Covey DF, Nomura DK, Ory DS & Zoncu R (2017) Lysosomal cholesterol activates mTORC1 via an SLC38A9–Niemann-Pick C1 signaling complex. *Science (80-.).* **355**, 1306–1311.

190 Laplante M & Sabatini DM (2009) mTOR signaling at a glance. *J. Cell Sci.* **122**, 3589–3594.

191 Mulcahy LA, Pink RC & Carter DRF (2014) Routes and mechanisms of extracellular vesicle uptake. *J. Extracell. Vesicles* **3**, 24641.

192 Edgar JR (2016) Q&A: What are exosomes, exactly? *BMC Biol.* **14**, 46.

193 Valadi H, Ekström K, Bossios A, Sjöstrand M, Lee JJ & Lötvall JO (2007) Exosome-mediated transfer of mRNAs and microRNAs is a novel mechanism of genetic exchange between cells. *Nat. Cell Biol.* **9**, 654–659.

194 Melo SA, Sugimoto H, O'Connell JT, Kato N, Villanueva A, Vidal A, Qiu L, Vitkin E, Perelman LT, Melo CA, Lucci A, Ivan C, Calin GA & Kalluri R (2014) Cancer Exosomes Perform Cell-Independent MicroRNA Biogenesis and Promote Tumorigenesis. *Cancer Cell* **26**, 707–721.

195 Zhang J, Li S, Li L, Li M, Guo C, Yao J & Mi S (2015) Exosome and Exosomal MicroRNA: Trafficking, Sorting, and Function. *Genomics. Proteomics Bioinformatics* **13**, 17–24.

196 Maxfield FR & McGraw TE (2004) Endocytic recycling. *Nat. Rev. Mol. Cell Biol.* **5**, 121–32.

197 Yamashiro DJ, Tycko B, Fluss SR & Maxfield FR (1984) Segregation of transferrin to a mildly acidic (pH 6.5) para-Golgi compartment in the recycling pathway. *Cell* **37**, 789–800.

198 Weigert R, Yeung AC, Li J & Donaldson JG (2004) Rab22a regulates the recycling of membrane proteins internalized independently of clathrin. *Mol. Biol. Cell* **15**, 3758–70.

199 Tan X, Thapa N, Choi S & Anderson RA (2015) Emerging roles of PtdIns(4,5)P 2 – beyond the plasma membrane. *J. Cell Sci.* **128**, 4047–4056.

200 Prigent M, Dubois T, Raposo G, Derrien V, Tenza D, Rossé C, Camonis J & Chavrier P (2003) ARF6 controls post-endocytic recycling through its downstream exocyst complex effector. *J. Cell Biol.* **163**, 1111–1121.

201 Montagnac G, Sibarita J-B, Loubéry S, Daviet L, Romao M, Raposo G, Chavrier P, Chavrier P, Houdusse A & Yamamoto KI (2009) ARF6 Interacts with JIP4 to control a motor switch mechanism regulating endosome traffic in cytokinesis. *Curr. Biol.* **19**, 184–95.

202 Husebye H, Aune MH, Stenvik J, Samstad E, Skjeldal F, Halaas Ø, Nilsen NJ, Stenmark H, Latz E, Lien E, Mollnes TE, Bakke O & Espevik T (2010) The Rab11a GTPase Controls Toll-like Receptor 4-Induced Activation of Interferon Regulatory Factor-3 on Phagosomes. *Immunity* **33**, 583–596.

203 Emery G, Hutterer A, Berdnik D, Mayer B, Wirtz-Peitz F, Gaitan MG & Knoblich JA (2005) Asymmetric Rab11 Endosomes Regulate Delta Recycling and Specify Cell Fate in the Drosophila Nervous System. *Cell* **122**, 763–773.

204 Burd CG (2011) Physiology and pathology of endosome-to-Golgi retrograde sorting. *Traffic* **12**, 948–55.

205 Ghosh RN, Mallet WG, Soe TT, McGraw TE & Maxfield FR (1998) An endocytosed TGN38 chimeric protein is delivered to the TGN after trafficking through the endocytic recycling compartment in CHO cells. *J. Cell Biol.* **142**, 923–36.

206 Mallet WG & Maxfield FR (1999) Chimeric forms of furin and TGN38 are transported with the plasma membrane in the trans-Golgi network via distinct endosomal pathways. *J. Cell Biol.* **146**, 345–59.

207 Molloy SS, Thomas L, VanSlyke JK, Stenberg PE & Thomas G (1994) Intracellular trafficking and activation of the furin proprotein convertase: localization to the TGN and recycling from the cell surface. *EMBO J.* **13**, 18–33.

208 Sandvig K, Garred Ø, Prydz K, Kozlov J V., Hansen SH & van Deurs B (1992) Retrograde transport of endocytosed Shiga toxin to the endoplasmic reticulum. *Nature* **358**, 510–512.

209 Lencer W & Tsai B (2003) The intracellular voyage of cholera toxin: going retro. *Trends Biochem. Sci.* **28**, 639–645.

210 Braulke T & Bonifacino JS (2009) Sorting of lysosomal proteins. *Biochim. Biophys. Acta* **1793**, 605–14.

211 Lin SX, Mallet WG, Huang AY & Maxfield FR (2004) Endocytosed cation-independent mannose 6-phosphate receptor traffics via the endocytic recycling compartment en route to the trans-Golgi network and a subpopulation of late endosomes. *Mol. Biol. Cell* **15**, 721–33.

212 McKenzie JE, Raisley B, Zhou X, Naslavsky N, Taguchi T, Caplan S & Sheff D (2012) Retromer guides STxB and CD8-M6PR from early to recycling endosomes, EHD1 guides STxB from recycling endosome to Golgi. *Traffic* **13**, 1140–59.

213 Barbero P, Bittova L & Pfeffer SR (2002) Visualization of Rab9-mediated vesicle transport from endosomes to the trans-Golgi in living cells. *J. Cell Biol.* **156**, 511–8.

214 Bonifacino JS & Hurley JH (2008) Retromer. *Curr. Opin. Cell Biol.* **20**, 427–36.

215 Seaman MNJ (2012) The retromer complex - endosomal protein recycling and beyond. *J. Cell Sci.* **125**, 4693–702.

216 van Weering JRT, Verkade P & Cullen PJ (2010) SNX–BAR proteins in phosphoinositide-mediated, tubular-based endosomal sorting. *Semin. Cell Dev. Biol.* **21**, 371–380.

217 Cullen PJ & Korswagen HC (2012) Sorting nexins provide diversity for retromer-dependent trafficking events. *Nat. Cell Biol.* **14**, 29–37.

218 Zhang P, Wu Y, Belenkaya TY & Lin X (2011) SNX3 controls Wingless/Wnt secretion through regulating retromer-dependent recycling of Wntless. *Cell Res.* **21**, 1677–1690.

219 Seaman MNJ (2004) Cargo-selective endosomal sorting for retrieval to the Golgi requires retromer. *J. Cell Biol.* **165**, 111–22.

220 Popoff V, Mardones GA, Tenza D, Rojas R, Lamaze C, Bonifacino JS, Raposo G & Johannes L (2007) The retromer complex and clathrin define an early endosomal retrograde exit site. *J. Cell Sci.* **120**, 2022–31.

221 Lu L & Hong W (2014) From endosomes to the trans-Golgi network. *Semin. Cell Dev. Biol.* **31**, 30–9.

222 Burd C & Cullen PJ (2014) Retromer: a master conductor of endosome sorting. *Cold Spring Harb. Perspect. Biol.* **6**, a016774.

223 Muhammad A, Flores I, Zhang H, Yu R, Staniszewski A, Planel E, Herman M, Ho L, Kreber R, Honig LS,

Ganetzky B, Duff K, Arancio O & Small SA (2008) Retromer deficiency observed in Alzheimer's disease causes hippocampal dysfunction, neurodegeneration, and A accumulation. *Proc. Natl. Acad. Sci.* **105**, 7327–7332.

224 Vardarajan BN, Bruesegem SY, Harbour ME, George-Hyslop P St., Seaman MNJ, Farrer LA, Seaman MNJ & Farrer LA (2012) Identification of Alzheimer disease-associated variants in genes that regulate retromer function. *Neurobiol. Aging* **33**, 2231.e15-2231.e30.

225 Fjorback AW, Seaman M, Gustafsen C, Mehmedbasic A, Gokool S, Wu C, Militz D, Schmidt V, Madsen P, Nyengaard JR, Willnow TE, Christensen EI, Mobley WB, Nykjaer A & Andersen OM (2012) Retromer Binds the FANSHY Sorting Motif in SorLA to Regulate Amyloid Precursor Protein Sorting and Processing. *J. Neurosci.* **32**, 1467–1480.

226 Small SA & Petsko GA (2015) Retromer in Alzheimer disease, Parkinson disease and other neurological disorders. *Nat. Rev. Neurosci.* **16**, 126–132.

227 Arribas J & Borroto A (2002) Protein ectodomain shedding. *Chem. Rev.* **102**, 4627–38.

228 Hayashida K, Bartlett AH, Chen Y & Park PW (2010) Molecular and cellular mechanisms of ectodomain shedding. *Anat. Rec. (Hoboken).* **293**, 925–37.

229 Arribas J, Coodly L, Vollmer P, Kishimoto TK, RoseJohn S & Massague J (1996) Diverse cell surface protein ectodomains are shed by a system sensitive to metalloprotease inhibitors. *J. Biol. Chem.* **271**, 11376–11382.

230 Reiss K & Saftig P (2009) The "A Disintegrin And Metalloprotease" (ADAM) family of sheddases: Physiological and cellular functions. *Semin. Cell Dev. Biol.* **20**, 126–137.

231 Black RA, Rauch CT, Kozlosky CJ, Peschon JJ, Slack JL, Wolfson MF, Castner BJ, Stocking KL, Reddy P, Srinivasan S, Nelson N, Boiani N, Schooley KA, Gerhart M, Davis R, Fitzner JN, Johnson RS, Paxton RJ, March CJ & Cerretti DP (1997) A metalloproteinase disintegrin that releases tumour-necrosis factor-α from cells. *Nature* **385**, 729–733.

232 Wauman J, De Ceuninck L, Vanderroost N, Lievens S & Tavernier J (2011) RNF41 (Nrdp1) controls type 1 cytokine receptor degradation and ectodomain shedding. *J. Cell Sci.* **124**, 921–32.

233 Edwards DR, Handsley MM & Pennington CJ (2008) The ADAM metalloproteinases. *Mol. Aspects Med.* **29**, 258–89.

234 Loechel F, Overgaard MT, Oxvig C, Albrechtsen R & Wewer UM (1999) Regulation of human ADAM 12 protease by the prodomain. Evidence for a functional cysteine switch. *J. Biol. Chem.* **274**, 13427–33.

235 Endres K, Anders A, Kojro E, Gilbert S, Fahrenholz F & Postina R (2003) Tumor necrosis factor-alpha converting enzyme is processed by proprotein-convertases to its mature form which is degraded upon phorbol ester stimulation. *Eur. J. Biochem.* **270**, 2386–2393.

236 Hinkle CL, Sunnarborg SW, Loiselle D, Parker CE, Stevenson M, Russell WE & Lee DC (2004) Selective Roles for Tumor Necrosis Factor α-converting Enzyme/ADAM17 in the Shedding of the Epidermal Growth Factor Receptor Ligand Family. *J. Biol. Chem.* **279**, 24179–24188.

237 Matthews V, Schuster B, Schütze S, Bussmeyer I, Ludwig A, Hundhausen C, Sadowski T, Saftig P, Hartmann D, Kallen K-J & Rose-John S (2003) Cellular Cholesterol Depletion Triggers Shedding of the Human Interleukin-6 Receptor by ADAM10 and ADAM17 (TACE). *J. Biol. Chem.* **278**, 38829–38839.

238 Taga T, Hibi M, Hirata Y, Yamasaki K, Yasukawa K, Matsuda T, Hirano T & Kishimoto T (1989) Interleukin-6 triggers the association of its receptor with a possible signal transducer, gp130. *Cell* **58**, 573–81.

239 Levine SJ (2004) Mechanisms of soluble cytokine receptor generation. *J. Immunol.* **173**, 5343–8.

240 Mizushima N (2007) Autophagy: process and function. *Genes Dev.* **21**, 2861–73.

241 Boya P, Reggiori F & Codogno P (2013) Emerging regulation and functions of autophagy. *Nat. Cell Biol.* **15**, 713–20.

242 Stolz A, Ernst A & Dikic I (2014) Cargo recognition and trafficking in selective autophagy. *Nat. Cell Biol.* **16**, 495–501.

243 Zaffagnini G & Martens S (2016) Mechanisms of Selective Autophagy. *J. Mol. Biol.* **428**, 1714–24.

244 Kaushik S, Bandyopadhyay U, Sridhar S, Kiffin R, Martinez-Vicente M, Kon M, Orenstein SJ, Wong E & Cuervo AM (2011) Chaperone-mediated autophagy at a glance. *J. Cell Sci.* **124**, 495–9.

245 Sahu R, Kaushik S, Clement CC, Cannizzo ES, Scharf B, Follenzi A, Potolicchio I, Nieves E, Cuervo AM & Santambrogio L (2011) Microautophagy of Cytosolic Proteins by Late Endosomes. *Dev. Cell* **20**, 131–139.

246 Xie Z & Klionsky DJ (2007) Autophagosome formation: core machinery and adaptations. *Nat. Cell Biol.* **9**, 1102–1109.

247 Kraft C & Martens S (2012) Mechanisms and regulation of autophagosome formation. *Curr. Opin. Cell Biol.* **24**, 496–501.

248 Amaya C, Fader CM & Colombo MI (2015) Autophagy and proteins involved in vesicular trafficking. *FEBS*

Lett. **589**, 3343–3353.

249 Matsuura A, Tsukada M, Wada Y & Ohsumi Y (1997) Apg1p, a novel protein kinase required for the autophagic process in Saccharomyces cerevisiae. *Gene* **192**, 245–50.

250 Kim J, Kundu M, Viollet B & Guan K-L (2011) AMPK and mTOR regulate autophagy through direct phosphorylation of Ulk1. *Nat. Cell Biol.* **13**, 132–141.

251 Russell RC, Tian Y, Yuan H, Park HW, Chang Y-Y, Kim J, Kim H, Neufeld TP, Dillin A & Guan K-L (2013) ULK1 induces autophagy by phosphorylating Beclin-1 and activating VPS34 lipid kinase. *Nat. Cell Biol.* **15**, 741–50.

252 Roberts R & Ktistakis NT (2013) Omegasomes: PI3P platforms that manufacture autophagosomes. *Essays Biochem.* **55**.

253 Dooley HC, Razi M, Polson HEJ, Girardin SE, Wilson MI & Tooze SA (2014) WIPI2 Links LC3 Conjugation with PI3P, Autophagosome Formation, and Pathogen Clearance by Recruiting Atg12–5-16L1. *Mol. Cell* **55**, 238–252.

254 Tanida I, Ueno T & Kominami E (2004) LC3 conjugation system in mammalian autophagy. *Int. J. Biochem. Cell Biol.* **36**, 2503–2518.

255 Hanada T, Noda NN, Satomi Y, Ichimura Y, Fujioka Y, Takao T, Inagaki F & Ohsumi Y (2007) The Atg12-Atg5 Conjugate Has a Novel E3-like Activity for Protein Lipidation in Autophagy. *J. Biol. Chem.* **282**, 37298–37302.

256 Kabeya Y, Mizushima N, Ueno T, Yamamoto A, Kirisako T, Noda T, Kominami E, Ohsumi Y & Yoshimori T (2000) LC3, a mammalian homologue of yeast Apg8p, is localized in autophagosome membranes after processing. *EMBO J.* **19**, 5720–5728.

257 Mari M, Griffith J, Rieter E, Krishnappa L, Klionsky DJ & Reggiori F (2010) An Atg9-containing compartment that functions in the early steps of autophagosome biogenesis. *J. Cell Biol.* **190**.

258 Rusten TE & Stenmark H (2009) How do ESCRT proteins control autophagy? *J. Cell Sci.* **122**, 2179–83.

259 Jiang P, Nishimura T, Sakamaki Y, Itakura E, Hatta T, Natsume T & Mizushima N (2014) The HOPS complex mediates autophagosome-lysosome fusion through interaction with syntaxin 17. *Mol. Biol. Cell* **25**, 1327–1337.

260 Carlsson SR & Simonsen A (2015) Membrane dynamics in autophagosome biogenesis. *J. Cell Sci.* **128**, 193–205.

261 Lippai M & Low P (2014) The role of the selective adaptor p62 and ubiquitin-like proteins in autophagy. *Biomed Res. Int.*

262 Bento CF, Renna M, Ghislat G, Puri C, Ashkenazi A, Vicinanza M, Menzies FM & Rubinsztein DC (2016) Mammalian Autophagy: How Does It Work? *Annu. Rev. Biochem.* **85**, 685–713.

263 Suzuki K & Ohsumi Y (2010) Current knowledge of the pre-autophagosomal structure (PAS). *FEBS Lett.* **584**, 1280–1286.

264 Lamb CA, Yoshimori T & Tooze SA (2013) The autophagosome: origins unknown, biogenesis complex. *Nat. Rev. Mol. Cell Biol.* **14**, 759–774.

265 Tan D, Cai Y, Wang J, Zhang J, Menon S, Chou H-T, Ferro-Novick S, Reinisch KM & Walz T (2013) The EM structure of the TRAPPIII complex leads to the identification of a requirement for COPII vesicles on the macroautophagy pathway. *Proc. Natl. Acad. Sci.* **110**, 19432–19437.

266 Abdullah JM, Li X, Nachtman RG & Jurecic R (2001) FLRF, a novel evolutionarily conserved RING finger gene, is differentially expressed in mouse fetal and adult hematopoietic stem cells and progenitors. *Blood Cells. Mol. Dis.* **27**, 320–33.

267 Joazeiro CA. & Weissman AM (2000) RING Finger Proteins: Mediators of Ubiquitin ligase activity. *Cell* **102**, 549–552.

268 Diamonti AJ, Guy PM, Ivanof C, Wong K, Sweeney C & Carraway KL (2002) An RBCC protein implicated in maintenance of steady-state neuregulin receptor levels. *Proc. Natl. Acad. Sci. U. S. A.* **99**, 2866–71.

269 Qiu X-B & Goldberg AL (2002) Nrdp1/FLRF is a ubiquitin ligase promoting ubiquitination and degradation of the epidermal growth factor receptor family member, ERBB3. *Proc. Natl. Acad. Sci. U. S. A.* **99**, 14843–8.

270 Olayioye MA, Neve RM, Lane HA & Hynes NE (2000) NEW EMBO MEMBERS' REVIEW: The ErbB signaling network: receptor heterodimerization in development and cancer. *EMBO J.* **19**, 3159–3167.

271 Yarden Y & Sliwkowski MX (2001) Untangling the ErbB signalling network. *Nat. Rev. Mol. Cell Biol.* **2**, 127–137.

272 Bouyain S & Leahy DJ (2007) Structure-based mutagenesis of the substrate-recognition domain of Nrdp1/FLRF identifies the binding site for the receptor tyrosine kinase ErbB3. *Protein Sci.* **16**, 654–61.

273 Fry WHD, Simion C, Sweeney C & Carraway KL (2011) Quantity control of the ErbB3 receptor tyrosine kinase at the endoplasmic reticulum. *Mol. Cell. Biol.* **31**, 3009–18.

274 Hatakeyama J, Wald JH, Rafidi H, Cuevas A, Sweeney C & Carraway KL (2016) The ER structural protein Rtn4A stabilizes and enhances signaling through the receptor tyrosine kinase ErbB3. *Sci. Signal.* **9**.

275 Cao Z, Wu X, Yen L, Sweeney C & Carraway KL (2007) Neuregulin-induced ErbB3 downregulation is mediated by a protein stability cascade involving the E3 ubiquitin ligase Nrdp1. *Mol. Cell. Biol.* **27**, 2180–8.

276 Wu X, Yen L, Irwin L, Sweeney C & Carraway KL (2004) Stabilization of the E3 ubiquitin ligase Nrdp1 by the deubiquitinating enzyme USP8. *Mol. Cell. Biol.* **24**, 7748–57.

277 Maddirevula S, Anuppalle M, Huh T-L, Kim SH & Rhee M (2011) *Nrdp1 governs differentiation of the melanocyte lineage via Erbb3b signaling in the zebrafish embryogenesis*.

278 Jing X, Infante J, Nachtman RG & Jurecic R (2008) E3 ligase FLRF (Rnf41) regulates differentiation of hematopoietic progenitors by governing steady-state levels of cytokine and retinoic acid receptors. *Exp. Hematol.* **36**, 1110–20.

279 Ye S, Xu H, Jin J, Yang M, Wang C, Yu Y & Cao X (2012) The E3 ubiquitin ligase neuregulin receptor degradation protein 1 (Nrdp1) promotes M2 macrophage polarization by ubiquitinating and activating transcription factor CCAAT/enhancer-binding Protein β (C/EBPβ). *J. Biol. Chem.* **287**, 26740–8.

280 Wang C, Chen T, Zhang J, Yang M, Li N, Xu X & Cao X (2009) The E3 ubiquitin ligase Nrdp1 "preferentially" promotes TLR-mediated production of type I interferon. *Nat. Immunol.* **10**, 744–52.

281 Zhu L, Bi W, Lu D, Zhang C, Shu X, Wang H, Qi R, Shi Q & Lu D (2015) Regulation of ubiquitin-specific processing protease 8 suppresses neuroinflammation. *Mol. Cell. Neurosci.* **64**, 74–83.

282 Zhang DL, Yu DH, Chen J, Fan S & Wang ZY (2015) Expression profiles and interaction suggest TBK1 can be regulated by Nrdp1 in response to immune stimulation in large yellow croaker Larimichthys crocea. *Fish Shellfish Immunol.* **46**, 745–752.

283 Yang M, Chen T, Li X, Yu Z, Tang S, Wang C, Gu Y, Liu Y, Xu S, Li W, Zhang X, Wang J & Cao X (2015) K33-linked polyubiquitination of Zap70 by Nrdp1 controls CD8+ T cell activation. *Nat. Immunol.* **16**, 1253–1262.

284 Elmore S (2007) Apoptosis: a review of programmed cell death. *Toxicol. Pathol.* **35**, 495–516.

285 Salvesen GS, Dixit VM, Vanags D., Orrenius S, Timkey T, Garcia-Calvo M, Houtzager V., Nordstrom P., Roy S, Vaillancourt J. & al. et (1997) Caspases: intracellular signaling by proteolysis. *Cell* **91**, 443–6.

286 White E (1996) Life, death, and the pursuit of apoptosis. *Genes Dev.* **10**, 1–15.

287 Li P, Nijhawan D, Budihardjo I, Srinivasula SM, Ahmad M, Alnemri ES & Wang X (1997) Cytochrome c and dATP-Dependent Formation of Apaf-1/Caspase-9 Complex Initiates an Apoptotic Protease Cascade. *Cell* **91**, 479–489.

288 Bump NJ, Hackett M, Hugunin M, Seshagiri S, Brady K, Chen P, Ferenz C, Franklin S, Ghayur T & Li P (1995) Inhibition of ICE family proteases by baculovirus antiapoptotic protein p35. *Science* **269**, 1885–8.

289 CLEM R & DUCKETT C (1997) The genes: unique arbitrators of cell death. *Trends Cell Biol.* **7**, 337–339.

290 Hauser HP, Bardroff M, Pyrowolakis G & Jentsch S (1998) A giant ubiquitin-conjugating enzyme related to IAP apoptosis inhibitors. *J. Cell Biol.* **141**, 1415–22.

291 Hao Y, Sekine K, Kawabata A, Nakamura H, Ishioka T, Ohata H, Katayama R, Hashimoto C, Zhang X, Noda T, Tsuruo T & Naito M (2004) Apollon ubiquitinates SMAC and caspase-9, and has an essential cytoprotection function. *Nat. Cell Biol.* **6**, 849–860.

292 Qiu X-B, Markant SL, Yuan J & Goldberg AL (2004) Nrdp1-mediated degradation of the gigantic IAP, BRUCE, is a novel pathway for triggering apoptosis. *EMBO J.* **23**, 800–10.

293 Chen Z, Naito M, Hori S, Mashima T, Yamori T & Tsuruo T (1999) A Human IAP-Family Gene, Apollon, Expressed in Human Brain Cancer Cells. *Biochem. Biophys. Res. Commun.* **264**, 847–854.

294 Shi H, Du J, Wang L, Zheng B, Gong H, Wu Y, Tang Y, Gao Y & Yu R (2014) Lower expression of Nrdp1 in human glioma contributes tumor progression by reducing apoptosis. *IUBMB Life* **66**, 704–710.

295 Shen JJ, Song Y, Shen JJ, Lin Y, Wu X, Yan Y, Niu M, Zhou L, Huang Y, Gao Y & Liu Y (2015) Nrdp1 is Associated with Neuronal Apoptosis in Lipopolysaccharide-Induced Neuroinflammation. *Neurochem. Res.* **40**, 971–979.

296 Naviglio S, Mattecucci C, Matoskova B, Nagase T, Nomura N, Di Fiore PP & Draetta GF (1998) UBPY: a growth-regulated human ubiquitin isopeptidase. *EMBO J.* **17**, 3241–50.

297 Hislop JN, Henry AG, Marchese A & von Zastrow M (2009) Ubiquitination regulates proteolytic processing of G protein-coupled receptors after their sorting to lysosomes. *J. Biol. Chem.* **284**, 19361–70.

298 Hasdemir B, Murphy JE, Cottrell GS & Bunnett NW (2009) Endosomal deubiquitinating enzymes control ubiquitination and down-regulation of protease-activated receptor 2. *J. Biol. Chem.* **284**, 28453–66.

299 Balut CM, Loch CM & Devor DC (2011) Role of ubiquitylation and USP8-dependent deubiquitylation in the endocytosis and lysosomal targeting of plasma membrane KCa3.1. *FASEB J.* **25**, 3938–48.

300 Mizuno E, Iura T, Mukai A, Yoshimori T, Kitamura N & Komada M (2005) Regulation of epidermal growth factor receptor down-regulation by UBPY-mediated deubiquitination at endosomes. *Mol. Biol. Cell* **16**, 5163–74.

301 Niendorf S, Oksche A, Kisser A, Löhler J, Prinz M, Schorle H, Feller S, Lewitzky M, Horak I & Knobeloch K-P (2007) Essential role of ubiquitin-specific protease 8 for receptor tyrosine kinase stability and endocytic trafficking in vivo. *Mol. Cell. Biol.* **27**, 5029–39.

302 Berlin I, Schwartz H & Nash PD (2010) Regulation of epidermal growth factor receptor ubiquitination and trafficking by the USP8·STAM complex. *J. Biol. Chem.* **285**, 34909–21.

303 Berlin I, Higginbotham KM, Dise RS, Sierra MI & Nash PD (2010) The deubiquitinating enzyme USP8 promotes trafficking and degradation of the chemokine receptor 4 at the sorting endosome. *J. Biol. Chem.* **285**, 37895–908.

304 Mizuno E, Kobayashi K, Yamamoto A, Kitamura N & Komada M (2006) A deubiquitinating enzyme UBPY regulates the level of protein ubiquitination on endosomes. *Traffic* **7**, 1017–31.

305 Row PE, Prior IA, McCullough J, Clague MJ & Urbé S (2006) The ubiquitin isopeptidase UBPY regulates endosomal ubiquitin dynamics and is essential for receptor down-regulation. *J. Biol. Chem.* **281**, 12618–24.

306 Bowers K, Piper SC, Edeling MA, Gray SR, Owen DJ, Lehner PJ & Luzio JP (2006) Degradation of endocytosed epidermal growth factor and virally ubiquitinated major histocompatibility complex class I is independent of mammalian ESCRTII. *J. Biol. Chem.* **281**, 5094–105.

307 Row PE, Liu H, Hayes S, Welchman R, Charalabous P, Hofmann K, Clague MJ, Sanderson CM & Urbé S (2007) The MIT domain of UBPY constitutes a CHMP binding and endosomal localization signal required for efficient epidermal growth factor receptor degradation. *J. Biol. Chem.* **282**, 30929–37.

308 Avvakumov G V, Walker JR, Xue S, Finerty PJ, Mackenzie F, Newman EM & Dhe-Paganon S (2006) Amino-terminal dimerization, NRDP1-rhodanese interaction, and inhibited catalytic domain conformation of the ubiquitin-specific protease 8 (USP8). *J. Biol. Chem.* **281**, 38061–70.

309 De Ceuninck L, Wauman J, Masschaele D, Peelman F & Tavernier J (2013) Reciprocal cross-regulation between RNF41 and USP8 controls cytokine receptor sorting and processing. *J. Cell Sci.* **126**, 3770–81.

310 Wijesuriya MT, De Ceuninck L, Masschaele D, Sanderson MR, Carias KV, Tavernier J & Wevrick R (2017) The Prader-Willi syndrome proteins MAGEL2 and necdin regulate cell surface abundance of the leptin receptor through ubiquitination pathways involving USP8 and RNF41. *Hum. Mol. Genet.* **26**, 4215–4230.

311 Pohl C, Jentsch S, Gould GW, Sweeney C, Carraway KL, Ricci R, Peter M, Sanderson CM, Urbe S, Noda T & al. et (2008) Final stages of cytokinesis and midbody ring formation are controlled by BRUCE. *Cell* **132**, 832–45.

312 Yen L, Cao Z, Wu X, Ingalla ERQ, Baron C, Young LJT, Gregg JP, Cardiff RD, Borowsky AD, Sweeney C & Carraway KL (2006) Loss of Nrdp1 enhances ErbB2/ErbB3-dependent breast tumor cell growth. *Cancer Res.* **66**, 11279–86.

313 Ingalla EQ, Miller JK, Wald JH, Workman HC, Kaur RP, Yen L, Fry WHD, Borowsky AD, Young LJT, Sweeney C & Carraway KL (2010) Post-transcriptional mechanisms contribute to the suppression of the ErbB3 negative regulator protein Nrdp1 in mammary tumors. *J. Biol. Chem.* **285**, 28691–7.

314 Jiao S, Liu W, Wu M, Peng C, Tang H & Xie X (2015) Nrdp1 expression to predict clinical outcome and efficacy of adjuvant anthracyclines-based chemotherapy in breast cancer: A retrospective study. *Cancer Biomarkers* **15**, 115–123.

315 Sithanandam G & Anderson LM (2008) The ERBB3 receptor in cancer and cancer gene therapy. *Cancer Gene Ther.* **15**, 413–48.

316 Chen L, Siddiqui S, Bose S, Mooso B, Asuncion A, Bedolla RG, Vinall R, Tepper CG, Gandour-Edwards R, Shi X, Lu X-H, Siddiqui J, Chinnaiyan AM, Mehra R, Devere White RW, Carraway KL & Ghosh PM (2010) Nrdp1-mediated regulation of ErbB3 expression by the androgen receptor in androgen-dependent but not castrate-resistant prostate cancer cells. *Cancer Res.* **70**, 5994–6003.

317 Savoy RM, Chen L, Siddiqui S, Melgoza FU, Durbin-Johnson B, Drake C, Jathal MK, Bose S, Steele TM, Mooso BA, D'Abronzo LS, Fry WH, Carraway KL, Mudryj M, Ghosh PM & Ghosh PM (2015) Transcription of Nrdp1 by the androgen receptor is regulated by nuclear filamin A in prostate cancer. *Endocr. Relat. Cancer* **22**, 369–386.

318 Brizzolara A, Benelli R, Venè R, Barboro P, Poggi A, Tosetti F & Ferrari N (2017) The ErbB family and androgen receptor signaling are targets of Celecoxib in prostate cancer. *Cancer Lett.* **400**, 9–17.

319 Shi H, Gong H, Cao K, Zou S, Zhu B, Bao H, Wu Y, Gao Y, Tang Y & Yu R (2015) Nrdp1-mediated ErbB3 degradation inhibits glioma cell migration and invasion by reducing cytoplasmic localization of p27Kip1. *J. Neurooncol.* **124**, 357–364.

320 Wu Y, Wang L, Bao H, Zou S, Fu C, Gong H, Gao Y, Tang Y, Yu R & Shi H (2016) Nrdp1S, short variant of Nrdp1, inhibits human glioma progression by increasing Nrdp1-mediated ErbB3 ubiquitination and degradation. *J. Cell. Mol. Med.* **20**, 422–9.

321 Printsev I, Yen L, Sweeney C & Carraway KL (2014) Oligomerization of the Nrdp1 E3 ubiquitin ligase is necessary for efficient autoubiquitination but not ErbB3 ubiquitination. *J. Biol. Chem.* **289**, 8570–8.

322 Benhenda S, Cougot D, Buendia M-A & Neuveut C (2009) Chapter 4 Hepatitis B Virus X Protein. In *Advances in cancer research* pp. 75–109.

323 Chen J-Y, Chen Y-J, Yen C-J, Chen W-S & Huang W-C (2016) HBx sensitizes hepatocellular carcinoma cells to lapatinib by up-regulating ErbB3. *Oncotarget* **7**, 473–89.

324 Cao K, Gong H, Qiu Z, Wen Q, Zhang B, Tang T, Zhou X, Cao T, Wang B, Shi H & Wang R (2016) Hepatitis B virus X protein reduces the stability of Nrdp1 to up-regulate ErbB3 in hepatocellular carcinoma cells. *Tumor Biol.* **37**, 10375–10382.

325 Byun S, Shin SH, Lee E, Lee J, Lee S-Y, Farrand L, Jung SK, Cho Y-Y, Um S-J, Sin H-S, Kwon Y-J, Zhang C, Tsang BK, Bode AM, Lee HJ, Lee KW & Dong Z (2015) The retinoic acid derivative, ABPN, inhibits pancreatic cancer through induction of Nrdp1. *Carcinogenesis* **36**, 1580–1589.

326 Paolini F, Curzio G, Melucci E, Terrenato I, Antoniani B, Carosi M, Mottolese M, Vici P, Mariani L & Venuti A (2016) Human papillomavirus 16 E2 interacts with neuregulin receptor degradation protein 1 affecting ErbB-3 expression in vitro and in clinical samples of cervical lesions. *Eur. J. Cancer* **58**, 52–61.

327 Sanchez-Soria P & Camenisch TD (2010) ErbB signaling in cardiac development and disease. *Semin. Cell Dev. Biol.* **21**, 929–935.

328 Zhang Y, Zeng Y, Wang M, Tian C, Ma X, Chen H, Fang Q, Jia L, Du J & Li H (2011) Cardiac-specific overexpression of E3 ligase Nrdp1 increases ischemia and reperfusion-induced cardiac injury. *Basic Res. Cardiol.* **106**, 371–383.

329 Zhang Y, Kang Y-M, Tian C, Zeng Y, Jia L-X, Ma X, Du J & Li H-H (2011) Overexpression of Nrdp1 in the Heart Exacerbates Doxorubicin-Induced Cardiac Dysfunction in Mice. *PLoS One* **6**, e21104.

330 Zhang Y, Jin SQ, Li WX, Gao GQ, Zhang K & Huang JL (2016) Association between RNF41 gene c.-206 T > A genetic polymorphism and risk of congenital heart diseases in the Chinese Mongolian population. *Genet. Mol. Res.* **15**.

331 Sun EG, Lee KH, Ko Y-S, Choi HJ, Yang J-I, Lee JH, Chung IJ, Paek Y-W, Kim H, Bae JA & Kim KK (2017) KITENIN functions as a fine regulator of ErbB4 expression level in colorectal cancer via protection of ErbB4 from E3-ligase Nrdp1-mediated degradation. *Mol. Carcinog.* **56**, 1068–1081.

332 Bae JA, Yoon S, Park S-Y, Lee JH, Hwang J-E, Kim H, Seo Y-W, Cha YJ, Hong SP, Kim H, Chung IJ & Kim KK (2014) An Unconventional KITENIN/ErbB4-Mediated Downstream Signal of EGF Upregulates c-Jun and the Invasiveness of Colorectal Cancer Cells. *Clin. Cancer Res.* **20**, 4115–4128.

333 Chen S-J, Lin J-H, Yao X-D, Peng B, Xu Y-F, Liu M & Zheng J-H (2016) Nrdp1-mediated degradation of BRUCE decreases cell viability and induces apoptosis in human 786-O renal cell carcinoma cells. *Exp. Ther. Med.* **12**, 597–602.

334 Thomasson M, Hedman H, Junttila TT, Elenius K, Ljungberg B & Henriksson R (2004) ErbB4 is downregulated in renal cell carcinoma A quantitative RT-PCR and immunohistochemical analysis of the epidermal growth factor receptor family. *Acta Oncol. (Madr).* **43**, 453–459.

335 Lewandowski KT & Piwnica-Worms H (2014) Phosphorylation of the E3 ubiquitin ligase RNF41 by the kinase Par-1b is required for epithelial cell polarity. *J. Cell Sci.* **127**, 315–27.

336 Wald JH, Hatakeyama J, Printsev I, Cuevas A, Fry WHD, Saldana MJ, VanderVorst K, Rowson-Hodel A, Angelastro JM, Sweeney C & Carraway KL (2017) Suppression of planar cell polarity signaling and migration in glioblastoma by Nrdp1-mediated Dvl polyubiquitination. *Oncogene*.

337 Allison MB & Myers MG (2014) 20 YEARS OF LEPTIN: Connecting leptin signaling to biological function. *J. Endocrinol.* **223**, 25–35.

338 Irizarry KA, Miller M, Freemark M & Haqq AM (2016) Prader Willi Syndrome. *Adv. Pediatr.* **63**, 47–77.

339 Mercer RE, Michaelson SD, Chee MJS, Atallah TA, Wevrick R & Colmers WF (2013) Magel2 Is Required for Leptin-Mediated Depolarization of POMC Neurons in the Hypothalamic Arcuate Nucleus in Mice. *PLoS Genet.* **9**, e1003207.

340 Pravdivyi I, Ballanyi K, Colmers WF & Wevrick R (2015) Progressive postnatal decline in leptin sensitivity of arcuate hypothalamic neurons in the Magel2-null mouse model of Prader-Willi syndrome. *Hum. Mol. Genet.* **24**, 4276–83.

341 Lang AE & Lozano AM (1998) Parkinson's Disease. *N. Engl. J. Med.* **339**, 1044–1053.

342 Kitada T, Asakawa S, Hattori N, Matsumine H, Yamamura Y, Minoshima S, Yokochi M, Mizuno Y & Shimizu N (1998) Mutations in the parkin gene cause autosomal recessive juvenile parkinsonism. *Nature* **392**,

605–608.

343 Shimura H, Hattori N, Kubo S, Mizuno Y, Asakawa S, Minoshima S, Shimizu N, Iwai K, Chiba T, Tanaka K & Suzuki T (2000) Familial Parkinson disease gene product, parkin, is a ubiquitin-protein ligase. *Nat. Genet.* **25**, 302–305.

344 Itier J-M, Ibanez P, Mena MA, Abbas N, Cohen-Salmon C, Bohme GA, Laville M, Pratt J, Corti O, Pradier L, Ret G, Joubert C, Periquet M, Araujo F, Negroni J, Casarejos MJ, Canals S, Solano R, Serrano A, Gallego E, Sanchez M, Denefle P, Benavides J, Tremp G, Rooney TA, Brice A & Garcia de Yebenes J (2003) Parkin gene inactivation alters behaviour and dopamine neurotransmission in the mouse. *Hum. Mol. Genet.* **12**, 2277–91.

345 Zhong L, Tan Y, Zhou A, Yu Q & Zhou J (2005) RING finger ubiquitin-protein isopeptide ligase Nrdp1/FLRF regulates parkin stability and activity. *J. Biol. Chem.* **280**, 9425–30.

346 Yu F & Zhou J (2008) Parkin is ubiquitinated by Nrdp1 and abrogates Nrdp1-induced oxidative stress. *Neurosci. Lett.* **440**, 4–8.

347 Greene JC, Whitworth AJ, Kuo I, Andrews LA, Feany MB & Pallanck LJ (2003) Mitochondrial pathology and apoptotic muscle degeneration in Drosophila parkin mutants. *Proc. Natl. Acad. Sci.* **100**, 4078–4083.

348 Tan Y, Yu F, Pereira A, Morin P & Zhou J (2011) *Suppression of Nrdp1 toxicity by Parkin in Drosophila models*.

349 Zhou A, Pan D, Yang X & Zhou J (2011) Overexpression of Nrdp1/FLRF sensitizes cells to oxidative stress. *Biochem. Biophys. Res. Commun.* **410**, 771–4.

350 Mo X, Liu D, Li W, Hu Z, Hu Y, Li J, Guo J, Tang B, Zhang Z, Bai Y & Xia K (2010) *Genetic screening for mutations in the Nrdp1 gene in Parkinson disease patients in a Chinese population*.

351 Narendra D, Tanaka A, Suen D-F & Youle RJ (2008) Parkin is recruited selectively to impaired mitochondria and promotes their autophagy. *J. Cell Biol.* **183**.

352 Soleimanpour SA, Gupta A, Bakay M, Ferrari AM, Groff DN, Fadista J, Spruce LA, Kushner JA, Groop L, Seeholzer SH, Kaufman BA, Hakonarson H & Stoffers DA (2014) The diabetes susceptibility gene Clec16a regulates mitophagy. *Cell* **157**, 1577–90.

353 Supale S, Li N, Brun T & Maechler P (2012) Mitochondrial dysfunction in pancreatic ? cells. *Trends Endocrinol. Metab.* **23**, 477–487.

354 Soleimanpour SA, Ferrari AM, Raum JC, Groff DN, Yang J, Kaufman BA & Stoffers DA (2015) Diabetes Susceptibility Genes Pdx1 and Clec16a Function in a Pathway Regulating Mitophagy in β-Cells. *Diabetes* **64**, 3475–84.

355 Durcan TM, Tang MY, Pérusse JR, Dashti EA, Aguileta MA, McLelland G-L, Gros P, Shaler TA, Faubert D, Coulombe B & Fon EA (2014) USP8 regulates mitophagy by removing K6-linked ubiquitin conjugates from parkin. *EMBO J.* **33**, 2473–91.

356 Jiang Y, Meng Q, Qi J, Shen H & Sun S (2015) MiR-497 promotes metastasis of colorectal cancer cells through Nrdp1 inhibition. *Tumour Biol.* **36**, 7641–7.

357 Basiorka AA, McGraw KL, De Ceuninck L, Griner LN, Zhang L, Clark JA, Caceres G, Sokol L, Komrokji RS, Reuther GW, Wei S, Tavernier J & List AF (2016) Lenalidomide Stabilizes the Erythropoietin Receptor by Inhibiting the E3 Ubiquitin Ligase RNF41. *Cancer Res.* **76**.

358 Kim S, Zhang S, Choi KH, Reister R, Do C, Baykiz AF & Gershenfeld HK (2009) An E3 ubiquitin ligase, Really Interesting New Gene (RING) Finger 41, is a candidate gene for anxiety-like behavior and beta-carboline-induced seizures. *Biol. Psychiatry* **65**, 425–31.

359 Lee Y-I, Giovinazzo D, Kang HC, Lee Y, Jeong JS, Doulias P-T, Xie Z, Hu J, Ghasemi M, Ischiropoulos H, Qian J, Zhu H, Blackshaw S, Dawson VL & Dawson TM (2014) Protein microarray characterization of the S-nitrosoproteome. *Mol. Cell. Proteomics* **13**, 63–72.

360 Nooren IMA & Thornton JM (2003) NEW EMBO MEMBER'S REVIEW: Diversity of protein-protein interactions. *EMBO J.* **22**, 3486–3492.

361 Stumpf MPH, Thorne T, de Silva E, Stewart R, An HJ, Lappe M & Wiuf C (2008) Estimating the size of the human interactome. *Proc. Natl. Acad. Sci.* **105**, 6959–6964.

362 Fields S & Song O (1989) A novel genetic system to detect protein-protein interactions. *Nature* **340**, 245–6.

363 Gingras A-C, Gstaiger M, Raught B & Aebersold R (2007) Analysis of protein complexes using mass spectrometry. *Nat. Rev. Mol. Cell Biol.* **8**, 645–54.

364 Söderberg O, Gullberg M, Jarvius M, Ridderstråle K, Leuchowius K-J, Jarvius J, Wester K, Hydbring P, Bahram F, Larsson L-G & Landegren U (2006) Direct observation of individual endogenous protein complexes in situ by proximity ligation. *Nat. Methods* **3**, 995–1000.

365 Boute N, Jockers R & Issad T (2002) The use of resonance energy transfer in high-throughput screening: BRET versus FRET. *Trends Pharmacol. Sci.* **23**, 351–354.

366 Eyckerman S, Verhee A, Van der Heyden J, Lemmens I, Van Ostade X, Vandekerckhove J & Tavernier J (2001) Design and application of a cytokine-receptor-based interaction trap. *Nat. Cell Biol.* **3**, 1114–1119.

367 Barrios-Rodiles M, Brown KR, Ozdamar B, Bose R, Liu Z, Donovan RS, Shinjo F, Liu Y, Dembowy J, Taylor IW, Luga V, Przulj N, Robinson M, Suzuki H, Hayashizaki Y, Jurisica I & Wrana JL (2005) High-throughput mapping of a dynamic signaling network in mammalian cells. *Science* **307**, 1621–5.

368 Roux KJ, Kim DI, Raida M & Burke B (2012) A promiscuous biotin ligase fusion protein identifies proximal and interacting proteins in mammalian cells. *J. Cell Biol.* **196**, 801–10.

369 Eyckerman S, Titeca K, Van Quickelberghe E, Cloots E, Verhee A, Samyn N, De Ceuninck L, Timmerman E, De Sutter D, Lievens S, Van Calenbergh S, Gevaert K & Tavernier J (2016) Trapping mammalian protein complexes in viral particles. *Nat. Commun.* **7**, 11416.

370 Petschnigg J, Groisman B, Kotlyar M, Taipale M, Zheng Y, Kurat CF, Sayad A, Sierra JR, Mattiazzi Usaj M, Snider J, Nachman A, Krykbaeva I, Tsao M-S, Moffat J, Pawson T, Lindquist S, Jurisica I & Stagljar I (2014) The mammalian-membrane two-hybrid assay (MaMTH) for probing membrane-protein interactions in human cells. *Nat. Methods* **11**, 585–92.

371 Weinrich D, Jonkheijm P, Niemeyer CM & Waldmann H (2009) Applications of protein biochips in biomedical and biotechnological research. *Angew. Chem. Int. Ed. Engl.* **48**, 7744–51.

372 Titeca K (2017) Novel technologies for the analysis of protein complexes. .

373 Rolland T, Taşan M, Charloteaux B, Pevzner SJ, Zhong Q, Sahni N, Yi S, Lemmens I, Fontanillo C, Mosca R, Kamburov A, Ghiassian SD, Yang X, Ghamsari L, Balcha D, Begg BE, Braun P, Brehme M, Broly MP, Carvunis A-R, Convery-Zupan D, Corominas R, Coulombe-Huntington J, Dann E, Dreze M, Dricot A, Fan C, Franzosa E, Gebreab F, Gutierrez BJ, Hardy MF, Jin M, Kang S, Kiros R, Lin GN, Luck K, MacWilliams A, Menche J, Murray RR, Palagi A, Poulin MM, Rambout X, Rasla J, Reichert P, Romero V, Ruyssinck E, Sahalie JM, Scholz A, Shah AA, Sharma A, Shen Y, Spirohn K, Tam S, Tejeda AO, Trigg SA, Twizere J-C, Vega K, Walsh J, Cusick ME, Xia Y, Barabási A-L, Iakoucheva LM, Aloy P, De Las Rivas J, Tavernier J, Calderwood MA, Hill DE, Hao T, Roth FP & Vidal M (2014) A Proteome-Scale Map of the Human Interactome Network. *Cell* **159**, 1212–1226.

374 Stynen B, Tournu H, Tavernier J & Van Dijck P (2012) Diversity in genetic in vivo methods for protein-protein interaction studies: from the yeast two-hybrid system to the mammalian split-luciferase system. *Microbiol. Mol. Biol. Rev.* **76**, 331–82.

375 Leanna CA & Hannink M (1996) The reverse two-hybrid system: a genetic scheme for selection against specific protein/protein interactions. *Nucleic Acids Res.* **24**, 3341–7.

376 Osborne MA, Dalton S & Kochan JP (1995) The yeast tribrid system--genetic detection of trans-phosphorylated ITAM-SH2-interactions. *Biotechnology. (N. Y).* **13**, 1474–8.

377 Licitra EJ & Liu JO (1996) A three-hybrid system for detecting small ligand-protein receptor interactions. *Proc. Natl. Acad. Sci. U. S. A.* **93**, 12817–21.

378 De Clercq DJH, Tavernier J, Lievens S & Van Calenbergh S (2016) Chemical Dimerizers in Three-Hybrid Systems for Small Molecule–Target Protein Profiling. *ACS Chem. Biol.* **11**, 2075–2090.

379 Johnsson N & Varshavsky A (1994) Split ubiquitin as a sensor of protein interactions in vivo. *Proc. Natl. Acad. Sci. U. S. A.* **91**, 10340–4.

380 Stagljar I, Korostensky C, Johnsson N & te Heesen S (1998) A genetic system based on split-ubiquitin for the analysis of interactions between membrane proteins in vivo. *Proc. Natl. Acad. Sci. U. S. A.* **95**, 5187–92.

381 Kerppola TK (2008) Bimolecular Fluorescence Complementation (BiFC) Analysis as a Probe of Protein Interactions in Living Cells. *Annu. Rev. Biophys.* **37**, 465–487.

382 Morell M, Ventura S & Avilés FX (2009) Protein complementation assays: Approaches for the in vivo analysis of protein interactions. *FEBS Lett.* **583**, 1684–1691.

383 Wehr MC, Laage R, Bolz U, Fischer TM, Grünewald S, Scheek S, Bach A, Nave K-A & Rossner MJ (2006) Monitoring regulated protein-protein interactions using split TEV. *Nat. Methods* **3**, 985–993.

384 Lievens S, Vanderroost N, Van der Heyden J, Gesellchen V, Vidal M & Tavernier J (2009) Array MAPPIT: High-Throughput Interactome Analysis in Mammalian Cells. *J. Proteome Res.* **8**, 877–886.

385 Lievens S, Van der Heyden J, Masschaele D, De Ceuninck L, Petta I, Gupta S, De Puysseleyr V, Vauthier V, Lemmens I, De Clercq DJH, Defever D, Vanderroost N, De Smet A-S, Eyckerman S, Van Calenbergh S, Martens L, De Bosscher K, Libert C, Hill DE, Vidal M & Tavernier J (2016) Proteome-scale Binary Interactomics in Human Cells. *Mol. Cell. Proteomics* **15**, 3624–3639.

386 Lievens S, Gerlo S, Lemmens I, De Clercq DJH, Risseeuw MDP, Vanderroost N, De Smet A-S, Ruyssinck E, Chevet E, Van Calenbergh S & Tavernier J (2014) Kinase Substrate Sensor (KISS), a mammalian in situ protein interaction sensor. *Mol. Cell. Proteomics* **13**, 3332–42.

387 Lemmens I (2003) Heteromeric MAPPIT: a novel strategy to study modification-dependent protein-protein

interactions in mammalian cells. *Nucleic Acids Res.* **31**, 75e–75.

388 Caligiuri M, Molz L, Liu Q, Kaplan F, Xu JP, Majeti JZ, Ramos-Kelsey R, Murthi K, Lievens S, Tavernier J & Kley N (2006) MASPIT: Three-hybrid trap for quantitative proteome fingerprinting of small molecule-protein interactions in mammalian cells. *Chem. Biol.* **13**, 711–722.

389 Uyttendaele I, Lavens D, Catteeuw D, Lemmens I, Bovijn C, Tavernier J & Peelman F (2012) Random mutagenesis MAPPIT analysis identifies binding sites for Vif and Gag in both cytidine deaminase domains of Apobec3G. *PLoS One* **7**, e44143.

390 Bovijn C, Desmet A-S, Uyttendaele I, Van Acker T, Tavernier J & Peelman F (2013) Identification of binding sites for myeloid differentiation primary response gene 88 (MyD88) and Toll-like receptor 4 in MyD88 adapter-like (Mal). *J. Biol. Chem.* **288**, 12054–66.

391 Vyncke L, Bovijn C, Pauwels E, Van Acker T, Ruyssinck E, Burg E, Tavernier J & Peelman F (2016) Reconstructing the TIR Side of the Myddosome: a Paradigm for TIR-TIR Interactions. *Structure* **24**, 437–47.

392 Ho Y, Gruhler A, Heilbut A, Bader GD, Moore L, Adams S-L, Millar A, Taylor P, Bennett K, Boutilier K, Yang L, Wolting C, Donaldson I, Schandorff S, Shewnarane J, Vo M, Taggart J, Goudreault M, Muskat B, Alfarano C, Dewar D, Lin Z, Michalickova K, Willems AR, Sassi H, Nielsen PA, Rasmussen KJ, Andersen JR, Johansen LE, Hansen LH, Jespersen H, Podtelejnikov A, Nielsen E, Crawford J, Poulsen V, Sørensen BD, Matthiesen J, Hendrickson RC, Gleeson F, Pawson T, Moran MF, Durocher D, Mann M, Hogue CW V., Figeys D & Tyers M (2002) Systematic identification of protein complexes in Saccharomyces cerevisiae by mass spectrometry. *Nature* **415**, 180–183.

393 Gavin A-C, Bösche M, Krause R, Grandi P, Marzioch M, Bauer A, Schultz J, Rick JM, Michon A-M, Cruciat C-M, Remor M, Höfert C, Schelder M, Brajenovic M, Ruffner H, Merino A, Klein K, Hudak M, Dickson D, Rudi T, Gnau V, Bauch A, Bastuck S, Huhse B, Leutwein C, Heurtier M-A, Copley RR, Edelmann A, Querfurth E, Rybin V, Drewes G, Raida M, Bouwmeester T, Bork P, Seraphin B, Kuster B, Neubauer G & Superti-Furga G (2002) Functional organization of the yeast proteome by systematic analysis of protein complexes. *Nature* **415**, 141–147.

394 Dunham WH, Mullin M & Gingras A-C (2012) Affinity-purification coupled to mass spectrometry: Basic principles and strategies. *Proteomics* **12**, 1576–1590.

395 Blagoev B, Kratchmarova I, Ong S-E, Nielsen M, Foster LJ & Mann M (2003) A proteomics strategy to elucidate functional protein-protein interactions applied to EGF signaling. *Nat. Biotechnol.* **21**, 315–318.

396 Choi-Rhee E, Schulman H & Cronan JE (2004) Promiscuous protein biotinylation by Escherichia coli biotin protein ligase. *Protein Sci.* **13**, 3043–50.

397 Kim DI, Jensen SC, Noble KA, KC B, Roux KH, Motamedchaboki K & Roux KJ (2016) An improved smaller biotin ligase for BioID proximity labeling. *Mol. Biol. Cell* **27**, 1188–1196.

398 Briggs JAG, Simon MN, Gross I, Kräusslich H-G, Fuller SD, Vogt VM & Johnson MC (2004) The stoichiometry of Gag protein in HIV-1. *Nat. Struct. Mol. Biol.* **11**, 672–675.

Scope of the thesis

RNF41 is an E3 ubiquitin ligase involved in the ubiquitination and degradation of many proteins such as ERBB3 receptors, BRUCE and parkin. Our lab previously showed that RNF41 influences the cell surface expression and signaling of the LR, LIFR and IL6R, three JAK2-associated type I cytokine receptors. Moreover, RNF41 was found to modulate the intracellular trafficking of these cytokine receptors. By ubiquitinating and suppressing USP8, RNF41 indirectly destablizes the ESCRT-0 complex, which inhibits these receptors from undergoing lysosomal degradation and subsequently reroutes them towards compartments for ectodomain shedding. This thesis aimed to further elucidate the function of RNF41 in intracellular trafficking through the identification of new interaction partners.

In the first part of the thesis we investigate the interaction between RNF41 and VPS52, a novel interaction partner identified via an initial array MAPPIT screen. This protein is involved in retrograde transport and recycling pathways and could therefore be implicated in, and further elaborate the functional effects of RNF41 in rerouting of cytokine receptors. This study was supported by a combination of random mutagenesis and MAPPIT that generates and identifies mutants specifically disrupting the interaction between RNF41 and VPS52.

The second part of the thesis describes the construction of the RNF41 interactome network. Data from newly performed high-throughput screens were merged with preexisting data from previously performed microarray MAPPIT and Y2H screens in order to build a high resolution and high confidence map of RNF41 interaction partners. A novel candidate partner, AP2S1, was selected from the high confidence map for further functional validation by determining its role in RNF41 mediated LR shedding, degradation and signaling.

We, and other groups, frequently observed a vesicular-like pattern for overexpressed RNF41 with immunofluorescence microscopy. In the last part of this thesis we attempt to characterize the RNF41-positive structures by using a number of known organelle and aggregate markers. In this way we hope to determine at which intracellular trafficking stages RNF41 exerts its function.

Results

RNF41 interacts with the VPS52 subunit of the GARP and EARP complexes

RNF41 (RING finger protein 41) is involved in the ubiquitination and downregulation of many substrates including BRUCE (BIR repeat containing ubiquitin-conjugating enzyme), parkin, USP8 (Ubiquitin-specific protease 8) and the ERBB3 receptor. It is also involved in the intracellular transport of several type I cytokine receptors such as the LR (leptin receptor), LIFR (leukaemia inhibitory factor receptor) and IL-6R (interleukin 6 receptor). We aimed to further elucidate the role of RNF41 in intracellular trafficking by identifying new interaction partners with the in-house developed Array MAPPIT (Mammalian Protein-Protein interaction trap) technology. This paper describes the identification of VPS52 (vacuolar protein sorting 52) as a novel RNF41 interaction partner. VPS52 is a subunit of the GARP (Golgi-associated retrograde protein) and the EARP (endosome-associated recycling protein) complexes which are involved in the sorting of cargo from the early endosomes towards the TGN or recycling endosomes, respectively. We show that via coiled coil domain interactions, RNF41 ubiquitinates and relocates VPS52 away from VPS53, another common subunit of the GARP and EARP complexes, towards RNF41 positive structures. This effect was lost when using an RNF41 mutant, specifically disrupting the interaction between RNF41 and VPS52, which was identified via a straightforward, high-throughput method combining random mutagenesis and MAPPIT.

The addendum describes the functional effects of RNF41 on EARP and GARP substrates, and the influence of VPS52 on known RNF41 functions. This data was obtained during the follow-up of this study and provides additional insights.

RNF41 interacts with the VPS52 subunit of the GARP and EARP complexes

Delphine Masschaele[1,2], Leentje De Ceuninck[1,2], Joris Wauman[1,2], Dieter Defever[1,2], Frank Stenner[3], Sam Lievens[1,2], Frank Peelman[1,2], Jan Tavernier[1,2]*

1 Cytokine Receptor Laboratory, Department of Biochemistry, Faculty of Medicine and Health Sciences, Ghent University, Ghent, Belgium, 2 VIB Medical Biotechnology Center, VIB, Ghent, Belgium, 3 Department of Oncology, University Hospital Basel, University of Basel, Basel, Switzerland

* jan.tavernier@vib-ugent.be

Abstract

RNF41 (Ring Finger Protein 41) is an E3 ubiquitin ligase involved in the intracellular sorting and function of a diverse set of substrates. Next to BRUCE and Parkin, RNF41 can directly ubiquitinate ErbB3, IL-3, EPO and RARα receptors or downstream signaling molecules such as Myd88, TBK1 and USP8. In this way it can regulate receptor signaling and routing. To further elucidate the molecular mechanism behind the role of RNF41 in intracellular transport we performed an Array MAPPIT (Mammalian Protein-Protein Interaction Trap) screen using an extensive set of proteins derived from the human ORFeome collection. This paper describes the identification of VPS52, a subunit of the GARP (Golgi-Associated Retrograde Protein) and the EARP (Endosome-Associated Recycling Protein) complexes, as a novel interaction partner of RNF41. Through interaction via their coiled coil domains, RNF41 ubiquitinates and relocates VPS52 away from VPS53, a common subunit of the GARP and EARP complexes, towards RNF41 bodies.

Introduction

Eukaryotic cells contain various types of organelles involved in the transport of proteins and lipids. Forward trafficking of cargo in the secretory pathway is counterbalanced by retrograde transport in which resident proteins and transport machinery components are transported back to their original compartment [1–3]. In the endocytic pathway, molecules are internalized at the plasma membrane and delivered to the early endosomes. These early or 'sorting' endosomes segregate cargo coming from the plasma membrane into different membrane subdomains. Certain proteins are targeted for lysosomal degradation through the late endosome, while other cargo bypass this step and undergo retrograde transport to the Golgi network, or recycle back to the plasma membrane directly from the endosomes or via the recycling endosomes [4–8]. Biosynthetic, endocytic and retrograde trafficking are highly regulated by the coordinated actions of tethering factors, SNAREs (Soluble N-Ethylmaleimide-Sensitive Factor Attachment Protein Receptors) and small G proteins from the Rab and Arl (Arf-like) family in order to maintain homeostasis of each organelle [9,10].

84

A key regulatory mechanism of intracellular transport is ubiquitination, which acts as a signal for internalization and sorting of receptors and adaptors [11–14]. The ESCRTs (Endosomal Sorting Complex Required for Transport) further mediate the sorting of ubiquitinated cargo into ILVs (intraluminal vesicles) of MVBs (multivesicular bodies) destined for lysosomal degradation [15,16]. Many E3 ligases have been identified to play a role in endocytosis and lysosomal sorting of membrane proteins. RING (really interesting new gene) finger E3 ligases act as a scaffold to coordinate ubiquitin transfer from an ubiquitin-conjugating E2 enzyme recruited by their RING domain to a specific substrate associated with their substrate binding domain. We previously reported that RNF41 (RING finger protein 41 or Nrdp1 (neuregulin receptor degradation protein-1) or FLRF (fetal liver ring finger) in mouse) controls the sorting and processing of JAK2-associated cytokine receptors including the LR (leptin receptor), LIFR (leukaemia inhibitory factor receptor) and IL6R (interleukin 6 receptor). RNF41 blocks lysosomal sorting and simultaneously enhances ectodomain shedding of these receptors by members of the ADAM (a disintegrin and metalloproteinase) family [17]. It does so by ubiquitinating, destabilizing and relocalizing the deubiquitinase USP8 (ubiquitin-specific protease 8). This leads to a destabilized ESCRT-0 complex, resulting in the rerouting of receptors from the lysosomal degradation pathway to compartments for ectodomain shedding [18]. RNF41 has been implicated in other signaling pathways; it directly ubiquitinates and subsequently downregulates the RARα (retinoic acid receptor alpha), the IL-3 (interleukin-3), EPO (erythropoietin) and ErbB3 receptors, independent of their respective ligands [19–22]. Moreover, RNF41 was reported to differentially regulate Myd88- and TRIF-dependent pathways of TLR4 (Toll-like receptor 4) by ubiquitinating adaptor proteins Myd88 (poly-lys48) and TBK1 (poly-lys63) respectively [23].

To further elucidate the function of RNF41 in intracellular transport we screened a human ORFeome collection containing around 8500 open reading frames in search of novel interaction partners of RNF41 using Array MAPPIT, a high-throughput mammalian two-hybrid screening method [24]. One newly identified RNF41 interaction partner was VPS52 (vacuolar protein sorting 52) which is a key component of two spatially distinct multisubunit tethering complexes, the GARP (Golgi-Associated Retrograde Protein) and EARP (Endosome-Associated Recycling Protein) complexes. The GARP complex is mainly located at the TGN (Trans Golgi Network) and consists of VPS52 together with Ang2, VPS53 and VPS54 [25–27]. This complex functions as a tethering factor for retrograde transport of cargo from endosomes to the TGN. As such, it participates in the delivery of internalized STxB (Shiga toxin B-subunit) and in the retrieval of the M6PR (mannose-6-phosphate receptor), the TGN-resident protein TGN46 and certain SNAREs to the TGN [25,28,29]. The GARP complex is also required for sphingolipid homeostasis and for post-Golgi anterograde transport of GPI-anchored and transmembrane proteins [30,31]. In the EARP complex, VPS54 is substituted by Syndetin while the other subunits are shared with the GARP complex, giving rise to a new tethering complex that associates with recycling endosomes and promotes the recycling of internalized transferrin receptor to the plasma membrane [32].

In this paper we show that RNF41 and VPS52 interact with each other via their CC (coiled coil) domains and demonstrate that RNF41 is able to ubiquitinate and relocate VPS52 from its subcellular location.

Results

VPS52 is a novel interaction partner of RNF41

Array MAPPIT, a high throughput two-hybrid screening method developed in our lab, was used to identify new interaction partners of RNF41 [24]. This method is based on complementation

of the JAK-STAT signaling pathway of type I cytokine receptors and allows the detection of protein-protein interactions in intact mammalian cells [33]. Screening was carried out with the RNF41 mutant C34S/H36Q bait, which lacks the ability to recruit an E2 conjugating enzyme. This prevents possible RNF41-dependent ubiquitination and degradation of interacting preys expressed in the system. The RNF41 mutant bait was screened against a human ORFeome collection that covered up to 8.500 preys (list available upon request). VPS52 appeared as one of the top ranked interaction partners of RNF41 amongst other known interaction partners like KDM3B, HOMER2 and ASB6 [34, 35] (Fig 1A). Binary MAPPIT retests confirmed that VPS52 specifically interacted with RNF41 and not with the bait receptor backbone (Fig 1B). AlphaScreen analysis further validated that E-tagged VPS52 specifically interacted with co-expressed Flag-tagged RNF41 in HEK293T cells, and not with a Flag-tagged mock construct, even though E-tagged VPS52 levels in the AlphaScreen lysate fraction were reduced upon RNF41 co-transfection (Fig 1C). Moreover, endogenous RNF41 could be precipitated using an antibody against endogenous VPS52 in HEK293T cells (Fig 1D) and *in vitro* GST-pull down analysis confirmed a direct interaction between VPS52 and RNF41 (Fig 1E). Confocal microscopy of transfected HeLa cells showed a perinuclear localization of VPS52 reminiscent of the trans-Golgi network, while RNF41 localized to punctate cytoplasmic structures. Upon co-transfection, RNF41 and E-tagged VPS52 colocalized in RNF41-positive structures, which we will further refer to as RNF41 bodies(Fig 1F). Of note, the amount of ectopically expressed RNF41 used for confocal experiments was similar to, or below endogenous levels of RNF41 (data not shown). Moreover, RNF41 has a potential myristoylation site at its N-terminus, which could account for membrane anchoring [21], and explain the vesicular pattern of RNF41 observed in Fig 1F. For this reason only C-terminal tagged constructs of RNF41 were used. No difference was observed between expression of N- or C-terminally tagged VPS52. Furthermore, co-immunoprecipitation and AlphaScreen data revealed that RNF41 exclusively interacts with VPS52 and not with the other GARP or EARP subunits (Fig 1G–1E).

L163 in the coiled-coil domain of RNF41 is required for interaction with VPS52 but not for RNF41oligomerization

To map the interaction of VPS52 on RNF41 we created several truncated forms of RNF41, which were tested in MAPPIT as bait proteins against the VPS52 prey (Fig 2A). The amino-terminal half of RNF41 (AA1-134; N-term) holds a RING domain and the carboxy-terminal half (AA135-317; C-term) consists of a CC domain (AA135-179; CC) and a substrate binding (AA179-317) domain [21]. Only the CC domain and C-terminal RNF41 bait, including the CC domain, interacted with VPS52 prey, demonstrating that the CC domain of RNF41 is necessary for interaction with VPS52 (Fig 2B). To further determine critical RNF41 amino acids involved in the interaction with VPS52, we used an approach that combined random mutagenesis with MAPPIT [36]. Briefly, the MAPPIT RNF41 bait protein was randomly mutated via error prone PCR, covering 113 of a total of 317 amino acids, a mutation yield of about 36% with approximately 26% single mutations. Putative RNF41 mutants were tested against the VPS52 prey or a JAK2-binding prey as a control for expression of the bait receptor. RNF41 mutants were selected based on a single amino acid mutation that strongly decreased the relative MAPPIT signal S1 Table. Mutations at position 163 reoccurred multiple times in the screen and binary MAPPIT retests clearly showed a disruption of the RNF41-VPS52 interaction using the RNF41 L163Q mutant bait (Fig 2B). The L163Q mutation was specific towards VPS52, as interaction between RNF41 and other interaction partners, such as USP8 [37] and ASB6 (manuscript in preparation), was not affected S1 Fig. Significantly, as for the L163Q mutant, all other RNF41 mutants found to disturb the interaction with VPS52 were located in
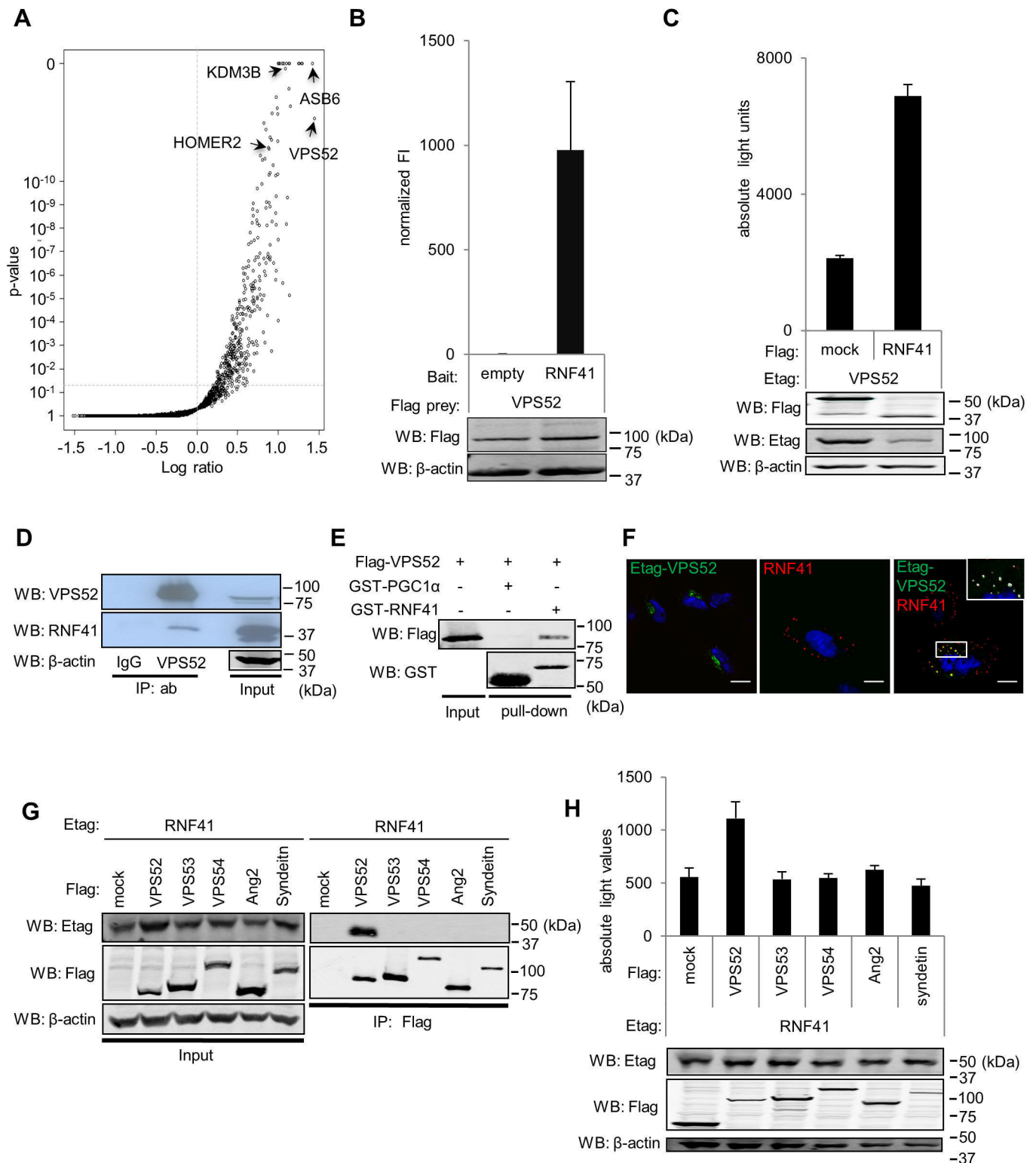
Fig 1. VPS52 is a novel interaction partner of RNF41. (A) Array MAPPIT screen result of the RNF41 C34S/H36Q bait against a library covering up to 8,500 preys shown as a volcano plot of the log ratio of normalized MAPPIT luciferase activity versus *P* value. **(B)** MAPPIT analysis of HEK293T cells transiently cotransfected with a vector encoding an RNF41 or empty bait, a VPS52 prey plasmid and the pXP2d2-rPAP1-luciferase reporter plasmid, followed by 24 hours Epo stimulation or left untreated. The luciferase signal is expressed as fold induction (stimulated/non stimulated), relative to the signal of a control JAK2 binding prey ± s.d. of triplicate measurements. Western blotting verified Flag-tagged prey expression and β-actin

levels (loading control). **(C)** AlphaScreen analysis of HEK293T cells transiently cotransfected with plasmids encoding E-tagged VPS52 and Flag-tagged RNF41 or SV40 large T antigen (SVT) as an irrelevant protein (mock). After 48 hours, cells were lysed and protein interactions were detected with the AlphaScreen FLAG^(TM) (M2) detection kit (PerkinElmer Life Sciences) by generation of a luminescent signal, displayed as absolute light units. Western blotting shows E and Flag-tagged protein expression and a β-actin loading control. **(D)** Co-immunoprecipitation of endogenous VPS52 and RNF41. HEK293T lysates were immunoprecipitated with anti-VPS52 or a control normal rabbit IgG. The immune complexes (first and second lane) and the input (third lane) were analyzed by immunoblotting with an antibody specific for RNF41 (middle panel). Anti-actin was used as a loading control **(E)** GST-pulldown of *Escherichia coli* BL21(DE3) cell lysates expressing GST-PGC1α (negative control, lane 2) or GST-RNF41 (lane 3) using glutathione sepharose beads and incubated with in vitro transcribed and translated Flag-tagged VPS52. Western blotting using anti-Flag and anti-GST antibodies reveals bead-bound protein complexes and expression of Flag-tagged VPS52 (lane 1). **(F)** Confocal microscopy of HeLa cells transfected with plasmids encoding either E-tagged VPS52 (left panel) or untagged RNF41 (middle panel), together with soluble IL5Rα plasmid as a control, or plasmids encoding E-tagged VPS52 and RNF41 (right panel). Cells were fixed and stained with DAPI (nuclei staining, blue), anti-Etag (secondary Alexa Fluor 488, green) and anti-RNF41 (secondary Alexa Fluor 568, red) antibodies. The inset shows a magnification of the boxed area. The white overlay represents the intersect between RNF41 and VPS52 with a threshold set on standard deviation using Volocity 6.3 software (Perkin Elmer, Waltham, MA, USA). Scale bar, 10μm. n = 3 or more for all performed experiments. **(G)** Co-immunoprecipitation analysis of HEK293T cells transiently cotransfected with plasmids encoding E-tagged RNF41 and Flag-tagged GARP/EARP subunits or soluble IL5Rα. Anti-Flag immunoprecipitates (right panel) and lysates (left panel) were visualized with anti-Flag, anti-Etag and anti-actin. **(H)** AlphaScreen analysis of HEK293T cells transiently cotransfected with plasmids encoding E-tagged RNF41 and Flag-tagged GARP/EARP subunits or SVT.

https://doi.org/10.1371/journal.pone.0178132.g001

the CC domain of RNF41 S2 Table. This marks VPS52 as the first RNF4 interaction partner that binds to its CC domain. Co-immunoprecipitation (Fig 2C) and AlphaScreen data (Fig 2D), where the RNF41 truncated forms were co-expressed with VPS52 in HEK293T cells, confirmed the MAPPIT results. Of note, the L163Q mutant showed no difference in stability compared to WT RNF41 (data not shown).

The program Logicoil [38], predicted the CC regions of RNF41 to form a trimer, which corresponds to the observations in a recently published paper based on chemical crosslinking and size exclusion chromatography [39] (Fig 2E). The trimeric coiled-coiled core does not consist merely of hydrophobic residues, but also has hydrophilic histidine and asparagine residues. Intermolecular salt bridges outside the core help to stabilize the coil. As RNF41 is able to trimerize via its CC domain, we examined whether the RNF41 L163Q mutation also affects RNF41 oligomerization. Immunoprecipitation and AlphaScreen analysis of transfected HEK293T cells showed that only RNF41ΔCC was able to impair RNF41 oligomerization (Fig 2F and 2G). We conclude that the CC region of RNF41, more specifically residue L163 located in this CC region, is necessary for its interaction with VPS52, while this L163 residue is redundant for RNF41 oligomerization.

D120, E124 and E127 in the CC domain of VPS52 interact with RNF41 and this interaction decreases RNF41 oligomerization

The Logicoil algorithm also predicted a CC domain in VPS52 between residues 120 and 151. We next created a truncated form of VPS52 without the CC domain (ΔCC), and one existing of only the CC domain (CC) (Fig 3A). We extended the CC domain from residues 109 to 151 as we observed optimal expression of the CC domain using this construct. Modeling of the CC region of VPS52 led to the prediction of a trimeric state with an extensive hydrophobic core (Fig 3B). MAPPIT analysis showed that the CC domain of VPS52 is essential and sufficient for binding with RNF41, as the VPS52 CC prey interacts with the RNF41 bait, while the VPS52 ΔCC prey does not (Fig 3C). Co-immunoprecipitation with ectopically expressed RNF41 and VPS52 mutant or truncated constructs in HEK293T cells verified the MAPPIT results (Fig 3D).

Since RNF41 and VPS52 interact with each other via their respective CC domains (Figs 2B, 2C, 3C and 3D), and RNF41 oligomerizes via its CC domain ([39] and Fig 2F and 2G), we examined whether VPS52 binding to RNF41 interferes with RNF41 oligomerization. VPS52 co-expression impeded the interaction between Flag-tagged and E-tagged RNF41 in
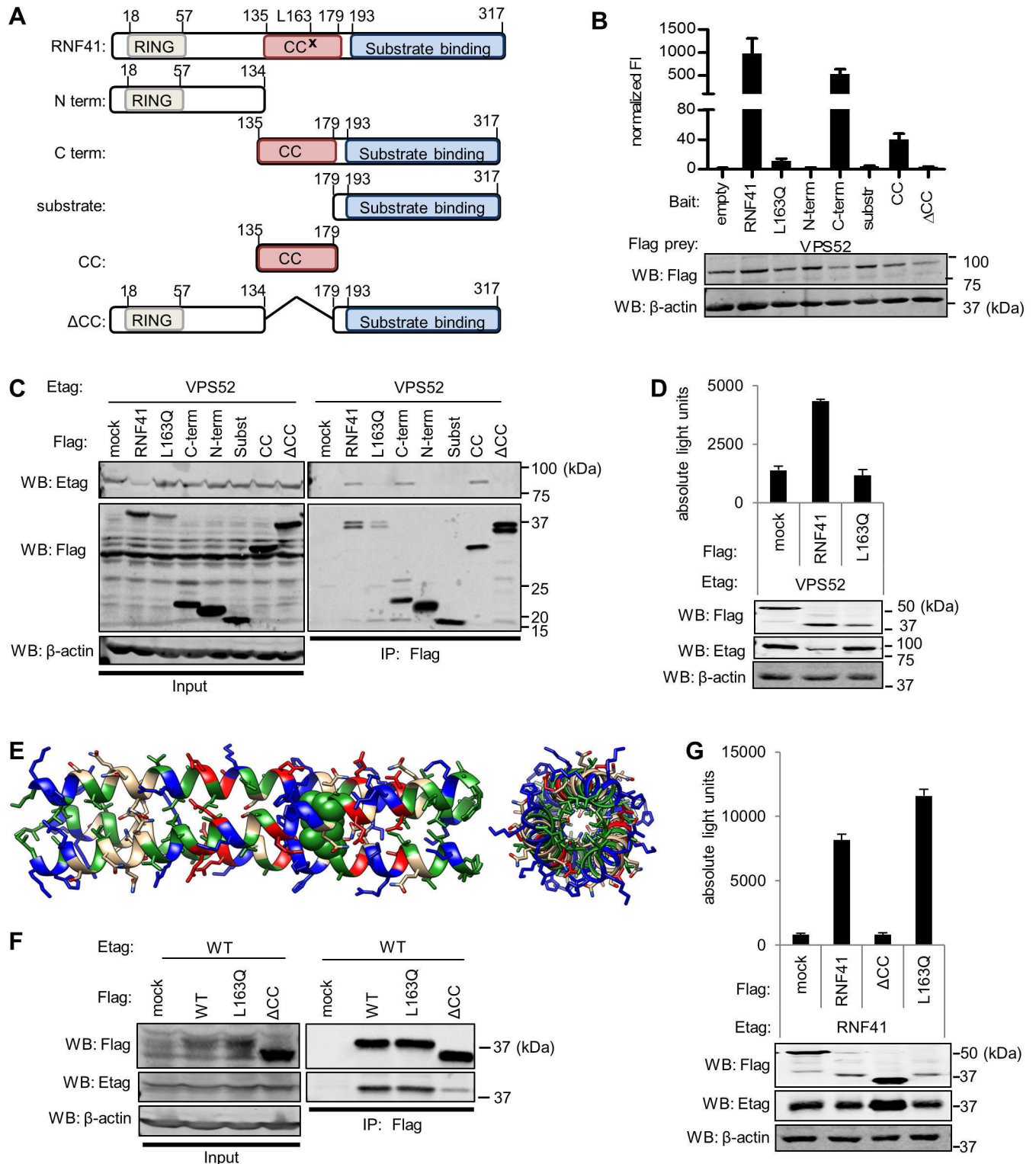
Fig 2. L163 in the RNF41 CC interacts with VPS52 but is not required for RNF41 oligomerization. (A) Schematic representation of the amino acid range, L163Q point mutation (indicated with x) and subdomain structure of the full length and truncated RNF41 constructs used to map the VPS52 interaction site. Domain designations: N term, the amino-terminal domain; RING, RING domain; C term, the carboxy-terminal domain; CC, the CC domain; ΔCC, RNF41 construct lacking the CC domain. (B) MAPPIT analysis of HEK293T cells transiently co-transfected with a vector encoding a VPS52 prey and an empty, wild type (WT), point mutated or truncated RNF41 bait. (C) Co-immunoprecipitation analysis of HEK293T cells transiently co-transfected with a plasmid encoding E-tagged VPS52 and Flag-tagged WT RNF41, L163Q, N-term, C-term, substrate binding

domain, RNF41 CC-gp130 (prey construct used to optimize expression), RNF41 ΔCC or soluble IL5Rα (mock). Also Anti-Flag immunoprecipitates (right panel) and lysates (input, left panel) were visualized with anti-Etag, anti-Flag and anti-actin (loading control). **(D)** AlphaScreen analysis of HEK293T cells transiently co-transfected with a vector encoding E-tagged VPS52 and Flag-tagged SVT (negative control), WT RNF41 or L163Q. **(E)** Side (left) and top (right) view of a model of trimeric RNF41 coiled-coils based on the RNF41 sequence using CC-builder and Logicoil. L163 is highlighted as green spheres. **(F)** Co-immunoprecipitation of HEK293T cells transiently co-transfected with E-tagged WT RNF41 and Flag-tagged RNF41, L163Q, RNF41 ΔCC or with Flag-tagged soluble IL5Rα (mock) shows that the L163Q mutation does not hamper RNF41 oligomerization. Anti-Flag immunoprecipitates (right panels) and lysates (left panels) were visualized with anti-Flag and anti-Etag. **(G)** AlphaScreen analysis of HEK293T cells transiently co-transfected with a plasmid encoding E-tagged RNF41 and Flag-tagged SVT, WT RNF41 and L163Q. n = 3 or more for all experiments performed.

AlphaScreen, whereas co-expression of the VPS52ΔCC mutant partially restored this interaction (Fig 3E). As RNF41 homotrimers are prone to auto-ubiquitination and degradation, disruption of RNF41 homotrimers lead to a more stabilized RNF41 expression [39]. We observed this in S2B Fig, where VPS52 co-expression increases RNF41 monomer expression compared to mock- or VPS52ΔCC- transfected cells. This was compensated for in Fig 3E. These results fit a hypothesis where CC RNF41 and VPS52 monomers can be interchangeable to form RNF41-VPS52 heterotrimers. The existence of such RNF41 and VPS52 heterotrimers is supported by molecular modeling that shows high electrostatic compatibility between the helices of RNF41 and VPS52: E153, K160 and K167 of RNF41 respectively face R125, D136 and E143 in VPS52. Furthermore, E165 and E169 in RNF41 are both able to interact with R145 in VPS52, and R148 in RNF41 can interact with D120, E124 and E127 in VPS52 (Fig 3F). Based on this model we selected three negatively charged residues, D120, E124 and E127 in VPS52 (Fig 3A and 3B) which proved to be important for the interaction with RNF41. MAPPIT and co-immunoprecipitation analysis demonstrated that this VPS52 DEE/RRA mutant prey disrupted the interaction with the RNF41 bait (Fig 3C and 3D).

RNF41 ubiquitinates and relocates VPS52

Since RNF41 is an E3 ubiquitin ligase, we next assessed ubiquitination of VPS52. In contrast to the L163Q mutant, expression of RNF41 clearly enhanced the endogenous ubiquitination status of Flag-tagged VPS52 (Fig 4A). As increased ubiquitination can result in protein degradation, we analyzed the effect of RNF41 on VPS52 protein expression. Interestingly, different conditions of cell lysis showed markedly contrasting results. Co-expression of RNF41 reduced VPS52 protein levels in the RIPA-soluble fraction (Fig 4B, middle) and caused co-enrichment of RNF41 and VPS52 in the sonicated RIPA-insoluble pellet fraction (Fig 4B, right), while total VPS52 levels remained unchanged when cells were physically disrupted by sonication in Laemmli loading buffer (Fig 4B, left). This indicates that RNF41 causes a partial redistribution of VPS52 to the detergent-insoluble fraction. This effect was lost when using a dominant negative (DN) RNF41, a RNF41 truncated form including residues 109 to 317, thus lacking the RING domain and myristoylation site but retaining the CC domain [20,21], or the L163Q mutant. This indicates that the E3 ligase activity and/or membrane anchoring of RNF41 and its specific interaction with VPS52 are necessary for this RNF41-dependent VPS52 redistribution. Moreover, enrichment of RNF41 and L163Q in the RIPA-insoluble pellet fraction (Fig 4B, right), contrary to DN abundancy in the RIPA-soluble fraction (Fig 4B, middle), indicates that the E3 ligase activity and/or membrane anchoring of RNF41 and not merely its oligomerization are required for RNF41 enrichment in the RIPA-insoluble pellet fraction.

We next used confocal microscopy to determine whether RNF41 altered the intracellular localization of VPS52 in HeLa cells. It is known that VPS52 mainly associates with the TGN, together with the three other subunits of the multimeric GARP complex i.e. VPS53, VPS54 and Ang2 [26,27]. However, VPS52 can also reside at recycling endosomes together with the
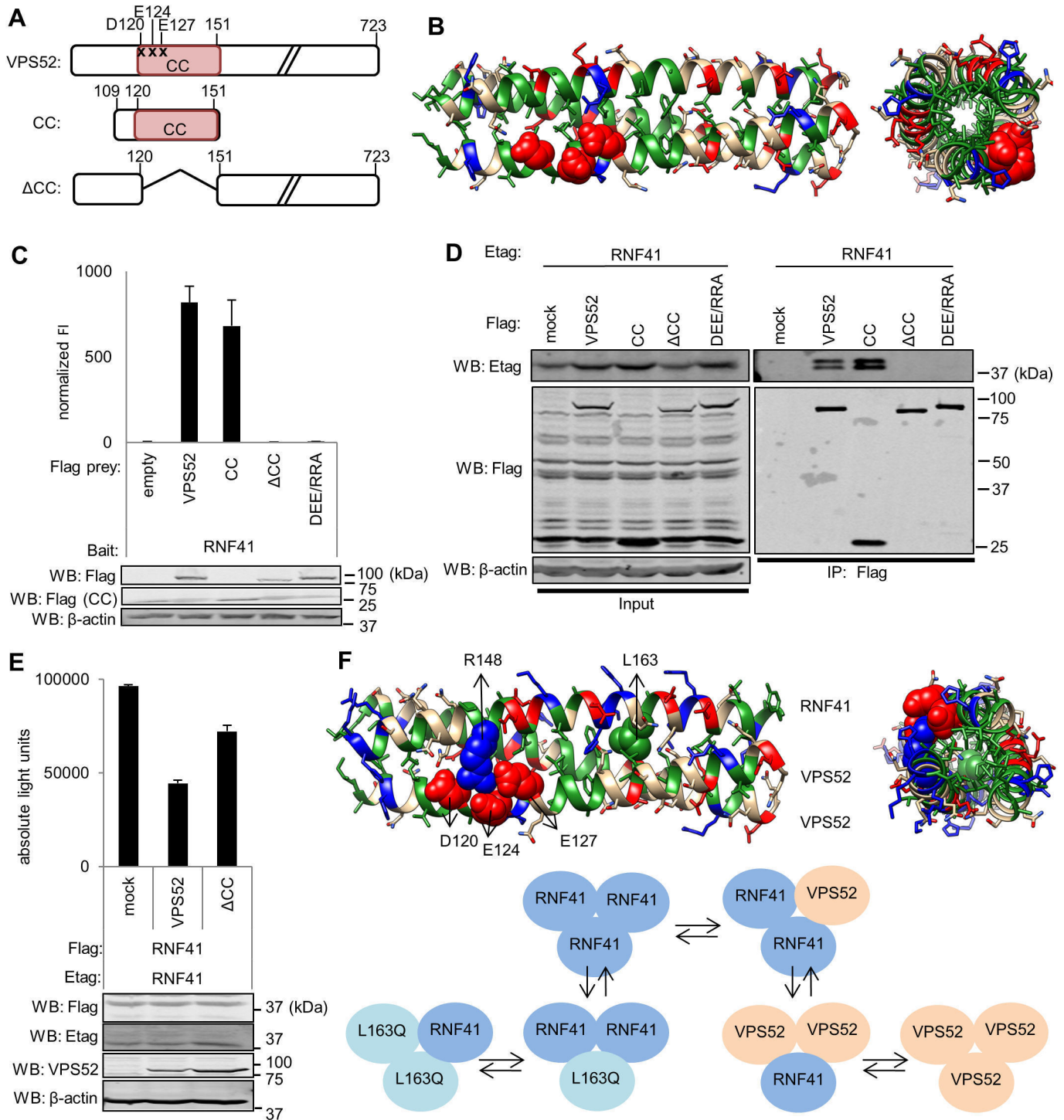
Fig 3. D120, E124 and E127 in the VPS52 CC interact with RNF41 resulting in decreased RNF41 oligomerization. (A) Schematic representation of the amino acid range, point mutations (indicated with x) and subdomain structure of the full length and truncated VPS52 constructs used to map the RNF41 interaction site. Domain designations as in Fig 2A. (B) Side (left) and top (right) view of a model of trimeric VPS52 coiled-coils based on the VPS52 sequence using CC-builder and Logicoil. D120, E124 and E127 are highlighted as red spheres. (C) MAPPIT analysis of HEK293T cells transiently co-transfected with a plasmid encoding an RNF41 bait and an empty; WT; mutated or truncated VPS52 prey. (D) Co-immunoprecipitation analysis of HEK293T cells transiently co-transfected with a vector encoding E-tagged RNF41 and Flag-tagged WT VPS52, VPS52CC-gp130 (prey construct used to optimize expression), VPS52ΔCC, VPS52 DEE/RRA or soluble IL5Rα (mock). Anti-Flag immunoprecipitates (right panel) and lysates (left panel) were visualized with anti-Etag, anti-Flag and anti-actin (loading control). (E) Ectopic expression of VPS52 hampers RNF41 oligomerization. AlphaScreen analysis of HEK293T cells transiently co-transfected with a plasmid encoding E-tagged and Flag-tagged RNF41

together with WT VPS52, VPS52ΔCC or soluble IL5Rα (mock). Values are means ± s.d from triplicate samples from one of three representative experiments. Data and statistical analysis of biological replicates are shown in S3 Fig. **(F)** Model of RNF41-VPS52 heterotrimeric coiled-coils, consisting of one RNF41 CC (upper coil) and two VPS52 CC (lower coils). R148 and L163 in RNF41 and D120, E124 and E127 in VPS52 are highlighted as blue, green and red spheres respectively. The scheme below depicts the proposed idea of interchangeable monomers between RNF41 and VPS52. n = 3 or more for all experiments.

https://doi.org/10.1371/journal.pone.0178132.g003

EARP components, VPS53, Ang2 and Syndetin [32]. To take into account both complexes, we studied the localization of the common GARP and EARP subunits VPS52 and VPS53, solely or together. While ectopically expressed E-tagged VPS52 mainly coincided with the TGN marker p230, RNF41 co-expression caused a redistribution of the large majority of VPS52 to RNF41-bodies with only little overlap between E-tagged VPS52 and p230 remaining (Fig 4C panel I). Localization to the TGN was restored in case of the RNF41 L163Q mutant. No relocalization was observed upon co-transfection of VPS53 and RNF41 or the L163Q mutant, where VPS53 still colocalized with GM130, a Golgi network marker (Fig 4C panel II). Moreover, RNF41 co-expression disrupted the well-established colocalization between VPS53 and E-tagged VPS52 (Fig 4D). Also here, RNF41 reroutes VPS52 away from VPS53, while overexpression of the L163Q mutant does not affect VPS52 localization. AlphaScreen analysis in HEK293T cells ascertained the disruption of the VPS52-VPS53 interaction by RNF41. Ectopic expression of RNF41 compromised the interaction between Flag-tagged VPS53 and E-tagged VPS52, whereas expression of the L163Q mutant did not show this effect (Fig 4E). Altogether, these results show that RNF41 is able to ubiquitinate and relocate VPS52 towards RNF41 bodies, thereby disrupting the interaction with VPS53, a common GARP and EARP subunit.

Discussion

In this paper, we identify VPS52, a subunit of two distinct tethering complexes, GARP and EARP, as a novel interaction partner of RNF41. VPS52 was identified using the high throughput screening method Array MAPPIT [24] and several other assays confirmed this interaction (Fig 1). Domain mapping revealed that the CC domain of RNF41, located in between the N-terminal RING and C-terminal substrate binding domain [21], is necessary and sufficient for interaction with VPS52 (Fig 2B and 2C). This is remarkable, as all other known RNF41 interaction partners such as USP8, ASB6 and ErbB3 interact with its substrate binding domain [22, 40] and Manuscript in preparation]. A combination of random mutagenesis and MAPPIT [36] of the entire RNF41 bait further enabled the identification of critical amino acids involved in the RNF41-VPS52 interface. In line with the domain mapping results, all residues necessary for the interaction with VPS52 were exclusively located in the CC domain of RNF41. We focused on a RNF41 mutant turning a hydrophobic leucine at position 163 into a polar, non-charged glutamine and found that this single residue is necessary for VPS52 interaction. VPS52 also contains an N-terminal CC domain, which proved to be essential for interaction with RNF41 (Fig 3C and 3D). *In silico* modeling of the CC domains of RNF41 and VPS52 lend further support that L163 was important for VPS52 interaction (Fig 3F) and identified a cluster of three residues in the CC domain of VPS52 that mediated the RNF41 interaction (Fig 3B). Next to the CC domain of RNF41, also membrane association is important for interaction with VPS52 as a RNF41 mutant lacking the putative myristoylation site no longer interacted with VPS52 (unpublished observation). Although not much is known about the protein structure of VPS52 and how it interacts with the GARP and EARP subunits, it has been proposed that the N-terminus holding the CC domain is involved in association with other GARP and possibly also EARP subunits [27,41,42]. Our findings provide the first evidence for the involvement of the RNF41 and VPS52 CC domains in a protein interaction.
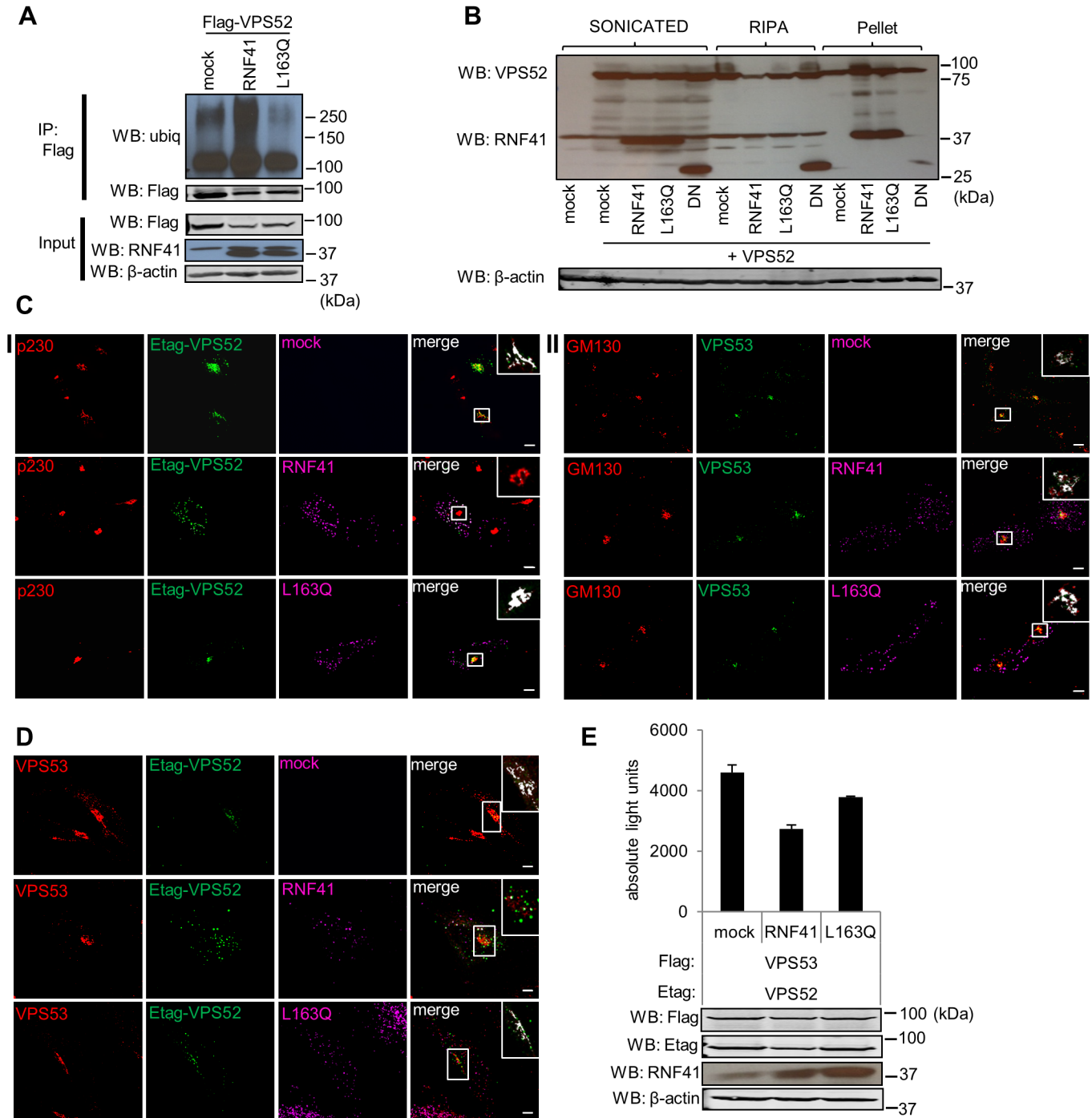
Fig 4. RNF41 ubiquitinates and relocates VPS52. (A) RNF41 enhances VPS52 ubiquitination. HEK293T cells co-transfected with a plasmid encoding Flag-tagged VPS52 and untagged RNF41, L163Q or soluble IL5Rα (mock) were incubated overnight with 5µM MG132 to inhibit proteasomal degradation. Flag-VPS52 was immunoprecipitated and ubiquitination was determined by Western Blotting with an anti-ubiquitin antibody (upper panels). Expression and loading controls were visualized using anti-Flag, RNF41 and anti-β-actin antibodies (lower panels). Statistical analysis is shown in S5A Fig. **(B)** RNF41 co-resides with VPS52 in the RIPA insoluble pellet fraction. HEK293T cells transiently co-transfected with a plasmid encoding untagged VPS52 and untagged RNF41, L163Q, DN RNF41 or soluble IL5Rα (mock) were either sonicated in 2x Laemmli buffer (left) or lysed with RIPA buffer (middle). Insoluble RIPA pellets were sonicated in 2x Laemmli buffer (right). Protein levels were detected by Western blotting using anti-VPS52, anti-RNF41 and anti-β-actin (loading control). Statistical analysis is shown in S5B Fig. **(C)** RNF41 relocates VPS52 and not VPS53. (I) Confocal microscopy of HeLa cells transiently transfected with a vector encoding E-tagged VPS52 together with soluble IL5Rα (mock, upper panel), untagged RNF41 (middle panel) or L163Q (lower panel) (right side shows merged images) were fixed and stained with antibodies against Etag (secondary Alexa Fluor 488, green), RNF41 (secondary Alexa Fluor 568, magenta) and Golgi marker p230

(secondary Alexa Fluor 647, red). (II) Same setup as in I, with co-transfection of VPS53 instead of E-tagged VPS52, and the use of anti-VPS53 (secondary Alexa Fluor 488, green) and co-staining with Golgi marker GM130 (secondary Alexa Fluor 647, red). n = 3 or more independent experiments. **(D)** Confocal microscopy and **(E)** AlphaScreen analysis show that Ectopic RNF41 expression disrupts the VPS52-VPS53 interaction. For confocal microscopy, HeLa cells were transiently transfected with a plasmid encoding E-tagged VPS52 and untagged VPS53 together with soluble IL5Rα (mock, upper panel), untagged RNF41 (middle panel) or L163Q (lower panel) (right side shows merged images), fixed and stained with antibodies against Etag (secondary Alexa Fluor 488, green), VPS53 (secondary Alexa Fluor 568, red) and RNF41 (secondary Alexa Fluor 647, magenta). The inset shows a magnification of the boxed area. The white overlay represents the intersect between the golgi marker and E-tagged VPS52 or VPS53 (C) or between E-tagged VPS52 and VPS53 (D) with a threshold set on standard deviation using Volocity 6.3 software. n = 3 or more independent experiments. Scale bar, 10μm. For AlphaScreen analysis, HEK293T cells were transiently co-transfected with a plasmid encoding E-tagged VPS52 and Flag-tagged VPS53 together with WT RNF41, L163Q or soluble IL5Rα (mock). Values are means ± s.d from triplicate samples from one of three representative experiments. Data and statistical analysis of biological replicates are shown in S3 Fig.

https://doi.org/10.1371/journal.pone.0178132.g004

Besides mediating heteromeric protein-protein interactions amongst a wide range of proteins, alpha-helical CC domains also have self-associating properties. By modeling its CCs, we predicted a trimeric state of RNF41. This is in line with cross-linking and size exclusion chromatography data indicating that RNF41 can self-assemble into a trimeric complex via its CC domain [39]. Similarly, the CC domains of VPS52 were predicted to form trimers (Figs 2E and 3B). Binding of RNF41 or VPS52 to RNF41 through their respective CC may not be mutually exclusive and CC homology modeling predicted that formation of RNF41-VPS52 heterotrimeric structures might occur (Fig 3F). Intertwining of the alpha-helices of the CC domains of RNF41 and VPS52 might lead to dynamic assembly and disassembly of homo- or heterotrimeric protein complexes. Supporting such model, we observed competition between RNF41-VPS52 interaction and RNF41 oligomerization. VPS52 hampered RNF41 oligomerization while VPS52 ΔCC, unable to interact with RNF41, did not affect RNF41 oligomerization (Fig 3E). Conversely, WT RNF41 and not the L163Q mutant reduced VPS52 oligomerization S2A Fig. RNF41 homotrimers are intrinsically instable due to auto-ubiquitination and subsequent proteasomal degradation. This can be counteracted by disrupting RNF41 homotrimerization through the introduction of an exogenous RNF41 CC domain or by CC domain deletion [39]. Similarly, disassembly of RNF41 homotrimers by RNF41-VPS52 complex formation might reduce RNF41 auto-ubiquitination, leading to more stabilized RNF41 expression. In accordance with this, we observed a marked increase in RNF41 monomer expression upon co-expression of VPS52, compared to mock- or VPS52ΔCC- transfected cells S2B Fig. In addition, unlike deletion of the complete CC domain, the RNF41 L163Q mutant did not impair RNF41 oligomerization (Fig 2F and 2G) or auto-ubiquitination (S4 Fig), while both disrupted VPS52 interaction (Fig 2B and 2C). This indicates that this single point mutation in the CC domain is not sufficient to disrupt RNF41 oligomerization and affect auto-ubiquitination. Changes in the oligomerization state of CCs are a widely accepted mechanism that occurs in intracellular transport. SNARE proteins are classical examples of unstructured monomers that can form stable hetero-oligomeric complexes through their CC regions [43]. The MTCs (multisubunit tethering complexes) like the GARP, exocyst and COG (conserved oligomeric Golgi) complex represent another group of multimeric protein complexes in which subunits can be exchanged. These complexes are linked by the presence of predicted short CC regions [44]. Binding of these short CCs is specific but not exclusive as they allow the interaction with different partners at different stages or locations. This is best exemplified by the GARP and EARP complex with the exchange of VPS54 for Syndetin [32] and could potentially be the case for the new RNF41-VPS52 complex.

RNF41 has multiple regulatory functions. Next to ubiquitinating BRUCE, Parkin and USP8 [18,45,46], it is known to downregulate ErbB3 and ErbB4 receptors, as well as several type I cytokine receptors such as the IL-3, EPO, IL-6, LIF and LR [17,19–22]. RNF41 often acts as a sorting signal in the transport of these cargo proteins. It reroutes IL6Rα, LIFRα and LR from the lysosomal degradation pathway to compartments where ectodomain shedding occurs by

ubiquitinating and suppressing USP8 [17,18]. Different functions of RNF41 can be ascribed to distinct locations as ER-localized RNF41 is responsible for downregulating steady state levels of signaling competent ErbB3 receptors by routing them to the ERAD pathway [47], while RNF41 present in endosomes can ubiquitinate internalized ErbB3 receptors and as such reroute them away from recycling pathways to the lysosomes for degradation [48]. All these known functions of RNF41 are mediated by its RING domain, and substrates are known to interact with its C-terminal substrate binding domain [18, 21]. Here, we present data implying a crucial role for the RNF41 CC domain in recruiting VPS52. RNF41, unlike the L163Q mutant, ubiquitinated VPS52 (Fig 4A). Moreover, we observed a reduction in VPS52 protein levels upon RNF41 expression in the soluble fraction of RIPA-lysed cells. Next to specific interaction between RNF41 and VPS52, this effect was also dependent on functional E3 ligase activity and/or membrane association as the L163Q mutant and a truncated RNF41 mutant with dominant-negative properties (DN RNF41 [20,21]) did not decrease VPS52 levels. Surprisingly, VPS52 levels were maintained when cells were lysed using sonication, pointing more towards an RNF41-dependent redistribution rather than degradation of VPS52 (Fig 4B). Previous studies showed that the GARP complex largely associates with the TGN, although the presence of vesicles coinciding with late, early and recycling endosomal markers were also reported, while the EARP complex localizes only to recycling endosomes [26, 29, 32, 41, 49]. In our hands, the expression pattern of the shared GARP and EARP subunits VPS52 and VPS53 primarily overlapped with Golgi markers. RNF41 relocated the majority of VPS52 away from the TGN towards RNF41 bodies, while VPS53 remained TGN associated (Fig 4C). This is also reflected in the reduced interaction between VPS52 and VPS53 upon RNF41 expression (Fig 4D–4E). These results are consistent with our data indicating that RNF41 solely interacts with VPS52, and not with the other GARP or EARP subunits (Fig 1G and 1H). It also further supports the observation that both RNF41 and VPS52 were enriched in the insoluble sonicated RIPA pellet fraction (Fig 4B), indicating that RNF41 is able to relocate part of VPS52 towards insoluble compartments. It remains to be determined which ubiquitin-chain linkage is responsible for the observed VPS52 ubiquitination, K63- and/or M1-linked chains that control localization of proteins would be in line with the observed relocalization of VPS52 by RNF41 (Komander et al, 2012). However, we cannot exclude the possibility of indirect VPS52 ubiquitination, since the mode of interaction with VPS52 (via the CC domain) differs from the other known RNF41 substrates (via the substrate binding domain). An alternative hypothesis is that RNF41 first recruits VPS52 through its CC domain, resulting in rerouting followed by ubiquitination at its new subcellular location by RNF41 or potentially another unidentified E3 ubiquitin ligase. It is possible that interactions with its CC region are reserved for proteins that regulate RNF41, as exemplified in literature where certain proteins like NS1, MAGEA1 and MAGEC2, are known to respectively interact with the CC domain of RING finger proteins TRIM25, TRIM31 and TRIM28 thereby inhibiting or enhancing their E3 ligase activity [50–52].

In conclusion, we identified VPS52, a component of the GARP and EARP complexes, as a novel interaction partner of RNF41 and show that they interact via their CC domains. RNF41 ubiquitinates and relocates VPS52 away from VPS53, another shared subunit of the GARP and EARP complexes, towards RNF41-positive structures. The nature of these RNF41 bodies which incorporate VPS52 remains to be fully elucidated.

Materials and methods

Plasmids and constructs

The generation of all sequence-verified constructs is shown in S3 Table.

Array and binary MAPPIT analysis

Array MAPPIT and the preparation of the prey and reporter reverse transfection mixture was previously described [24]. The screened prey collection entails 8.569 full length human ORF preys selected from the human ORFeome collection version 5.1 (http://horfdb.dfci.harvard.edu/hv5). For binary MAPPIT, 1 x 10^4 HEK293T cells (www.atcc.org, mycoplasma negative) were seeded in a 96-well and transfected with 50 ng of STAT3-dependent pXP2d2-rPAP1-luciferase reporter, 250 ng bait and prey constructs using calcium phosphate. Cells were left untreated or stimulated for 24 hours with human Erythropoietin (5 ng/ml). Luciferase activity from triplicate samples was measured by chemiluminescence in an EnVision plate reader (PerkinElmer) and expressed as fold induction (stimulated/non-stimulated relative light units) relative to the signal generated by a JAK2 binding prey, which corrects for possible varying expression levels of the different baits used. Random mutagenesis of RNF41 bait was performed as described in Uyttendaele *et al*, 2012.

AlphaScreen

2 x 10^5 HEK293T cells were seeded in a 6-well and transfected with 1 μg of both E- and Flag-tagged proteins using calcium phosphate. In the condition where E- and Flag tagged RNF41 are co-expressed with VPS52, only 250 ng of RNF41 was transfected. AlphaScreen experiments were performed according to the manufacturer's protocol (PerkinElmer). 48 h later, cells were lysed in TAP lysis buffer (50 mM Tris–HCl pH 7.5, 125 mM NaCl, 5% glycerol, 0.2% NP40, 1.5 mM MgCl2, 25 mM NaF, 1 mM Na_3VO_4 and Complete^{TM} Protease Inhibitor without EDTA Cocktail (Roche)). Lysates were incubated for 2 hours at 4˚C with 0.7 mg/ml biotinylated anti-E-tag antibody, subsequently incubated for 1 hour at 4˚C with the AlphaScreen FLAG™ (M2) detection kit (PerkinElmer Life Sciences) acceptor beads, and finally for 30 minutes at room temperature with streptavidin donor beads. Samples were measured in triplicate using the EnVision plate reader (PerkinElmer). Expression was analyzed by Western Blotting.

GST-pulldown

BL21(DE3) cells were transformed with GST-constructs. Protein production was induced by 0.2 mM isopropyl-D-thiogalactoside at A600 of 0.6. The bacteria were cultured overnight at 25˚C. After centrifugation at 5000 r.p.m. for 10 minutes, the bacterial pellet was resuspended and sonicated in NETN buffer (20 mM Tris-HCl pH 8; 100 mM NaCl; 6 mM MgCl2; 1 mM EDTA; 0.5% NP40; 1% DTT and Complete^{TM} Protease Inhibitor Cocktail from Roche). The lysate was centrifuged at 12,000 r.p.m. for 10 minutes to obtain the soluble GST proteins in the supernatant. GST proteins were immobilized on Glutathione Sepharose 4B beads (GE Healthcare) for 1 hour at 4˚C and washed three times with NETN buffer. Flag-tagged VPS52, expressed using the TNT T7 Quick Coupled Transcription/Translation System (Promega), was incubated overnight with the GST beads. The beads were washed with NETN buffer and Flag-tagged proteins bound to the GST-proteins were eluted by 10 minutes boiling in 2x SDS gel loading buffer and analyzed by Western blotting.

Western blot analysis

1.5 x 10^5 HEK293T cells were seeded in a 12-well and co-transfected with 1μg of each construct. Cells were washed with PBS, and lysed in RIPA buffer (50 mM Tris-HCl pH 8.0; 200 mM NaCl; 0.05% SDS; 2 mM EDTA; 1% NP-40; 0.5% deoxycholic acid; 1 mM Na3VO4; 1mM NaF; and Complete^{TM} Protease Inhibitor Cocktail (Roche)), or in 2x SDS gel laemmli buffer (62.5 mM Tris- HCl pH 6.8, 3% SDS, 10% glycerol, 5% β-mercaptoethanol and 0.01%

Bromophenol Blue sodium salt) and sonicated using the Bioruptor Plus (Diagenode). After boiling, cell lysates were resolved by SDS-PAGE and transferred to nitrocellulose membranes (Amersham Biosciences). Blots were blocked in Odyssey blocking buffer (LICOR), when using Odyssey infrared imaging (LICOR) or in 5% milk upon ECL (enhanced chemiluminescence) detection. Rabbit anti-VPS52 (1:1500, kind gift from F. Stenner-Liewen) and rabbit anti-RNF41 (1:10.000; Bethyl) were revealed by SuperSignal West Pico Chemiluminescent Substrate (Pierce) using peroxidase-conjugated anti-rabbit antibody (1:10.000, Jackson ImmunoResearch), diluted in milk blocking buffer. Mouse anti-β-actin (1:5000, Sigma) and anti-mouse Dylight 680-conjugated antibody (1:15.000, Pierce) diluted in Odyssey blocking buffer + 0.1% Tween20 was used as a loading control. The following antibodies were used for expression controls in other experiments: anti-Flag rabbit or mouse (1:5000 and 1:10.000, Sigma), anti-E-tag mouse (1: 10.000, Phadia) and anti-GST rabbit (1:5000, Abcam) revealed with anti-rabbit or anti-mouse DyLight 800- or DyLight 680-conjugated antibody (1:15,000, Pierce) diluted in Odyssey blocking buffer +0.1% Tween20. For visualization of the ubiquitin signal we used mouse anti-ubiquitin (VU-1, 1: 1000, LifeSensors), revealed with peroxidase-conjugated anti-mouse antibody (1:10.000, Jackson ImunoResearch), diluted in milk blocking buffer.

Co-immunoprecipitation analysis

HEK293T cells (1.8×10^6 in a 60 mm petri dish) were transfected with 3μg of each construct for 48 hours and cell extracts were prepared in lysis buffer (50 mM Tris HCl pH 7.5; 125 mM NaCl, 0.2% NP40; 1.5 mM MgCl2; 5% glycerol and Complete™ Protease Inhibitor Cocktail from Roche) followed by two freezing rounds of 10 minutes at -80˚C. The lysates were cleared by centrifugation and precleared with sepharose 4B beads (Sigma) followed by incubation overnight at 4˚C with 20μl of monoclonal anti-flag M2 agarose beads (Sigma) to precipitate the Flag-tagged proteins. Immunoprecipitates were washed three times with lysisbuffer and eluted from the beads using Flag peptide (200μg/ml, Sigma). After adding 5x SDS gel loading buffer, samples were analyzed by Western blotting. For endogenous Co-IPs, HEK293T cells were lysed and prepared as described above, After preclearing, 1 ml of lysate was incubated overnight with 1.5 μg of rabbit anti-VPS52 or normal rabbit IgG (Santa Cruz Biotechnology). Subsequently, lysates were incubated with protein A sepharose beads (Sigma) for 2 hours at 4˚C. The beads were washed three times and resuspended in 2 x SDS gel loading buffer.

Ubiquitination assay

HEK293T cells (1.8×10^6 in a 60 mm petri dish) were transfected with 6μg of each construct together with 3μg of Flag-tagged VPS52. The next day, cells were washed and treated overnight with 5 μM MG132 in serum-free OPTIMEM medium (Invitrogen). 48h post-transfection, cells were washed with PBS and lysed in 250 μl of SDS lysis buffer (2% SDS, 150 mM NaCl, 10 mM Tris-HCl, pH 8.0, 2 mM sodium orthovanadate, 50 mM sodium fluoride, 10 mM N-ethyl-maleimide and Complete™ Protease Inhibitor without EDTA Cocktail from Roche). Lysates were sonicated using the Bioruptor Plus (Diagenode), boiled for 10 minutes and diluted in 2250 μl dilution buffer (10 mM Tris-HCl, pH 8.0, 150 mM NaCl, 2 mM EDTA, 1% Triton X-100) for 30–60 minutes at 4˚C under rotation. The lysates were cleared by centrifugation for 30 minutes and precleared with sepharose 4B beads (Sigma) followed by incubation overnight at 4˚C with 20μl of monoclonal anti-flag M2 agarose beads (Sigma) to precipitate the Flag-tagged proteins. Immunoprecipitates were washed three times with wash buffer (10 mM Tris-HCl, pH 8.0, 1 M NaCl, 1 mM EDTA, 1% NP-40) and resuspended in 2x SDS gel loading buffer followed by Western blot analysis.

Confocal microscopy

1.5×10^5 HeLa cells (www.atcc.org, mycoplasma negative) were seeded on No.1.5 glass coverslips (Zeiss) in a 6 well coated with poly-L-lysine (Sigma-Aldrich). The next day, cells were transfected with 100 ng of construct using JetPrime (Polyplus). 24 hours later, cells were rinsed with PBS and fixed for 15 minutes at room temperature in 4% paraformaldehyde. Cells were washed with 100mM phosphate buffer (100 mM Na_2HPO_4; 100 mM NaH_2PO_4, pH 7.4), permeabilized and blocked in blocking buffer (20 mM phosphate buffer; 100 mM NaCl; 0.23% Triton X-100 and 10% donkey serum) for 30 minutes. Samples were incubated for 1.5 hours at room temperature with goat anti-Etag (1:2000, Bethyl), mouse anti-RNF41 (1:500, Santa Cruz), rabbit anti-p230 (1:800, Santa Cruz), goat anti-GM130 (1:150, Santa Cruz) or rabbit anti-VPS53 (1:1500, Abcam). After washing in blocking buffer without donkey serum, cells were incubated for 1 hour at room temperature with donkey anti-goat Alexa Fluor 488 or 647, donkey anti-mouse Alexa Fluor 568 or 647 and donkey anti-rabbit Alexa Fluor 647, 488 or 568. Images were acquired using a 60x 1.35 NA objective on an Olympus IX-81 laser scanning confocal microscope. Intersect was determined using a threshold set on standard deviation intensity in the Volocity 6.3 software (Perkin Elmer, Waltham, MA, USA). Noise removal was done with medium filters.

Supporting information

S1 Table. Random mutagenesis combined with MAPPIT, single mutants.
Table representing all single RNF41 mutants resulting from the screen. Column 1 and 2 show the positions and mutations in RNF41. Column 3, 4 and 5 represent the relative MAPPIT signals of the preys tested against the RNF41 mutants, with EFH1A, a JAK2 binder, as a positive control. The relative MAPPIT signal was calculated as the median of the normalized MAPPIT value, which is the result of the fold induction of each mutant divided by the median of the fold induction of the six WT controls on that plate.
(XLSX)

S2 Table. Random mutagenesis combined with MAPPIT, specific single mutants.
Table representing only the specific single mutants for interaction with VPS52 or ASB6.
(XLSX)

S3 Table. Generation and origin of the constructs used in this paper.
(XLSX)

S1 Fig. L163Q specifically disrupts interaction with VPS52. MAPPIT analysis of HEK293T cells transiently co-transfected with a plasmid encoding an empty, VPS52, ASB6 or USP8 prey together with a RNF41 or L163Q bait.
(TIF)

S2 Fig. (A) Ectopic expression of RNF41 hampers VPS52 oligomerization. AlphaScreen analysis of HEK293T cells transiently co-transfected with a plasmid encoding an E-tagged and Flag-tagged VPS52 together with untagged WT RNF41, L163Q or sol IL5Rα (mock). Values are means ± s.d from triplicate samples from one of three representative experiments. Data and statistical analysis of biological replicates are shown in S3 Fig. **(B) Ectopic expression of VPS52 hampers RNF41 oligomerization and auto-ubiquitination thereby stabilizing RNF41.** HEK293T cells transiently co-transfected with a plasmid encoding an E-tagged and Flag-tagged RNF41 together with WT VPS52, VPS52ΔCC or sol IL5Rα (mock).
(TIF)

S3 Fig. Data and statistical analysis of biological replicates from AlphaScreen experiments in Figs 3E, 4E and S2. One-way ANOVA (randomized block design) showed a marginal significant difference (Fig 3E: P = 0.0983; Fig 4E: P = 0.1106; S2 Fig: P = 0.0693).
(TIF)

S4 Fig. L163Q does not influence RNF41 auto-ubiquitination. HEK293T cells co-transfected with pMet7-vectors encoding Flag-tagged RNF41, L163Q, ΔCC or sol IL5Rα (mock), together with HA-ubiquitin were incubated overnight with 5μM MG132 and 25μM chlolorquine to inhibit proteasomal or lysosomal degradation. Flag immunoprecipitation followed by anti-HA staining revealed the ubiquitination state of the RNF41 mutants.
(TIF)

S5 Fig. Statistical analysis of biological replicates from the data in Fig 4A and 4B. The Western Blots in Fig 4A and 4B, together with biological replicates, were quantified using Image J. **(A)** The ubiquitination signal was normalized for the amount of immunoprecipitated Flag-tagged VPS52 and compared between the mock, RNF41 and L163Q condition. A one-way ANOVA (randomized block design) showed a significant difference in VPS52 ubiquitination between the RNF41 and mock or L163Q transfected cells (p<0.01). **(B)** For each condition (i.e. mock, RNF41, L163Q and DN ectopic expression) the amount of VPS52 in the soluble RIPA and insoluble pellet fraction was compared to the total amount of VPS52 in the sonicated fraction. These results were subjected to a two-way ANOVA with post-hoc comparison (Bonferroni correction) that showed statistical difference between RNF41 and mock or L163Q (p<0.05) for the RIPA fraction and between RNF41 and mock or L163Q (p<0.001) for the pellet fraction.
(TIF)

Acknowledgments

Author Contributions

Conceptualization: DM LDC JW JT.

Investigation: DD SL.

Resources: FS.

Software: FP.

Supervision: JT.

Writing – original draft: DM.

**Writing – review & editing:** JT FP.

References

1. Tokarev AA, Alfonso A, Segev N. Overview of Intracellular Compartments and Trafficking Pathways. Landes Bioscience; 2000.

2. Bonifacino JS, Glick BS. The mechanisms of vesicle budding and fusion. Cell. 2004; 116(2):153–66. PMID: 14744428

3. Bonifacino JS, Rojas R. Retrograde transport from endosomes to the trans-Golgi network. Nat Rev Mol Cell Biol. 2006; 7(8):568–79. https://doi.org/10.1038/nrm1985 PMID: 16936697

99

4. Hsu VW, Bai M, Li J. Getting active: protein sorting in endocytic recycling. Nat Rev Mol Cell Biol. 2012; 13(5):323–8. https://doi.org/10.1038/nrm3332 PMID: 22498832

5. Scott CC, Vacca F, Gruenberg J. Endosome maturation, transport and functions. Semin Cell Dev Biol. 2014; 31:2–10. https://doi.org/10.1016/j.semcdb.2014.03.034 PMID: 24709024

6. Maxfield FR, McGraw TE. Endocytic recycling. Nat Rev Mol Cell Biol. 2004; 5(2):121–32. https://doi.org/10.1038/nrm1315 PMID: 15040445

7. Platta HW, Stenmark H. Endocytosis and signaling. Curr Opin Cell Biol. 2011; 23(4):393–403. https://doi.org/10.1016/j.ceb.2011.03.008 PMID: 21474295

8. Sannerud R, Saraste J, Goud B. Retrograde traffic in the biosynthetic-secretory route: pathways and machinery. Curr Opin Cell Biol. 2003; 15(4):438–45. PMID: 12892784

9. Chia PZC, Gleeson PA. Membrane tethering. F1000Prime Rep. 2014; 6:74. https://doi.org/10.12703/P6-74 PMID: 25343031

10. Cai H, Reinisch K, Ferro-Novick S. Coats, tethers, Rabs, and SNAREs work together to mediate the intracellular destination of a transport vesicle. Dev Cell. 2007; 12(5):671–82. https://doi.org/10.1016/j.devcel.2007.04.005 PMID: 17488620

11. Acconcia F, Sigismund S, Polo S. Ubiquitin in trafficking: the network at work. Exp Cell Res. 2009; 315 (9):1610–8. https://doi.org/10.1016/j.yexcr.2008.10.014 PMID: 19007773

12. Hicke L. A New Ticket for Entry into Budding Vesicles—Ubiquitin. Cell. 2001; 106(5):527–30. PMID: 11551499

13. Piper RC, Lehner PJ. Endosomal transport via ubiquitination. Trends Cell Biol. 2011; 21(11):647–55. https://doi.org/10.1016/j.tcb.2011.08.007 PMID: 21955996

14. Piper RC, Dikic I, Lukacs GL. Ubiquitin-dependent sorting in endocytosis. Cold Spring Harb Perspect Biol. 2014; 6(1):a016808. https://doi.org/10.1101/cshperspect.a016808 PMID: 24384571

15. Williams RL, Urbé S. The emerging shape of the ESCRT machinery. Nat Rev Mol Cell Biol. 2007; 8 (5):355–68. https://doi.org/10.1038/nrm2162 PMID: 17450176

16. Hurley JH. ESCRT complexes and the biogenesis of multivesicular bodies. Curr Opin Cell Biol. 2008; 20(1):4–11. https://doi.org/10.1016/j.ceb.2007.12.002 PMID: 18222686

17. Wauman J, De Ceuninck L, Vanderroost N, Lievens S, Tavernier J. RNF41 (Nrdp1) controls type 1 cytokine receptor degradation and ectodomain shedding. J Cell Sci. 2011; 124(Pt 6):921–32. https://doi.org/10.1242/jcs.078055 PMID: 21378310

18. De Ceuninck L, Wauman J, Masschaele D, Peelman F, Tavernier J. Reciprocal cross-regulation between RNF41 and USP8 controls cytokine receptor sorting and processing. J Cell Sci. 2013; 126(Pt 16):3770–81. https://doi.org/10.1242/jcs.131250 PMID: 23750007

19. Jing X, Infante J, Nachtman RG, Jurecic R. E3 ligase FLRF (Rnf41) regulates differentiation of hematopoietic progenitors by governing steady-state levels of cytokine and retinoic acid receptors. Exp Hematol. 2008; 36(9):1110–20. https://doi.org/10.1016/j.exphem.2008.04.001 PMID: 18495327

20. Diamonti AJ, Guy PM, Ivanof C, Wong K, Sweeney C, Carraway KL. An RBCC protein implicated in maintenance of steady-state neuregulin receptor levels. Proc Natl Acad Sci U S A. 2002; 99(5):2866–71. https://doi.org/10.1073/pnas.052709799 PMID: 11867753

21. Qiu X-B, Goldberg AL. Nrdp1/FLRF is a ubiquitin ligase promoting ubiquitination and degradation of the epidermal growth factor receptor family member, ErbB3. Proc Natl Acad Sci U S A. 2002; 99 (23):14843–8. https://doi.org/10.1073/pnas.232580999 PMID: 12411582

22. Bouyain S, Leahy DJ. Structure-based mutagenesis of the substrate-recognition domain of Nrdp1/FLRF identifies the binding site for the receptor tyrosine kinase ErbB3. Protein Sci. 2007; 16(4):654–61. https://doi.org/10.1110/ps.062700307 PMID: 17384230

23. Wang C, Chen T, Zhang J, Yang M, Li N, Xu X, et al. The E3 ubiquitin ligase Nrdp1 "preferentially" promotes TLR-mediated production of type I interferon. Nat Immunol. 2009; 10(7):744–52. https://doi.org/10.1038/ni.1742 PMID: 19483718

24. Lievens S, Vanderroost N, Van der Heyden J, Gesellchen V, Vidal M, Tavernier J. Array MAPPIT: High-Throughput Interactome Analysis in Mammalian Cells. J Proteome Res. 2009; 8(2):877–86. https://doi.org/10.1021/pr8005167 PMID: 19159283

25. Conibear E, Cleck JN, Stevens TH. Vps51p mediates the association of the GARP (Vps52/53/54) complex with the late Golgi t-SNARE Tlg1p. Mol Biol Cell. 2003; 14(4):1610–23. https://doi.org/10.1091/mbc.E02-10-0654 PMID: 12686613

26. Liewen H, Meinhold-Heerlein I, Oliveira V, Schwarzenbacher R, Luo GR, Wadle A, et al. Characterization of the human GARP (Golgi associated retrograde protein) complex. Exp Cell Res. 2005; 306 (1):24–34. https://doi.org/10.1016/j.yexcr.2005.01.022 PMID: 15878329

100

27. Pérez-Victoria FJ, Schindler C, Magadán JG, Mardones GA, Delevoye C, Romao M, et al. Ang2/fat-free is a conserved subunit of the Golgi-associated retrograde protein complex. Mol Biol Cell. 2010; 21 (19):3386–95. https://doi.org/10.1091/mbc.E10-05-0392 PMID: 20685960

28. Conibear E, Stevens TH. Vps52p, Vps53p, and Vps54p form a novel multisubunit complex required for protein sorting at the yeast late Golgi. Mol Biol Cell. 2000; 11(1):305–23. PMID: 10637310

29. Pérez-Victoria FJ, Mardones GA, Bonifacino JS. Requirement of the human GARP complex for mannose 6-phosphate-receptor-dependent sorting of cathepsin D to lysosomes. Mol Biol Cell. 2008; 19 (6):2350–62. https://doi.org/10.1091/mbc.E07-11-1189 PMID: 18367545

30. Fröhlich F, Petit C, Kory N, Christiano R, Hannibal-Bach H-K, Graham M, et al. The GARP complex is required for cellular sphingolipid homeostasis. Elife. 2015; 4:e08712.

31. Hirata T, Fujita M, Nakamura S, Gotoh K, Motooka D, Murakami Y, et al. Post-Golgi anterograde transport requires GARP-dependent endosome-to-TGN retrograde transport. Mol Biol Cell. 2015; 26 (17):3071–84. https://doi.org/10.1091/mbc.E14-11-1568 PMID: 26157166

32. Schindler C, Chen Y, Pu J, Guo X, Bonifacino JS. EARP is a multisubunit tethering complex involved in endocytic recycling. Nat Cell Biol 17(5), 639–50. 2015; 17(5):639–50. https://doi.org/10.1038/ncb3129 PMID: 25799061

33. Eyckerman S, Verhee A, Van der Heyden J, Lemmens I, Van Ostade X, Vandekerckhove J, et al. Design and application of a cytokine-receptor-based interaction trap. Nat Cell Biol. 2001; 3:1114–9. https://doi.org/10.1038/ncb1201-1114 PMID: 11781573

34. Kim S, Zhang S, Choi KH, Reister R, Do C, Baykiz AF, et al. An E3 ubiquitin ligase, Really Interesting New Gene (RING) Finger 41, is a candidate gene for anxiety-like behavior and beta-carboline-induced seizures. Biol Psychiatry. 2009; 65(5):425–31. https://doi.org/10.1016/j.biopsych.2008.09.015 PMID: 18986647

35. Rolland T, Taşan M, Charloteaux B, Pevzner SJ, Zhong Q, Sahni N, et al. A Proteome-Scale Map of the Human Interactome Network. Cell. 2014; 159(5):1212–26. https://doi.org/10.1016/j.cell.2014.10.050 PMID: 25416956

36. Uyttendaele I, Lavens D, Catteeuw D, Lemmens I, Bovijn C, Tavernier J, et al. Random mutagenesis MAPPIT analysis identifies binding sites for Vif and Gag in both cytidine deaminase domains of Apobec3G. PLoS One. 2012; 7(9):e44143. https://doi.org/10.1371/journal.pone.0044143 PMID: 22970171

37. Wu X, Yen L, Irwin L, Sweeney C, Carraway KL. Stabilization of the E3 ubiquitin ligase Nrdp1 by the deubiquitinating enzyme USP8. Mol Cell Biol. 2004; 24(17):7748–57. https://doi.org/10.1128/MCB.24.17.7748-7757.2004 PMID: 15314180

38. Vincent TL, Green PJ, Woolfson DN. LOGICOIL—multi-state prediction of coiled-coil oligomeric state. Bioinformatics. 2013; 29(1):69–76. https://doi.org/10.1093/bioinformatics/bts648 PMID: 23129295

39. Printsev I, Yen L, Sweeney C, Carraway KL. Oligomerization of the Nrdp1 E3 ubiquitin ligase is necessary for efficient autoubiquitination but not ErbB3 ubiquitination. J Biol Chem. 2014; 289(12):8570–8. https://doi.org/10.1074/jbc.M113.527036 PMID: 24519943

40. Avvakumov G V, Walker JR, Xue S, Finerty PJ, Mackenzie F, Newman EM, et al. Amino-terminal dimerization, NRDP1-rhodanese interaction, and inhibited catalytic domain conformation of the ubiquitin-specific protease 8 (USP8). J Biol Chem. 2006; 281(49):38061–70. https://doi.org/10.1074/jbc.M606704200 PMID: 17035239

41. Pérez-Victoria FJ, Bonifacino JS. Dual roles of the mammalian GARP complex in tethering and SNARE complex assembly at the trans-golgi network. Mol Cell Biol. 2009; 29(19):5251–63. https://doi.org/10.1128/MCB.00495-09 PMID: 19620288

42. Chou H-T, Dukovski D, Chambers MG, Reinisch KM, Walz T. CATCHR, HOPS and CORVET tethering complexes share a similar architecture. Nat Struct Mol Biol. 2016; 23(8):761–3. https://doi.org/10.1038/nsmb.3264 PMID: 27428774

43. Fasshauer D. Structural insights into the SNARE mechanism. Biochim Biophys Acta—Mol Cell Res. 2003; 1641(2–3):87–97.

44. Whyte JRC, Munro S. Vesicle tethering complexes in membrane traffic. J Cell Sci. 2002; 115 (13):2627–37.

45. Qiu X-B, Markant SL, Yuan J, Goldberg AL. Nrdp1-mediated degradation of the gigantic IAP, BRUCE, is a novel pathway for triggering apoptosis. EMBO J. 2004; 23(4):800–10. https://doi.org/10.1038/sj.emboj.7600075 PMID: 14765125

46. Zhong L, Tan Y, Zhou A, Yu Q, Zhou J. RING finger ubiquitin-protein isopeptide ligase Nrdp1/FLRF regulates parkin stability and activity. J Biol Chem. 2005; 280(10):9425–30. https://doi.org/10.1074/jbc.M408955200 PMID: 15632191
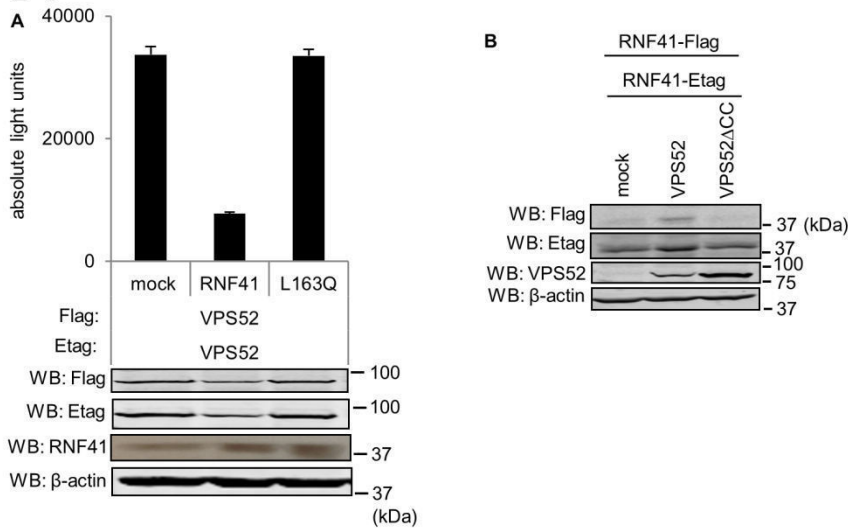
47. Fry WHD, Simion C, Sweeney C, Carraway KL. Quantity control of the ErbB3 receptor tyrosine kinase at the endoplasmic reticulum. Mol Cell Biol. 2011; 31(14):3009–18. https://doi.org/10.1128/MCB. 05105-11 PMID: 21576364

48. Cao Z, Wu X, Yen L, Sweeney C, Carraway KL. Neuregulin-induced ErbB3 downregulation is mediated by a protein stability cascade involving the E3 ubiquitin ligase Nrdp1. Mol Cell Biol. 2007; 27(6):2180–8. https://doi.org/10.1128/MCB.01245-06 PMID: 17210635

49. Pérez-Victoria FJ, Abascal-Palacios G, Tascón I, Kajava A, Magadán JG, Pioro EP, et al. Structural basis for the wobbler mouse neurodegenerative disorder caused by mutation in the Vps54 subunit of the GARP complex. Proc Natl Acad Sci U S A. 2010; 107(29):12860–5. https://doi.org/10.1073/pnas. 1004756107 PMID: 20615984

50. Gack MU, Albrecht RA, Urano T, Inn K-S, Huang I-C, Carnero E, et al. Influenza A virus NS1 targets the ubiquitin ligase TRIM25 to evade recognition by the host viral RNA sensor RIG-I. Cell Host Microbe. 2009; 5(5):439–49. https://doi.org/10.1016/j.chom.2009.04.006 PMID: 19454348

51. Kozakova L, Vondrova L, Stejskal K, Charalabous P, Kolesar P, Lehmann AR, et al. The melanoma-associated antigen 1 (MAGEA1) protein stimulates the E3 ubiquitin-ligase activity of TRIM31 within a TRIM31-MAGEA1-NSE4 complex. Cell Cycle. 2015; 14(6):920–30. https://doi.org/10.1080/15384101. 2014.1000112 PMID: 25590999

52. Doyle JM, Gao J, Wang J, Yang M, Potts PR. MAGE-RING protein complexes comprise a family of E3 ubiquitin ligases. Mol Cell. 2010; 39(6):963–74. https://doi.org/10.1016/j.molcel.2010.08.029 PMID: 20864041
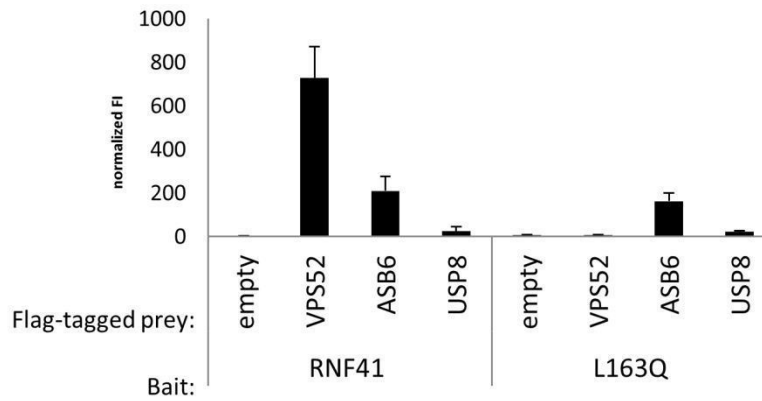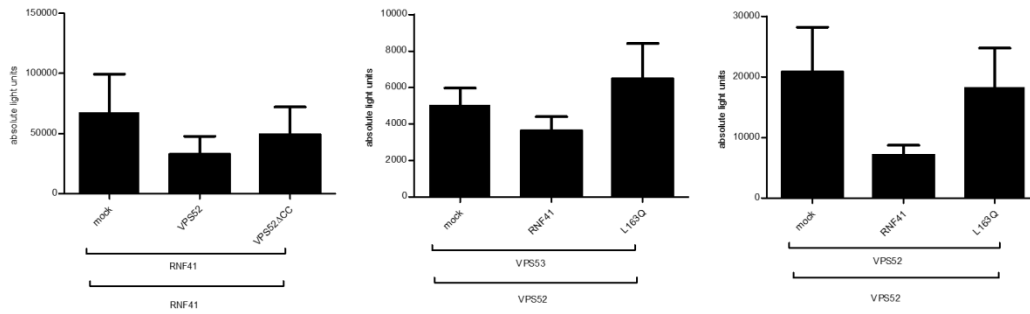
S1_Fig

S1 Fig. L163Q specifically disrupts interaction with VPS52. MAPPIT analysis of HEK293T cells transiently co-transfected with a plasmid encoding an empty, VPS52, ASB6 or USP8 prey together with a RNF41 or L163Q bait.

S2_Fig

S2 Fig. (A) **Ectopic expression of RNF41 hampers VPS52 oligomerization**. AlphaScreen analysis of HEK293T cells transiently co-transfected with a plasmid encoding an E-tagged and Flag-tagged VPS52 together with untagged WT RNF41, L163Q or sol IL5Rα (mock). Values are means ± s.d from triplicate samples from one of three representative experiments. Data and statistical analysis of biological replicates are shown in S3 Fig. (B) **Ectopic expression of VPS52 hampers RNF41 oligomerization and auto-ubiquitination thereby stabilizing RNF41**. HEK293T cells transiently co-transfected with a plasmid encoding an E-tagged and Flag-tagged RNF41 together with WT VPS52, VPS52ΔCC or sol IL5Rα (mock).
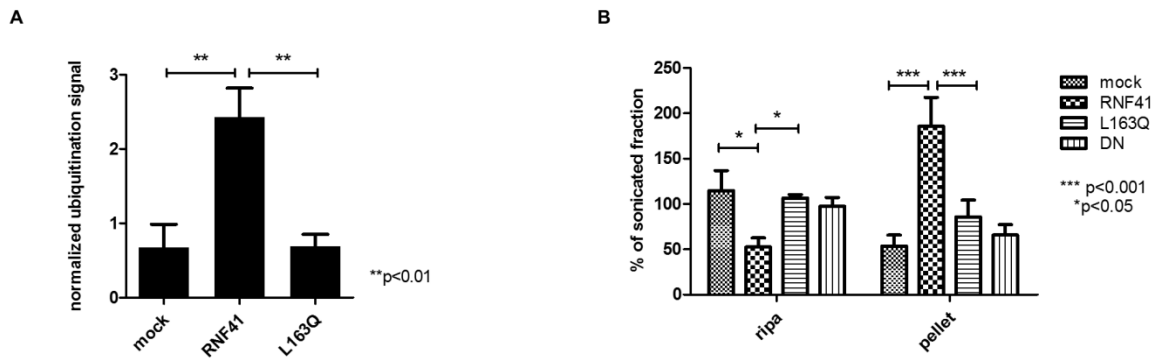
S3_Fig

S3 Fig. Data and statistical analysis of biological replicates from AlphaScreen experiments in Figs 3E, 4E and S2. One-way ANOVA (randomized block design) showed a marginal significant difference (Fig 3E: P = 0.0983; Fig 4E: P = 0.1106; S2 Fig: P = 0.0693).

S4_Fig
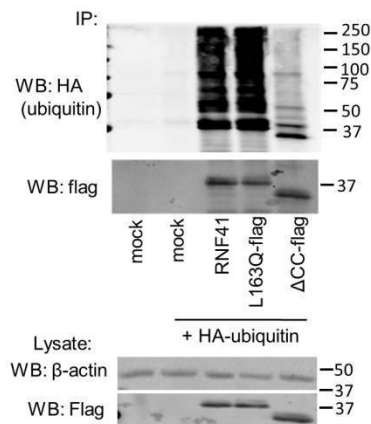
S4 Fig. L163Q does not influence RNF41 auto-ubiquitination. HEK293T cells co-transfected with pMet7-vectors encoding Flag-tagged RNF41, L163Q, ΔCC or sol IL5Rα (mock), together with HA-ubiquitin were incubated overnight with 5μM MG132 and 25μM chlolorquine to inhibit proteasomal or lysosomal degradation. Flag immunoprecipitation followed by anti-HA staining revealed the ubiquitination state of the RNF41 mutants.

S5 Fig. Statistical analysis of biological replicates from the data in Fig 4A and 4B. The Western Blots in Fig 4A and 4B, together with biological replicates, were quantified using Image J. (A) The ubiquitination signal was normalized for the amount of immunoprecipitated Flag-tagged VPS52 and compared between the mock, RNF41 and L163Q condition. A one-way ANOVA (randomized block design) showed a significant difference in VPS52 ubiquitination between the RNF41 and mock or L163Q transfected cells ($p<0.01$). (B) For each condition (i.e. mock, RNF41, L163Q and DN ectopic expression) the amount of VPS52 in the soluble RIPA and insoluble pellet fraction was compared to the total amount of VPS52 in the sonicated fraction. These results were subjected to a two-way ANOVA with post-hoc comparison (Bonferroni correction) that showed statistical difference between RNF41 and mock or L163Q ($p<0.05$) for the RIPA fraction and between RNF41 and mock or L163Q ($p<0.001$) for the pellet fraction.

S1 Table

position AA	mutation	ASB6	VPS52	EFH1A
61	T61K	0,36953379	0,9765057	1,76387244
61	T61M	0,81138884	0,9205568	0,57520708
69	P69S	0,26674214	1,0171002	1,24527236
70	R70L	0,29473992	0,9133219	1,52407841
77	S77P	0,23317792	0,8492693	1,50581454
77	S77L	0,39010404	0,8320182	1,25147287
83	C83Y	0,44192332	0,8713712	0,97628475
84	D84N	0,53683349	0,5856752	0,81151709
84	D84H	0,20569557	0,7694646	0,80168029
87	V87M	0,61083071	0,7898355	1,30962211
88	F88L	0,7052382	0,8216528	0,9502522
89	G89C	0,59263895	0,7043611	0,98598522
95	R95W	0,71101018	0,5756181	0,97809111
98	N98Y	0,70216297	0,8069333	0,94798535
98	N98K	0,53783121	0,814843	0,69769663
99	L99P	0,39546577	0,8087754	1,60896744
99	L99H	0,599362	0,8735778	1,10681031
104	S104R	0,93735962	0,6996397	0,91254602
106	C106Y	0,0303103	1,1247857	1,89875227
108	H108L	0,40391465	0,6113655	1,58700698
109	N109D	0,39682419	0,6581925	1,61009644
112	R112W	0,60085023	0,8032191	0,5779027
112	R112Q	0,43723491	0,7779057	1,03485664
116	C116R	0,65947628	0,2729743	0,84368137
118	Q118L	0,13541155	1,033833	2,08993146
119	G119C	0,44310937	0,223739	0,98768949
120	C120R	0,25577075	0,3047095	3,83534916
121	G121V	0,89125768	0,4572335	1,14480579
123	E123K	0,4249667	0,5712967	1,20344867
124	M124I	0,51394861	0,1958864	1,24007061
125	P125H	0,59638946	0,7874175	1,35386965
125	P125S	0,40353784	0,7269915	1,77422282
126	K126R	0,57686988	0,9245272	1,05453877
128	E128G	0,89576424	1,1337548	0,84111114
128	E128G	0,45919151	0,6058244	0,81726463
131	N131I	0,31523403	0,9275294	0,67591963
131	N131Y	0,74638044	1,0611953	1,19637756
132	H132Y	0,36382778	0,4360728	1,86941938
132	H132D	0,58719157	0,4493198	0,64406366
132	H132Y	0,26170408	0,4604682	2,55686161
133	N133S	0,77775007	0,7981179	0,99617495
133	N133I	0,71741573	0,6657585	1,06049731
135	I135N	0,58615098	0,2547316	1,26975014
137	H137R	0,64231627	0,0737958	0,96691063

137	H137L	0,13247004	0,0381617	1,250844
138	L138M	0,53022579	0,8138754	0,92516765
138	L138Q	1,12159729	0,0137276	1,25982683
145	Q145H	0,63460622	1,0098923	1,12321961
145	Q145P	0,69613933	0,007918	1,65567993
148	R148C	0,74732301	0,0249683	0,56571647
153	E153V	0,36930322	0,8740117	1,24213892
154	K154N	0,39995637	1,0830125	1,27193649
158	E158D	0,60540626	0,8338607	1,42900827
159	H159Y	0,66878298	0,1825419	1,0885409
159	H159L	0,29299475	1,0356296	1,36760387
160	K160I	0,29829513	0,3138894	1,42107399
162	Q162H	0,91147987	0,444721	1,15373185
162	Q162H	0,10568623	0,4294918	1,5335004
163	L163Q	0,90016639	0,0172903	0,73068434
163	L163P	0,78227081	0,0123849	2,27892326
166	Q166L	0,60097216	1,083836	1,00260842
170	I170T	0,69004037	0,0422675	1,59038753
170	I170N	1,08606692	0,0083806	1,56940262
173	L173I	0,73222053	0,5874012	0,66896773
177	M177I	0,58005133	0,4477608	0,87087843
181	R181L	0,41147357	1,0420746	1,42487205
189	N189Y	0,38893986	0,7095052	0,90633139
190	L190P	0,75336332	0,6450948	1,19609293
191	E191V	0,50056665	0,6676948	1,21310995
194	I194N	0,45496932	0,795848	0,92522264
196	Y196H	0,59914826	0,5100577	1,10397687
196	Y196H	0,79911322	0,6675553	1,6046442
197	N197D	0,40769161	0,7204851	1,07986732
202	W202C	0,20399165	0,6176285	0,82454233
202	W202R	0,03475107	0,226162	1,44722133
202	W202G	0,30338769	0,6579043	1,22299636
203	V203M	0,2891222	0,8123217	1,55712024
209	A209V	0,8418015	0,9964533	0,56552768
210	R210T	0,6312329	0,9108947	0,73449505
212	T212S	0,67697595	0,8496229	1,20198263
212	T212I	0,41666707	1,0510252	1,75015759
213	R213C	1,27536555	1,0030178	1,62772469
214	W214C	0,06938865	0,2534766	1,86723334
214	W214R	0,02466675	0,2558658	2,04787534
215	G215E	1,05631278	0,7737422	1,01054552
215	G215E	0,73419574	0,8905318	1,56391109
217	M217V	1,00201168	0,8358497	0,87630082
217	M217V	0,7050458	1,0304211	1,17864915
217	M217T	0,02390221	0,2068466	2,84426797
219	S219L	0,0250253	0,3320982	2,7125154

220	T220A	0,07583181	0,9542239	0,69473643
220	T220A	0,08262559	0,8179446	1,29958976
224	V224M	0,49805743	0,8622194	1,78376505
225	L225H	0,26953317	0,7184912	4,38121763
226	Q226K	0,47316154	0,8199195	0,8427934
227	A227T	0,33329783	0,6797115	2,99979382
230	K230E	0,63474093	0,8833858	1,03930697
230	K230E	0,32020533	0,9607123	2,19294952
233	L233D	0,03386514	0,2386468	1,70000543
235	E235G	0,44818036	0,8241216	1,71725224
236	S236N	0,07795108	0,4113383	0,77694015
237	G237D	0,4990214	0,6722196	1,55562555
238	C238S	0,10641084	0,5620076	1,63988696
238	C238S	0,02143371	0,3581456	1,03879535
239	P239H	0,05584209	0,4554081	2,63663451
241	S241Y	0,28236384	0,6284714	2,43537669
242	I242V	0,57361819	1,05869	1,46452623
242	I242N	0,01752322	0,3926028	1,33901094
243	V243A	0,1735202	0,6690218	2,34624823
244	N244I	0,55590401	0,7774884	1,83675393
246	L246P	0,02036139	0,1353056	2,22176205
247	I247N	0,04962493	0,6955627	3,44135717
247	247N	0,34294189	0,72627	1,49723382
251	H251Q	0,2423014	0,6258655	0,95378616
255	W255C	0,0160425	0,218247	1,52967704
256	P256A	0,04424429	0,4732772	3,10481799
258	G258D	0,14379154	0,6231628	1,67786724
260	A260V	0,0883241	0,8177156	2,57269432
261	T261A	0,6031658	0,8845948	1,09522172
262	L262Q	0,03561199	0,768548	1,90280073
262	L262P	0,06217264	0,7424845	2,66096872
263	E263K	0,38895868	1,0035017	1,88776407
265	R265I	0,02153525	0,1855592	2,02042303
265	R265I	0,02471793	0,3074393	1,77281739
266	Q266H	0,01869853	0,0036522	1,52683597
268	N268I	0,0479824	0,440682	3,38603192
268	N268Y	0,57904903	0,8842708	0,97521592
268	N268S	1,8977434	1,5231281	1,67949586
270	R270H	0,45870775	0,7547494	0,79869686
271	Y271D	0,12039595	0,778755	1,66866256
276	V276E	0,66315592	0,9360612	1,38424629
276	V276A	0,32247799	0,6845931	1,17607085
276	V276M	0,0631523	0,4767385	1,06595941
276	V276A	0,54079229	0,9443168	1,17664623
277	A227D	0,79301777	0,9468914	1,09701436
278	Y278H	0,04926894	0,2899932	1,79121952

281	P281T	0,51625353	0,7722161	3,49617351
284	Q284Y	0,45139053	0,6588139	2,83838955
285	A285V	1,38189036	0,6686424	1,64653189
285	A285T	0,04514166	0,2800539	4,68300979
286	V286G	0,03397093	0,4031727	1,79444051
287	V287A	0,47048914	0,8759703	1,97940248
289	M289I	0,39101166	0,8616651	1,90447005
289	M289V	0,03401168	0,2555988	1,92115812
289	M289V	0,23919631	0,8042051	1,90156195
294	N294K	0,01448356	0,1920535	2,15082707
295	H295Y	0,27135391	0,628407	2,74143467
295	H295Y	0,1559407	0,6193911	2,16052302
296	M296R	0,05835019	0,3139475	2,26912644
298	D298G	0,44532592	0,8200294	1,37310982
298	D298G	0,254024	1,0540513	3,55073719
300	M300K	0,41055777	0,7614755	2,3358728
300	M300L	1,26435444	0,9676143	0,77333363
307	V307F	0,02649419	0,2068875	1,84447728
308	M308V	0,61321524	0,8115375	0,74176665
310	F310Y	0,22394057	0,7988185	2,50516772
310	F310L	0,01485981	0,2373833	1,56290907
310	F310I	0,01761029	0,28476	1,63835576
312	H312Q	0,51944572	0,7122444	1,51638264
312	H312R	0,89871509	0,9056529	1,08823494
313	G313D	0,10274408	0,5284451	1,28689031

S2 Table

position AA	mutation	ASB6	VPS52	EFH1A
106	C106Y	0,03031	1,12479	1,89875
118	Q118L	0,13541	1,03383	2,08993
137	H137R	0,64232	0,0738	0,96691
138	L138Q	1,1216	0,01373	1,25983
145	Q145P	0,69614	0,00792	1,65568
148	R148C	0,74732	0,02497	0,56572
159	H159Y	0,66878	0,18254	1,08854
163	L163Q	0,90017	0,01729	0,73068
163	L163P	0,78227	0,01238	2,27892
170	I170T	0,69004	0,04227	1,59039
170	I170N	1,08607	0,00838	1,5694
202	W202C	0,20399	0,61763	0,82454
203	V203M	0,28912	0,81232	1,55712
220	T220A	0,07583	0,95422	0,69474
220	T220A	0,08263	0,81794	1,29959
247	I247N	0,04962	0,69556	3,44136
258	G258D	0,14379	0,62316	1,67787
260	A260V	0,08832	0,81772	2,57269
262	L262Q	0,03561	0,76855	1,9028
262	L262P	0,06217	0,74248	2,66097
276	V276M	0,06315	0,47674	1,06596
289	M289V	0,2392	0,80421	1,90156
298	D298G	0,25402	1,05405	3,55074
310	F310Y	0,22394	0,79882	2,50517
313	G313D	0,10274	0,52845	1,28689

S3 Table				
pMG1-VPS52	huORF5.1	pMG1	LR reaction	
pMET7-VPS52-Flag		pMET7-Flag		
pMET7-Etag-VPS52		Etag-pMET7		
pMET7-VPS52-Etag		pMET7-Etag		
		(De Ceuninck et al, 2013; Lievens et al, 2009)		
pCLG-RNF41 C34S/H36Q bait	pSEL-RNF41	pCLG	SacI-NotI + mutagenesis	5'-GTACAGGCACCTCATTGTGAACATGCTTTCTGCAACGCC-3'
	(De Ceuninck et al, 2013)			5'-GGCGTTGCAGAAAGCTTGTTCACTATGAGGTGCCTGTAC-3'
RNF41 C34S/H36Q bait	pCLG-RNF41 C34S/H36Q	pSEL	SacI-NotI	
RNF41 C43S/H36Q L163Q bait	RNF41 C34S/H36Q bait		mutagenesis	5'-GAACACAAACACCAGCAGGCGGAGCAGAAGCGAGACATCCAGC-3'
pMET7-RNF41L163Q	pMET7-RNF41 (De Ceuninck et al, 2013)			5'-GCTGGATGTCTCGCTTCTGCTCCGCCTGCTGGTGTTTGTGTTC-3'
pMET7-RNF41L163Q-Flag	pMET7-RNF41-Flag			
RNF41 N-terminal bait	pMET7-RNF41-Etag	pSEL-FKBP12 (Eyckerman et al, 2001)	SacI-NotI	5'-GCGGAGCTCGATGGGGTATGATGTAACCCGTTTCC-3'
				5'-CGCGCGGCCGCTTAGCAGTTATGGTTGGGCAGCTC-3'
RNF41 C-terminal bait	pMET7-RNF41-Etag	pSEL-FKBP12	SacI-NotI	5'-GCGGAGCTCGATTAAGCACCTGCGCTCAGTGG-3'
				5'-CGCGCGGCCGCTTATATCTCTTCCACGCCATGCG-3'
RNF41 substrate binding bait	pMET7-RNF41-Etag	pSEL-FKBP12	SacI-NotI	5'-GCGGAGCTCGGCAATCCGCAGTGTC-3'
				5'-CGCGCGGCCGCTTATATCTCTTCCACGCCATGCG-3'
RNF41 CC bait	pMET7-RNF41-Etag	pSEL-FKBP12	SacI-NotI	5'-GCCGAGCTCCATGATTAAGCACCTGCGCTCAGTGG-3'

	(Wauman et al, 2011)			5'- CCTGCGGCCGCTTTAACGCATGTATGCCTTTAGCAGC-3'
pMET7-VPS52	pMET7-VPS52-Flag		mutagenesis	5'-GCCCAACTTCTGACCAACTTTC-3'
				5'-GAAAGTTGGTCAGAAGTTGGGC-3'
pMET7-VPS52 DEE/RRA-Flag	pMET7-VPS52-Flag		mutagenesis	5'-TCTCTACACAACCAGATCACAGCCTGTCGTGCAGTCCTGCGGCGA A TGGCGCAGATGTTGGGAGCTTTTCAGG-3'
pMG1-VPS52 DEE/RRA	pMG1-VPS52			5'-CACTCTGAAAAGCTCCCAACATCTGCGCCATTCGCCGCAGGACTG CA CGACAGGCTGTGATCTGGTTGTGTAGAGA-3'
pMET7-VPS52ΔCC-Flag	pMet7-VPS52-Flag		Mutagenesis 1	5'-CAACCAGATCACAGCCTGTGATGTCGACCTGGAGCGAATGGAGC -3'
				5'-GCTCCATTCGCTCCAGGTCGACATCACAGGCTGTGATCTGGTTG-3'
			Mutagenesis 2	5'-CTGAGATCCGGACACTGCAGGAAGTCGACGGAGCCATGAACATT CGAC-3'
			+ SalI digest	5'-GTCGAATGTTCATGGCTCCGTCGACTTCCTGCAGTGTCCGGATCT CAG-3'
pMET7-VPS52ΔCC	pMET7-VPS52ΔCC -FLag	pMET7	EcoRV-DraIII	
pMG-VPS52ΔCC		pMG1		
pMG1-VPS52 CC	pMET7-VPS52	pMG1	EcoRI-NotI	5'-GCCGAATTCGCCATGGCTGTCCTGGAGCG-3'
				5'-GCGCGGCCGCTTTATGACTGTTCCTGCAG-3' or
pMET7-VPS52 CC-Flag		pMET7-flag		5'-GCGCGGCCGCTTGACTGTTCCTGCAGTG-3'
pcDNA3.1-Flag-VPS52	pMET7-Flag-VPS52	pCDNA3.1 vector	Mutagenesis + AflII-XbaI	5'-TGCGGGCCCTTAAGCATGGATTAC-3'
				5'-GTAATCCATGCTTAAGGGCCCGCA-3'
pMET7-RNF41-Flag	pMET7-RNF41-Etag		XhoI-XbaI	5'-TCGAGGATTACAAGGATGACGACGATAAGTAAT-3'
pMET7-RNF41 Nterm-Flag	pMET7-RNF41 Nterm-Etag			5'- CTAGATTACTTATCGTCGTCATCCTTGTAATCC-3'
pMET7- C-term-Flag	pMEt7-RNF41 Cterm-Etag			
pMET7-RNF41 CC-Flag	pMet7-RNF41-Flag	pMET7	EcoRI-NotI	5'-GCCGAATTCACCATGATTAAGCACCTGCGC-3'

				5'-CCTGCGGCCGCTCCCACGCATGTATGCCTTTAGCAGC-3'
pMET7-substr-Flag	pSEL-RNF41 substr	pMET7	EcoRI-NotI	5'-GCGAATTCGCCATGGCAATCCGCAGTGTCAACCCC-3'
				5'-CTAGATTAGCGGCCGCGTATCTCTTCCACGCCATGCGCAAA-3'
pMET7-RNF41ΔCC-Flag	pMET7-RNF41-Flag		Mutagenesis 1	5'-CCCAACCATAACTGCGATATCCACCTGCGCTCAGTG-3'
pMET7-RNF41ΔCC-Etag	pMET7-RNF41-Etag		Mutagenesis 2	5'-CACTGAGCGCAGGTGGATATCGCAGTTATGGTTGGG-3'
pSEL-RNF41ΔCC = RNF41ΔCC bait	pSEL-RNF41		+ EcoRV digest	5'-CTGCTAAAGGCATACGATATCGCAATCCGCAGTGTC-3'
				5'-GACACTGCGGATTGCGATATCGTATGCCTTTAGCAG-3'
pMET7-VPS53	Hela cDNA	pMET7	EcoRI-PsiI	5'-GTCCGGAGAATTCGCCATGATGGAGGAGGAGGAACTGGAGTTCG-3'
				5'-CCCTTATAAGCGGCCGCCCCCCTACAGTCTCTTTTTAATGAGTTTCTC-3'
pMET7-VPS53-Flag	Hela cDNA	pMET7-Flag	EcorI-NotI	5'-GTCCGGAGAATTCGCCATGATGGAGGAGGAGGAACTGGAGTTCG-3'
				5'-GGCCGCGGCCGCCCCCACAGTCTCTTTTTAATGAG-3'

pXP2d2-rPAP1-luficerase reporter; pMET7-Flag-SVT; PMET7-RNF41 DN (Wauman et al, 2011)

pGEX-4T-GST-RNF41; pMet7-sIL-5Rα (De Ceuninck et al, 2013)

RNF41 does not affect STxB transport

We established that RNF41 relocalizes VPS52 and in this way disrupts the interaction between VPS52 and VPS53, a shared subunit of the GARP and EARP complexes. Therefore, we examined the importance of RNF41 in retrograde transport and endocytic recycling, two pathways regulated by the GARP and EARP complex respectively [1,2]. We first focused on retrograde transport by examining the GARP-dependent delivery of the Shiga toxin B-subunit (STxB) to the TGN [1,3]. Uptake experiments of Cy3-labeled STxB (STxB-Cy3) in mock-transfected HeLa cells were in line with previous reports showing correct STxB retrograde transport and delivery to the TGN [4] (Fig A1). Remarkably, RNF41-overexpressing cells showed no difference in retrograde delivery of STxB to the TGN, as StxB-Cy3 still localized to the Golgi ribbon. Also, in cells expressing dominant negative (DN) RNF41 or ΔCC, STxB was correctly transported to the Golgi region, resembling the situation in control cells. It is noteworthy that, at similar expression levels, DN RNF41 and RNF41 ΔCC show a different expression pattern compared to WT RNF41 in confocal microscopy. These truncated forms do not show the vesicular dots we usually observe with RNF41 or the L163Q mutant, but seem to be dispersed almost homogenously throughout the cytoplasm of the HeLa cells.
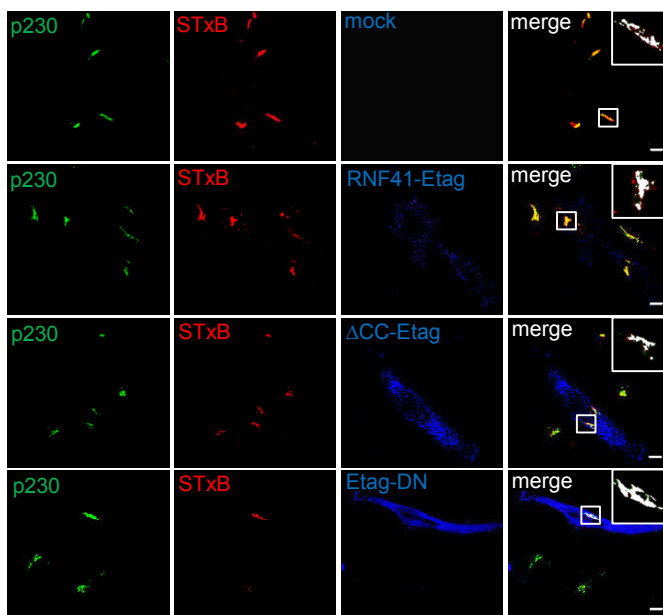
Figure A1: Ectopic RNF41 expression does not interfere with STxB transport. Confocal microscopy of HeLa cells transiently transfected with a plasmid encoding soluble IL5Rα (mock), E-tagged WT RNF41, E-tagged DN RNF41 or E-tagged RNF41ΔCC. Cells were incubated on ice with 1 µg/ml STxB-Cy3 (red) for 30 min and chased in complete medium for 60 min prior to fixation and immunostaining using anti-Etag antibody (secondary Alexa Fluor 488, blue) and anti-p230 (secondary Alexa Fluor 647, green). The inset shows a magnification of the boxed area. The white overlay represents the intersect between p230 and StxB with a threshold set on standard deviation using Volocity 6.3 software. n=3 or more independent experiments. Scale bar, 10µm.

RNF41 delays Transferrin recycling

Live cell imaging of transferrin (Tf-568) uptake in HeLa cells was used to examine endocytic recycling of the transferrin receptor. Significantly enhanced retention of Tf-568 was observed in cells expressing RNF41-EGFP compared to the control cells, but not in ΔCC-EGFP expressing cells (Fig A2). Overexpression of the L163Q-EGFP mutant showed only marginal differences in transferrin recycling compared to WT RNF41, which could be explained by possible oligomerization with endogenous RNF41 (data not shown). We attempted to circumvent this problem by depleting cells of RNF41 and performing rescue experiments with an RNF41 WT-EGFP or L16Q-EGFP rescue construct. Unfortunately, we were unable to obtain sufficient silencing of RNF41 and lack antibodies to detect endogenous RNF41 with confocal microscopy (see discussion thesis). Together this indicates that RNF41 delays the recycling of internalized transferrin but, at this point, we are unable to confirm whether this is due to its interaction with VPS52. It should be noted that we observed no effects on transferrin internalization with any of the overexpressed constructs (data not shown).
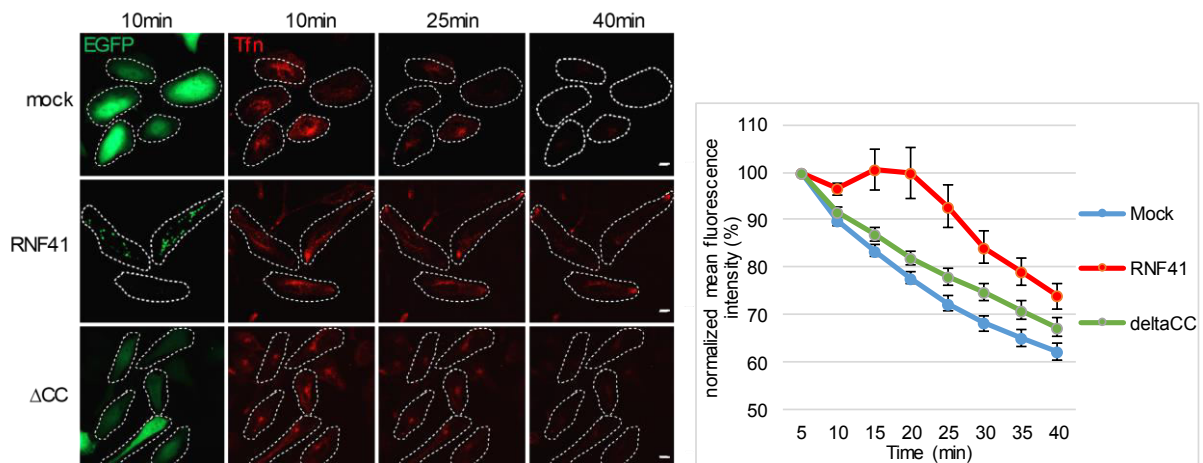
Figure A2: Ectopic RNF41 expression delays transferrin recycling. Live cell imaging using a Spinning disc confocal microscope of HeLa cells transiently transfected with a plasmid encoding Flag-tagged EGFP (mock), WT RNF41-EGFP or RNF41ΔCC-EGFP. After 24h, cells were labeled with AlexaFluor-568 conjugated transferrin (Tf) for 20min on ice, allowed to internalize for 10 min at 37°C, washed and chased with holo-Tf in DHB medium for the indicated time. The normalized mean intensity of Tf-568 in transfected cells (timepoint 1=100%) was plotted as function of time using the Volocity 6.3-software package (Perkin Elmer, Waltham, MA, USA). Values are means ± s.e.m. (n=3), P<0.01 (one-way ANOVA with a Tukey's multiple comparison post-hoc test) for mock and ΔCC compared to RNF41 for the analysed timepoints (10, 25 and 40 minutes). Transfected cells are indicated with dotted lines.

VPS52 does not influence the RNF41 mediated shedding or degradation of the LR

We previously reported the influence of RNF41 on LR (leptin receptor) routing [5,6]. Here, ectopic RNF41 expression blocks cathepsin L-mediated C-terminal stub (CTS) formation of the LR. This CTS is visualized after overnight incubation with the lysosomal inhibitor, chloroquine. Concomitantly, RNF41 enhanced LR ectodomain shedding resulting in increased soluble LR [5]. To investigate whether the interaction with VPS52 was involved in this RNF41-induced LR rerouting, we tested the L163Q mutant and silencing of VPS52 in this setup. As expected, RNF41 expression blocks the CTS

generation in HEK293T cells expressing HA-tagged LR, whereas DN RNF41, lacking the RING domain, generated a CTS (Fig A3). The cell culture supernatant from the same transfected cells was collected to analyze soluble LR levels. Here, RNF41 enhances soluble LR levels, while DN RNF41 had no effect. Like WT RNF41, the RNF41 L163Q mutant inhibits CTS formation and increases soluble LR levels, suggesting that VPS52 is not involved in this particular function of RNF41. Likewise, silencing of VPS52 did not hamper the RNF41-mediated increase in LR ectodomain shedding nor the blocked CTS formation. Silencing of VPS52 did however decrease basal LR ectodomain shedding, implying that VPS52 could be involved in LR recycling. On the other hand, ectopic expression of VPS52 did not enhance LR shedding. Collectively, our observations indicate that VPS52 is not involved in the RNF41-mediated effects on LR rerouting.
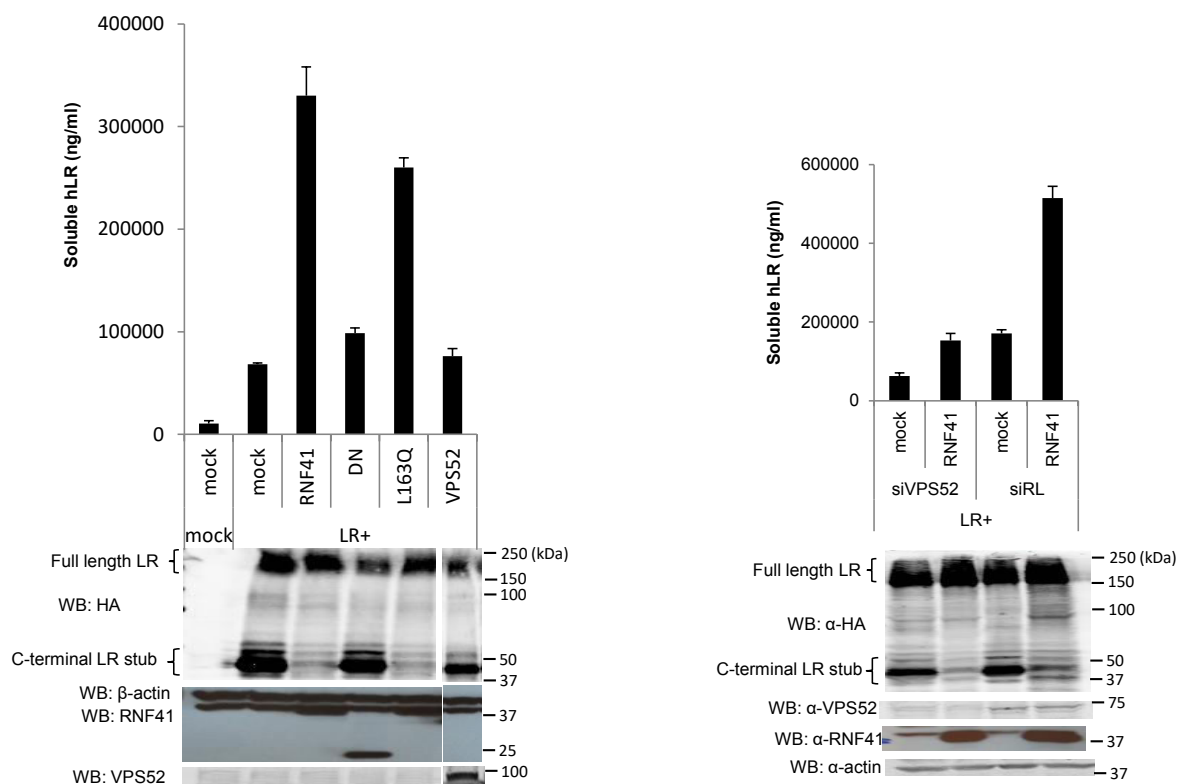
Figure A3: Overexpression or silencing of VPS52 does not influence the RNF41 mediated shedding or degradation of the LR. HEK293T cells were silenced for VPS52 (siVPS52) or treated with an irrelevant siRNA (Renilla, siRL) and/or were transiently co-transfected with a plasmid encoding a C-terminally HA-tagged LR and RNF41, DN RNF41, L163Q, VPS52 or solIL5Rα as a negative control (mock). Cell lysates were subjected to western blot analysis after overnight incubation with chloroquine. Full length LR and stub are visualized with anti-HA antibody. At the same time cell media supernatants from the transfected cells were collected and analyzed for soluble LR levels. Quantification was done by ELISA.

References

1 Pérez-Victoria FJ, Mardones GA & Bonifacino JS (2008) Requirement of the human GARP complex for mannose 6-phosphate-receptor-dependent sorting of cathepsin D to lysosomes. *Mol. Biol. Cell* **19**, 2350–62.

2 Schindler C, Chen Y, Pu J, Guo X & Bonifacino JS (2015) EARP is a multisubunit tethering complex involved in endocytic recycling. *Nat. Cell Biol. 17(5), 639–50.* **17**, 639–50.

3 Pérez-Victoria FJ, Schindler C, Magadán JG, Mardones GA, Delevoye C, Romao M, Raposo G & Bonifacino JS (2010) Ang2/fat-free is a conserved subunit of the Golgi-associated retrograde protein complex. *Mol. Biol. Cell* **21**, 3386–95.

4 Johannes L, Tenza D, Antony C & Goud B (1997) Retrograde transport of KDEL-bearing B-fragment of Shiga toxin. *J. Biol. Chem.* **272**, 19554–61.

5 Wauman J, De Ceuninck L, Vanderroost N, Lievens S & Tavernier J (2011) RNF41 (Nrdp1) controls type 1 cytokine receptor degradation and ectodomain shedding. *J. Cell Sci.* **124**, 921–32.

6 De Ceuninck L, Wauman J, Masschaele D, Peelman F & Tavernier J (2013) Reciprocal cross-regulation between RNF41 and USP8 controls cytokine receptor sorting and processing. *J. Cell Sci.* **126**, 3770–81.

A high confidence interactome for RNF41 built on multiple orthogonal assays

This paper describes the generation of a high-confidence RNF41 (RING finger protein 41) interactome map based on several co-purification screens. Virotrap, BioID (proximity-dependent biotin identification) and AP-MS (Affinity Purification-Mass Spectrometry) were combined with known datasets from previously performed microarray MAPPIT (Mammalian Protein-Protein Interaction Trap) and Y2H (Yeast Two-Hybrid) screens. This first RNF41 interactome provides a unique tool for further elucidation of the role of RNF41. We selected AP2S1 (Adaptor related Protein complex 2 Sigma 1 subunit), a newly identified RNF41 interaction partner, for more detailed analysis. We were able to link AP2S1 with leptin receptor signaling and found that RNF41 stabilizes and relocates this protein.

A high confidence interactome for RNF41 built on multiple orthogonal assays

Delphine Masschaele[1,2], Joris Wauman[1,2], Giel Vandemoortele[1,2], Delphine De Sutter[1,2], Leentje De Ceuninck[1,2], Sven Eyckerman[1,2†*] and Jan Tavernier[1,2†*]

[1]Department of Biochemistry, Faculty of Medicine and Health Sciences, Ghent University, Albert Baertsoenkaai 3, B-9000 Ghent, Belgium
[2]Center for Medical Biotechnology, VIB, Albert Baertsoenkaai 3, B-9000 Ghent, Belgium
† Shared senior author
* Shared corresponding author
Email: sven.eyckerman@vib-ugent.be ; jan.tavernier@vib-ugent.be

Tel: +32 (0)9 264 9218 ; +32 (0)9 264 9302

Abstract

Ring finger protein 41 (RNF41) is an E3 ubiquitin ligase involved in the ubiquitination and degradation of many proteins including ERBB3 receptors, BIRC6 and parkin. Next to this, RNF41 regulates the intracellular trafficking of certain JAK2-associated cytokine receptors by ubiquitinating and suppressing USP8 which in turn destabilizes the ESCRT-0 complex. To further elucidate the function of RNF41 we used different orthogonal approaches to reveal the RNF41 protein complex: Affinity Purification-Mass Spectrometry, BioID and Virotrap. We combined these results with known datasets for RNF41 obtained with microarray MAPPIT and Y2H screens. This way, we establish a comprehensive high resolution interactome network comprising 175 candidate protein partners. To remove potential methodological artifacts from this network, we distilled the data into a high confidence interactome map by retaining a total of 19 protein hits identified in two or more of the orthogonal methods. AP2S1, a novel RNF41 interaction partner, was selected from this high confidence interactome for further functional validation. We reveal a role for AP2S1 in leptin and LIF receptor signaling and show that RNF41 stabilizes and relocates AP2S1.

Key words

High confidence interactome, Interactomics, AP-MS, BioID, Virotrap, Y2H, Microarray MAPPIT, RNF41, AP2S1, Cytokine receptor signaling

1

<u>Introduction</u>

The high heterogeneity that underlies protein protein interactions (PPIs) resulted in the development of many different approaches to study these interactions. One set of methods, the so-called binary methods, test the specific interaction between two candidate proteins using a reporter read-out[1], while other approaches aim at purifying the intact complex followed by identification of protein partners using mass spectrometry (MS)[2]. There is currently no universal method to obtain a comprehensive view of a full interactome. A valid strategy to approach this issue is by combining different complementary or orthogonal methods to establish a high confidence interactome. While this can indeed reveal additional protein partners, virtually all methods suffer from the presence of false positive associations. These can be explained by the nature of the method (e.g. proteins with transactivation activity in the yeast two-hybrid system (Y2H)), or by the simple fact that many of the methods rely on forced expression of the bait protein (and even of the prey protein for the binary methods), a condition that can lead to many artifacts[3]. These false positives contaminate the interaction profile leading to an overestimation of the number of candidate partner proteins. Another way to use these complementary datasets relates to the generation of a confidence score based on the recurrent detection of specific partners with orthogonal methods. This concept was pioneered for the binary methods[4] and is now starting to be explored with the MS-based methods[5–7].

RING finger protein 41 (RNF41, or NRDP1 (neuregulin receptor degradation protein-1)) is an E3 ubiquitin ligase with multiple roles including regulation of intracellular cargo trafficking. Next to its N-terminal RING finger domain responsible for recruiting E2 conjugating enzymes, it contains a coiled-coil domain, necessary for trimerization[8,9], followed by a C-terminal substrate binding domain, which mediates interaction with a broad variety of proteins[10]. RNF41 ubiquitinates and degrades BIRC6 (or BRUCE), an inhibitor of apoptosis, and parkin, a protein involved in Parkinson's disease[11,12]. Next to degradation, ubiquitination by RNF41 can also lead to subcellular relocalization, as demonstrated for VPS52, a protein involved in tethering of cargo to the Golgi network or recycling endosomes[9]. Moreover, differential ubiquitination of adaptor proteins MYD88 and TBK1 by RNF41 regulates Toll-like receptor 4 (TLR4) signaling resulting in suppressed production of proinflammatory cytokines and enhanced IFN-β production, respectively[13]. Next to downregulation of cytokine type I interleukin-3 (IL-3) and erythropoietin (EPO) receptors, RNF41 further controls the differentiation of myeloid progenitors and activates macrophages by respectively downregulating the transcription factor retinoic acid receptor α (RARα) and upregulating CCAAT/Enhancer-binding protein β (C/EBPβ)[14,15]. Furthermore, RNF41 can ubiquitinate and degrade ERBB3 receptors, thereby regulating their steady state levels. RNF41 located at the ER reroutes signaling competent ERBB3 receptors to the ERAD pathway, while it tags the internalized ERBB3 receptors for lysosomal degradation[16,17]. By downregulating parkin, BIRC6 and ERBB3, RNF41 is implicated in disorders such as Parkinson's disease[18] and cardiomyopathies[19,20] and in many cancers, like breast cancer[21,22], prostate cancer[23,24], glioma[25–27] and pancreatic cancer[28]. Our previous studies indicated that RNF41 modulates the intracellular trafficking of the leptin receptor (LR), leukaemia inhibitory factor receptor (LIFR) and the interleukin-6 receptor (IL-6R), three JAK2-associated type I cytokine receptors[29]. By ubiquitinating and suppressing USP8, RNF41 indirectly destabilizes the ESCRT-0 complex, which inhibits these receptors from undergoing lysosomal degradation and

2

subsequently reroutes them towards compartments for ectodomain shedding, resulting in the increased release of soluble receptors by ADAM proteases[30]. Furthermore, RNF41 was shown to attenuate LR, LIFR and IL-6R signaling by a yet unknown mechanism[29]. RNF41 itself is transcriptionally regulated by LPS stimulation[13,31] and the androgen receptor[32]. Its regulation at posttranslational level is mostly accomplished by mechanisms modulating the ubiquitination state of RNF41, such as autoubiquitination or deubiquitination by USP8[33], as well as proteins stabilizing[34], destabilizing[35], or sequestering RNF41[36].

In this paper we generate a network of RNF41 interaction partners using a set of complementary MS-based approaches Virotrap, BioID and AP-MS, and combine them with data obtained from previously performed binary RNF41 interaction screens to further complete the RNF41 interactome network. By pooling these datasets we obtained a high resolution interactome map for RNF41 and further condensed this into a high-confidence RNF41 interactome dataset respectively identifying 175 and 19 candidate proteins. Since Adaptor related Protein complex 2 Sigma 1 subunit (AP2S1) is implicated in clathrin-mediated endocytosis (CME), we validated this newly identified RNF41 interaction partner based on known RNF41 functional assays involving LR signaling and trafficking. We found that AP2S1, which affects LR signaling, is stabilized and relocated by RNF41.

Results

High resolution and high confidence interactome profiling of RNF41

Based on the concept as originally outlined for binary methods to obtain a confidence score[4], we applied different MS-based methods in combination with binary methods and database information to obtain a comprehensive view of the RNF41 interactome (Fig 1). With the exception of Y2H, all screens were carried out with the RNF41 C34S/H36Q mutant preventing E3 ubiquitin ligase activity and subsequent possible RNF41-dependent ubiquitination and degradation of interacting proteins, including RNF41 itself, thereby safeguarding its stability[10]. A classical AP-MS approach was performed by expression of a FLAG-tagged RNF41 C34S/H36Q protein in HEK293T cells in triplicate, while control cells were transfected with a FLAG-tagged EGFP construct. After lysis and purification, protein complexes were analyzed by mass spectrometry. The volcano plot shows the enriched proteins for a false discovery rate of 1% (Fig 2A and Supplementary Fig 2). The list of candidate binding proteins (Supplementary Table S2 and Supplementary Table S3 for spectral counts) contains both known (BIRC6, HOMER2, …) and novel proteins (KIAA1598 or SHOOTIN, NAV1, AP2S1, CCP110, …). As a first orthogonal approach, we investigated labeling of proximal proteins using the BioID technology. A FLAG-tagged promiscuous BirA* protein was cloned in frame on the C-terminus of RNF41 in a doxycycline-inducible expression vector. After recombination-assisted integration, expression of the construct was induced by doxycycline and verified by Western blot analysis (Supplementary Fig S1). To limit overexpression effects, a low doxyxycline level was chosen for the BioID experiments. We used the same liquid chromatography (LC) settings for peptide separations, and the same instrument and settings for MS analysis. The volcano plot in Figure 2A (extended in Supplementary Fig 2; Supplementary Table S2 and S3) shows the comparison of 4 induced RNF41-BirA*samples vs. 4 non-induced control samples. The strong binding of BIRC6 is confirmed here as the data suggest that the protein is in close proximity to RNF41. As expected, protein

3

levels of RNF41 and BirA* (separate entries in the proteomics database) are highly similar. As a third orthogonal method, we also made use of the Virotrap technology[41] where expression of RNF41 C34S/H36Q fused to GAG leads to the secretion of virus-like particles containing the RNF41 bait protein and its associated protein partners. Analysis of RNF41 was repeated for this study with the protocol described in Titeca et al.,[37] to allow a side-by-side comparison with the AP-MS and BioID conditions. LC-MS conditions were again the same for the 4 RNF41 samples and the 4 controls analyzed in the Virotrap study (Fig 2A, Supplementary Fig. 2; Supplementary Table S2 and S3). BIRC6 is clearly enriched in the particles containing RNF41 bait protein.

By comparing the list of significantly enriched proteins for the different methods (Supplementary Table S4), we clearly observe overlapping and unique proteins (Fig 2B). This is a reflection of the different approaches with their unique advantages and disadvantages, resulting in their specific sets of missing partners (false negatives). While the design of experiments mostly prevents false positives in the lists, we cannot formally exclude their presence. For instance, the presence of BirA* in the BioID sample can lead to false associations with this exogenous protein.

To further characterize the interaction profile of RNF41, we added data obtained with the MAPPIT technology[39] and data from high throughput Y2H analysis[42] (Fig 2B; Supplementary Table S4). Out of the 175 candidate proteins in this high resolution interactome map, 15 were detected before according to BioGRID[3.4] (entries in database on April 2017). Visualization of these candidate interactions in STRING (Version 10.5[43]) reveals known associations, including known RNF41 interactions (Supplementary Fig S6). Based on function and localization, some associations are likely incorrect (e.g. the network around XRN1, related to mRNA metabolism and transcriptional regulation). To obtain a high confidence interactome, we selected only proteins that were detected by two or more orthogonal approaches. In this case we did not include the BioGRID data[44] to avoid bias because of overlap with our approaches. This resulted in a short list of 19 high confidence interactions with RNF41 (Fig 2C) with 12 proteins also detected in the BioGRID data (Supplementary Table 2). While this list comprises several well characterized RNF41 interaction partners such as BIRC6 and USP8[11,30,33], it also reveals candidate interaction that were not previously known according to STRING, such as KIAA1598, NAV1 and AP2S1. Several of these novel interaction partners, i.e. KIAA1598, TACC1 and ENOPH1, were validated via co-immunoprecipitation (Supplementary Fig S7). KIAA1598 and NAV1 are proteins involved in axon outgrowth and guidance, thus regulating neuronal polarization[45–47]. Recently, RTN4A, an ER-structural protein, was characterized as a new interaction partner of RNF41[36]. This protein is, just like KIAA1598 and NAV1, involved in axon growth, which further illustrates the potential of orthogonal screens to identify functionally related proteins. Moreover, RNF41 has been implicated in the regulation of cell polarity in different ways. RNF41 downregulated VANGL-dependent non-canonical Wnt signaling, a pathway necessary for planar cell polarity in neuronal development[48], while phosphorylation of RNF41 by Par-1b is required for its role in epithelial cell polarity[49]. For further functional validation, we selected AP2S1 from the high confidence list of candidate interactions based on its involvement in clathrin-mediated endocytosis (CME) which could have implications in RNF41-mediated JAK2-associated type I cytokine receptor trafficking and signaling.
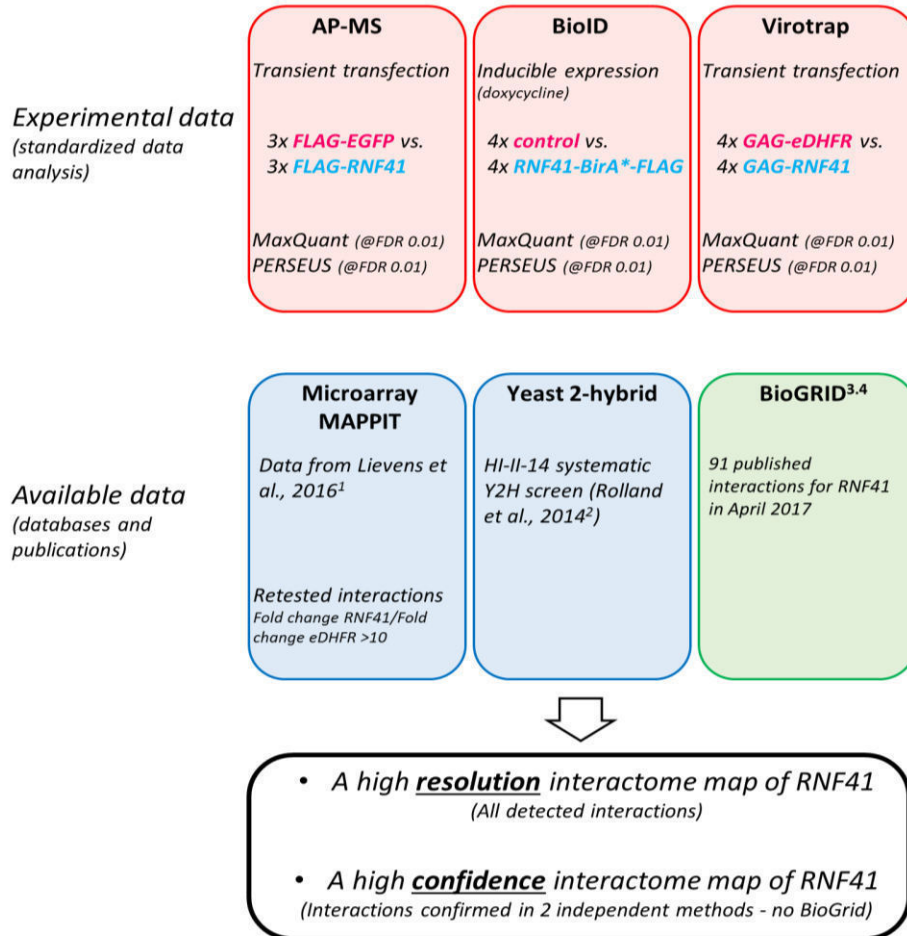
4

Figure 1. Overview of the orthogonal MS-based approaches to analyze protein complexes. The design of the different experiments in HEK293T cells (AP-MS and Virotrap) and in Flp-In™ T-REx 293 cells (BioID) is shown. Database searches and statistical analysis were performed in the same way for the different experiments. The lower part of the overview shows additional data sources (Microarray MAPPIT[39] and Y2H[42]) that were used for the generation of high resolution and high confidence views on the RNF41 interactome, and BioGRID[44] that was used to assess overlap.
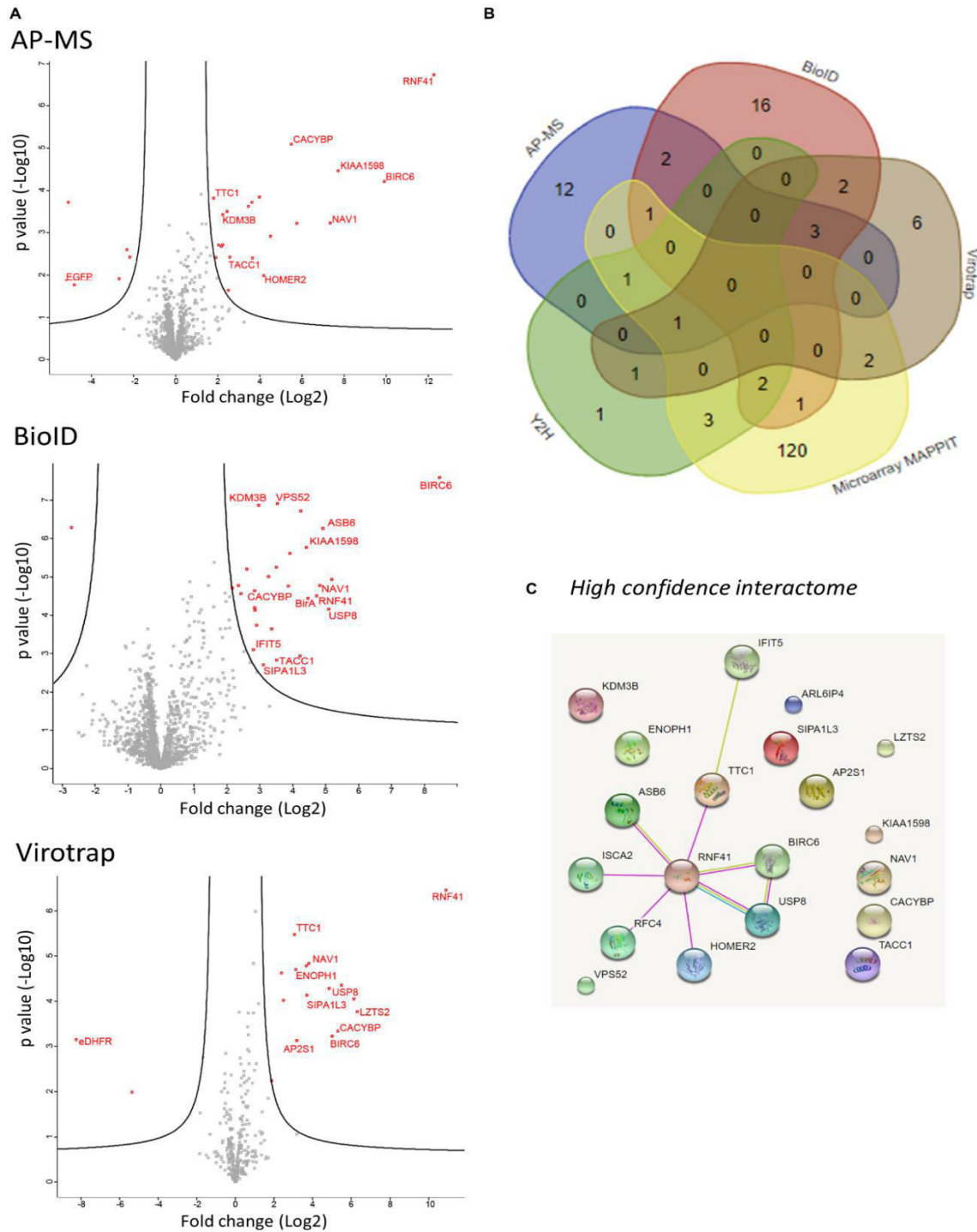
Figure 2. Comprehensive interaction profiling for RNF41. (A) Volcano plots for the different MS-based approaches showing the difference in protein quantity (X-axis, log2) against the p-value (Y-axis, -log10). FDR was set at 1% and S0 value was 1 for the 3 different approaches. Volcano plots with all significant proteins annotated are visualized in Supplementary Fig S2. Correlation between samples for the different MS-based approaches are given in

Supplementary Fig S3-5 **(B)** Venn diagram showing the overlap in number of proteins between the different approaches (http://bioinformatics.psb.ugent.be/webtools/Venn/) The data for this Venn diagram is presented in Supplementary Table S4. **(C)** The high-confidence interactome of RNF41. A STRING search was performed to reveal functional protein association networks (http://string-db.org/)[43] using candidate proteins that were identified in 2 orthogonal methods (19 proteins in addition of RNF41).

AP2S1 depletion increases LR signaling but does not hamper RNF41-mediated effects on the LR.

Our lab previously reported the influence of RNF41 on type I cytokine receptor signaling and routing[29,30]. We first sought to determine whether depletion of AP2S1 could modify these known RNF41-mediated effects. We demonstrated before that RNF41 expression inhibits LR signaling and blocks cathepsin L-mediated C-terminal stub (CTS) formation of the LR. This CTS is visualized upon treatment with the lysosomal inhibitor chloroquine and serves as a read-out for lysosomal LR sorting. Concomitantly, RNF41 stimulates LR recycling and enhances receptor ectodomain shedding by metalloproteases of the ADAM family leading to increased soluble LR[29,30]. We therefore assessed whether silencing of AP2S1 would influence trafficking of the LR. CTS generation in the lysates of LR transfected HEK293T cells treated with chloroquine and ELISA analysis of soluble LR levels in their conditioned medium was used to evaluate the effect on LR routing. Depletion AP2S1 did not hamper the RNF41-induced increase in LR ectodomain shedding nor the blocked CTS formation (Fig 3A). We next evaluated the effect of depleted AP2S1 on the RNF41-dependent attenuation of LR signaling. STAT3 luciferase reporter assays in HEK293T cells transfected with the LR showed no significant difference in RNF41 inhibited LR signaling. We noticed a clear increase in basal LR signaling upon silencing of AP2S1 when compared to the non-targeting (NT) control (Fig 3B). In addition, similar to the effects observed with ectopically expressed LR, silencing of AP2S1 also potentiated signaling of the endogenous LIFR in HEK293T cells. This increase in LR and LIFR signaling is comparable with the enhanced LR and LIFR signaling provoked by depletion of RNF41 (Fig 3C). In conclusion, AP2S1 did not influence the RNF41-mediated effects on LR trafficking or signaling itself, but its depletion did increase basal LR and LIFR signaling similar to depletion of RNF41.

7
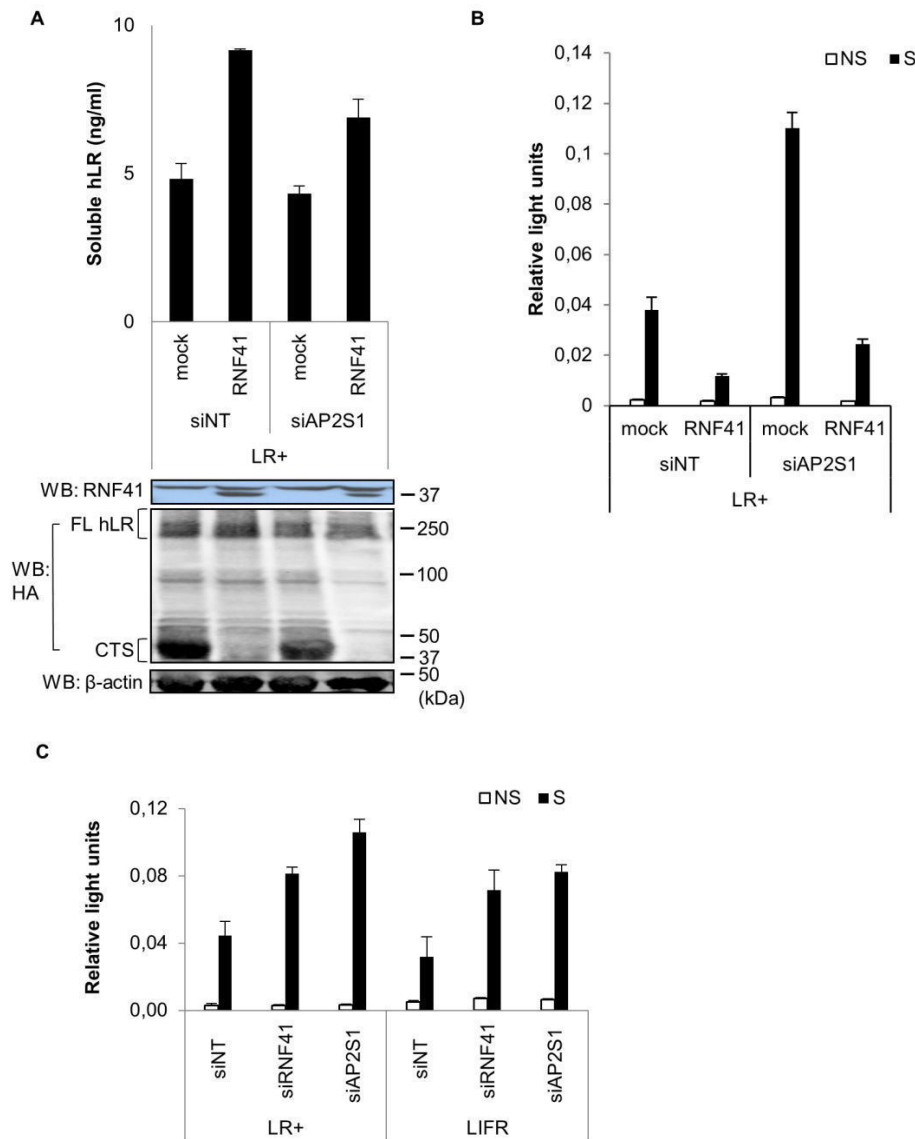
Figure 3. AP2S1 depletion increases LR signaling but does not hamper RNF41-mediated effects on the LR. (A) LR shedding and degradation. HEK293T cells were silenced (72h) for AP2S1 or treated with a non-targeting siRNA (siNT) and were transiently co-transfected with a plasmid encoding a C-terminally HA-tagged LR and RNF41 or soluble IL5Rα (mock). Cell lysates were subjected to western blot analysis after overnight incubation with chloroquine. Full length LR and stub are visualized with anti-HA antibody. At the same time cell media supernatants from the transfected cells were collected and analyzed for soluble LR levels. Quantification was done by ELISA. Values are means ± s.d. from triplicate samples from one of three representative experiments. **(B)** LR signaling. HEK293T cells were silenced (72h) for AP2S1 or treated with siNT and were transiently co-transfected with C-terminally HA-tagged LR and RNF41 or soluble IL5Rα (mock) together with a STAT3-dependent luciferase reporter gene. Cells were stimulated with leptin (black bars) or left untreated (white bars). Absolute luciferase counts of triplicate measurements normalized for transfection efficiency from one biological replicate are represented (means ± s.d.). **(C)** Basal LR and LIFR signaling. HEK293T cells were silenced (72h) for RNF41, AP2S1 or treated with NT siRNA, followed by co-transfection of LR or soluble IL5Rα (for endogenous LIFR signaling) and a STAT3-luciferase reporter gene. Cells were stimulated with leptin or LIF (black bars) or left untreated (white bars).

8

Absolute luciferase counts of triplicate measurements normalized for transfection efficiency from one biological replicate are represented (means ± s.d.). n=3 for all experiments, data and statistical analysis of biological replicates are shown in Supplementary Fig S8.

RNF41 stabilizes and relocates AP2S1

Binary MAPPIT allowed us to further investigate the RNF41-AP2S1 interaction interface using different subdomains of RNF41 as bait to test against the AP2S1 prey. Next to full length RNF41 we used an N-terminal construct, which holds the RING domain (AA1-134); a C-terminal construct, which contains the CC domain (AA135-179) and the substrate binding domain; a construct bearing only the substrate binding domain (AA179-317); and a truncated construct, ΔCC, which lacks the CC domain. Clearly, AP2S1 specifically interacts with the substrate binding domain of RNF41 (Fig 4A). As interactions with this domain are primarily used for RNF41 substrates that undergo ubiquitination, we tested RNF41-dependent ubiquitination of AP2S1. Surprisingly, we were unable to show that RNF41 ubiquitinates AP2S1 (Supplementary Fig S9). This is corroborated by *in vitro* GST-pulldown experiments revealing an indirect interaction between RNF41 and AP2S1 (Fig 4B). We next investigated whether the interaction between both proteins affects their stability. Depletion of AP2S1 in HEK293T and HeLa cells did not influence RNF41 expression levels, nor did silencing of RNF41 affect AP2S1 levels (Supplementary Fig S10). We therefore studied the effect of ectopically expressed RNF41 on AP2S1 protein expression in HEK293T cells. Co-expression of RNF41 significantly stabilized FLAG-tagged AP2S1 protein levels compared to the mock control. Moreover, RNF41 prevented AP2S1 from undergoing proteasomal degradation since this effect was lost when cells were incubated with the proteasomal inhibitor MG132 (Fig 4C). Consistent with the absence of AP2S1 ubiquitination by RNF41, this AP2S1 stabilization appeared to be independent of the RNF41 E3 ligase function as the C34S/H36Q mutant, lacking the ability to recruit an E2 conjugating enzyme (CS/HQ[10]), still stabilized AP2S1. Furthermore, we did not observe this stabilizing effect on AP2S1 when using dominant negative (DN; AA 109-317[10,50]) or Gly2Ala (G2A) mutated RNF41. This suggests a need for RNF41 membrane-anchoring as DN RNF41 lacks the RING domain and a possible myristoylation site, while the mutated glycine at position 2 of the G2A mutant disrupts this potential myristoylation site. Constructs lacking the CC domain (ΔCC) or only expressing the CC domain, which are known to disturb endogenous RNF41 oligomerization[8] appear to further destabilize AP2S1 (Fig 4C). These results can be explained by an RNF41-mediated relocalization of AP2S1. This is further supported by confocal microscopy, as ectopically expressed RNF41 and the C34S/H36Q mutant stabilize FLAG-tagged AP2S1 and redistribute it from a more diffuse and plasma membrane-located pattern towards cytosolic RNF41-positive structures (Fig 4D). DN RNF41 together with the G2A mutant and the CC domain closely resemble the control condition where we observe a more diffuse staining of AP2S1, while ectopic expression of ΔCC enhanced this diffuse pattern of FLAG-tagged AP2S1 (Fig 4D). Since RNF41 expression is upregulated upon LPS stimulation in RAW264.7 cells[13], we also asked whether LPS stimulation could in this way result in stabilized AP2S1. Unfortunately, we were not able to reproduce the LPS-mediated increased RNF41 expression in RAW264.7 cells, nor in HEK-blue[TM] TLR4 or THP-1 cells (Supplementary Fig S11).

9

Altogether, these results indicate that AP2S1 indirectly interacts with the substrate binding domain of RNF41 and is not ubiquitinated by RNF41. Moreover, RNF41 protects AP2S1 from proteasomal degradation thereby stabilizing and relocating it away from its conventional location. Membrane anchoring and oligomerization of RNF41 appear to be necessary for these effects on AP2S1.
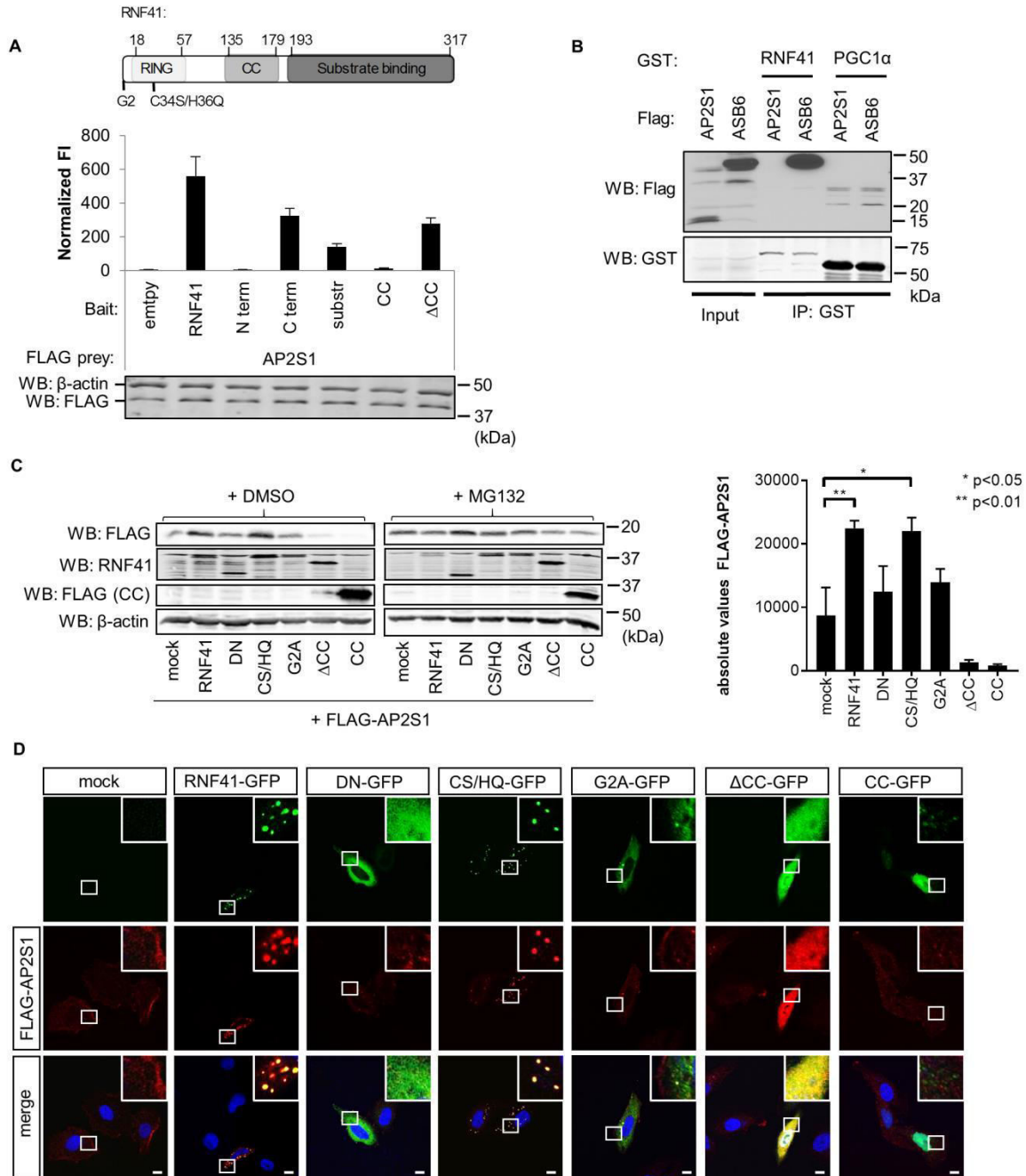

Figure 4. RNF41 stabilizes and relocates AP2S1. (A) Left, MAPPIT analysis in HEK293T cells transiently co-transfected with plasmids encoding an AP2S1 prey together with empty, RNF41 WT or RNF41 subdomain bait and the pXP2d2-rPAP1-luciferase reporter plasmid. The next day, cells were stimulated with EPO or left untreated for

24 hours. The luciferase signal is expressed as fold induction (stimulated/non stimulated), relative to the signal of a control JAK2 binding prey ± s.d. of triplicate measurements. Western blotting verified Flag-tagged prey expression and β-actin levels (loading control). MAPPIT data with empty and JAK2 binding control preys are shown in Supplementary Fig S12. Right, representation of full length RNF41 with indicated subdomains and point mutations (N-term: AA1-134; C-term: AA 135-317). **(B)** GST-pulldown analysis. Escherichia coli BL21(DE3) cell lysates expressing GST-RNF41 or GST-PGC1α (negative control) were incubated with in vitro transcribed and translated FLAG-tagged AP2S1 and ASB6 (positive control). Glutatione sepharose beads precipitated the complexes which were revealed via Western blotting using anti-FLAG and anti-GST antibodies. **(C)** Effect on expression levels of AP2S1. HEK293T cells transiently co-transfected with a plasmid encoding FLAG-tagged AP2S1 and untagged WT, mutated or truncated RNF41, FLAG-tagged RNF41 CC-gp130 (prey construct used to optimize expression), or soluble IL5Rα (mock) were treated overnight with 5μM DMSO (left) or 5μM MG132 (right) prior to sonication in 2x Laemmli buffer. Protein levels were determined by Western Blotting using anti-FLAG, anti-RNF41 or anti-β-actin (loading control) antibodies. A one-way ANOVA of three quantified biological replicates showed a significant difference in FLAG-AP2S1 levels between mock and RNF41 ($p<0.01$) and between mock and CS/HQ ($p<0.05$), Values are means ± s.e.m. **(D)** RNF41 redistributes AP2S1. Confocal microscopy of HeLa cells transiently transfected with a vector encoding FLAG-tagged AP2S1 and soluble IL5Rα (mock), GFP-tagged WT, mutated or truncated RNF41 (green) were fixed and stained with Dapi (blue) and anti-FLAG antibody (secondary Alexa Fluor 568, red). The insets show a magnification of the boxed area. Scale bar, 10μm. n=3 for all performed experiments.

Discussion

To further characterize the RNF41 interactome and hence further explore the function of RNF41, we performed several co-purification screens, e.g. Virotrap, a method based on viral particle sorting; BioID, a proximity biotinylation approach and affinity purification-mass spectrometry (AP-MS), and pooled these results with known datasets from a mammalian two-hybrid microarray MAPPIT and a human proteome-wide Y2H screen[39,42]. The different PPI technologies all have intrinsic strengths and weaknesses, of which the presence of false positives and false negatives represents a limitation inherent to almost all PPI methods. This is supported by a number of observations in the available data sets. The AP-MS experiments failed to reveal USP8 and ASB6, proteins that were validated by different orthogonal methods, and that were functionally validated ([30,39]; De Ceuninck et al, manuscript in preparation). The absence of these proteins can be explained by degradation during lysis and purification. USP8 degradation is likely prevented in the virus-like cage that is used in the Virotrap method[41]. Both USP8 and ASB6 were readily detectable with BioID. Biotinylation of proximal proteins by BirA* occurs in the intact cells before the actual lysis step which may help in the detection of these partners. This may also explain the detection of VPS52 in the BioID data. Note also that lysines are typically biotinylated by the BirA* activity. This modification may prevent ubiquitination and can thus prevent degradation of some of the candidate interacting proteins. In addition, our MS-based approaches were performed in a single cellular context (i.e. in HEK293 cells), therefore limiting the interactome to the proteins that are expressed in these cells. The binary approaches microarray MAPPIT and Y2H were performed using an arrayed proteome-wide library of prey proteins which corrects the absence of proteins that are not endogenously expressed in the cells. While MAPPIT allows the detection of indirect interactions when the bridging partners are present in the cellular background (i.e. HEK293T cells), this is much less likely in the Y2H system which will mainly detect direct partners. Combining these orthogonal datasets allowed

11

us to generate a high-resolution interactome of RNF41, containing 175 candidate proteins, which revealed several functional clusters including proteins involved in ubiquitination and in receptor signaling pathways. Interpretation of this network should be performed with caution. This is exemplified by the presence of the XRN1 cluster, as the functional link between RNF41 and mRNA metabolism is not obvious at present (Supplementary Fig S6). From this list, 19 proteins were identified by two or more methods, supporting the high quality of the RNF41 interactome (Fig 2C). Altogether, these orthogonal assays proved to be complementary, providing both new and previously identified interaction partners of RNF41. Novel candidate proteins such as KIAA1598 and NAV1, which are, similarly to RNF41 and its recently discovered interaction partner RTN4A, implicated in cell polarization underscore the adequacy of our interactome profiling approach to reveal functional relevant links[36,45–47,49]. We selected the novel RNF41 candidate partner AP2S1 from the high confidence map for further functional validation.

AP2S1 is the sigma subunit of the clathrin adaptor protein AP-2, a key player of CME, one of the major mechanisms for internalization of transmembrane proteins from the plasma membrane[51]. Therefore, AP2S1 might be functionally related to the well-established role of RNF41 in receptor trafficking and signaling[10,13,14,29]. The heterotetrameric AP-2 complex, comprises two large subunits, α and β2, a medium subunit μ2 and a small subunit σ2[52]. Plasma membrane binding triggers a conformational change in AP-2, which allows it to select and interact with internalization motifs in the cytoplasmic tail of cargo, followed by clathrin recruitment. In this way, AP-2 acts as a central 'hub' for CME[53,54]. In an attempt to validate AP2S1 as a novel RNF41 interaction partner we implemented an RNAi strategy in the hope of linking this protein with the previously described RNF41 functions in LR shedding, degradation and signaling[29]. Depletion of AP2S1 revealed no changes in RNF41-mediated enhanced LR ectodomain shedding or decreased CTS formation, or on RNF41-induced attenuated LR signaling (Fig 3A-B). We did however observe that AP2S1 depletion increased basal LR and endogenous LIFR signaling. This potentiated signaling corresponds to the enhanced signaling in RNF41-depleted cells (Fig 3C). This suggests that AP2S1 has an inhibitory effect on LR signaling, which is further enhanced by ectopic RNF41 expression (Fig 3B). This is in line with our observation that RNF41 stabilizes AP2S1, and hence, potentiates its inhibitory effect on LR signaling (Fig 4C). Next to this, RNF41 itself inhibits LR signaling via an unknown mechanism[29], possibly entailing other interaction partners, such as the E3 ligase ASB6, which indirectly interacts with the LR via IRS4 (De Ceuninck et al., unpublished observations). This underscores the versatile nature of RNF41 function depending on its interaction partners that are likely spatially and temporally separated.

Other than the involvement of clathrin and dynamin[55], there is a lack of information regarding LR internalization and whether this can regulate its signaling. Therefore, our results can be interpreted in different ways depending on the notion if LR signaling occurs at the plasma membrane or whether LR signaling requires internalization, although we cannot exclude the occurrence of signaling both at the plasma membrane and after internalization. If AP-2 and thus AP2S1 are involved in LR internalization and LR signaling occurs at the plasma membrane, then AP2S1 silencing would block internalization, resulting in enhanced LR signaling, which is in accordance with our results. However, we observed that ectopic expression of a DN dynamin mutant (dynamin K44A), which is known to block CME, resulted in inhibited LR signaling, indicating that LR internalization is required for its signaling (Supplementary Fig

12

S13). In this case, depletion of AP2S1 should, similarly to DN dynamin, inhibit signaling. Since we detect the opposite, i.e. enhanced signaling upon AP2S depletion, it is possible that AP2S1 and AP-2 are not involved in LR endocytosis, and that other adaptor proteins may regulate its internalization. In line herewith, there are currently no reports on a putative dileucine or tyrosine-based motif in the LR, which are recognized by the σ2 or μ2 subunit of AP-2 respectively. It is known that CME acquires different adaptor proteins for mediating endocytosis, making AP-2 dispensable for certain cargo. This is exemplified by the EGF and LDL receptors, where AP-2 depletion does not hamper EGFR and LDLR CME, whereas Tfn endocytosis is blocked[56].

Mapping the RNF41-AP2S1 interface using distinct RNF41 subdomains revealed that the RNF41 substrate binding domain mediates AP2S1 binding (Fig 4A). Interactions with this C-terminal domain are generally reserved for proteins like BIRC6, USP8 and ERBB3, that are ubiquitinated by RNF41[11,57,58]. Remarkably, we did not detect changes in the ubiquitination state of AP2S1 by RNF41 (Supplementary Fig S9). Since ubiquitination is a hallmark for protein stability or trafficking, it was surprising to find that RNF41 stabilizes AP2S1, independent of its E3 ubiquitin ligase function. Stabilization of AP2S1 when using RNF41 C34S/H36Q, a RING domain mutant unable to exert ubiquitination[10], confirmed this result (Fig 4C). This stabilization could be visualized using confocal microscopy, where AP2S1, typically distributed homogenously throughout the cytoplasma with a predominance for the plasma membrane, overlapped with RNF41 and the C34S/H36Q mutant in RNF41-positive structures. This also points towards a redistribution of AP2S1 by RNF41 (Fig 4D). The identity of these RNF41-positive structures remains to be elucidated. Both myristoylation and oligomerization of RNF41 appeared to be necessary for its stabilizing effect on AP2S1. RNF41 has a possible myristoylation site, characterized by the Met-Gly sequence at its N-terminus[10]. A G2A mutant, disrupting this site and DN RNF41, lacking the N-terminus, did not mediate this effect on AP2S1, which was also seen with confocal microscopy. Furthermore, RNF41 ΔCC and the RNF41 CC domain, both disrupting RNF41 oligomerization[8], did not affect AP2S1 stability (Fig 4C-D). Moreover, AP2S1 underwent proteasomal degradation, since incubation with the proteasomal inhibitor MG132 stabilized AP2S1 levels. Thus it is likely that, by its relocalization, RNF41 prevents AP2S1 from proteasomal degradation (Fig 4C).

Lack of RNF41-mediated ubiquitination of AP2S1 can also be explained by the observation of the indirect interaction between RNF41 and AP2S1 (Fig 4B). The identification of an indirect interactor in the high-confidence interactome nicely attributes to our orthogonal approach as AP2S1 appeared as a candidate interactor of RNF41 in both Virotrap and microarray MAPPIT, two methods allowing the detection of weak, transient and indirect interactions. We and others have previously determined that USP8 and ASB6 require, similar to AP2S1, the substrate binding domain of RNF41[9,30,57]). MAPPIT analysis revealed that RNF41 mutants specifically disrupting interaction with ASB6 and/or USP8 also resulted in a loss of AP2S1 binding. However, we did not detect an interaction between AP2S1 and ASB6 or USP8, indicating that the RNF41-AP2S1 interaction is not mediated by any of these proteins (Supplementary Fig S14). Since AP2S1 indirectly interacts with the substrate binding domain of RNF41 (Fig 4A-B), and RNF41 prevented AP2S1 from proteasomal degradation (Fig 4C), it is conceivable that RNF41 directly interacts, via its substrate binding domain, with another currently unknown E3 ligase, which under normal circumstances may ubiquitinate AP2S1 and target it for proteasomal degradation. RNF41 may inhibit the

13

function of this unknown E3 ligase thus preventing proteasomal degradation of AP2S1. Zhong, et al., described a similar situation where RNF41 degrades the E3 ligase parkin thereby stabilizing CDCrel-1, a parkin substrate[12]. Moreover, the Virotrap dataset revealed three potential E3 ubiquitin ligases, including CACYBP, BIRC6 and TTC1, who could possibly mediate this effect. On the other hand, RNF41 prevented AP2S1 from proteasomal degradation, depending on its myristoylation and oligomerization state. RNF41 could perhaps, by membrane anchoring or hetero-oligomerization with other, unknown proteins, reroute AP2S1 in complex with the unknown E3 ligase, towards compartments which can be visualized as RNF41-positive structures.

Furthermore, Arg15 mutations in AP2S1 are known to cause familial hypocalciuric hypercalcemia type 3 (FHH3), a calcium homeostasis disorder that affects parathyroid glands, kidney and bone. These mutations likely disrupt the interaction between AP-2 and the cytoplasmic tail of the calcium sensing receptor, thereby reducing its endocytosis and decreasing the sensitivity of the cells to extracellular calcium[59]. These AP2S1 Arg15 mutations did not disrupt interaction with RNF41, suggesting that RNF41 is not implicated in FHH3 (Supplementary Fig S14)

In conclusion, by employing complementary MS-based methods Virotrap, BioID and AP-MS screens and combining these results with publicly available data retrieved from microarray MAPPIT and Y2H screens we were able to generate high resolution and high confidence interactome maps for RNF41. As we show for AP2S1, these maps provide a useful resource for further functional analysis of RNF41.

Experimental procedures

Plasmids and constructs
The generation of all sequence-verified constructs is shown in Supplementary Table S1.

Co-purification methods
For every AP-MS condition we seeded 2 PD150 dishes with 8 x 10^6 HEK293T cells 48 hours before transfection. After PolyEthylene Imine (PEI)-based transfection for 8 hours using 14.5 µg of pMET7-FLAG-RNF41 C34S/H36Q or pMET7-FLAG-EGFP (controls), cells were scraped the next day in ice cold PBS. After removal of PBS by pelleting the cell material, pellets were weighed and 400 µl lysis buffer (50 mM HEPES-KOH pH 8.0, 100 mM KCl, 2 mM EDTA, 0.1 % NP40, 10 % glycerol, 1 mM DTT, 0.5 mM PMSF, Protease inhibitor cocktail tablet [Roche], 0.25 mM Na_3VO_4, 50 mM glycerophosphate, 10 mM NaF) was added for every 100 mg of pelleted cell material. 50 µl of prewashed MyOne Streptavidin T1 beads (Thermo Fisher Scientific) were pre-incubated with 5 µl BioM2 antibody (Sigma). The beads were added after washing to the pre-cleared lysates (20 min 16000 x g 4°C) and left to bind complexes for 2 hours at 4°C by end-over-end rotation. After washing, beads were incubated overnight with 750 ng trypsin, followed by an additional incubation step with 250 ng trypsin for 4 hours after removal of the beads. After acidification, peptides were analyzed by liquid chromatography - mass spectrometry (LC-MS) using a Thermo Scientific™ Q Exactive™ Hybrid Quadrupole-Orbitrap Mass Spectrometer.

The pDEST-pCDNA5-RNF41 C34S/H36Q-BirA*-FLAG-C-term vector was stably integrated in the genome of Flp-In™ T-REx 293 cells using the Flp-In™ reaction according to the manufacturer's protocol. Inducible

14

expression of the fusion construct was verified by Western blot using anti-FLAG antibody (M2, Sigma). 80 μg of cleared lysates were loaded on 4-12 % gradient gels. For BioID experiments, 2 PD150 dishes were seeded the day before doxycycline induction for each sample. Cells were treated with doxycycline (4 repeat samples) for 48 hours or left untreated as controls (4 repeat control samples) the day after transfection. At around 85 % confluency cells were washed and collected in PBS. After removal of PBS, the cells were lysed using ice-cold RIPA lysis buffer (50 mM TRIS-HCl pH 7.5, 150 mM NaCl, 1 % NP40, 1 mM EGTA, 0.1 % SDS, 0.5 % Sodium Deoxycholate, 250 U Benzonase and Protease inhibitor cocktail [Sigma 1/500]). Lysates were cleared after sonication by 15 min at 16000 x g and at 4°C. 150 μl bed volume of pre-washed Streptavidin Sepharose® High Performance Beads (GE) was added to each sample and was allowed to bind biotinylated proteins for 3 hours at 4°C by end-over-end rotation. After extensive washing of the beads, on bead trypsin digest and LC-MS was performed as described for the AP-MS approach.

Virotrap experiments were performed essentially as described in Titeca et al.[37]. Briefly, HEK293T cells were seeded in T75 bottles the day before transfection with pMET7-GAG-RNF41 C34S/H36Q or with a pMET7-GAG-eDHFR control construct, combined with expression vectors for VSV-G and FLAG-VSV-G. Cell supernatants were harvested 40 hours after transfection and were cleared by low-speed centrifugation and by filtering (0.45 μm). Supernatants were then incubated with MyOne Streptavidin T1 beads loaded with BioM2 antibody. Two hours after binding, beads containing Virotrap particles were washed, and particles were released by competition with FLAG-peptide. After removal of the beads, samples were processed with Amphipols and digested using trypsin. After acidification, peptides were analyzed by LC-MS using a Thermo Scientific™ Q Exactive™ Hybrid Quadrupole-Orbitrap Mass Spectrometer. Analysis was performed on 4 independent transfections for RNF41 and control experiments.

The peptide mixtures were first loaded on a trapping column (made in-house, 100 μm I.D. × 20 mm, 5 μm beads C18 Reprosil-HD, Dr. Maisch, Ammerbuch-Entringen, Germany). After flushing from the trapping column, the sample was loaded on an analytical column (made in-house, 75 μm I.D. × 150 mm, 5 μm beads C18 Reprosil-HD, Dr. Maisch) packed in the nanospray needle (PicoFrit SELF/P PicoTip emitter, PF360-75-15-N-5, NewObjective, Woburn, USA). The samples were loaded and separated with a linear gradient from 98 % solvent A' (0.1 % formic acid in water) to 40 % solvent B' (0.08 % formic acid in water/acetonitrile, 20/80 (v/v)) in 30 min at a flow rate of 300 nl/min. This was followed by a 15 min wash reaching 99 % solvent B'. The Q Exactive instrument was operated in data-dependent, positive ionization mode, automatically switching between MS and MS/MS acquisition for the 10 most abundant peaks in a given MS spectrum. The source voltage was 3.4 kV, and the capillary temperature was 275°C. One MS1 scan (m/z 400–2000, AGC target 3×10^6 ions, maximum ion injection time 80 ms) acquired at a resolution of 70,000 (at 200 m/z) was followed by up to 10 tandem MS scans (resolution 17,500 at 200 m/z) of the most intense ions fulfilling the defined selection criteria (AGC target 5×10^4 ions, maximum ion injection time 80 ms, isolation window 2 Da, fixed first mass 140 m/z, spectrum data type: centroid, minimum AGC target 1000, intensity threshold 1.4×10^4, exclusion of unassigned, 1, 5-8, and >8 charged precursors, peptide match preferred, exclude isotopes on, dynamic exclusion time 12 sec). The HCD

collision energy was set to 25% Normalized Collision Energy and the polydimethylcyclosiloxane background ion at 445.120025 Da was used for internal calibration (lock mass).

All MS data was searched using MAXQUANT (version 1.5.7.4) against the human SwissProt database (Jan 2017; complemented with GAG, VSV-G and eDHFR sequences for Virotrap; complemented with EGFP for AP-MS, and BirA* for BioID), with 4,5 ppm and 20 ppm tolerance on precursor and fragment mass respectively, with trypsin/P settings allowing up to 2 missed cleavages, and with methionine oxidation and N-terminal acetylation formation as variable modifications. Minimum peptide length was set to 7, maximum peptide mass was 4,600 Da. PSM FDR and protein FDR were set to 0.01. Min. peptides and min. razor + unique peptides were set to 1. The searches were performed together with the corresponding control samples to allow matching of MS spectra between runs. Contaminants and identifications against the REVERSE database were removed in the PERSEUS (version 1.5.5.3) analysis after the log2 transformation of the non-normalized protein LFQ ratios. A two-sided t-test was performed with multiple testing correction using 1000 randomizations. FDR was set at 1 % with the S0 curve set at 1.

The mass spectrometry proteomics data have been deposited to the ProteomeXchange Consortium via the PRIDE [38] partner repository with the dataset identifier PXD007794.

Microarray and binary MAPPIT analysis

Microarray MAPPIT and the preparation of the prey and reporter reverse transfection mixture was previously described[39]. RNF41 C34S/H36Q was used as bait and screened against a 15K ORF prey collection (The human ORFeome v8.1[40]). For binary MAPPIT, 1 x 10^4 HEK293T cells (www.atcc.org, mycoplasma negative) were seeded in a 96-well plate and transfected with 50 ng of STAT3-dependent pXP2d2-rPAP1-luciferase reporter, 250 ng bait and prey constructs using calcium phosphate. Cells were left untreated or stimulated for 24 hours with human Erythropoietin (5 ng/ml). Luciferase activity from triplicate samples was measured by chemiluminescence in an Envision plate reader (PerkinElmer) and expressed as fold induction (stimulated/non-stimulated relative light units) relative to the signal generated by a JAK2 binding prey, thereby correcting for varying expression levels of the different used baits.

Western Blot analysis

1.5 x 10^5 HEK293T cells were seeded in a 12-well plate and co-transfected with 1 µg of each construct. Cells were incubated overnight with 5µM of DMSO or MG132 followed by lysis in 2x SDS gel laemmli buffer (62.5 mM Tris-HCl pH 6.8, 3% SDS, 10% glycerol, 5% β-mercaptoethanol and 0.01% Bromophenol Blue sodium salt) and sonicated using the Bioruptor Plus (Diagenode). After boiling, cell lysates were resolved by SDS-PAGE and transferred to nitrocellulose membranes (Amersham Biosciences). Blots were blocked in Odyssey blocking buffer (LICOR). Rabbit anti-RNF41 (1:10.000; Bethyl), mouse anti-FLAG (1:10.000; Sigma) and mouse anti-β-actin (1:5000, Sigma) were revealed by Odyssey infrared imaging (LICOR) using anti-rabbit or anti-mouse Dylight 680-conjugated antibody (1:15.000, Pierce) diluted in Odyssey blocking buffer + 0.1% Tween20. Rat-anti HA (1:5000, Roche (3F10)) was used for expression control in other experiments, revealed with anti-rat Dylight 680-conjugated antibody (1:15.000, Pierce) diluted in Odyssey blocking buffer + 0.1% Tween. For some experiments rabbit-anti RNF41 was revealed

16

by SuperSignal West Pico Chemiluminescent Substrate (Pierce) for detection via ECL (enhanced chemiluminescence), using peroxidase-conjugated anti-rabbit antibody (1:10.000, Jackson ImmunoResearch), diluted in milk blocking buffer.

LR shedding and degradation

1.25×10^5 HEK293T cells in a 12-well plate were reverse transfected with 50 nM siRNA using Dharmafect 1 (Dharmacon). Transient knockdown was accomplished using AP2S1 siRNA (L-011833-01-0005, Dharmacon and non-targeting siRNA (D-001810-10-0020, Dharmacon). The next day, cells were transfected with 1 µg of pMet7-hLR-HA together with 0.5 µg of pMet7-RNF41 or pMet7-solIL5Rα. 48 hours later, cells were incubated overnight in serum-free OPTIMEM medium with 25 µM chloroquine. The next morning, cell supernatant was collected to detect soluble LR by ELISA with the Human Leptin R DuoSet (R&D systems), and cells were simultaneously lysed for CTS cleavage analysis using western blotting.

Luciferase reporter assay

2×10^5 HEK293T cells in a 6-well plate were reverse transfected as described above with the addition of RNF41 siRNA (D-006922-02-0020, Dharmacon). Cells were transfected the next day with 0.1 µg pMet7-hLR-HA together with 0.2 µg of pXP2d2-rPAP1-luciferase reporter and 0.2 µg of a β-gal reporter construct to correct for transfection efficiency with or without 1 µg of pMet7-RNF41 or pMet7-solIL5Rα. 24 hours later, cells were washed, transferred to a 96-well plate and stimulated with mouse leptin (100 ng/ml) or human LIF (10 ng/ml) or were left untreated for 24 hours. Luciferase activity from triplicate samples was measured by chemiluminescence in an Envision plate reader (PerkinElmer) and expressed as fold induction (stimulated/non-stimulated relative light units) or as relative light units normalized for transfection efficiency.

GST-pulldown assay

Escherichia (E.) coli strain BL21(DE3) was transformed with vectors containing GST-RNF41 or GST-PGC1α. Production of protein was induced by 0.2 mM isopropyl-D-thiogalactoside at A600 of 0.6. The bacteria were further cultured ON at 25°C. After centrifugation at 5000 rpm for 10 min, the bacterial pellet was resuspended and sonicated in NETN buffer (20 mM Tris-HCl pH 8; 100 mM NaCl; 6 mM $MgCl_2$; 1 mM EDTA; 0.5 % NP40; 1 % DTT and protease inhibitor cocktail Complete (Roche)). The *E.coli* lysate was centrifugated at 12000 rpm for 10 min allowing separation of the soluble GST proteins in the supernatant. The GST proteins were immobilized on Glutathione Sepharose 4B beads (GE Healthcare) for 1 hour at 4°C. After incubation the beads were washed three times with NETN buffer. N-terminal FLAG-tagged AP2S1 or ASB6, produced using the TNT T7 Quick Coupled Transcription/Translation System (Promega), was added to the beads-GST protein mixture. After ON incubation the beads were washed three times with NETN buffer. The bound proteins were eluted by boiling in 2x SDS gel laemmli buffer for 10 minutes and analyzed by SDS-PAGE and immunoblotting. The following antibodies, rabbit anti-GST (Abcam) and mouse anti-FLAG (Sigma), were used for GST proteins and the FLAG-tagged protein respectively.

17

Confocal microscopy

1.5 x 10^4 HeLa cells (www.atcc.org, mycoplasma negative) were seeded on μ-Slide 8 well plates (Ibidi), coated with poly-L-lysine (Sigma-Aldrich). The next day, cells were transfected with 100 ng of construct using JetPrime (Polyplus). 24 hours later, cells were rinsed with PBS and fixed for 15 minutes at room temperature in 4% paraformaldehyde. Cells were washed with 100mM phosphate buffer (100 mM Na$_2$HPO$_4$; 100 mM NaH$_2$PO$_4$, pH 7.4), permeabilized and blocked in blocking buffer (20 mM phosphate buffer; 100 mM NaCl; 0.23% Triton X-100 and 10% donkey serum) for 30 minutes. Samples were incubated for 1.5 hours at room temperature with mouse anti-FLAG (1:5.000, Sigma). After washing in blocking buffer without donkey serum, cells were incubated for 1 hour at room temperature with donkey anti-mouse Alexa Fluor 568 (1:1000, Molecular Probes) and DAPI (1:100, Molecular Probes). Images were acquired using a 60x 1.35 NA objective on an Olympus IX-81 laser scanning confocal microscope and analyzed using Image J software.

SUPPORTING INFORMATION

Supplementary Figure S1. Inducible expression of a FLAG-tagged RNF41 C34S/H36Q-BirA*fusion construct in Flp-In™ T-REx 293 cells.

Supplementary Figure S2. Volcano plots for the different MS-based approaches showing all detected proteins.

Supplementary Figure S3. Correlation plots of the LFQ intensities for the AP-MS experiments.

Supplementary Figure S4. Correlation plots of the LFQ intensities for the BioID experiments.

Supplementary Figure S5. Correlation plots of the LFQ intensities for the Virotrap experiments.

Supplementary Figure S6. The high resolution interactome of RNF41.

Supplementary Figure S7. Co-immunoprecipitation of E-tagged RNF41 and FLAG-tagged KIAA1598, TACC1 and ENOPH1.

Supplementary Figure S8. Statistical analysis of 3 biological replicates from data in Figure 3.

Supplementary Figure S9. RNF41 does not ubiquitinate AP2S1.

Supplementary Figure S10. Effect of AP2S1 depletion on RNF41 and vice versa.

Supplementary Figure S11. Effect of LPS on RNF41 protein expression.

Supplementary Figure S12. Extended MAPPIT data from Figure 4A.

Supplementary Fig S13: LR internalization is necessary for LR signaling.

Supplementary Fig S14: AP2S1 Arg mutations do not influence RNF41 interaction, and AP2S1 does not interact with ASB6 or USP8.

Supplementary Table S1: Generation of constructs.

Supplementary Table S2: Protein lists obtained with the different methods used in this study.

Supplementary Table S3: Spectral counts for the different proteins detected in the MS-based approaches.

Supplementary Table S4: Overlap of detected proteins between the different methods and between BioGRID.

Notes

The mass spectrometry proteomics data have been deposited to the ProteomeXchange Consortium via the PRIDE [38] partner repository with the dataset identifier PXD007794

19

References

(1) Stynen, B.; Tournu, H.; Tavernier, J.; Van Dijck, P. Diversity in genetic in vivo methods for protein-protein interaction studies: from the yeast two-hybrid system to the mammalian split-luciferase system. *Microbiol. Mol. Biol. Rev.* **2012**, *76*, 331–82.

(2) Smits, A. H.; Vermeulen, M. Characterizing Protein-Protein Interactions Using Mass Spectrometry: Challenges and Opportunities. *Trends Biotechnol.* **2016**, *34*, 825–34.

(3) Gibson, T. J.; Seiler, M.; Veitia, R. A. The transience of transient overexpression. *Nat. Methods.* **2013**, *10*, 715–721.

(4) Braun, P.; Tasan, M.; Dreze, M.; Barrios-Rodiles, M.; Lemmens, I.; Yu, H.; Sahalie, J. M.; Murray, R. R.; Roncari, L.; de Smet, A.-S.; Venkatesan, K.; Rual, J.-F.; Vandenhaute, J.; Cusick, M. E.; Pawson, T.; Hill, D. E.; Tavernier, J.; Wrana, J. L.; Roth, F. P.; Vidal, M. An experimentally derived confidence score for binary protein-protein interactions. *Nat. Methods.* **2009**, *6*, 91–97.

(5) Couzens, A. L.; Knight, J. D. R.; Kean, M. J.; Teo, G.; Weiss, A., Dunham, W. H.; Lin, Z.-Y.; Bagshaw, R. D., Sicheri, F.; Pawson, T.; Wrana, J. L.; Choi, H.; Gingras, A.-C. Protein Interaction Network of the Mammalian Hippo Pathway Reveals Mechanisms of Kinase-Phosphatase Interactions. *Sci. Signal.* **2013**, *6*, rs15-rs15.

(6) Lambert, J.-P.; Tucholska, M.; Go, C.; Knight, J. D. R.; Gingras, A.-C. Proximity biotinylation and affinity purification are complementary approaches for the interactome mapping of chromatin-associated protein complexes. *J. Proteomics.* **2015**, *118*, 81–94.

(7) Kastritis, P. L.; O'Reilly, F. J.; Bock, T.; Li, Y.; Rogon, M. Z.; Buczak, K.; Romanov, N.; Betts, M. J.; Bui, K. H.; Hagen, W. J.; Hennrich, M. L.; Mackmull, M.-T.; Rappsilber, J.; Russell, R. B.; Bork, P.; Beck, M.; Gavin, A.-C. Capturing protein communities by structural proteomics in a thermophilic eukaryote. *Mol. Syst. Biol.* **2017**, *13*, 936.

(8) Printsev, I.; Yen, L.; Sweeney, C.; Carraway, K. L. Oligomerization of the Nrdp1 E3 ubiquitin ligase is necessary for efficient autoubiquitination but not ErbB3 ubiquitination. *J. Biol. Chem.* **2014**, *289*, 8570–8.

(9) Masschaele, D.; De Ceuninck, L.; Wauman, J.; Defever, D.; Stenner, F.; Lievens, S.; Peelman, F.; Tavernier, J. RNF41 interacts with the VPS52 subunit of the GARP and EARP complexes. *PLoS One*. **2017**, *12*, e0178132.

(10) Qiu, X.-B.; Goldberg, A. L. Nrdp1/FLRF is a ubiquitin ligase promoting ubiquitination and degradation of the epidermal growth factor receptor family member, ErbB3. *Proc. Natl. Acad. Sci. U. S. A.* **2002**, *99*, 14843–8.

(11) Qiu, X.-B.; Markant, S. L.; Yuan, J.; Goldberg, A. L. Nrdp1-mediated degradation of the gigantic IAP, BRUCE, is a novel pathway for triggering apoptosis. *EMBO J.* **2004**, *23*, 800–10.

(12) Zhong, L.; Tan, Y.; Zhou, A.; Yu, Q.; Zhou, J. RING finger ubiquitin-protein isopeptide ligase Nrdp1/FLRF regulates parkin stability and activity. *J. Biol. Chem.* **2005**, *280*, 9425–30.

(13) Wang, C.; Chen, T.; Zhang, J.; Yang, M.; Li, N.; Xu, X.; Cao, X. The E3 ubiquitin ligase Nrdp1 "preferentially" promotes TLR-mediated production of type I interferon. *Nat. Immunol.* **2009**, *10*, 744–52.

(14) Jing, X.; Infante, J.; Nachtman, R. G.; Jurecic, R. E3 ligase FLRF (Rnf41) regulates differentiation of hematopoietic progenitors by governing steady-state levels of cytokine and retinoic acid receptors. *Exp. Hematol.* **2008**, *36*, 1110–20.

(15) Ye, S.; Xu, H.; Jin, J.; Yang, M.; Wang, C.; Yu, Y.; Cao, X. The E3 ubiquitin ligase neuregulin receptor degradation protein 1 (Nrdp1) promotes M2 macrophage polarization by ubiquitinating and activating transcription factor CCAAT/enhancer-binding Protein β (C/EBPβ). *J. Biol. Chem.* **2012**, *287*, 26740–8.

(16) Fry, W. H. D.; Simion, C.; Sweeney, C.; Carraway, K. L. Quantity control of the ErbB3 receptor tyrosine kinase at the endoplasmic reticulum. *Mol. Cell. Biol.* **2011,** *31*, 3009–18.

(17) Cao, Z.; Wu, X.; Yen, L.; Sweeney, C.; Carraway, K. L. Neuregulin-induced ErbB3 downregulation is mediated by a protein stability cascade involving the E3 ubiquitin ligase Nrdp1. *Mol. Cell. Biol.* **2007,** *27*, 2180–8.

(18) Yu, F.; Zhou, J. Parkin is ubiquitinated by Nrdp1 and abrogates Nrdp1-induced oxidative stress. *Neurosci. Lett.* **2008,** *440*, 4–8.

(19) Zhang, Y.; Zeng, Y.; Wang, M.; Tian, C.; Ma, X.; Chen, H.; Fang, Q.; Jia, L.; Du, J.; Li, H. Cardiac-specific overexpression of E3 ligase Nrdp1 increases ischemia and reperfusion-induced cardiac injury. *Basic Res. Cardiol.* **2001,** *106*, 371–383.

(20) Zhang, Y.; Jin, S. Q.; Li, W. X.; Gao, G. Q.; Zhang, K.; Huang, J. L. Association between RNF41 gene c.-206 T > A genetic polymorphism and risk of congenital heart diseases in the Chinese Mongolian population. *Genet. Mol. Res.* **2016**, *15*, gmr.15028089.

(21) Yen, L.; Cao, Z.; Wu, X.; Ingalla, E. R. Q.; Baron, C.; Young, L. J. T.; Gregg, J. P.; Cardiff, R. D.; Borowsky, A. D.; Sweeney, C.; Carraway, K. L. Loss of Nrdp1 enhances ErbB2/ErbB3-dependent breast tumor cell growth. *Cancer Res.* **2006**, *66*, 11279–86.

(22) Ingalla, E. Q.; Miller, J. K.; Wald, J. H.; Workman, H. C.; Kaur, R. P.; Yen, L.; Fry, W. H. D.; Borowsky, A. D.; Young, L. J. T.; Sweeney, C.; Carraway, K. L. Post-transcriptional mechanisms contribute to the suppression of the ErbB3 negative regulator protein Nrdp1 in mammary tumors. *J. Biol. Chem.* **2010,** *285*, 28691–7.

(23) Chen, L.; Siddiqui, S.; Bose, S.; Mooso, B.; Asuncion, A.; Bedolla, R. G.; Vinall, R.; Tepper, C. G.; Gandour-Edwards, R.; Shi, X.; Lu, X.-H.; Siddiqui, J.; Chinnaiyan, A. M.; Mehra, R.; Devere White, R. W.; Carraway, K. L.; Ghosh, P. M. Nrdp1-mediated regulation of ErbB3 expression by the androgen receptor in androgen-dependent but not castrate-resistant prostate cancer cells. *Cancer Res.* **2010,** *70*, 5994–6003.

(24) Brizzolara, A.; Benelli, R.; Venè, R.; Barboro, P.; Poggi, A.; Tosetti, F.; Ferrari, N. The ErbB family and androgen receptor signaling are targets of Celecoxib in prostate cancer. *Cancer Lett.* **2017,** *400*, 9–17.

(25) Shi, H.; Du, J.; Wang, L.; Zheng, B.; Gong, H.; Wu, Y.; Tang, Y.; Gao, Y.; Yu, R. Lower expression of Nrdp1 in human glioma contributes tumor progression by reducing apoptosis. *IUBMB Life.* **2014,** *66*, 704–710.

(26) Shi, H.; Gong, H.; Cao, K.; Zou, S.; Zhu, B.; Bao, H.; Wu, Y.; Gao, Y.; Tang, Y.; Yu, R. Nrdp1-mediated ErbB3 degradation inhibits glioma cell migration and invasion by reducing cytoplasmic localization of p27Kip1. *J. Neurooncol.* **2015,** *124*, 357–364.

(27) Wu, Y.; Wang, L.; Bao, H.; Zou, S.; Fu, C.; Gong, H.; Gao, Y.; Tang, Y.; Yu, R.; Shi, H. Nrdp1S, short variant of Nrdp1, inhibits human glioma progression by increasing Nrdp1-mediated ErbB3 ubiquitination and degradation. *J. Cell. Mol. Med.* **2016,** *20*, 422–9.

(28) Byun, S.; Shin, S. H.; Lee, E.; Lee, J.; Lee, S.-Y.; Farrand, L.; Jung, S. K.; Cho, Y.-Y.; Um, S.-J.; Sin, H.-S.; Kwon, Y.-J.; Zhang, C.; Tsang, B. K.; Bode, A. M.; Lee, H. J.; Lee, K. W.; Dong, Z. The retinoic acid derivative, ABPN, inhibits pancreatic cancer through induction of Nrdp1. *Carcinogenesis.* **2015,** *36*,

21

1580–1589.

(29) Wauman, J.; De Ceuninck, L.; Vanderroost, N.; Lievens, S.; Tavernier, J. (2011) RNF41 (Nrdp1) controls type 1 cytokine receptor degradation and ectodomain shedding. *J. Cell Sci.* **2011,** *124*, 921–32.

(30) De Ceuninck, L.; Wauman, J.; Masschaele, D.; Peelman, F.; Tavernier, J. Reciprocal cross-regulation between RNF41 and USP8 controls cytokine receptor sorting and processing. *J. Cell Sci.* **2013,** *126*, 3770–81.

(31) Shen, J. J.; Song, Y.; Shen, J. J.; Lin, Y.; Wu, X.; Yan, Y.; Niu, M.; Zhou, L.; Huang, Y.; Gao, Y.; Liu, Y. Nrdp1 is Associated with Neuronal Apoptosis in Lipopolysaccharide-Induced Neuroinflammation. *Neurochem. Res.* **2015,** *40*, 971–979.

(32) Savoy, R. M.; Chen, L.; Siddiqui, S.; Melgoza, F. U.; Durbin-Johnson, B.; Drake, C.; Jathal, M. K.; Bose, S.; Steele, T. M.; Mooso, B. A.; D'Abronzo, L. S.; Fry, W. H.; Carraway, K. L.; Mudryj, M.; Ghosh, P. M. Transcription of Nrdp1 by the androgen receptor is regulated by nuclear filamin A in prostate cancer. *Endocr. Relat. Cancer.* **2015,** *22*, 369–386.

(33) Wu, X.; Yen, L.; Irwin, L.; Sweeney, C.; Carraway, K. L. Stabilization of the E3 ubiquitin ligase Nrdp1 by the deubiquitinating enzyme USP8. *Mol. Cell. Biol.* **2004,** *24*, 7748–57.

(34) Soleimanpour, S. A.; Gupta, A.; Bakay, M.; Ferrari, A. M.; Groff, D. N.; Fadista, J.; Spruce, L. A.; Kushner, J. A.; Groop, L.; Seeholzer, S. H.; Kaufman, B. A.; Hakonarson, H.; Stoffers, D. A. The diabetes susceptibility gene Clec16a regulates mitophagy. *Cell.* **2014,** *157*, 1577–90.

(35) Cao, K.; Gong, H.; Qiu, Z.; Wen, Q.; Zhang, B.; Tang, T.; Zhou, X.; Cao, T.; Wang, B.; Shi, H.; Wang, R. Hepatitis B virus X protein reduces the stability of Nrdp1 to up-regulate ErbB3 in hepatocellular carcinoma cells. *Tumor Biol.* **2016,** *37*, 10375–10382.

(36) Hatakeyama, J.; Wald, J. H.; Rafidi, H.; Cuevas, A.; Sweeney, C.; Carraway, K. L. The ER structural protein Rtn4A stabilizes and enhances signaling through the receptor tyrosine kinase ErbB3. *Sci. Signal.* **2016,** *9*, ra65.

(37) Titeca, K.; Van Quickelberghe, E.; Samyn, N.; De Sutter, D.; Verhee, A.; Gevaert, K.; Tavernier, J.; Eyckerman, S. Analyzing trapped protein complexes by Virotrap and SFINX. *Nat. Protoc.* **2017,** *12*, 881–898.

(38) Vizcaíno, J. A.; Deutsch, E. W.; Wang, R.; Csordas, A.; Reisinger, F.; Ríos, D.; Dianes, J. A.; Sun, Z.; Farrah, T.; Bandeira, N.; Binz, P.-A.; Xenarios, I.; Eisenacher, M.; Mayer, G.; Gatto, L.; Campos, A.; Chalkley, R. J.; Kraus, H.-J.; Albar, J. P.; Martinez-Bartolomé, S.; Apweiler, R.; Omenn, G. S.; Martens, L.; Jones, A. R.; Hermjakob, H. ProteomeXchange provides globally coordinated proteomics data submission and dissemination. *Nat. Biotechnol.* **2014,** *32*, 223–6.

(39) Lievens, S.; Van der Heyden, J.; Masschaele, D.; De Ceuninck, L.; Petta, I.; Gupta, S.; De Puysseleyr, V.; Vauthier, V.; Lemmens, I.; De Clercq, D. J. H.; Defever, D.; Vanderroost, N.; De Smet, A.-S.; Eyckerman, S.; Van Calenbergh, S.; Martens, L.; De Bosscher, K.; Libert, C.; Hill, D. E.; Vidal, M.; Tavernier, J. Proteome-scale Binary Interactomics in Human Cells. *Mol. Cell. Proteomics.* **2016,** *15*, 3624–3639.

(40) Yang, X.; Boehm, J. S.; Yang, X.; Salehi-Ashtiani, K.; Hao, T.; Shen, Y.; Lubonja, R.; Thomas, S. R.; Alkan, O.; Bhimdi, T.; Green, T. M.; Johannessen, C. M.; Silver, S. J.; Nguyen, C.; Murray, R. R.; Hieronymus, H.; Balcha, D.; Fan, C.; Lin, C.; Ghamsari, L.; Vidal, M.; Hahn, W. C.; Hill, D. E.; Root, D. E. A public genome-scale lentiviral expression library of human ORFs. *Nat. Methods.* **2011,** *8*, 659–661.

(41) Eyckerman, S.; Titeca, K.; Van Quickelberghe, E.; Cloots, E.; Verhee, A.; Samyn, N.; De Ceuninck, L.; Timmerman, E.; De Sutter, D.; Lievens, S.; Van Calenbergh, S.; Gevaert, K.; Tavernier, J. Trapping

22

mammalian protein complexes in viral particles. *Nat. Commun.* **2016***, 7*, 11416.

 (42) Rolland, T.; Taşan, M.; Charloteaux, B.; Pevzner, S. J.; Zhong, Q.; Sahni, N.; Yi, S.; Lemmens, I.; Fontanillo, C.; Mosca, R.; Kamburov, A.; Ghiassian, S. D.; Yang, X.; Ghamsari, L.; Balcha, D.; Begg, B. E.; Braun, P.; Brehme, M.; Broly, M. P.; Carvunis, A.-R.; Convery-Zupan, D.; Corominas, R.; Coulombe-Huntington, J.; Dann, E.; Dreze, M.; Dricot, A.; Fan, C.; Franzosa, E.; Gebreab, F.; Gutierrez, B. J.; Hardy, M. F.; Jin, M.; Kang, S.; Kiros, R.; Lin, G. N.; Luck, K.; MacWilliams, A.; Menche, J.; Murray, R. R.; Palagi, A.; Poulin, M. M.; Rambout, X.; Rasla, J.; Reichert, P.; Romero, V.; Ruyssinck, E.; Sahalie, J. M.; Scholz, A.; Shah, A. A.; Sharma, A.; Shen, Y.; Spirohn, K.; Tam, S.; Tejeda, A. O.; Trigg, S. A.; Twizere, J.-C.; Vega, K.; Walsh, J.; Cusick, M. E.; Xia, Y.; Barabási, A.-L.; Iakoucheva, L. M.; Aloy, P.; De Las Rivas, J.; Tavernier, J.; Calderwood, M. A.; Hill, D. E.; Hao, T.; Roth, F. P.; Vidal, M. A Proteome-Scale Map of the Human Interactome Network. *Cell.* **2014,** *159*, 1212–1226.

(43) Szklarczyk, D.; Franceschini, A.; Wyder, S.; Forslund, K.; Heller, D.; Huerta-Cepas, J.; Simonovic, M.; Roth, A.; Santos, A.; Tsafou, K. P.; Kuhn, M.; Bork, P.; Jensen, L. J.; von Mering, C. STRING v10: protein-protein interaction networks, integrated over the tree of life. *Nucleic Acids Res.* **2015,** *43*, D447–D452.

 (44) Chatr-Aryamontri, A.; Oughtred, R.; Boucher, L.; Rust, J.; Chang, C.; Kolas, N. K.; O'Donnell, L.; Oster, S.; Theesfeld, C.; Sellam, A.; Stark, C.; Breitkreutz, B.-J.; Dolinski, K.; Tyers, M. The BioGRID interaction database: 2017 update. *Nucleic Acids Res.* **2017**, *45*, D369–D379.

 (45) Toriyama, M.; Shimada, T.; Kim, K. B.; Mitsuba, M.; Nomura, E.; Katsuta, K.; Sakumura, Y.; Roepstorff, P.; Inagaki, N. Shootin1: A protein involved in the organization of an asymmetric signal for neuronal polarization. *J. Cell Biol.* **2006,** *175*, 147–57.

(46) Shimada, T.; Toriyama, M.; Uemura, K.; Kamiguchi, H.; Sugiura, T.; Watanabe, N.; Inagaki, N. Shootin1 interacts with actin retrograde flow and L1-CAM to promote axon outgrowth. *J. Cell Biol.* **2008,** *181*, 817–29.

(47) van Haren, J.; Boudeau, J.; Schmidt, S.; Basu, S.; Liu, Z.; Lammers, D.; Demmers, J.; Benhari, J.; Grosveld, F.; Debant, A.; Galjart, N. Dynamic Microtubules Catalyze Formation of Navigator-TRIO Complexes to Regulate Neurite Extension. *Curr. Biol.* **2014,** *24,* 1778-1785.

(48) Wald, J. H.; Hatakeyama, J.; Printsev, I.; Cuevas, A.; Fry, W. H. D.; Saldana, M. J.; VanderVorst, K.; Rowson-Hodel, A.; Angelastro, J. M.; Sweeney, C.; Carraway, K. L. Suppression of planar cell polarity signaling and migration in glioblastoma by Nrdp1-mediated Dvl polyubiquitination. *Oncogene.* **2017**, *56*, 1068-1081.

(49) Lewandowski, K. T.; Piwnica-Worms, H. (2014) Phosphorylation of the E3 ubiquitin ligase RNF41 by the kinase Par-1b is required for epithelial cell polarity. *J. Cell Sci.* **2017,** *127*, 315–27.

(50) Diamonti, A. J.; Guy, P. M.; Ivanof, C.; Wong, K.; Sweeney, C.; Carraway, K. L. An RBCC protein implicated in maintenance of steady-state neuregulin receptor levels. *Proc. Natl. Acad. Sci. U. S. A.* **2002,** *99*, 2866–71.

 (51) Kirchhausen, T.; Owen, D.; Harrison, S. C. Molecular structure, function, and dynamics of clathrin-mediated membrane traffic. *Cold Spring Harb. Perspect. Biol.* **2014,** *6*, a016725.

(52) Collins, B. M.; McCoy, A. J.; Kent, H. M.; Evans, P. R.; Owen, D. J. Molecular Architecture and Functional Model of the Endocytic AP2 Complex. *Cell.* **2002,** *109*, 523–535.

(53) Jackson, L. P.; Kelly, B. T.; McCoy, A. J.; Gaffry, T.; James, L. C.; Collins, B. M.; Höning, S.; Evans, P. R.; Owen, D. J. A large-scale conformational change couples membrane recruitment to cargo binding in the AP2 clathrin adaptor complex. *Cell.* **2010,** *141*, 1220–9.

23

(54) Kelly, B. T.; Graham, S. C.; Liska, N.; Dannhauser, P. N.; Höning, S.; Ungewickell, E. J.; Owen, D. J. AP2 controls clathrin polymerization with a membrane-activated switch. *Science.* **2014,** *345*, 459–463.

(55) Tu, H.; Hsuchou, H.; Kastin, A. J.; Wu, X.; Pan, W. Unique leptin trafficking by a tailless receptor. *FASEB J.* **2010,** *24*, 2281–91.

(56) Motley, A.; Bright, N. A.; Seaman, M. N. J.; Robinson, M. S. Clathrin-mediated endocytosis in AP-2-depleted cells. *J. Cell Biol.* **2003,** *162*, 909–18.

(57) Avvakumov, G. V; Walker, J. R.; Xue, S.; Finerty, P. J.; Mackenzie, F.; Newman, E. M.; Dhe-Paganon, S. Amino-terminal dimerization, NRDP1-rhodanese interaction, and inhibited catalytic domain conformation of the ubiquitin-specific protease 8 (USP8). *J. Biol. Chem.* **2006,** *281*, 38061–70.

(58) Bouyain, S.; Leahy, D. J. Structure-based mutagenesis of the substrate-recognition domain of Nrdp1/FLRF identifies the binding site for the receptor tyrosine kinase ErbB3. *Protein Sci.* **2007,** *16*, 654–61.

(59) Nesbit, M. A.; Hannan, F. M.; Howles, S. A.; Reed, A. A. C.; Cranston, T.; Thakker, C. E.; Gregory, L.; Rimmer, A. J.; Rust, N.; Graham, U.; Morrison, P. J.; Hunter, S. J.; Whyte, M. P.; McVean, G.; Buck, D.; Thakker, R. V. Mutations in AP2S1 cause familial hypocalciuric hypercalcemia type 3. *Nat. Genet.* **2013,** *45*, 93–7.

For TOC use only:
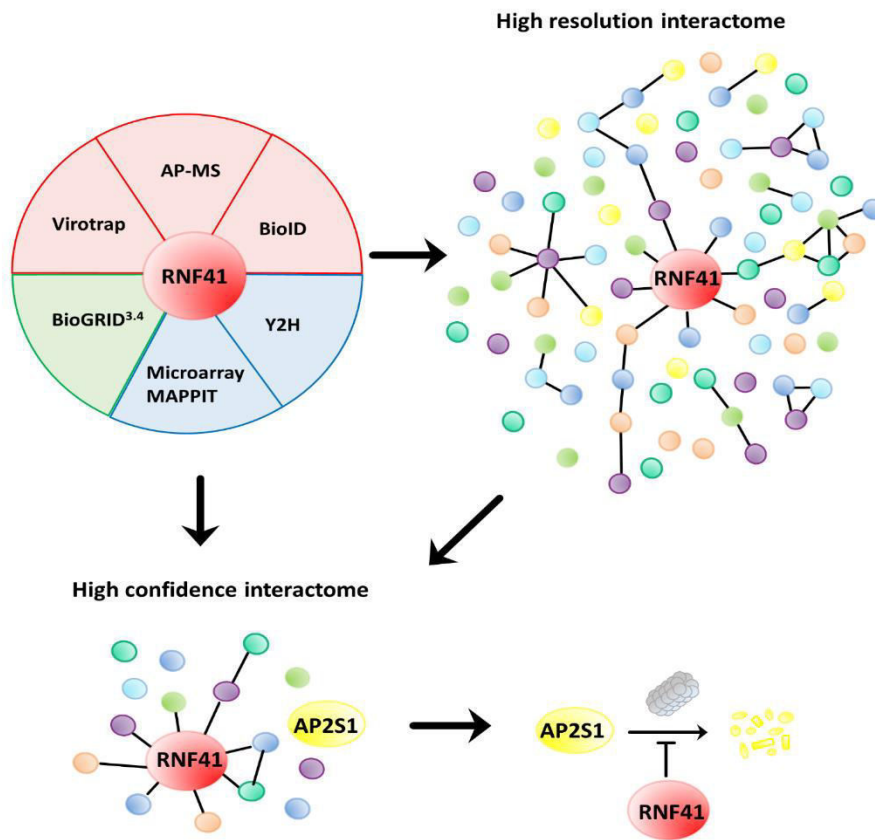
Supplementary Figures
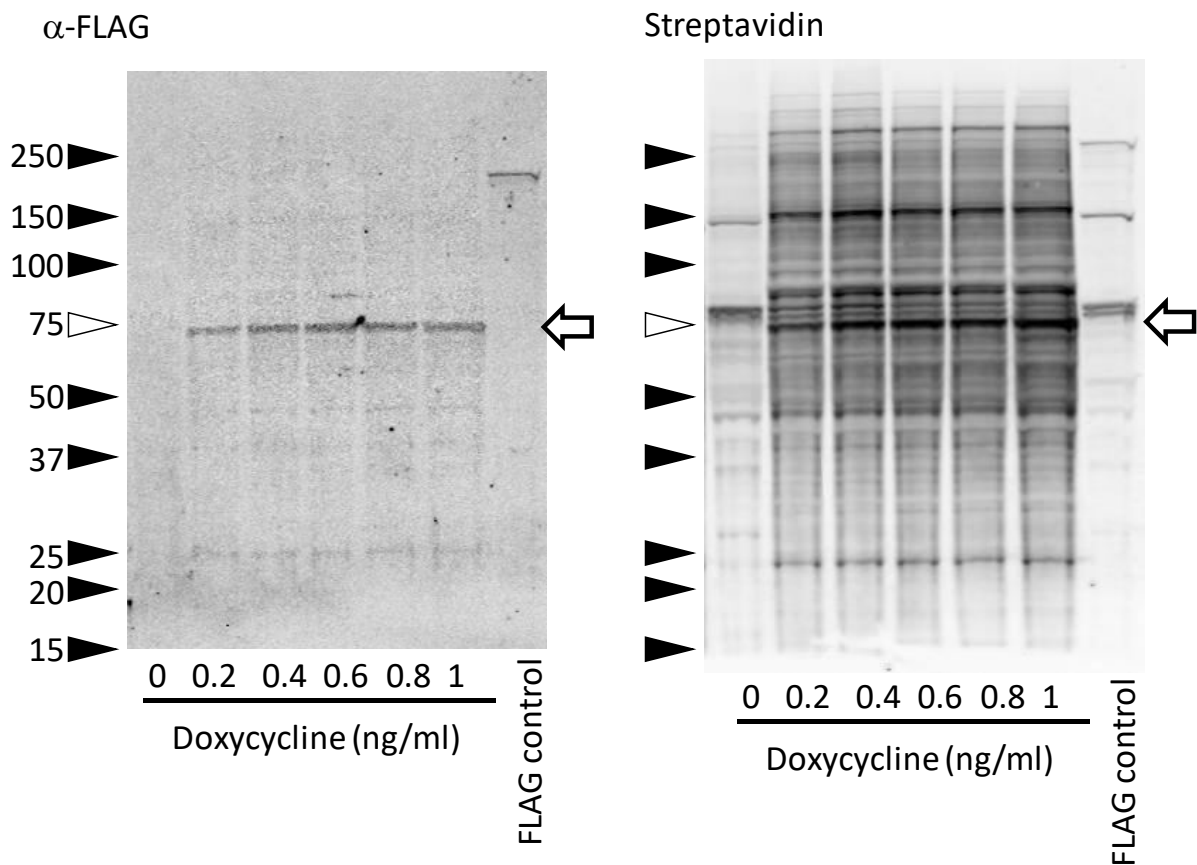
Supplementary Figure S1. Inducible expression of a FLAG-tagged RNF41 C34S/H36Q-BirA*fusion construct in Flp-In™ T-REx 293 cells. After treatment with doxycycline, cells were lysed and cleared lysates were loaded for PAGE. After blotting, expression of the fusion protein was revealed by anti-FLAG antibodies (left panel). In the panel on the right, biotinylated proteins are revealed by fluorescently-labeled streptavidin.
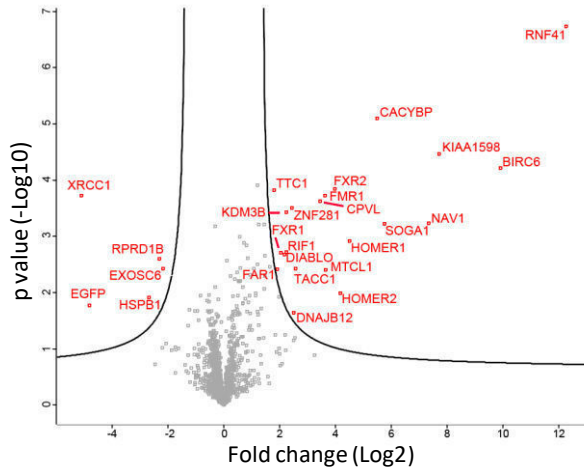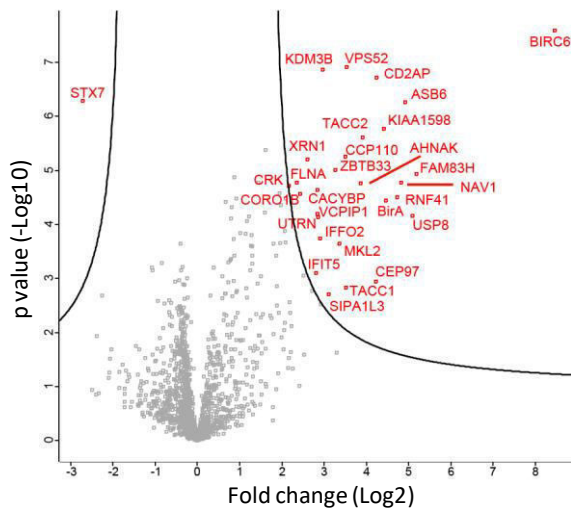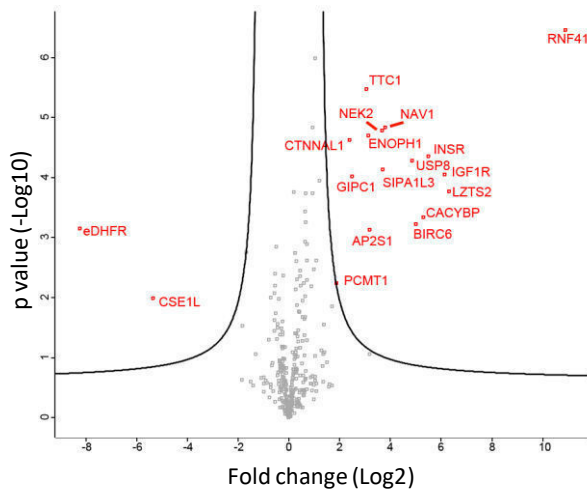
Supplementary Figure S2. Volcano plots for the different MS-based approaches showing the difference in protein quantity (X-axis, log2) against the p-value (Y-axis, -log10). FDR was set at 1% and S0 value was 1 for the 3 different approaches. All significant proteins are annotated in these plots.
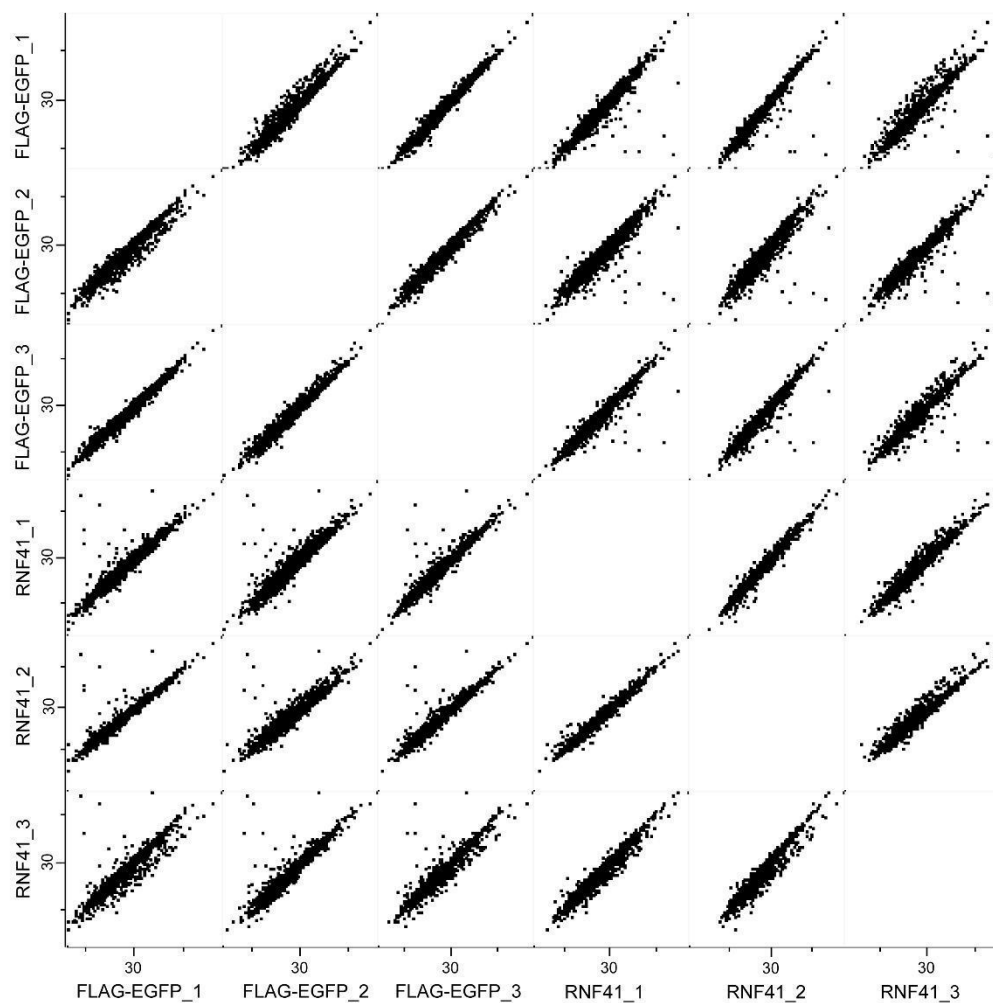
Supplementary Figure S3. Correlation plots of the LFQ intensities for the AP-MS experiments. LFQ intensities for the different samples were compared in a pairwise fashion and presented in scatter plots.
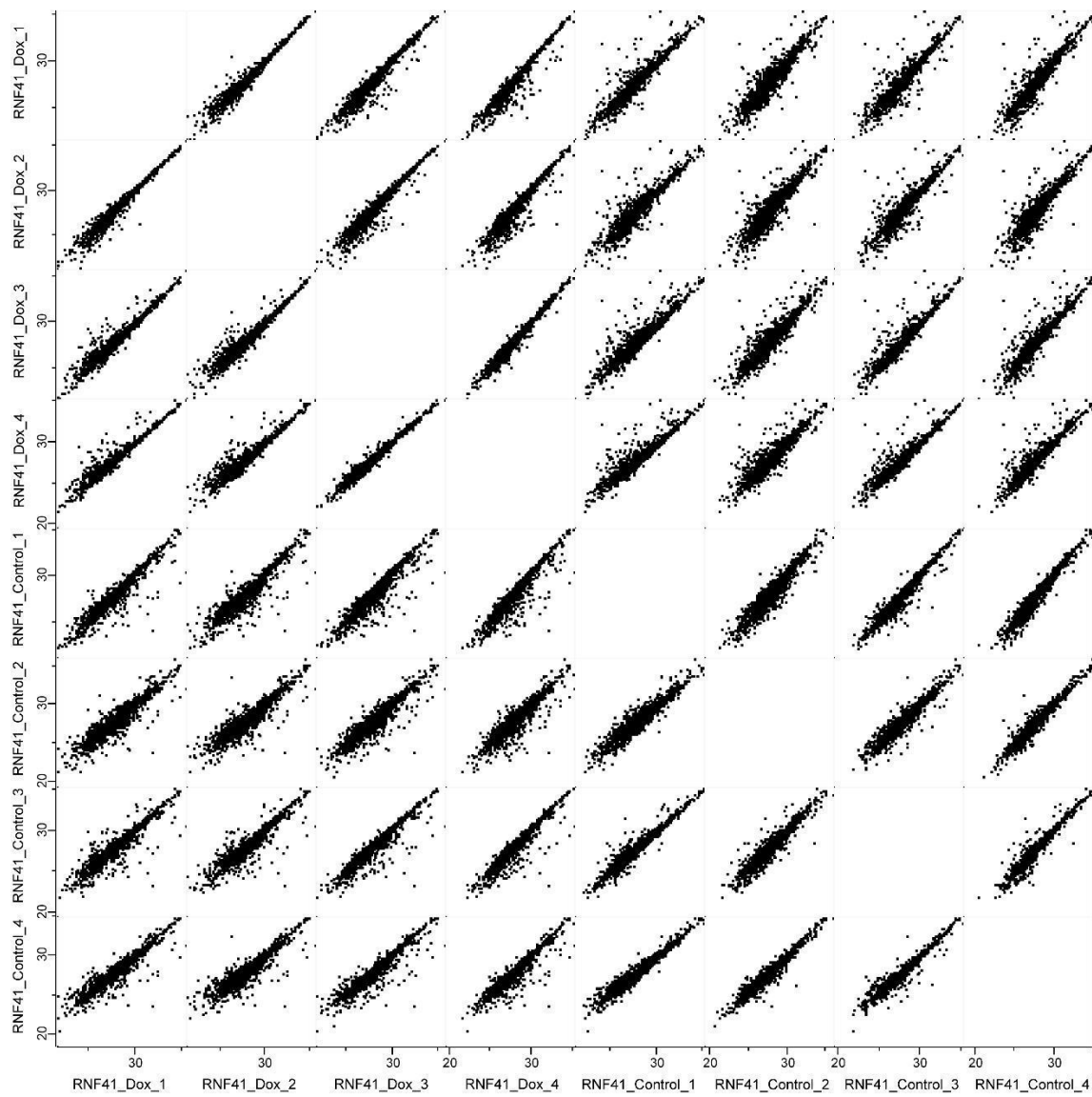
Supplementary Figure S4. Correlation plots of the LFQ intensities for the BioID experiments. LFQ intensities for the different samples were compared in a pairwise fashion and presented in scatter plots.
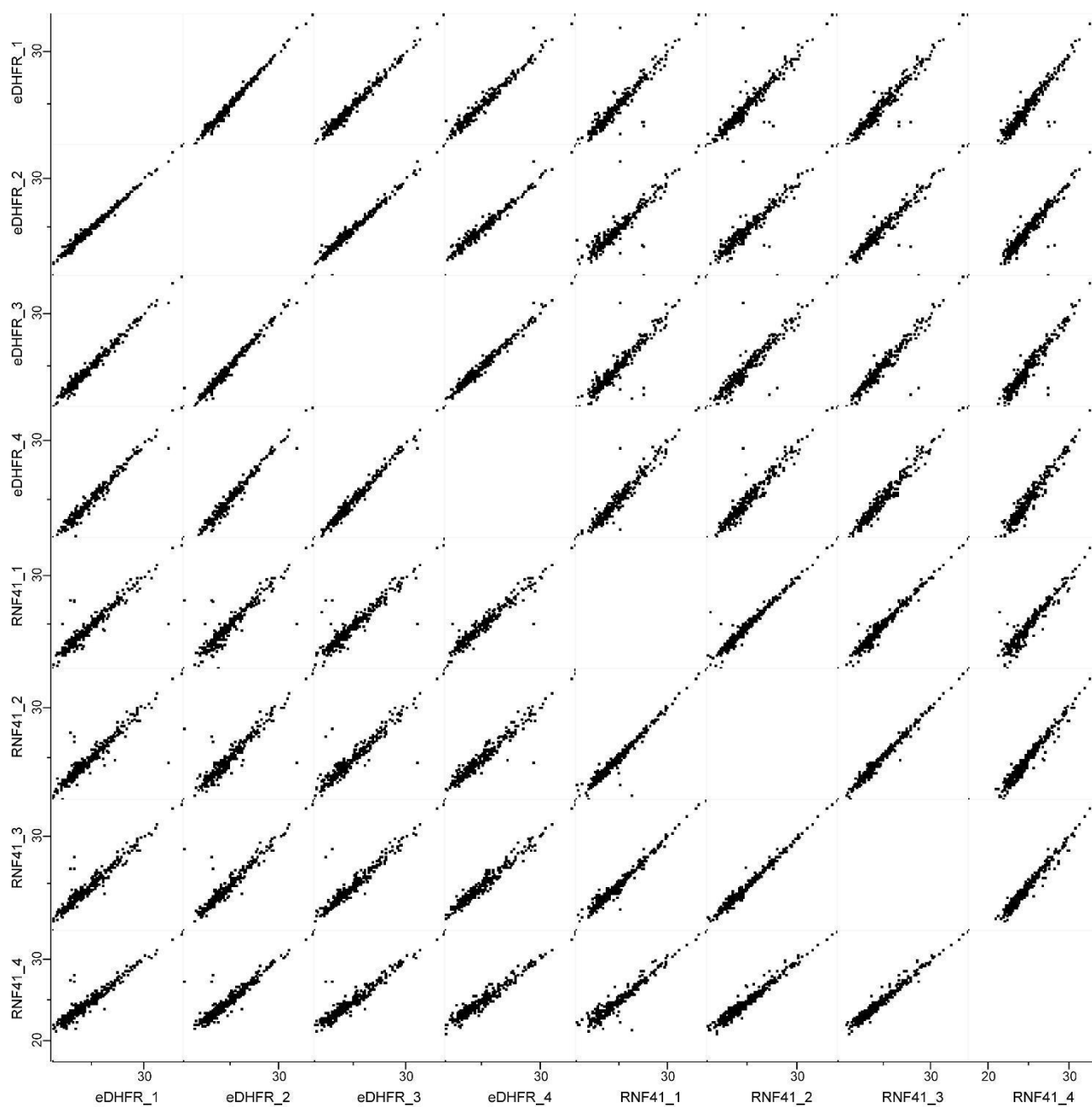
Supplementary Figure S5. Correlation plots of the LFQ intensities for the Virotrap experiments. LFQ intensities for the different samples were compared in a pairwise fashion and presented in scatter plots.

29
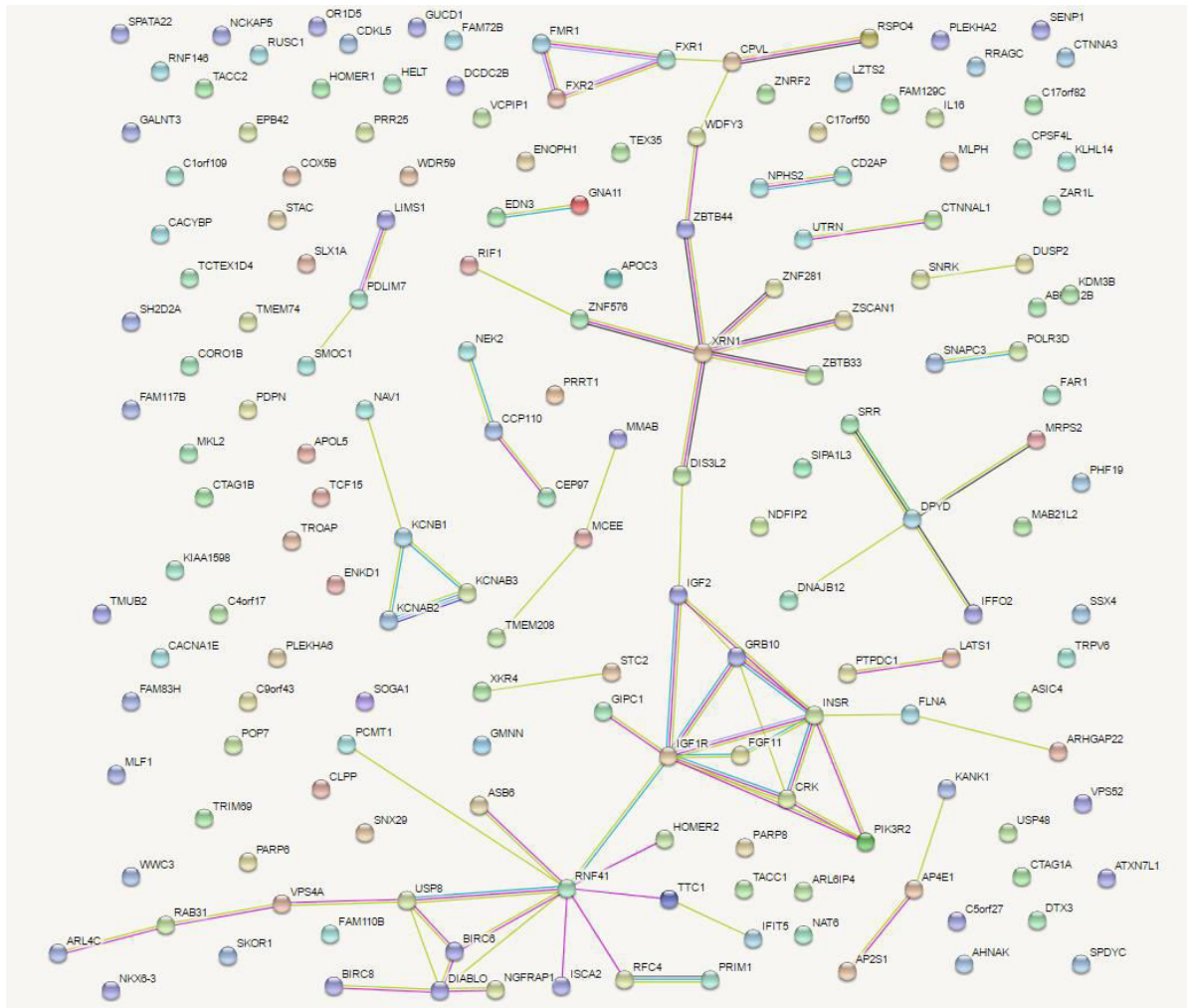
Supplementary Figure S6. The high resolution interactome of RNF41. All candidate partner proteins from the different experimental approaches and from Y2H and microarray MAPPIT were combined in a single list and analyzed in STRING to reveal functional protein association networks (http://string-db.org/)[34].
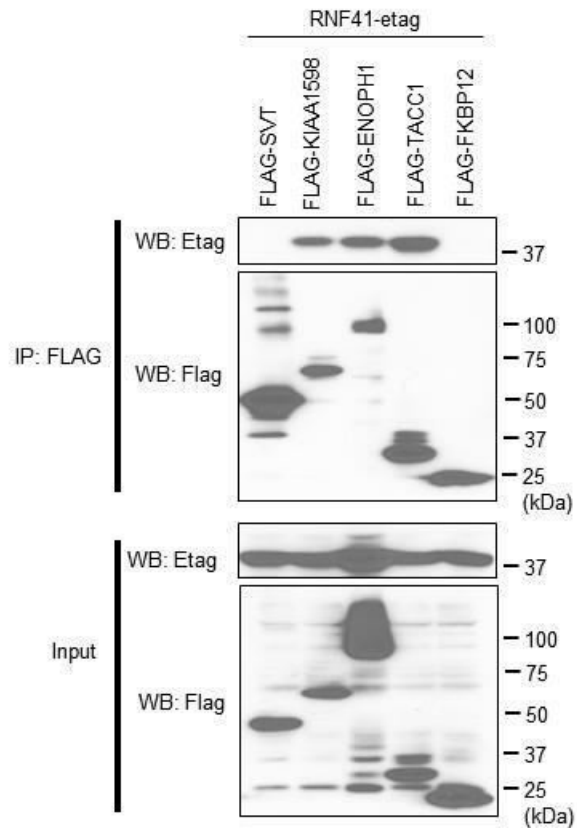
Supplementary Figure S7. Co-immunoprecipitation of E-tagged RNF41 and FLAG-tagged KIAA1598, TACC1 and ENOPH1. HEK293T cells were transiently transfected with E-tagged RNF41 and FLAG-tagged KIAA1598, TACC1, ENOPH1 and FLAG-tagged SVT and FKBP12 as negative controls. Anti-FLAG immunoprecipitates (upper panels) and lysates (Input, lower panels) were visualized using anti-Etag and anti-FLAG.
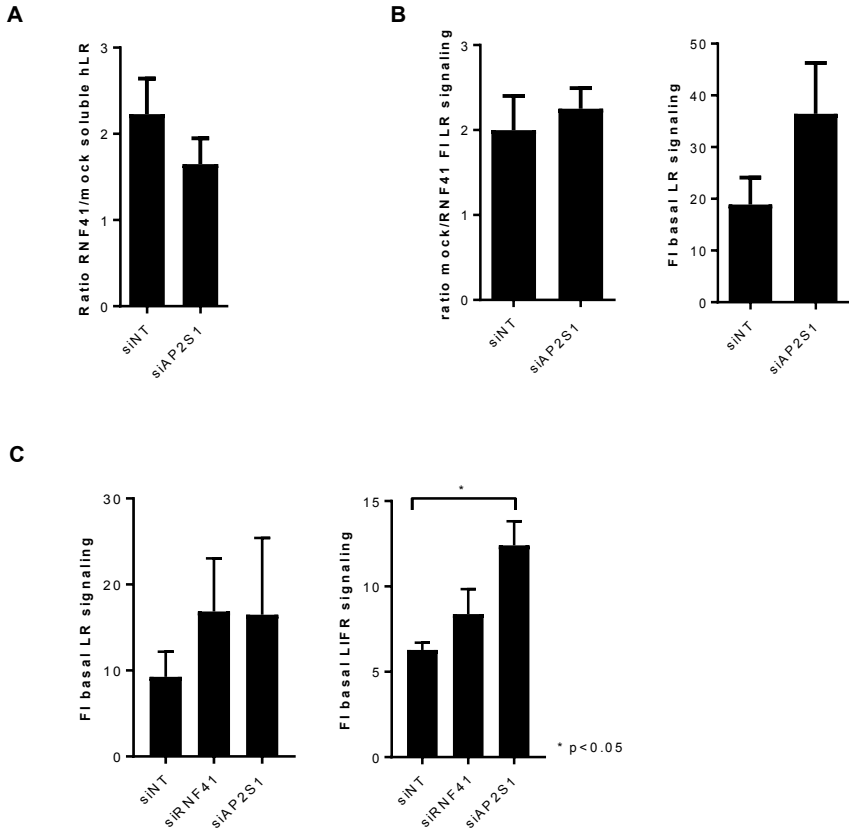
Supplementary Figure S8. Statistical analysis of 3 biological replicates from data in Figure 3. (A) Fig 3A.
A two-tailed Mann-Whitney test showed no significant difference in LR shedding for the RNF41/mock ratio between siAP2S1 and the siNT control. Values are means ± s.e.m. **(B) Fig 3B.** Left, a two-tailed Mann-Whitney test showed no significant difference in LR signaling for the mock/RNF41 ratio of the FI (S/NS values) between siAP2S1 and the siNT control. Right, although the three biological replicates show the same trend, i.e. enhanced signaling with siAP2S1, no statistical significant difference in LR signaling for the FI (S/NS values) was observed between the different siRNA treatments using a two-tailed Mann-Whitney test. Values are means ± s.e.m**. (C) Fig 3C.** Left, a one-way ANOVA showed no significant difference in LR signaling for the FI (S/NS values) between siAP2S1 and the siNT control, although we do observe enhanced LR signaling when silencing AP2S1 throughout all 3 biological replicates. Right, a one-way ANOVA showed a significant increase in LIFR signaling for the FI (S/NS values) when cells are treated with siAP2S1 compared to the siNT control (p<0.05). Values are means ± s.e.m.
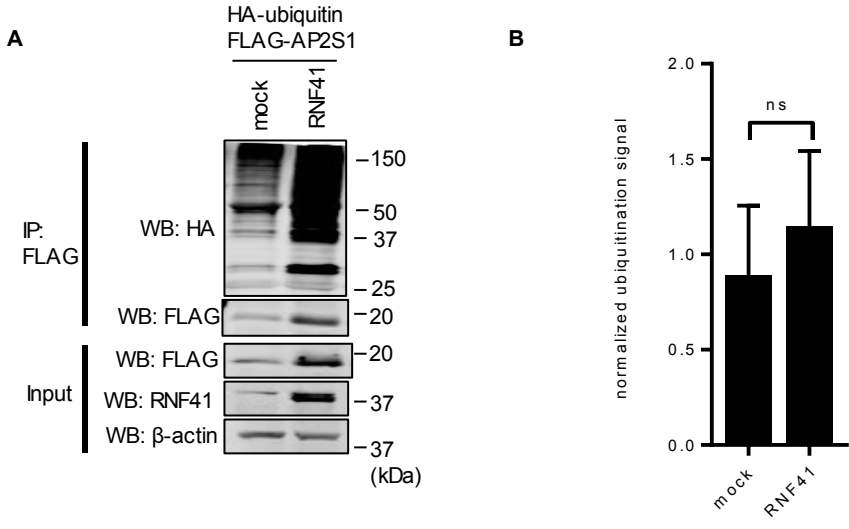
Supplementary Figure S9. RNF41 does not ubiquitinate AP2S1. (A) HEK293T cells were transiently co-transfected with plasmids encoding FLAG-tagged AP2S1, HA-ubiquitin and either WT RNF41 or soluble IL5Rα (mock). FLAG immunoprecipitation followed by anti-HA staining revealed the ubiquitination state of AP2S1. Expression was verified using anti-FLAG, anti-RNF41 and anti-β-actin (loading control) antibodies. **(B)** The Western Blot from (A) was quantified together with two other biological replicates using Image J. The ubiquitination signal was normalized for the amount of immunoprecipitated FLAG-tagged AP2S1 and compared between the mock and RNF41 condition. A two-tailed Mann-Whitney test showed no significant difference in AP2S1 ubiquitination between the RNF41 and mock transfected cells.
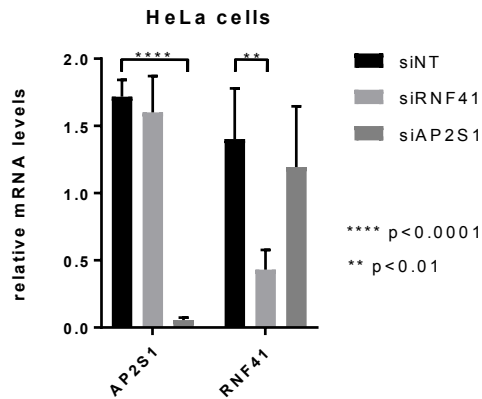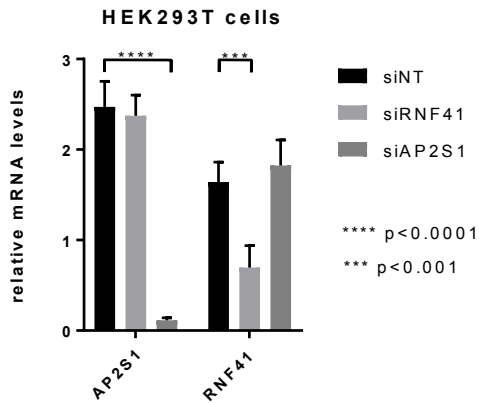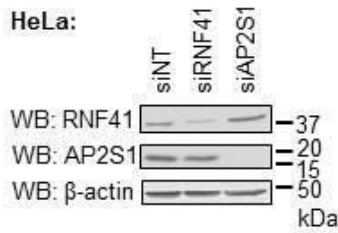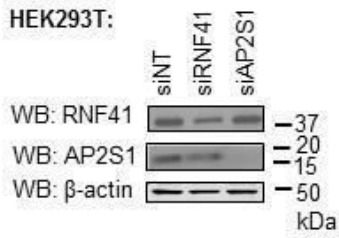
Supplementary Figure S10. Effect of AP2S1 depletion on RNF41 and vice versa. HEK293T and HeLa cells were silenced for 72h using siRNA against RNF41 or AP2S1. Protein expression levels were analyzed by Western Blotting using antibodies against RNF41, AP2S1 or β-actin (loading control) and mRNA levels were checked via RT-qPCR. A one-way ANOVA of three biological replicates showed significant knockdown of both AP2S1 and RNF41 mRNA levels in HEK293T and HeLa cells using siAP2S1 and siRNF41 respectively.
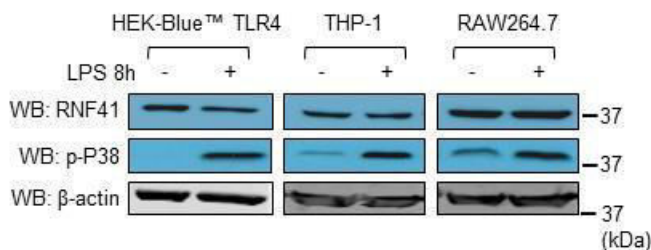

Supplementary Figure S11. Effect of LPS on RNF41 protein expression. HEK-Blue™ TLR4, THP-1 and RAW264.7 cells were incubated with LPS for 8 hours. RNF41 protein levels were analyzed by Western Blotting using antibodies against RNF41, p-P38 (confirmation for LPS activation) or β-actin (loading control), n=3.
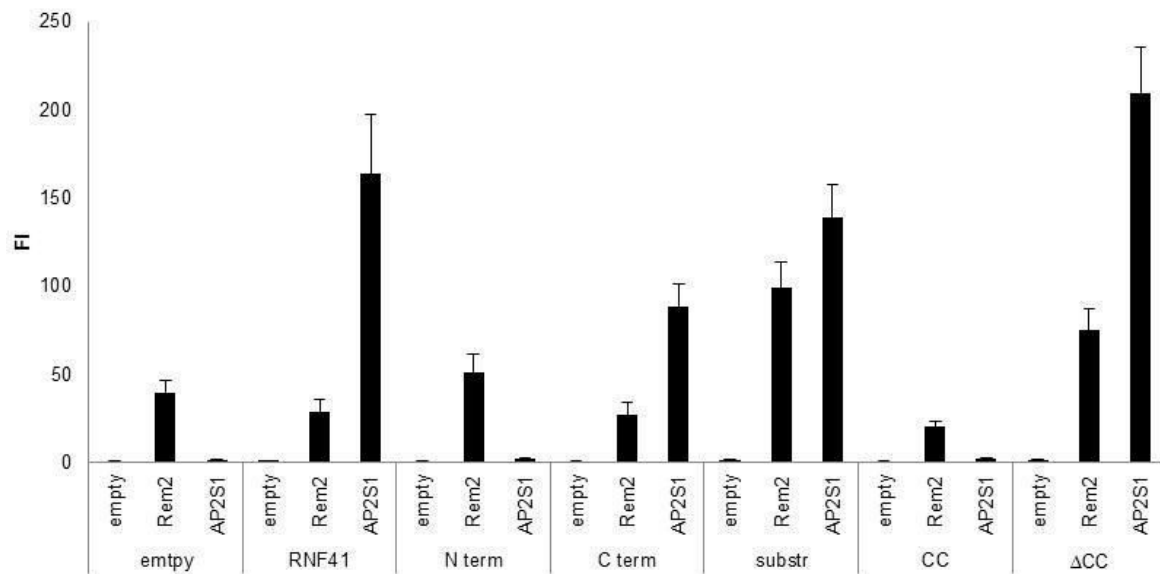
Supplementary Figure S12. Extended MAPPIT data from Figure 4A, with empty (unfused gp130) and JAK2 binding (Rem2-gp130) prey as a negative and positive control respectively to confirm specificity and bait expression.
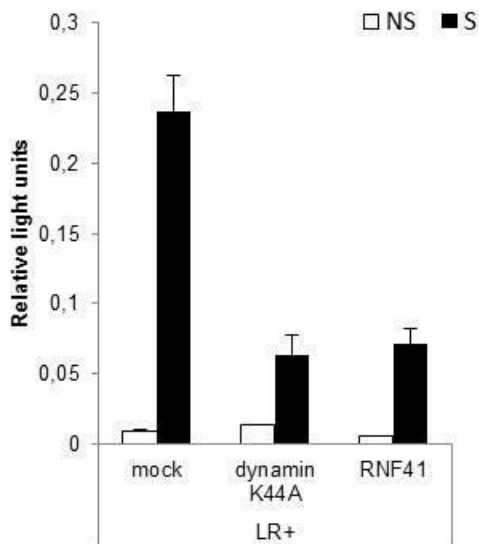
Supplementary Fig S13: LR internalization is necessary for LR signaling. HEK293T cells were transiently co-transfected with C-terminally HA-tagged LR and DN dynamin K44A, RNF41 or soluble IL5Rα (mock) together with a STAT3-dependent luciferase reporter gene. Cells were stimulated with leptin (black bars) or left untreated (white bars). Absolute luciferase counts of triplicate measurements normalized for transfection efficiency from one biological replicate are represented (means ± s.d.).

35
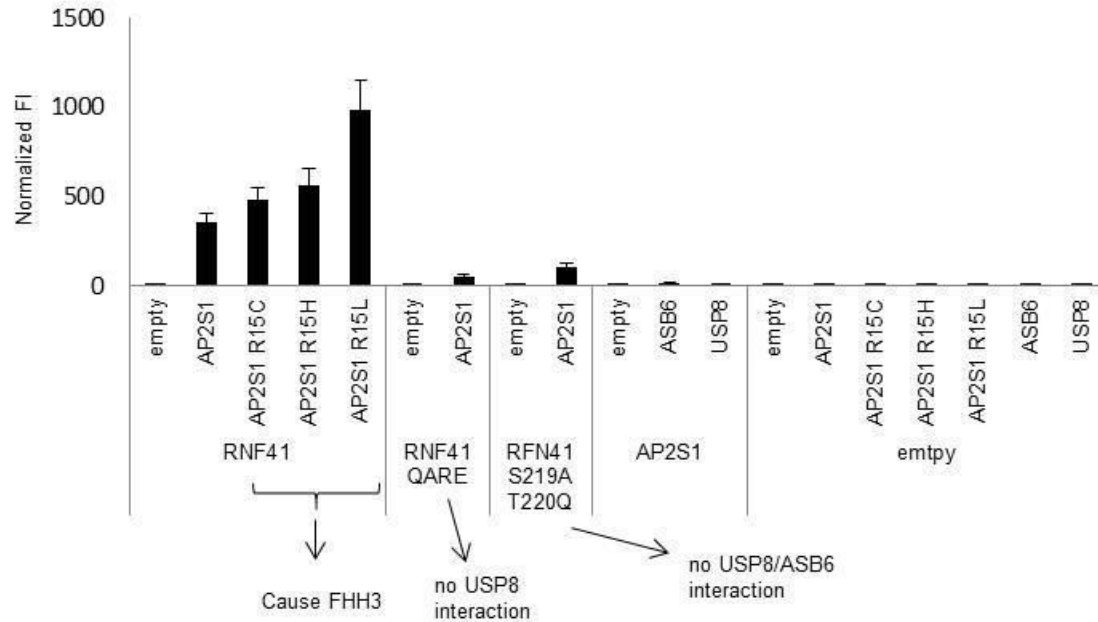
Supplementary Fig S14: AP2S1 Arg mutations do not influence RNF41 interaction, and AP2S1 does not interact with ASB6 or USP8. MAPPIT analysis in HEK293T cells transiently co-transfected with plasmids encoding WT or mutated AP2S1, ASB6 or USP8 prey together with empty, RNF41 WT or mutated RNF41 bait and the pXP2d2-rPAP1-luciferase reporter plasmid. The next day, cells were stimulated with EPO or left untreated for 24 hours. The luciferase signal is expressed as fold induction (stimulated/non stimulated), relative to the signal of a control JAK2 binding prey ± s.d. of triplicate measurements.

Supplementary Tables

Supplementary Table S1. Generation of constructs.

Supplementary Table S2: Protein lists obtained with the different methods used in this study. Perseus tables with differential proteins (FDR 0.01% S0=1) are shown for AP-MS, BioID and Virotrap experiments. For microarray MAPPIT the full list of retested candidates obtained for a genome-wide screen is shown. Interactions were also tested for a eDHFR control bait. Only positive interactions that have a 10 fold higher induction over control were retained for further analysis. The results obtained for different high throughput studies with the yeast 2 hybrid for RNF41 are displayed in the Y2H tab. The BioGRID tab shows the list of protein interactions present in the BioGRID3.4 database (April 2017) with references to the original publications.

Supplementary Table S3: Spectral counts for the different proteins detected in the MS-based approaches. Spectral counts are presented for all individual samples that were analyzed by MS.

Supplementary Table S4: Overlap of detected proteins between the different methods and between BioGRID. The data presented here were used as input in the Venn diagram shown in Figure 2B.

Supplementary Table S1.				
Construct	Template	cloning Vector	cloning site	primers
pDEST-pCDNA5-RNF41 C34S/H36Q-BirA*-Flag	pMet7-GAG-RNF41 C34S/H36Q	pDEST-pCDNA5-BirA*-Flag (Couzens et al, 2013)	LR reaction	5'-GGGGACAAGTTTGTACAAAAAAGCAGGCTCAACCATGGGGTATGATGTAACCCG-3'
				5'-GGGGACCACTTTGTACAAGAAAGCTGGGTCTGCGGCCGCTATCTCTTCC-3'
pMG1-AP2S1 = prey	huORF5.1	pMG1 (Lievens et al, 2009)	LR reaction	
pMG1-RNF41 CC = prey	pSel-RNF41 CC	pMG1	SalI-XbaI	
pMet7-FLAG-AP2S1	huORF5.1	pMet7-FLAG (Lievens et al, 2009)	LR reaction	
pMet7-RNF41 G2A	pMet7-RNF41		mutagenesis	5'-GCTGCGGAATTCGCCATGGCATATGATGTAACCCGTTTCCAGGGGG-3'
				5'-CCCCCTGGAAACGGGTTACATCATATGCCATGGCGAATTCCGCAGC-3'
pMet7-RNF41 ΔCC	pMet7-RNF41		Mutagenesis 1	5'-CCCAACCATAACTGCGATATCCACCTGCGCTCAGTG-3'
			Mutagenesis 2	5'-CACTGAGCGCAGGTGGATATCGCAGTTATGGTTGGG-3'
			+ EcoRV digest	5'-CTGCTAAAGGCATACGATATCGCAATCCGCAGTGTC-3'
				5'-GACACTGCGGATTGCGATATCGTATGCCTTTAGCAG-3'
pMet7-RNF41-GFP	pMet7-RNF41	pMet7-GFP (Wauman et al, 2011)	NheI-EcoRI	5'-GAGCTAGCATGGGGTATGATGTAACCCG-3'
				5'-CGCGAATTCTATCTCTTCCACGCCATGCG-3'
pMet7-RNF41 DN-GFP	pMet7-RNF41 DN	pMet7-RNF41-GFP	NheI-SalI	5'-GGCGCTAGCGGCATGAACCCGAAGCGGCCTGTGAC-3'
				5'-GCCGTCGACGTATCTCTTCCACGCCATGCGCAAAT-3'
pMet7-RNF41 C34S/H36Q-GFP	pMet7-RNF41-GFP		mutagenesis	5'-GTACAGGCACCTCATAGTGAACAAGCTTTCTGCAACGCC-3'
				5'-GGCGTTGCAGAAAGCTTGTTCACTATGAGGTGCCTGTAC-3'
pMet7-RNF41 G2A-GFP	pMet7-RNF41-GFP		mutagenesis	5'-GCTGCGGAATTCGCCATGGCATATGATGTAACCCGTTTCCAGGGGG-3'
				5'-CCCCCTGGAAACGGGTTACATCATATGCCATGGCGAATTCCGCAGC-3'

156

pMet7-RNF41 ΔCC-GFP	pSEL-RNF41ΔCC	pMET7-RNF41-GFP	BbvCI-AfeI	
pMet7-RNF41 CC-GFP	pMet7-RNF41 CC-FLAG (Masschaele et al, 2017)	pMet7-RNF41-GFP	NheI-SalI	5'-GGCGCTAGCACCATGATTAAGCACCTGCGCTCAG-3'
				5'-GGCGCTAGCACCATGATTAAGCACCTGCGCTCAG-3'
pCDNA3,1-T7-FLAG-AP2S1	pMET7-FLAG-AP2S1	pCDNA3.1 vector	AflII-XbaI	GCCCTTAAGGCCATGGATTACAAGGATGACG
				GGCCTCTAGATTAAACCACTTTGTACAAGAAAGTTGGGC
pCDNA3,1-T7-FLAG-ASB6	huORF5,1; pMET7-FLAG-ASB6	pCDNA3.1 vector	AflII-XbaI	TGCGGGCCCTTAAGCATGGATTAC
				GTAATCCATGCTTAAGGGCCCGCA

pMet7-GAG-RNF41 C34S/H36Q (Eyckerman et al, 2016)
pMet7-GAG-eDHFR (Eyckerman et al, 2016)
pMet7-FLAG-RNF41 C34S/H36Q (Eyckerman et al, 2016)
pMet7-FLAG-GFP (Eyckerman et al, 2016)
pSel-RNF41 = bait (De Ceuninck et al, 2013)
pSel-RNF41 C34S/H36Q = bait (De Ceuninck et al, 2013)
pSel-RNF41 N-terminal = bait (Masschaele et al, 2017)
pSel-RNF41 C-terminal = bait (Masschaele et al, 2017)
pSel-RNF41 substrate binding = bait (Masschaele et al, 2017)
pSel-RNF41 CC = bait (Masschaele et al, 2017)
pSel-RNF41ΔCC = bait (Masschaele et al, 2017)
pXP2d2-rPAP1-luficerase reporter (wauman et al, 2011)
pMet7-hLR-HA (Wauman et al, 2011)
pMet7-sIL-5Rα (De Ceuninck et al, 2013)
pMet7-RNF41 (De Ceuninck et al, 2013)
pMet7-RNF41 DN (wauman et al, 2011)
pMet7-RNF41 (C34S/H36Q) (De Ceuninck et al, 2013)
pGEX-4T-GST-RNF41 (Masschaele et al, 2017)
pGEX-4T-GST-PGC1α (Masschaele et al, 2017)

Supplementary Table S4: Overlap of detected proteins between the different methods and between BioGRID3.4. The data presented here were used as input in the Venn diagram shown in Figure 2B.

All interactors	AP-MS	BioID	Virotrap	ay MAPPIT	Y2H	BioGRID3.4	Combined (no BioGRID)	Combined all
RNF41	**1**	**1**	**1**	**0**	**1**	**1**	**4**	**5**
TTC1	1	0	1	1	1	1	4	5
BIRC6	1	1	1	0	0	1	3	4
CACYBP	1	1	1	0	0	1	3	4
NAV1	1	1	1	0	0	1	3	4
KIAA1598	1	1	0	1	0	0	3	3
HOMER2	1	0	0	1	1	1	3	4
ASB6	0	1	0	1	1	1	3	4
VPS52	0	1	0	1	1	1	3	4
KDM3B	1	1	0	0	0	0	2	2
TACC1	1	1	0	0	0	0	2	2
SIPA1L3	0	1	1	0	0	0	2	2
USP8	0	1	1	0	0	1	2	3
LZTS2	0	0	1	0	1	1	2	3
AP2S1	0	0	1	1	0	0	2	2
ENOPH1	0	0	1	1	0	0	2	2
IFIT5	0	1	0	1	0	0	2	2
ARL6IP4	0	0	0	1	1	1	2	3
ISCA2	0	0	0	1	1	1	2	3
RFC4	0	0	0	1	1	1	2	3
CPVL	1	0	0	0	0	0	1	1
DIABLO	1	0	0	0	0	0	1	1
DNAJB12	1	0	0	0	0	0	1	1
FAR1	1	0	0	0	0	0	1	1
FMR1	1	0	0	0	0	0	1	1
FXR1	1	0	0	0	0	0	1	1
FXR2	1	0	0	0	0	0	1	1
HOMER1	1	0	0	0	0	0	1	1
MTCL1	1	0	0	0	0	1	1	2
RIF1	1	0	0	0	0	0	1	1
SOGA1	1	0	0	0	0	1	1	2
ZNF281	1	0	0	0	0	0	1	1
CTNNAL1	0	0	1	0	0	0	1	1
GIPC1	0	0	1	0	0	0	1	1
IGF1R	0	0	1	0	0	0	1	1
INSR	0	0	1	0	0	0	1	1
NEK2	0	0	1	0	0	0	1	1
PCMT1	0	0	1	0	0	0	1	1
AHNAK	0	1	0	0	0	0	1	1
BirA	0	1	0	0	0	0	1	1
CCP110	0	1	0	0	0	0	1	1
CD2AP	0	1	0	0	0	0	1	1
CEP97	0	1	0	0	0	0	1	1
CORO1B	0	1	0	0	0	0	1	1
CRK	0	1	0	0	0	0	1	1
FAM83H	0	1	0	0	0	0	1	1
FLNA	0	1	0	0	0	0	1	1
IFFO2	0	1	0	0	0	0	1	1
MKL2	0	1	0	0	0	0	1	1
TACC2	0	1	0	0	0	0	1	1
UTRN	0	1	0	0	0	0	1	1
VCPIP1	0	1	0	0	0	0	1	1
XRN1	0	1	0	0	0	0	1	1
ZBTB33	0	1	0	0	0	0	1	1
C1orf109	0	0	0	0	1	1	1	2
ABHD12B	0	0	0	1	0	0	1	1
AP4E1	0	0	0	1	0	0	1	1
APOC3	0	0	0	1	0	0	1	1
APOL5	0	0	0	1	0	0	1	1
ARHGAP22	0	0	0	1	0	0	1	1
ARL4C	0	0	0	1	0	0	1	1
ASIC4	0	0	0	1	0	0	1	1

ATXN7L1	0	0	0	1	0	0	1	1
BIRC8	0	0	0	1	0	0	1	1
C16orf48	0	0	0	1	0	0	1	1
C17orf50	0	0	0	1	0	0	1	1
C17orf82	0	0	0	1	0	0	1	1
C1orf49	0	0	0	1	0	0	1	1
C22orf13	0	0	0	1	0	0	1	1
C4orf17	0	0	0	1	0	0	1	1
C5orf27	0	0	0	1	0	0	1	1
C9orf43	0	0	0	1	0	0	1	1
CACNA1E	0	0	0	1	0	0	1	1
CDKL5	0	0	0	1	0	0	1	1
CLPP	0	0	0	1	0	0	1	1
COX5B	0	0	0	1	0	0	1	1
CPSF4L	0	0	0	1	0	0	1	1
CSNK1G2-AS1	0	0	0	1	0	0	1	1
CTAG1A	0	0	0	1	0	0	1	1
CTAG1B	0	0	0	1	0	0	1	1
CTNNA3	0	0	0	1	0	0	1	1
DCDC2B	0	0	0	1	0	0	1	1
DIS3L2	0	0	0	1	0	0	1	1
DPYD	0	0	0	1	0	0	1	1
DTX3	0	0	0	1	0	0	1	1
DUSP2	0	0	0	1	0	0	1	1
EDN3	0	0	0	1	0	0	1	1
EPB42	0	0	0	1	0	0	1	1
FAM110B	0	0	0	1	0	0	1	1
FAM117B	0	0	0	1	0	0	1	1
FAM129C	0	0	0	1	0	0	1	1
FAM72B	0	0	0	1	0	0	1	1
FGF11	0	0	0	1	0	0	1	1
GALNT3	0	0	0	1	0	0	1	1
GMNN	0	0	0	1	0	0	1	1
GNA11	0	0	0	1	0	0	1	1
GRB10	0	0	0	1	0	0	1	1
HELT	0	0	0	1	0	0	1	1
IGF2	0	0	0	1	0	0	1	1
IL16	0	0	0	1	0	0	1	1
KANK1	0	0	0	1	0	0	1	1
KCNAB2	0	0	0	1	0	0	1	1
KCNAB3	0	0	0	1	0	0	1	1
KCNB1	0	0	0	1	0	0	1	1
KLHL14	0	0	0	1	0	0	1	1
LATS1	0	0	0	1	0	0	1	1
LIMS1	0	0	0	1	0	0	1	1
LOC554206	0	0	0	1	0	0	1	1
LOC84989	0	0	0	1	0	0	1	1
MAB21L2	0	0	0	1	0	0	1	1
MCEE	0	0	0	1	0	0	1	1
MLF1	0	0	0	1	0	0	1	1
MLPH	0	0	0	1	0	0	1	1
MMAB	0	0	0	1	0	0	1	1
MRPS2	0	0	0	1	0	0	1	1
NAT6	0	0	0	1	0	0	1	1
NBLA00301	0	0	0	1	0	0	1	1
NCKAP5	0	0	0	1	0	0	1	1
NDFIP2	0	0	0	1	0	0	1	1
NGFRAP1	0	0	0	1	0	0	1	1
NKX6-3	0	0	0	1	0	0	1	1
NPHS2	0	0	0	1	0	0	1	1
OR1D5	0	0	0	1	0	0	1	1
PARP6	0	0	0	1	0	0	1	1
PARP8	0	0	0	1	0	0	1	1
PDLIM7	0	0	0	1	0	0	1	1
PDPN	0	0	0	1	0	0	1	1
PHF19	0	0	0	1	0	0	1	1
PIK3R2	0	0	0	1	0	0	1	1

159

PLEKHA2	0	0	0	1	0	0	1	1
PLEKHA6	0	0	0	1	0	0	1	1
POLR3D	0	0	0	1	0	0	1	1
POP7	0	0	0	1	0	0	1	1
PRIM1	0	0	0	1	0	0	1	1
PRR25	0	0	0	1	0	0	1	1
PRRT1	0	0	0	1	0	0	1	1
PTPDC1	0	0	0	1	0	0	1	1
RAB31	0	0	0	1	0	0	1	1
RNF146	0	0	0	1	0	0	1	1
RRAGC	0	0	0	1	0	0	1	1
RSPO4	0	0	0	1	0	0	1	1
RUSC1	0	0	0	1	0	0	1	1
SENP1	0	0	0	1	0	0	1	1
SH2D2A	0	0	0	1	0	0	1	1
SKOR1	0	0	0	1	0	0	1	1
SLX1A	0	0	0	1	0	0	1	1
SMOC1	0	0	0	1	0	0	1	1
SNAPC3	0	0	0	1	0	0	1	1
SNRK	0	0	0	1	0	0	1	1
SNX29	0	0	0	1	0	0	1	1
SPATA22	0	0	0	1	0	0	1	1
SPDYC	0	0	0	1	0	0	1	1
SRR	0	0	0	1	0	0	1	1
SSX4	0	0	0	1	0	0	1	1
STAC	0	0	0	1	0	0	1	1
STC2	0	0	0	1	0	0	1	1
TCF15	0	0	0	1	0	0	1	1
TCTEX1D4	0	0	0	1	0	0	1	1
TMEM208	0	0	0	1	0	0	1	1
TMEM74	0	0	0	1	0	0	1	1
TMUB2	0	0	0	1	0	0	1	1
TRIM69	0	0	0	1	0	0	1	1
TROAP	0	0	0	1	0	0	1	1
TRPV6	0	0	0	1	0	0	1	1
USP48	0	0	0	1	0	0	1	1
VPS4A	0	0	0	1	0	0	1	1
WDFY3	0	0	0	1	0	0	1	1
WDR59	0	0	0	1	0	0	1	1
WWC3	0	0	0	1	0	0	1	1
XKR4	0	0	0	1	0	0	1	1
ZAR1L	0	0	0	1	0	0	1	1
ZBTB44	0	0	0	1	0	0	1	1
ZNF576	0	0	0	1	0	0	1	1
ZNRF2	0	0	0	1	0	0	1	1
ZSCAN1	0	0	0	1	0	0	1	1
ADRB2	0	0	0	0	0	1	0	1
APP	0	0	0	0	0	1	0	1
C1GALT1C1	0	0	0	0	0	1	0	1
CD247	0	0	0	0	0	1	0	1
CEP192	0	0	0	0	0	1	0	1
CLASP1	0	0	0	0	0	1	0	1
CLEC16A	0	0	0	0	0	1	0	1
CREB3	0	0	0	0	0	1	0	1
ELAVL1	0	0	0	0	0	1	0	1
ERBB3	0	0	0	0	0	1	0	1
ERBB4	0	0	0	0	0	1	0	1
EVI5	0	0	0	0	0	1	0	1
H3F3A	0	0	0	0	0	1	0	1
IL23A	0	0	0	0	0	1	0	1
ITSN2	0	0	0	0	0	1	0	1
KIFC3	0	0	0	0	0	1	0	1
LEPR	0	0	0	0	0	1	0	1
LPGAT1	0	0	0	0	0	1	0	1
MARK2	0	0	0	0	0	1	0	1
MARK4	0	0	0	0	0	1	0	1
MNAT1	0	0	0	0	0	1	0	1

N4BP3	0	0	0	0	0	1	0	1
NPAT	0	0	0	0	0	1	0	1
Osgep	0	0	0	0	0	1	0	1
P4HA1	0	0	0	0	0	1	0	1
PARK2	0	0	0	0	0	1	0	1
RASIP1	0	0	0	0	0	1	0	1
RCN1	0	0	0	0	0	1	0	1
RFWD3	0	0	0	0	0	1	0	1
RNF166	0	0	0	0	0	1	0	1
SF1	0	0	0	0	0	1	0	1
SUGT1	0	0	0	0	0	1	0	1
TADA2A	0	0	0	0	0	1	0	1
TRIM32	0	0	0	0	0	1	0	1
TRIM8	0	0	0	0	0	1	0	1
TSG101	0	0	0	0	0	1	0	1
UBASH3A	0	0	0	0	0	1	0	1
UBASH3B	0	0	0	0	0	1	0	1
UBE2D3	0	0	0	0	0	1	0	1
UBE2K	0	0	0	0	0	1	0	1
UBE2U	0	0	0	0	0	1	0	1
UBE2Z	0	0	0	0	0	1	0	1
UPF3A	0	0	0	0	0	1	0	1
ZAP70	0	0	0	0	0	1	0	1

The role of RNF41 in selective autophagy

We and others have previously reported a vesicular pattern for overexpressed RNF41 (RING finger protein 41) in different cell types such as HeLa, COS, MDA-MB-468 and NIH/3T3 cells (De Ceuninck et al., 2013; Masschaele et al., 2017; Diamonti et al., 2002; Qiu et al., 2002; Qiu et al., 2004). In this paper we attempt to characterize these RNF41 bodies and find that they colocalize with p62, an autophagy receptor. Moreover, silencing of RNF41 decreases endogenous p62 and LC3B-II. RNF41 depletion also results in decreased phosphorylated TBK1, which is necessary for the increased affinity between p62 and ubiquitinated autophagic cargo. Furthermore, RNF41 interacted with autophagy related proteins Beclin1, ATG14, WIPI2 and ATG5 that are involved in autophagosome formation. All together, this points towards a role for RNF41 in the early steps of autophagosome biogenesis which leads to the selective autophagy pathway aggrephagy. This new established link between RNF41 and autophagy further elucidates the role of RNF41 in intracellular trafficking, as autophagy shares several components of the molecular machinery involved in intracellular trafficking pathways.

The role of RNF41 in selective autophagy

Delphine Masschaele[1,2], Leentje De Ceuninck[1,2], Joris Wauman[1,2] and Jan Tavernier[1,2*]

[1]Cytokine Receptor Laboratory, Department of Biochemistry, Faculty of Medicine and Health Sciences, Ghent University, Ghent, Belgium
[2]VIB Medical Biotechnology Center, VIB, Ghent, Belgium
* Corresponding author
Email: jan.tavernier@vib-ugent.be

Abstract

RNF41 is an E3 ubiquitin ligase involved in the ubiquitination of several substrates. As such it is implicated in intracellular trafficking, yet its role is not fully elucidated. To further unravel its function we aimed to characterize the RNF41 bodies observed with confocal microscopy by using various organelle and aggregate markers. This paper describes the colocalization between RNF41 and p62, an autophagy receptor. RNF41 depletion revealed a role for RNF41 in maintaining p62 and phosphorylated TBK1 levels. This, in combination with the novel detected interactions between RNF41 and Beclin1, ATG14, WIPI2 and ATG5, suggests that RNF41 functions in autophagosome biogenesis leading to the aggrephagy pathway.

Introduction

Autophagy is a multistep process initiating with the formation of an isolation membrane that expands and sequesters a portion of the cytoplasm and eventually generates a double-membraned vesicle called the autophagosome. This autophagosome subsequently fuses with the lysosome resulting in the degradation of the cytoplasmic cargo [1]. Autophagosome biogenesis is regulated by the hierarchical action of four protein complexes all containing ATG (autophagy-related genes) proteins. Initiation of the isolation membrane requires the ULK kinase complex composed of ULK1/2, ATG13, FIP200 and ATG101 which is inhibited by the amino acid sensor mTORC1 (mammalian target of rapamycin complex 1) under nutrient-rich conditions but activated upon starvation. This is followed by membrane nucleation, which depends on the class III PI3K complex I, consisting of Beclin1, VPS34, VPS15 and ATG14. Finally, two ubiquitin-like conjugation systems, ATG5-ATG12-ATG16 and LC3 (or ATG8) coordinate the elongation and closure of the autophagosome [2]. Autophagy was generally thought to be a non-selective, bulk degradation process, however, increasing evidence illustrates that this can also be a highly selective process that mediates the clearance of specific cargo such as aggregated proteins (aggrephagy), mitochondria (mitophagy), ribosomes (ribophagy) and pathogens (xenophagy) [3]. This selectivity is achieved through autophagy receptors such as p62 (or SQSTM1 (sequestosome-1)), NBR1 (Neighbor of BRCA gene 1), NDP52 (nuclear dot protein 52 kDa) and OPTN (optineurin), which all contain ubiquitin binding domains and LC3-interacting regions necessary for recognizing cargo and autophagosomal membrane, respectively [3].

The multifunctional protein p62 was the first discovered mammalian autophagy receptor [4]. It encompasses multiple domains which contribute to its versatile function by interacting with various binding partners involved in autophagy and in signaling pathways that regulate antioxidant response,

inflammation and metabolism. p62 contains an N-terminal PB1 (Phox-BEM1) domain that is responsible for self-oligomerisation and also interacts with aPKC and ERK1. This is followed by a ZZ-type zinc finger domain and a TBD (TRAF6-binding domain) domain which respectively interact with RIP1 and TRAF6 to regulate the NFκB pathway. p62 also contains two NLS (nuclear localization signals), one located in between the zinc finger and TBD and the other located after the TBD, and a NES (nuclear export signal). The p62 C-terminus holds the LIR (LC3-interacting region) and UBA (ubiquitin-associated domain) domain that mediate the interaction between the autophagic machinery and the ubiquitinated autophagic cargo ultimately resulting in autophagic clearance. The affinity of this UBA domain for ubiquitinated substrates is greatly enhanced by CK2 (casein kinase 2) and TBK1 (TANK-binding kinase 1)-mediated Ser403 phosphorylation [5–7]. Finally, a KIR (Keap1-interacting region) domain, located in between the LIR and UBA domain interacts with Keap1, a Cullin3-ubiquitin E3 ligase complex adaptor protein. This interaction results in the release of transcription factor Nrf2 resulting in an antioxidant response [8–10].

In this paper we demonstrate for the first time a role for RNF41 (RING finger protein 41) in autophagy. RNF41 is an E3 ubiquitin ligase that mediates the ubiquitination and degradation of several interaction partners such as the inhibitor of apoptosis BRUCE, parkin, a protein involved in Parkinson's disease, and the ERBB3, IL-3 (interleukin-3) and EPO (erythropoietin) receptors [11–14]. RNF41 hereby reduces the signaling of the IL-3R and EPOR, and attenuates the signaling of other JAK2-associated type I cytokine receptors including the LR (leptin receptor), LIFR (Leukaemia inhibitory factor receptor) and IL-6R (interleukin-6 receptor) [15,16]. RNF41 is also implicated in intracellular transport where it modulates the trafficking of the LR, LIFR and IL-6R [15]. This is accomplished by ubiquitinating and suppressing the deubiquitinase USP8, thereby indirectly destabilizing the ESCRT-0 complex, a complex required for proper internalization of cargo into multivesicular bodies leading to the degradation pathway. In this way, RNF41 inhibits receptors from undergoing lysosomal degradation and subsequently reroutes them towards compartments for ectodomain shedding [17]. Moreover, RNF41 also relocalizes VPS52, a subunit of two distinct tethering complexes that are involved in the sorting of cargo to the Golgi network or recycling endosomes [18]. This study describes the colocalization between p62 and RNF41 and reveals the involvement of RNF41 in maintaining p62 levels. This links RNF41 to autophagy, which further clarifies the role of RNF41 in intracellular trafficking since autophagy is considered to share many features with membrane trafficking pathways, including budding of vesicles, movement along microtubule tracks and tethering and fusion with late endosomes and lysosomes. Interactions between RNF41 and several autophagy-related proteins including Beclin1, ATG14, WIPI2 and ATG5, together with the effect of RNF41 on phosphorylated TBK1 imply that RNF41 functions in autophagosome formation.

Results

RNF41 bodies colocalize with autophagy receptor p62 but not with lysosome or autophagosome markers

We and others previously reported a vesicular pattern for overexpressed RNF41 in several cell lines such as COS cells, MDA-MB-468 cells, NIH/3T3 and HeLa cells [11,13,17–19]. A potential myristoylation site, marked by the Met-Gly sequence at the N-terminus of RNF41 can account for membrane anchoring and thus explain its vesicular localization [13]. However, experimental evidence

for this membrane attachment is currently missing and it is still not clear whether these RNF41 bodies represent vesicles or aggregates. Therefore, we set out to characterize these RNF41 bodies by testing a number of known organelle and aggregate markers. Although we could not detect colocalization between ectopically expressed RNF41 and well known early and late endosomal makers, we did observe a clear colocalization with p62, an autophagy receptor for cargo material such as aggregated proteins (Fig 1A). Since p62 plays an important role in autophagy, we additionally tested LC3B, a well-established autophagy marker and the lysosome marker LAMP1. We did not detect any colocalization between these markers and the RNF41 bodies that co-stained with p62, implying that the RNF41 bodies are not closed autophagosomes or autolysosomes (Fig 1B).
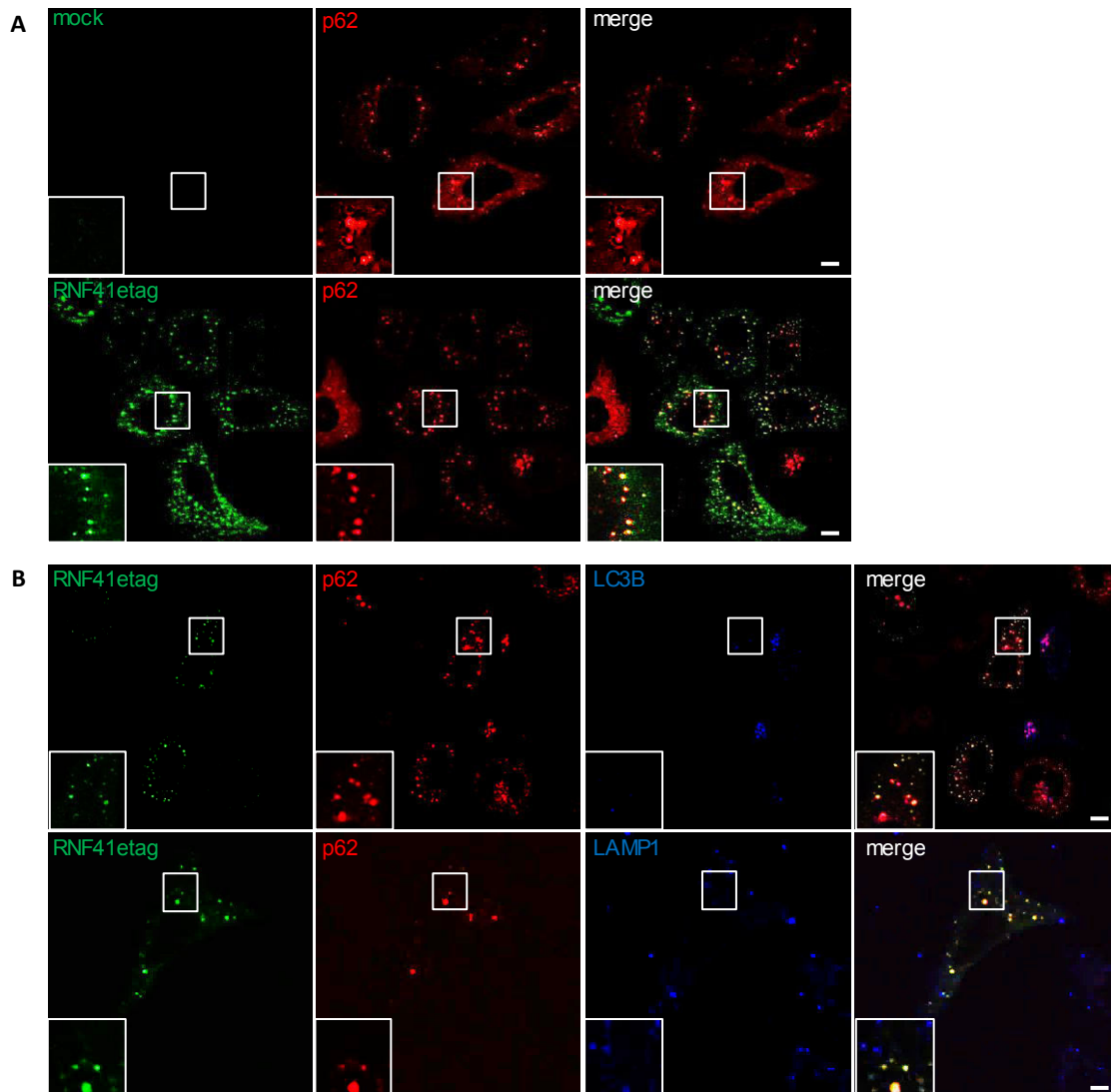
Figure 1. HeLa cells transiently transfected with a vector encoding E-tagged RNF41 or soluble IL5Rα (mock) were fixed and stained with anti-Etag (secondary Alexa Fluor 488, green) and anti-p62 (secondary Alexa Fluor 568, red) **(A)**, and co-stained with anti-LAMP1 (secondary Alexa Fluor 647, blue) or anti-LC3B (secondary Alexa Fluor 647, blue) **(B)**. The insets show a magnification of the boxed area. Scale bar, 10µm. n=3 for all experiments.

RNF41 depletion decreases p62 and LC3B-II

Since RNF41 colocalizes with p62, it is easily presumed that these RNF41 bodies represent aggregates that are eventually cleared by aggrephagy. However, the observed effects of RNF41 on this autophagy receptor indicate a functional role for RNF41 in the clearance of aggregates. Ectopic expression of RNF41 did not affect p62 levels, whereas RNF41 even partial silencing clearly decreases p62. Likewise, partial depletion of RNF41 also decreases the lipidated form of LC3B, LC3B-II, while ectopic RNF41 expression enhances LC3B-II (Fig 2A). We next investigated whether induced autophagy, and thus lysosomal degradation is responsible for the reduced p62 and LC3B-II levels upon RNF41 depletion. Incubating HeLa cells with the vacuolar ATPase inhibitor Bafilomycin A1 that blocks autophagosome turnover at the lysosome does not result in an accumulation of p62 and LC3B-II. Conversely, the siNT control condition shows a clear accumulation of LC3B-II upon Bafilomycin A1 treatment (Fig 2B). This suggests that the decrease in p62 and LC3B-II upon RNF41 depletion is not a consequence of enhanced autophagy and that RNF41 is important for maintaining p62 and LC3B-II levels. To determine whether silencing of RNF41 possibly blocks the induction of autophagy we attempted to promote autophagy using rapamycin. Under normal circumstances, this should result in enhanced LC3B-II and decreased p62 levels. Unfortunately, we were not able to reproduce these effects and thus could not further investigate this hypothesis (Fig 2B). It is worth mentioning that silencing of p62 did not affect the levels of RNF41 (Suppl Fig 1).
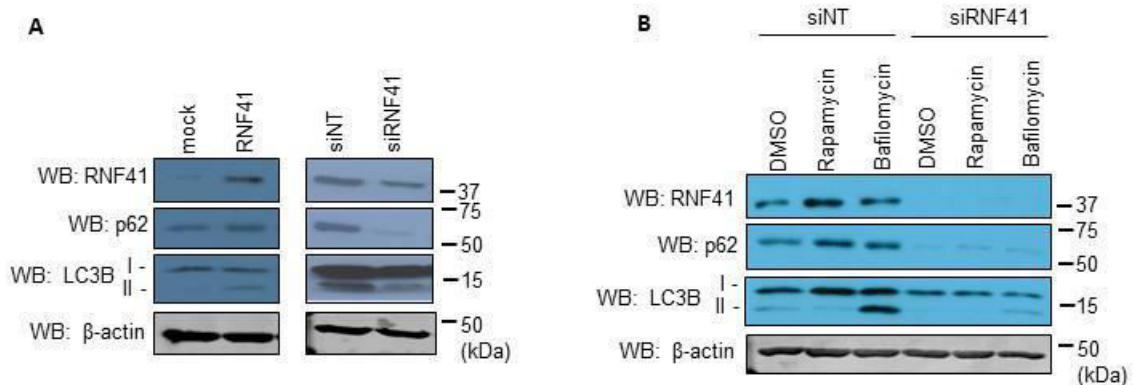
Figure 2: **(A)** HeLa cells were transiently co-transfected with a plasmid encoding RNF41 or soluble IL5Rα (mock), or were silenced (96h) for RNF41 or treated with a non-targeting siRNA (siNT). The protein levels of RNF41, p62 and LC3B were determined by Western Blotting using anti-RNF41, anti-p62, anti-LC3B or anti-β-actin (loading control) antibodies. n=3. **(B)** HeLa cells were silenced (96h) for RNF41 or treated with siNT and incubated for 2 hours with 200nM of DMSO, Rapamycin or Bafilomycin A1 prior to sonication. Protein levels were analyzed by Western Blotting using antibodies against RNF41, p62, LC3B or β-actin (loading control). n=3.

RNF41 interacts with several autophagy-related proteins

The previous results implicate that RNF41 plays a role in the early steps of autophagy, therefore, we investigated whether RNF41 interacted with other well known ATGs and ATG-related proteins. For this we performed binary MAPPIT (Mammalian Protein-Protein Interaction Trap), an in-house developed technology to detect protein-protein interactions in intact mammalian cells [20]. We first wanted to establish the interaction between RNF41 and p62 since we detect a clear colocalization between these two proteins (Fig 1A). Next to this, we also wanted to verify the known interaction between TBK1 and RNF41, described by Wang et al., as TBK1 is known to cofractionate and colocalize

with p62 and is thereby involved in autophagy [6,21]. Surprisingly, RNF41 bait did not interact with TBK1 prey, nor with p62 prey (Fig 3). Co-immunoprecipitation analysis confirmed these results and also failed to show an interaction between RNF41 and TBK1 or p62 (Suppl Fig 2). We could also not detect an interaction between RNF41 and RPTOR (Regulatory-associated protein of mTOR), a substrate binding subunit of mTORC1 and its downstream effector, ULK1 [22,23]. However, RNF41 clearly interacted with Beclin1 and ATG14, two members of the class III PI3K complex I, and with its effector protein WIPI2. Next to this, RNF41 also interacted with the ATG5 subunit of the ATG5-ATG12-ATG16 ubiquitin-like conjugation system. No clear interaction was observed between RNF41 and the other ubiquitin-like conjugation system, LC3B nor with ATG3, a protein necessary for LC3 lipidation (Fig 3; [2]). These results suggest that RNF41 is implicated in autophagosome formation, since it interacts with various proteins involved in this process.
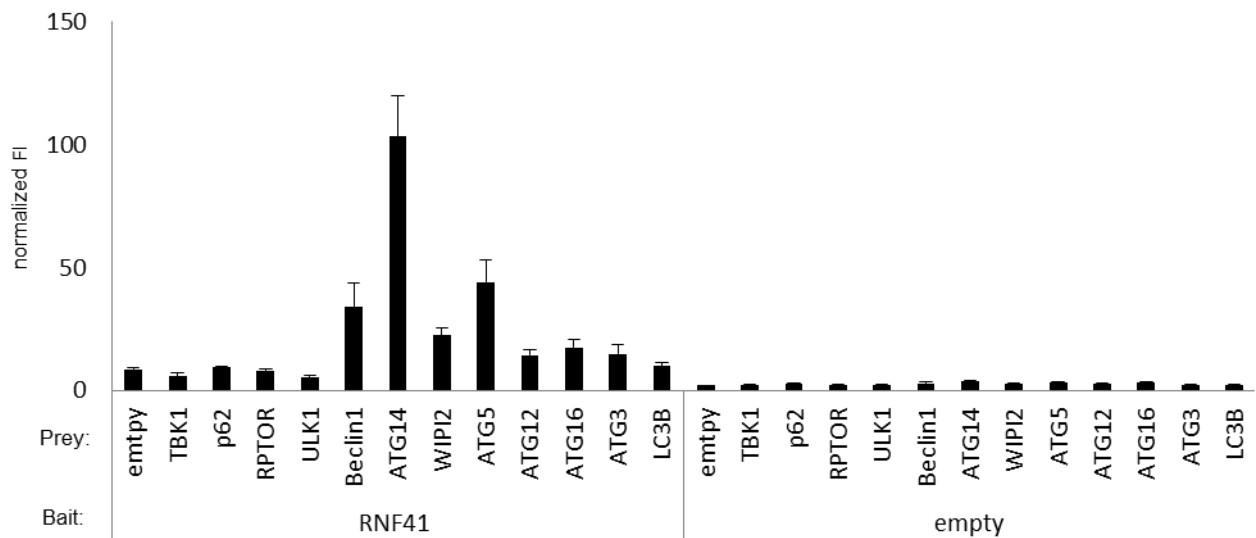
Figure 3: MAPPIT analysis of HEK293T cells transiently co-transfected with plasmids encoding several autophagy-related prey proteins together with an empty or RNF41 bait and the pXP2d2-rPAP1-luciferase reporter plasmid. The next day, cells were stimulated with Epo or left untreated for 24 hours. The luciferase signal is expressed as fold induction (stimulated/non stimulated), relative to the signal of a control JAK2 binding prey ± s.d. of triplicate measurements. n=3.

RNF41 contributes to TBK1 phosphorylation

Although we could not confirm the interaction between TBK1 and RNF41 (Fig 3), we did further investigate the functional link between RNF41 and TBK1. TBK1 is activated by phosphorylation of Ser172 and in turn phosphorylates the UBA domain of p62 thereby strengthening the p62-polyubiquitin interaction [5–7,24]. Via confocal microscopy we were able to confirm the colocalization between activated, and thus phosphorylated, TBK1 and p62 in HeLa cells. Moreover, we also detected colocalization between the RNF41 bodies and these p62 and p-S172 TBK1 positive structures (Fig 4A). Additionally, next to reducing p62 and LC3B levels, silencing of RNF41 also decreased the levels of phosphorylated TBK1, but did not influence the total amount of TBK1 (Fig 4B). This suggests that RNF41 contributes to TBK1 phosphorylation. Furthermore, silencing of RNF41 also strongly decreased the levels of ARF6, a small GTPase that was shown to promote autophagosome formation independent of mTORC activation (Fig 4B; [25]). All together, these findings further argue for a role of RNF41 in autophagosome biogenesis.
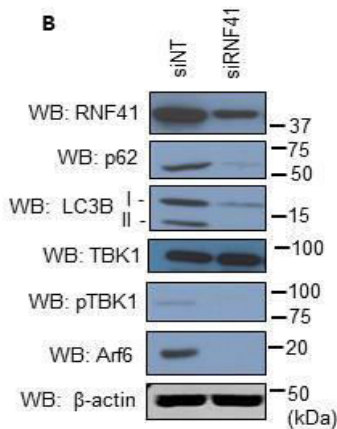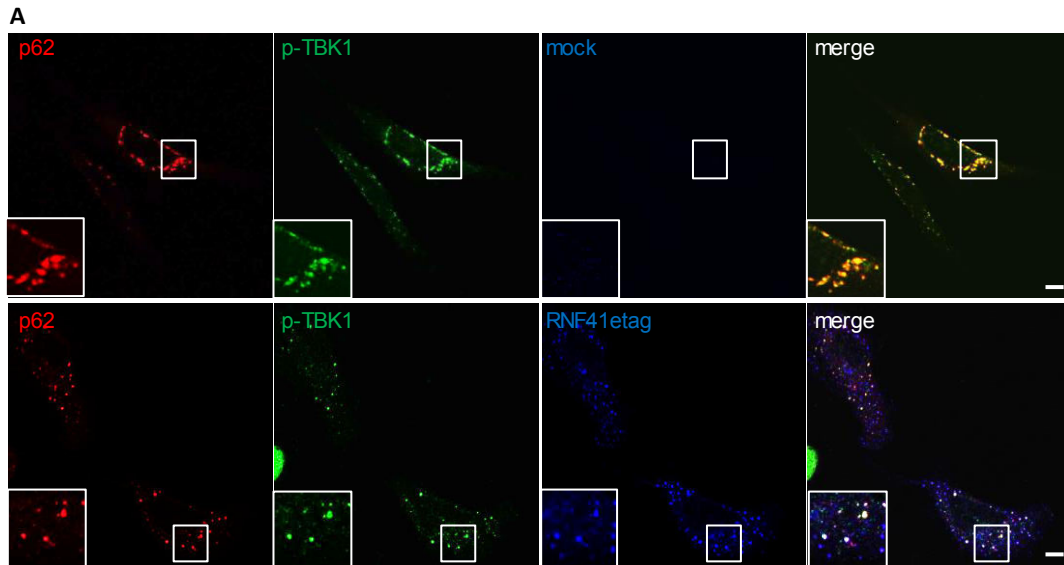
Figure 4: **(A)** HeLa cells transiently transfected with a vector encoding E-tagged RNF41 or soluble IL5Rα (mock) were fixed and stained with anti-Etag (secondary Alexa Fluor 647, blue), anti-p62 (secondary Alexa Fluor 568, red) and anti-pS172-TBK1 (secondary Alexa Fluor 488, green). The insets show a magnification of the boxed area. Scale bar, 10μm. n=2. **(B)** HeLa cells were silenced (96h) for RNF41 or treated with siNT. Protein levels were analyzed by Western Blotting using antibodies against RNF41, p62, LC3B, TBK1, p-TBK1, ARF6 or β-actin (loading control). n=3.

Discussion

The vesicular pattern of ectopically expressed RNF41 prompted us to further characterize these structures using several organelle and aggregate markers. Most interestingly, p62, an autophagic cargo receptor colocalized with these RNF41-bodies (Fig 1A). Moreover, transient silencing of RNF41 decreased endogenous p62 and the lipidated form of LC3B, LC3B-II (Fig 2A). This is not due to an increase of autophagic flux, but rather indicates a defect or delay earlier in the process, prior to autolysosomal degradation since treatment of the RNF41-depleted cells with the lysosome acidification inhibitor Bafilomycin A1 did not result in an accumulation of p62 or LC3B-II (Fig 2B). Additionally, RNF41 failed to colocalize with LC3B or LAMP1 (Fig 1B), which points to a role for RNF41 in autophagy, likely in the early stages at the isolation membrane, where p62 sequesters ubiquitinated cargo into aggregates prior to recruitment of LC3B and formation of the autophagosomes. In support of this, Bjørkøy, et al., described two populations of p62 bodies in the cytosol, where a first population appeared as large protein aggregates, called sequestrosomes, that were resistant to detergent extraction and did not colocalize with Lysotracker whereas another lysotracker-positive p62 population represented detergent dissolvable membrane-enclosed

autophagsomes [26]. Our previous studies also detected ectopically expressed RNF41 in the insoluble pellet fraction of RIPA-lysed cells, which suggests that the RNF41 bodies are, like sequestrosomes, detergent resistant [17,18]. More evidence for the involvement of RNF41 in autophagosome formation emerged from interaction studies with MAPPIT. Here, RNF41 interacted with Beclin1 and ATG14, two components of the class III PI3K complex I involved in isolation membrane nucleation (Fig 3). This complex, consisting of Beclin1, VPS34, VPS15 and ATG14 generates PI(3)P (phosphatidylinositol (3)-phosphate) on the surface of the isolation membrane, which results in the recruitment of WIPI2 [27,28]. WIPI2 also interacted with RNF41, and this protein targets the first ubiquitin-like conjugating complex ATG5-ATG12-ATG16 to the PI(3)P enriched isolation membrane, which is necessary for isolation membrane elongation (Fig 3; [29]). Additionally, MAPPIT also showed an interaction between RNF41 and the ATG5 subunit of this conjugating complex, but not with the second ubiquitin-like conjugation system that mediates the lipidation of LC3B. Even though these interactions could be indirect, this further implies that the action of RNF41 is situated somewhere at the isolation membrane, between the nucleation and elongation process and is consistent with the fact that p62 also localizes to this isolation membrane, independent of LC3B ([30], Fig 5)

TBK1 is an essential regulator of the innate immune response against pathogens and also plays a role in the selective autophagy pathways xenophagy, mitophagy and aggrephagy by phosphorylating autophagy receptors OPTN and p62 [6,7,31,32]. Moreover, Wang et al described the interaction between RNF41 and TBK1, where RNF41 leads to K63-linked polyubiquitination of TBK1 [21]. We assumed that TBK1 would be an ideal candidate to further establish the role of RNF41 in autophagy since TBK1, similarly to our observations for RNF41, colocalizes with p62 ([6]; Fig 1A). Despite the lack of interaction between RNF41 and TBK1 in MAPPIT and Co-IP (Fig 3 and Suppl Fig 2), we indeed noticed colocalisation between phosphorylated TBK1 and RNF41 (Fig 4A). It is described in literature that K63-linked polyubiquitination of TBK1 is required for Ser172 phosphorylation resulting in its activation [33]. As RNF41 is one of the E3 ligases involved in TBK1 K63-linked polyubiquitination, it is therefore plausible that RNF41 is required for this activation of TBK1. Indeed, RNF41 depletion resulted in a decrease of phosphorylated, and thus activated, TBK1 (Fig 4B). Since activated TBK1 phosphorylates the UBA domain of p62 and thereby increases the binding affinity of p62 for ubiquitin chains on autophagic cargo [5], it is possible that RNF41 in this way regulates p62 recruitment to autophagic cargo. On the other hand, we cannot exclude the possibility that RNF41 directly ubiquitinates autophagic cargo, and as such mediates the binding of p62 to these cargo. Further evidence for a role of RNF41 in the early stages of autophagosome biogenesis emanates from the effect of RNF41 on ARF6. Figure 4B showed that RNF41 depletion also decreased the levels of ARF6, a small GTPase that modulates autophagosome formation by influencing membrane delivery to the autophagosome formation site via the production of PI(4,5)P2 (phosphatidylinositol 4,5-bisphosphate), and by regulating phospholipase D activity independent of mTORC [25].
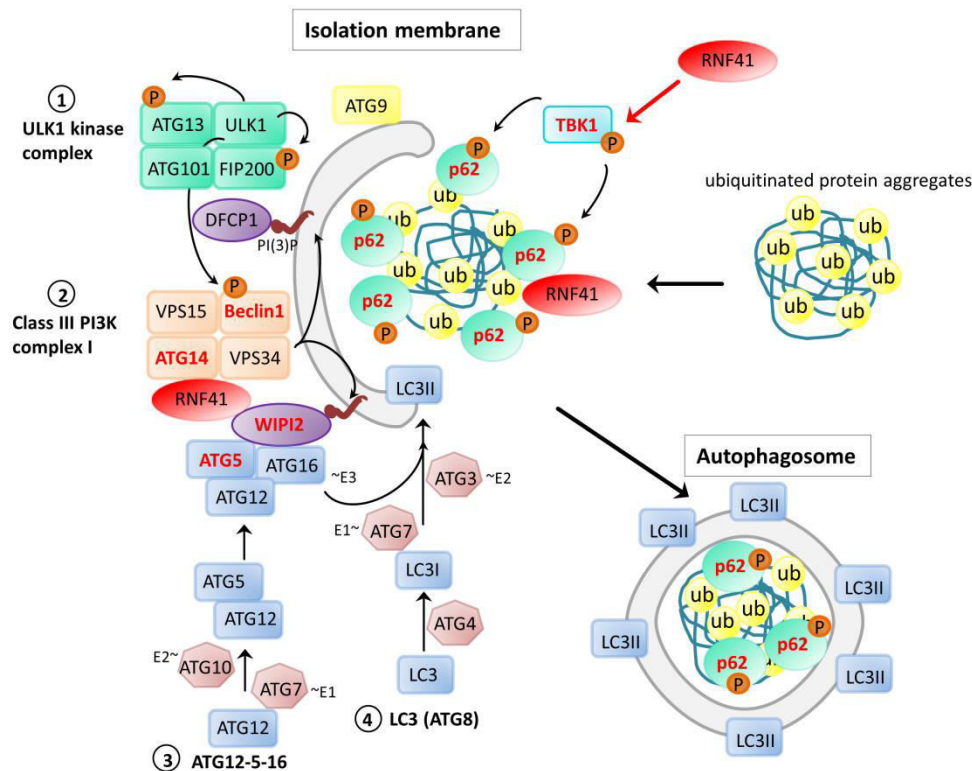
Figure 5. Overview of RNF41 implicated in autophagosome formation. Autophagosome formation is initiated by (1) the ULK1 kinase complex (ULK1, ATG13, FIP200, ATG101) and (2) the Class III PI3K complex I (Beclin1, VPS34, VPS15, ATG14) which are recruited to the isolation membrane. (3) The ATG12-ATG5-ATG16 complex and (4) LC3-II are formed via an ubiquitin-like conjugation system and are subsequently recruited to the isolation membrane where they play a role in the elongation process. Our results suggest that RNF41 interacts with Beclin1 and ATG14 of the Class III PI3K complex I, its effector WIPI2, and with ATG5 of the first ubiquitin-like conjugation complex, prior to LC3 recruitment. Next to this, phosphorylated and activated TBK1 in turn phosphorylates p62, which is recruited to and binds ubiquitinated protein aggregates and is targeted to the isolation membrane. Our results indicate that RNF41 is required for phosphorylated TBK1 and in this way maintains p62 levels. Proteins that interact with RNF41 or are regulated by RNF41 are indicated in red.

Although p62 depletion shows little effect on autophagy due to the presence of other autophagy receptors such as NBR1, NDP52 and OPTN [34,35], p62 is critical for aggregation of ubiquitinated proteins and thereby has a protective effect on cell survival [36,37]. Also, dysfunctional p62 resulting in impaired aggrephagy is involved in many neurodegenerative diseases such as ALS (amyotrophic lateral sclerosis), frontotemporal dementia and huntington's disease and also causes Paget disease, a bone disorder [26,38]. Therefore it is imperative to determine proteins involved in the regulation or dysregulation of p62, such as RNF41. At this time, it is still unclear why silencing of RNF41, even with only partial knockdown efficiencies, results in decreased endogenous p62 (Fig 2A). We hypothesize that silencing of RNF41 inhibits TBK1 activation and thereby the phosphorylation of p62, which in turn could possibly enhance the turnover of p62 by proteasomal degradation. Indeed, next to autophagic degradation, p62 also undergoes proteasomal degradation [39]. Here, the E3 ligase

parkin ubiquitinates p62 and is in this way responsible for its proteasomal degradation. The authors also suggest that mutated parkin or impaired E3 ligase activity of parkin could possibly result in an increase in the level of p62. Since RNF41 is known to degrade parkin [12], silencing of RNF41 should stabilize parkin and thus decrease the levels of p62, which would be in concordance with our observations. Experiments using the proteasomal inhibitor MG132 should help clarifing this hypothesis (Fig 6).
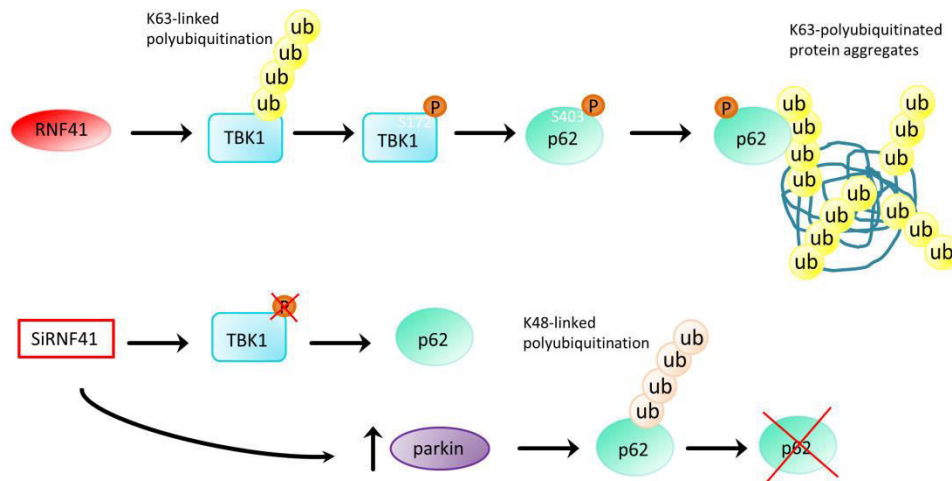
Figure 6. Hypothesis of RNF41 function. RNF41 is involved in K63-linked polyubiquitination of TBK1. This type of ubiquitination is necessary for phosphorylation of Ser172 in TBK1, which leads to TBK1 activation. Phosphorylated and activated TBK1 can phosphorylate Ser403 in p62, resulting in an increased binding affinity for K63-linked polyubiquitinated chains on autophagic cargo. Silencing of RNF41 inhibits TBK1 phosphorylation and activation, thus resulting in decreased levels of phosphorylated p62. Silencing of RNF41 also inhibits the degradation of parkin, which can lead to parkin-mediated K48-linked polyubiquitination of p62, resulting in its proteasomal degradation, which would explain the loss of p62.

Parkin and USP8, another RNF41 interacting protein, were shown to be involved in the selective autophagic pathway mitophagy. Parkin is recruited to the depolarized mitochondria and activated by PINK1 (PTEN-induced putative kinase protein 1) [40]. This recruitment also depends on the deubiquitinating enzyme USP8, which removes non-canonical K6-linked ubiquitin chains from parkin [41]. Activated parkin results in the K63-linked polyubiquitination of outer mitochondrial membrane proteins, which are recognized and clustered by p62 and destined for mitophagy [42]. Although these RNF41 interaction partners are involved in mitophagy, we did not observe colocalization between our RNF41 bodies that co-stained with p62 and mitochondria (Suppl Fig 3). CCCP (carbonyl cyanide m-chlorophenylhydrazone) treatment which severely reduces the mitochondrial membrane potential and generally induces parkin recruitment to depolarized mitochondria also failed to show colocalization between RNF41 and mitochondria (Suppl Fig 3; [40]). Moreover, Durcan et al. described that the USP8 effect on mitophagy was not associated with its function in the ESCRT pathway, further suggesting that the RNF41-USP8 interaction only acts at the latter stage, and probably not affects mitophagy [41]. Instead, we argue for a role of RNF41 in aggrephagy. In this selective autophagic pathway, misfolded and aggregated proteins are polyubiquitinated (K63-linked) and selectively recognized by HDAC6 (histone deacetylase 6). HDAC6 links the polyubiquitinated cargo to dynein which results in delivery towards the microtubule organizing center to form the aggresome. Here, the K63-linked polyubiquitin chains are recognized by p62 or by other autophagic receptors which recruit further autophagic machinery and subsequently lead to autophagic clearance

172

[43]. HDAC6 was also identified as an RNF41 interaction partner in an arrayMAPPIT screen performed in our lab, where the RNF41 bait was tested against a large collection of about 8500 preys derived from the human ORFeome collection (data not shown). Furthermore, parkin was also found to be a key regulator of aggrephagy, by mediating K63-linked polyubiquitination of misfolded proteins when proteasomal degradation is impaired. This promotes the recruitment p62 and further autophagic machinery leading to autophagic clearance [44]. We observed sequestering of parkin by RNF41 suggesting that RNF41 can also be recruited to the aggregated proteins by its interaction with parkin and as such function in the aggrephagy pathway (Suppl Fig 4). Expression of mutant huntingtin results in the upregulation of p62, which protects the cell from toxicity by linking these ubiquitinated polyglutamine protein aggregates to the autophagic machinery [26,45]. This could be used to evaluate whether RNF41 indeed plays a role in aggrephagy, as silencing of RNF41 should result in an accumulation of these mutant huntingtin aggregates.

In conclusion, we detect colocalization between RNF41 and p62, and observe that RNF41 is necessary for maintaining p62 and phosphorylated TBK1 levels. Interactions between RNF41 and autophagy-related proteins Beclin1, ATG14, WIPI2 and ATG5 further suggest that RNF41 is implicated in autophagosome formation leading to the selective autophagy pathway aggrephagy.

Materials and methods

Constructs
The pXP2d2-rPAP1-luficerase reporter and pMet7-RNF41-Etag vector were previously described [15], as were the pSEL-RNF41 bait, pSEL-emtpy, pMG1-emtpy, pMG1-Rem2, pMet7-RNF41, and pMet7-sIL-5Rα vectors [17]. pMG1-p62, pMG1-TBK1, pMG1-RPTOR, pMG1-LC3B, pMG1-Beclin1, pMG1-ULK1, pMG1-ATG16, pMG1-ATG5, pMG1-ATG12, pMG1-ATG3, pMG1-ATG14 and pMG1-WIPI2 were generated via an LR reaction (Invitrogen) to transfer the genes from a Gateway entry clone of the human ORFeome v5.1 collection to a previously described pMG1 destination vector [46]. All constructs were verified by DNA sequence analysis.

Confocal microscopy
1.5×10^4 HeLa cells (www.atcc.org, mycoplasma negative) were seeded on μ-Slide 8 well plates (Ibidi), coated with poly-L-lysine (Sigma-Aldrich). The next day, cells were transfected with 10 ng of construct using JetPrime (Polyplus). 24 hours later, cells were rinsed with PBS and fixed for 15 minutes at room temperature in 4% paraformaldehyde. Cells were washed with 100mM phosphate buffer (100 mM Na_2HPO_4; 100 mM NaH_2PO_4, pH 7.4), permeabilized and blocked in blocking buffer (20 mM phosphate buffer; 100 mM NaCl; 0.23% Triton X-100 and 10% donkey serum) for 30 minutes. Samples were incubated for 1.5 hours at room temperature with goat anti-Etag (1:2000, Bethyl), mouse anti-p62 (1:200, BD Bioscience), rat anti-LAMP (1:500, Abcam), rabbit anti-LC3B (1:1000, MBL international) or rabbit anti-p-TBK1 (1:120, Cell Signaling). After washing in blocking buffer without donkey serum, cells were incubated for 1 hour at room temperature with donkey anti-goat Alexa Fluor 488 or 647, donkey anti-mouse Alexa Fluor 568, donkey anti-rat Alexa Fluor 647 or donkey anti-rabbit Alexa Fluor 647 or 488 (1:1000, Molecular Probes). Images were acquired using a 60x 1.35 NA objective on an Olympus IX-81 laser scanning confocal microscope and analyzed using Image J software.

Western Blot analysis

2×10^5 HeLa cells were seeded in a 12-well plate and transfected with 1µg of pMet7-sIL-5Rα or pMet7-RNF41. After 48h, cells were lysed in 2x SDS gel laemmli buffer (62.5 mM Tris-HCl pH 6.8, 3% SDS, 10% glycerol, 5% β-mercaptoethanol and 0.01% Bromophenol Blue sodium salt) and sonicated using the Bioruptor Plus (Diagenode). For silencing, 2×10^5 HeLa cells in a 6-well plate were reverse transfected with 50 nM siRNA using Dharmafect 1 (Dharmacon). Transient knockdown was accomplished using RNF41 siRNA (D-006922-02-0020, Dharmacon) and non-targeting siRNA (D-001810-10-0020, Dharmacon). After 48h, cells were detached and 1.5×10^5 of the silenced HeLa cells were re-seeded in a 12-well plate and lysed via sonication after another 48h. For the perturbation experiment, the re-seeded cells were incubated for 2 hours with 200nM of DMSO (Sigma), Rapamycin (Sigma) or Bafilomcin A1 (Sigma) prior to cell lysis with sonication. After boiling, cell lysates were resolved by SDS-PAGE and transferred to nitrocellulose membranes (Amersham Biosciences). Blots were blocked in Odyssey blocking buffer (LICOR). Mouse anti-β-actin (1:5000, Sigma) was revealed by Odyssey infrared imaging (LICOR) using anti-mouse Dylight 680-conjugated antibody (1:15.000, Pierce) diluted in Odyssey blocking buffer + 0.1% Tween20. Rabbit anti-RNF41 (1:10.000; Bethyl), mouse-anti p62 (1:1000, BD Bioscience), rabbit anti-LC3B (1:1000, Cell Signaling), rabbit anti-TBK1 (1:2000, Abcam), rabbit anti-p-TBK1 (1:1000, Cell Signaling) and mouse anti-ARF6 (1:500, Santa Cruz) were revealed with SuperSignal West Pico Chemiluminescent Substrate (Pierce) for detection via ECL (enhanced chemiluminescence), using peroxidase-conjugated anti-rabbit or mouse antibody (1:10.000, Jackson ImmunoResearch), diluted in milk blocking buffer.

Binary MAPPIT analysis

For binary MAPPIT, 1×10^4 HEK293T cells (www.atcc.org, mycoplasma negative) were seeded in a 96-well plate and transfected with 50 ng of STAT3-dependent pXP2d2-rPAP1-luciferase reporter, 250 ng bait and prey constructs using calcium phosphate. Cells were left untreated or stimulated for 24 hours with human Erythropoietin (5 ng/ml). Luciferase activity from triplicate samples was measured by chemiluminescence in an Envision plate reader (PerkinElmer) and expressed as fold induction (stimulated/non-stimulated relative light units) relative to the signal generated by a JAK2 binding prey (Rem2), thereby correcting for varying expression levels of the different used baits.

Suppl Fig 1:
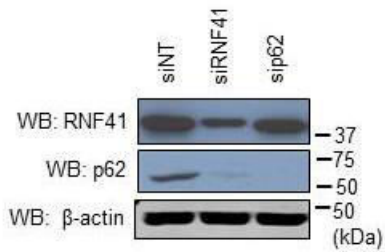
Suppl Fig 1. HeLa cells were silenced (96h) for RNF41, p62 or treated with siNT. Protein levels were analyzed by Western Blotting using antibodies against RNF41, p62 or β-actin (loading control). n=3.

Suppl Fig 2:
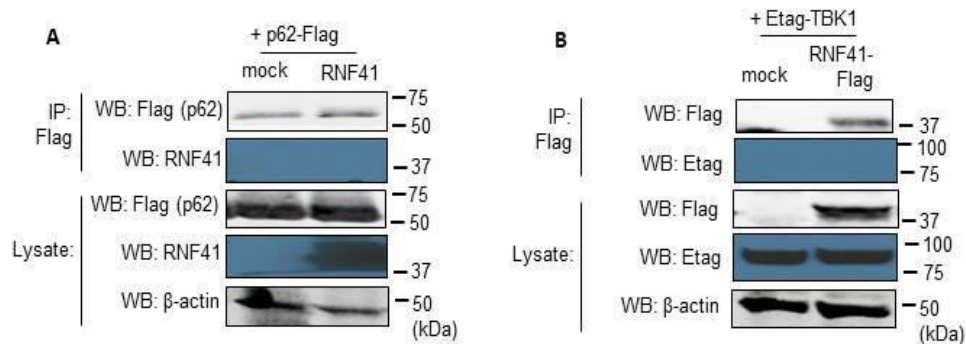
Suppl Fig 2. **(A)** Co-immunoprecipitation analysis of HEK293T cells transiently co-transfected with a plasmid encoding Flag-tagged p62 and RNF41 or soluble IL5Rα (mock). Anti-Flag immunoprecipitates (upper panels) and lysates (lower panels) were visualized with anti-Flag, anti-RNF41 and anti-actin (loading control). n=3. **(B)** Co-immunoprecipitation analysis of HEK293T cells transiently co-transfected with a plasmid encoding E-tagged TBK1 and Flag-tagged RNF41 or soluble IL5Rα (mock). Anti-Flag immunoprecipitates (upper panels) and lysates (lower panels) were visualized with anti-Flag, anti-Etag and anti-actin (loading control). n=3.

Suppl Fig 3:
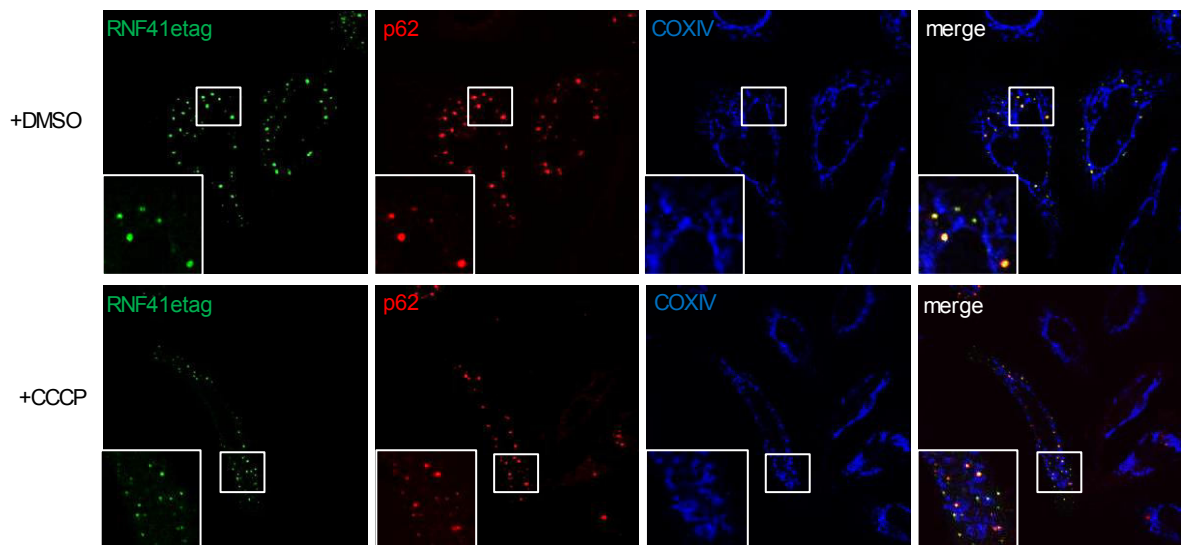
Suppl Fig 3. HeLa cells transiently transfected with a vector encoding E-tagged RNF41 were treated with 20μM DMSO or CCCP for 4hours prior to fixing and staining with anti-Etag (secondary Alexa Fluor 488, green), anti-p62 (secondary Alexa Fluor 568, red) and anti-COXIV (secondary Alexa Fluor 647, blue). COXIV was used to identify the inner membrane of mitochondria. The insets show a magnification of the boxed area. n=1.

Suppl Fig 4:
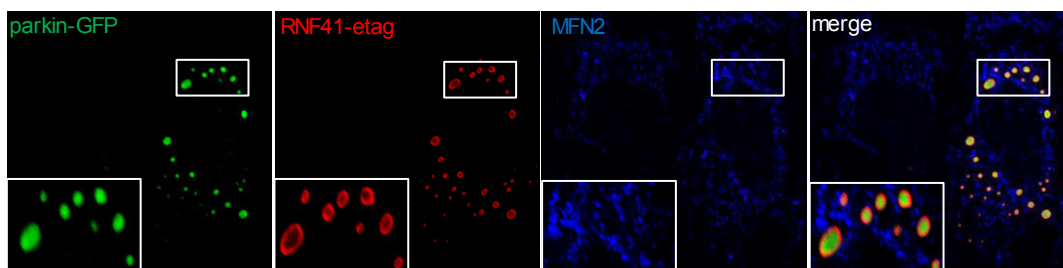
Suppl Fig 4. U2OS cells, stably expressing GFP-parkin, were transiently transfected with a vector encoding E-tagged RNF41. After fixation, cells were stained with anti-Etag (secondary Alexa Fluor 568, red) and anti-MFN2 (secondary Alexa Fluor 647, blue). MFN2 (mitofusin 2) embedded in the outer membrane of mitochondria was used to identify mitochondria. The insets show a magnification of the boxed area. n=3.

References

1 Mizushima N (2007) Autophagy: process and function. *Genes Dev.* **21**, 2861–73.

2 Shibutani ST & Yoshimori T (2014) A current perspective of autophagosome biogenesis. *Cell Res.* **24**, 58–68.

3 Stolz A, Ernst A & Dikic I (2014) Cargo recognition and trafficking in selective autophagy. *Nat. Cell Biol.* **16**, 495–501.

4 Shin J (1998) P62 and the sequestosome, a novel mechanism for protein metabolism. *Arch. Pharm. Res.* **21**, 629–33.

5 Matsumoto G, Wada K, Okuno M, Kurosawa M & Nukina N (2011) Serine 403 phosphorylation of p62/SQSTM1 regulates selective autophagic clearance of ubiquitinated proteins. *Mol. Cell* **44**, 279–89.

6 Pilli M, Arko-Mensah J, Ponpuak M, Roberts E, Master S, Mandell MA, Dupont N, Ornatowski W, Jiang S, Bradfute SB, Bruun J-A, Hansen TE, Johansen T & Deretic V (2012) TBK-1 promotes autophagy-mediated antimicrobial defense by controlling autophagosome maturation. *Immunity* **37**, 223–34.

7 Matsumoto G, Shimogori T, Hattori N & Nukina N (2015) TBK1 controls autophagosomal engulfment of polyubiquitinated mitochondria through p62/SQSTM1 phosphorylation. *Hum. Mol. Genet.* **24**, 4429–42.

8 Lin X, Li S, Zhao Y, Ma X, Zhang K, He X & Wang Z (2013) Interaction domains of p62: a bridge between p62 and selective autophagy. *DNA Cell Biol.* **32**, 220–7.

9 Lippai M & Low P (2014) The role of the selective adaptor p62 and ubiquitin-like proteins in autophagy. *Biomed Res. Int.*

10 Katsuragi Y, Ichimura Y & Komatsu M (2015) p62/SQSTM1 functions as a signaling hub and an autophagy adaptor. *FEBS J.* **282**.

11 Qiu X-B, Markant SL, Yuan J & Goldberg AL (2004) Nrdp1-mediated degradation of the gigantic IAP, BRUCE, is a novel pathway for triggering apoptosis. *EMBO J.* **23**, 800–10.

12 Zhong L, Tan Y, Zhou A, Yu Q & Zhou J (2005) RING finger ubiquitin-protein isopeptide ligase Nrdp1/FLRF regulates parkin stability and activity. *J. Biol. Chem.* **280**, 9425–30.

13 Qiu X-B & Goldberg AL (2002) Nrdp1/FLRF is a ubiquitin ligase promoting ubiquitination and degradation of the epidermal growth factor receptor family member, ErbB3. *Proc. Natl. Acad. Sci. U. S. A.* **99**, 14843–8.

14 Jing X, Infante J, Nachtman RG & Jurecic R (2008) E3 ligase FLRF (Rnf41) regulates differentiation of hematopoietic progenitors by governing steady-state levels of cytokine and retinoic acid receptors. *Exp. Hematol.* **36**, 1110–20.

15 Wauman J, De Ceuninck L, Vanderroost N, Lievens S & Tavernier J (2011) RNF41 (Nrdp1) controls type 1 cytokine receptor degradation and ectodomain shedding. *J. Cell Sci.* **124**, 921–32.

16 Basiorka AA, McGraw KL, De Ceuninck L, Griner LN, Zhang L, Clark JA, Caceres G, Sokol L, Komrokji RS, Reuther GW, Wei S, Tavernier J & List AF (2016) Lenalidomide Stabilizes the Erythropoietin Receptor by Inhibiting the E3 Ubiquitin Ligase RNF41. *Cancer Res.* **76**.

17 De Ceuninck L, Wauman J, Masschaele D, Peelman F & Tavernier J (2013) Reciprocal cross-regulation between RNF41 and USP8 controls cytokine receptor sorting and processing. *J. Cell Sci.* **126**, 3770–81.

18 Masschaele D, De Ceuninck L, Wauman J, Defever D, Stenner F, Lievens S, Peelman F & Tavernier J (2017) RNF41 interacts with the VPS52 subunit of the GARP and EARP complexes. *PLoS One* **12**, e0178132.

19 Diamonti AJ, Guy PM, Ivanof C, Wong K, Sweeney C & Carraway KL (2002) An RBCC protein implicated in maintenance of steady-state neuregulin receptor levels. *Proc. Natl. Acad. Sci. U. S. A.* **99**, 2866–71.

20 Eyckerman S, Verhee A, Van der Heyden J, Lemmens I, Van Ostade X, Vandekerckhove J & Tavernier J (2001) Design and application of a cytokine-receptor-based interaction trap. *Nat. Cell Biol.* **3**, 1114–1119.

21 Wang C, Chen T, Zhang J, Yang M, Li N, Xu X & Cao X (2009) The E3 ubiquitin ligase Nrdp1 "preferentially" promotes TLR-mediated production of type I interferon. *Nat. Immunol.* **10**, 744–52.

22 Hara K, Maruki Y, Long X, Yoshino K, Oshiro N, Hidayat S, Tokunaga C, Avruch J & Yonezawa K (2002) Raptor, a binding partner of target of rapamycin (TOR), mediates TOR action. *Cell* **110**, 177–89.

23 Hosokawa N, Hara T, Kaizuka T, Kishi C, Takamura A, Miura Y, Iemura S, Natsume T, Takehana K, Yamada N, Guan J-L, Oshiro N & Mizushima N (2009) Nutrient-dependent mTORC1 association with the ULK1-Atg13-FIP200 complex required for autophagy. *Mol. Biol. Cell* **20**, 1981–91.

24 Ma X, Helgason E, Phung QT, Quan CL, Iyer RS, Lee MW, Bowman KK, Starovasnik MA & Dueber EC (2012) Molecular basis of Tank-binding kinase 1 activation by transautophosphorylation. *Proc. Natl. Acad. Sci. U. S. A.* **109**, 9378–83.

25 Moreau K, Ravikumar B, Puri C & Rubinsztein DC (2012) Arf6 promotes autophagosome formation via effects on phosphatidylinositol 4,5-bisphosphate and phospholipase D. *J. Cell Biol.* **196**, 483–96.

26 Bjørkøy G, Lamark T, Brech A, Outzen H, Perander M, Overvatn A, Stenmark H & Johansen T (2005) p62/SQSTM1 forms protein aggregates degraded by autophagy and has a protective effect on huntingtin-

induced cell death. *J. Cell Biol.* **171**, 603–14.

27 Russell RC, Tian Y, Yuan H, Park HW, Chang Y-Y, Kim J, Kim H, Neufeld TP, Dillin A & Guan K-L (2013) ULK1 induces autophagy by phosphorylating Beclin-1 and activating VPS34 lipid kinase. *Nat. Cell Biol.* **15**, 741–50.

28 Roberts R & Ktistakis NT (2013) Omegasomes: PI3P platforms that manufacture autophagosomes. *Essays Biochem.* **55**.

29 Dooley HC, Razi M, Polson HEJ, Girardin SE, Wilson MI & Tooze SA (2014) WIPI2 Links LC3 Conjugation with PI3P, Autophagosome Formation, and Pathogen Clearance by Recruiting Atg12–5-16L1. *Mol. Cell* **55**, 238–252.

30 Itakura E & Mizushima N (2011) p62 Targeting to the autophagosome formation site requires self-oligomerization but not LC3 binding. *J. Cell Biol.* **192**, 17–27.

31 Weidberg H & Elazar Z (2011) TBK1 mediates crosstalk between the innate immune response and autophagy. *Sci. Signal.* **4**, pe39.

32 Korac J, Schaeffer V, Kovacevic I, Clement AM, Jungblut B, Behl C, Terzic J & Dikic I (2013) Ubiquitin-independent function of optineurin in autophagic clearance of protein aggregates. *J. Cell Sci.* **126**, 580–592.

33 Tu D, Zhu Z, Zhou AY, Yun C, Lee K-E, Toms A V, Li Y, Dunn GP, Chan E, Thai T, Yang S, Ficarro SB, Marto JA, Jeon H, Hahn WC, Barbie DA & Eck MJ (2013) Structure and ubiquitination-dependent activation of TANK-binding kinase 1. *Cell Rep.* **3**, 747–58.

34 Korolchuk VI, Mansilla A, Menzies FM & Rubinsztein DC (2009) Autophagy Inhibition Compromises Degradation of Ubiquitin-Proteasome Pathway Substrates. *Mol. Cell* **33**, 517–527.

35 Zaffagnini G & Martens S (2016) Mechanisms of Selective Autophagy. *J. Mol. Biol.* **428**, 1714–24.

36 Komatsu M, Waguri S, Koike M, Sou Y-S, Ueno T, Hara T, Mizushima T, Iwata J-I, Ezaki J, Murata S, Hamazaki J, Nishito Y, Iemura S, Natsume T, Yanagawa T, Uwayama J, Warabi E, Yoshida H, Ishii T, Kobayashi A, Yamamoto M, Yue Z, Uchiyama Y, Kominami E & Tanaka K (2007) Homeostatic Levels of p62 Control Cytoplasmic Inclusion Body Formation in Autophagy-Deficient Micee. *Cell* **131**, 1149–1163.

37 Wooten MW, Hu X, Babu JR, Seibenhener ML, Geetha T, Paine MG & Wooten MC (2006) Signaling, polyubiquitination, trafficking, and inclusions: sequestosome 1/p62's role in neurodegenerative disease. *J. Biomed. Biotechnol.* **2006**, 62079.

38 Rea SL, Majcher V, Searle MS & Layfield R (2014) SQSTM1 mutations – Bridging Paget disease of bone and ALS/FTLD. *Exp. Cell Res.* **325**, 27–37.

39 Song P, Li S, Wu H, Gao R, Rao G, Wang D, Chen Z, Ma B, Wang H, Sui N, Deng H, Zhang Z, Tang T, Tan Z, Han Z, Lu T, Zhu Y & Chen Q (2016) Parkin promotes proteasomal degradation of p62: implication of selective vulnerability of neuronal cells in the pathogenesis of Parkinson's disease. *Protein Cell* **7**, 114–29.

40 Narendra D, Tanaka A, Suen D-F & Youle RJ (2008) Parkin is recruited selectively to impaired mitochondria and promotes their autophagy. *J. Cell Biol.* **183**.

41 Durcan TM, Tang MY, Pérusse JR, Dashti EA, Aguileta MA, McLelland G-L, Gros P, Shaler TA, Faubert D, Coulombe B & Fon EA (2014) USP8 regulates mitophagy by removing K6-linked ubiquitin conjugates from parkin. *EMBO J.* **33**, 2473–91.

42 Narendra D, Kane LA, Hauser DN, Fearnley IM & Youle RJ (2010) p62/SQSTM1 is required for Parkin-induced mitochondrial clustering but not mitophagy; VDAC1 is dispensable for both. *Autophagy* **6**, 1090–106.

43 Lamark T & Johansen T (2012) Aggrephagy: Selective Disposal of Protein Aggregates by Macroautophagy. *Int. J. Cell Biol.* **2012**, 1–21.

44 Chin L-S, Olzmann JA & Li L (2010) Parkin-mediated ubiquitin signalling in aggresome formation and autophagy. *Biochem. Soc. Trans.* **38**, 144–9.

45 Nagaoka U, Kim K, Jana NR, Doi H, Maruyama M, Mitsui K, Oyama F & Nukina N (2004) Increased expression of p62 in expanded polyglutamine-expressing cells and its association with polyglutamine inclusions. *J. Neurochem.* **91**, 57–68.

46 Lievens S, Vanderroost N, Van der Heyden J, Gesellchen V, Vidal M & Tavernier J (2009) Array MAPPIT: High-Throughput Interactome Analysis in Mammalian Cells. *J. Proteome Res.* **8**, 877–886.

Discussion and
future prospects

The in-house developed MAPPIT (Mammalian Protein-Protein Interaction Trap) technique proved to be a highly valuable tool to analyze PPIs (protein-protein interactions) [1]. The high-throughput screening platforms array MAPPIT and microarray MAPPIT allow the extensive screening for new interaction partners of a protein of interest [2,3]. A common feature of PPI screening methods is the presence of technical false positive hits. In the case of MAPPIT these false positives usually interact with the LR tail of the MAPPIT bait receptor or bind with JAK2. Through the years this list of intrinsic false positives became well defined and was excluded from subsequent MAPPIT screening analyses. On the other hand, such screening artifacts could also serve as internal controls to determine expression of the bait chimera. RNF41 (RING finger protein 41), more specifically RNF41-encoding preys with truncated RING domains, were frequently detected as false positives. These truncated preys resembled DN (dominant negative) RNF41, as they lack the functional RING domain responsible for recruiting the ubiquitination machinery. Such RNF41 DN effect was first described for the ERBB3 and ERBB4 receptors as its expression resulted in enhanced signaling [4]. Our lab therefore decided to further investigate the functional significance of RNF41 in LR (leptin receptor) signaling and indeed found that RNF41 suppressed LR signaling, and in extension also LIFR (leukaemia inhibitory factor receptor), IL-6R (interleukin 6 receptor), EPOR (erythropoietin receptor) and IL-3R (interleukin 3 receptor) signaling [5]. Moreover, further research uncovered a role for RNF41 in the intracellular trafficking of these JAK2-associated type I cytokine receptors. RNF41 was found to reroute these receptors from the lysosomal degradation pathway to compartments for ectodomain shedding by ubiquitinating and suppressing the deubiquitinase USP8 (Ubiquitin-specific protease 8) which leads to a destabilized ESCRT-0 complex [6].

RNF41 interacts with the VPS52 subunit of the GARP and EARP complexes

In the first part of this thesis we further explored the molecular mechanisms underlying the role of RNF41 in intracellular rerouting by focusing on newly identified RNF41 interaction partners from an initial array MAPPIT screen. VPS52 (vacuolar protein sorting 52), which is a component of two spatially distinct multisubunit tethering complexes GARP (Golgi-associated retrograde protein) and EARP (endosome-associated recycling protein), appeared as one of the top-ranked hits. These complexes mediate transport of cargo from the endosomes to the TGN (trans-Golgi network) or to the PM (plasma membrane), respectively. We therefore reasoned that this RNF41-VPS52 interaction could potentially be involved in the effects of RNF41 on intracellular transport of the LR. Detailed interaction analysis revealed that RNF41 and VPS52 interacted with each other via their coiled-coil domains. This was confirmed by a screen that combined random mutagenesis with MAPPIT to reveal RNF41 mutants that specifically disrupted the interaction between RNF41 and VPS52, which were al located in the RNF41 coiled-coil domain. This approach also led to the identification of the RNF41 L163Q mutant which was used throughout the paper to determine the specificity of the RNF41-VPS52 interaction in the observed RNF41-provoked effects. RNF41 ubiquitinated and relocated VPS52 away from VPS53, which is another shared subunit of the GARP and EARP complexes. This relocalisation of VPS52 towards RNF41-positive structures, which we refer to as RNF41-bodies, depended on the E3 ligase activity and membrane anchoring potential of RNF41 since DN RNF41, lacking both features, RNF41 C34S/H36Q, with impaired E3 ligase activity (unpublished observations), and RNF41 G2A, with a mutated myristoylation site necessary for membrane anchoring, did not exhibit this effect. In line with other reports [7], we established that both RNF41 and VPS52 oligomerize, and our results indicated that VPS52 hindered this RNF41 oligomerization and vice versa. Molecular modeling of the coiled-coil regions of one RNF41 and two VPS52 monomers

accentuates a high electrostatic compatibility between the RNF41 and VPS52 coiled-coils, where positively charged basic amino acids, such as Arg and Lys, frequently face negatively charged acidic amino acids, like Asp and Glu. Therefore, we envisioned a complex where the RNF41 and VPS52 monomers are interchangeable, thereby cycling between a new RNF41-VPS52 complex and existing RNF41 complexes, GARP or EARP complexes. Exchange between coiled-coil proteins is often observed in intracellular trafficking. SNARE (soluble N-ethylmaleimide-sensitive factor attachment protein receptor) proteins, for example, can assemble into stable four-helix bundle SNARE complexes via their coiled-coil containing SNARE motifs. A single SNARE protein can hereby get incorporated in multiple SNARE complexes and in this way regulate multiple fusion events [8,9]. Moreover, the GARP and EARP multisubunit tethering complexes share the VPS51, VPS52 and VPS53 subunits, while the exchange of VPS54 in GARP for Syndetin in EARP defines the specificity of the location of these complexes [10]. Furthermore, the coiled-coil tethering factor p115 is able to interact with the coiled-coil tether Giantin on COPI (coat protein complex I) vesicles. This is followed by binding with coiled-coil tether GM130 on the Golgi in order to link COPI vesicles with the Golgi [11], which further illustrates the sequential interaction potential of coiled-coil domains. In the future we could make use of SEC-MALS (Size exclusion chromatography- Multi-angle light scattering) to determine the oligomeric state of the RNF41, VPS52 or RNF41-VPS52 complexes. This biochemical approach enables accurate molecular weight determination of proteins, oligomers and complexes where the SEC column separates molecules by size, while MALS calculates the molar mass of eluting proteins based on the intensity of light scattering [12].

At this point it is unclear what type of ubiquitin linkage is responsible for the RNF41-mediated ubiquitination of VPS52 or whether this is direct or via the recruitment of other E3 ligases. Since this ubiquitination does not result in the degradation of VPS52 we are inclined to exclude K48-chains, and believe that this ubiquitination could involve K63- and/or M1-linked chains. These chains are usually implicated in regulating protein localization and are thus in line with the observed relocalization of VPS52 by RNF41 [13]. Experiments with appropriate antibodies or K48, K63 and M1 mutants together with an in vitro ubiquitin assay should allow to determine the type of ubiquitination and whether this ubiquitination of VPS52 by RNF41 is direct or indirect.

Considering that RNF41 relocates VPS52 and thereby hampers the interaction between VPS52 and the GARP or EARP complex, we further investigated the influence of RNF41 on known substrates of these complexes and added the results in the addendum of this paper. Since the GARP complex participates in the retrograde transport of Shiga toxin B-subunit (STxB) and depletion of any of the GARP subunits altered STxB distribution [14,15], we expected RNF41 to mimic this effect. Surprisingly, RNF41 did not hamper STxB transport to the TGN. We next examined the EARP complex, which is involved in the recycling of internalized transferrin receptor back to the plasma membrane [10]. Ectopic RNF41 expression clearly interfered with the transferrin recycling pathway and resulted in an accumulation of transferrin, resembling the situation of VPS52 depleted cells [10]. Since expression of the L163Q mutant also resulted in accumulated transferrin, we were not able to ascribe this effect to the RNF41-VPS52 interaction (unpublished data). However, we can also not exclude this, as the L163Q mutant is still able to oligomerize with WT RNF41, which could explain the lack of functional effect. Unfortunately, we cannot determine the effect of RNF41 silencing on transferrin recycling or STxB transport at this point due to poor silencing efficiencies and failing endogenous RNF41 antibodies for immunofluorescence. We reason that RNF41 interacts with and relocalizes VPS52 destined for the EARP complex. This may explain why the GARP complex remains

functional but transferrin recycling, mediated by the EARP complex, is inhibited. This is similar to a situation described by Otto et al, where overexpression of the t-SNARE STX6 (syntaxin 6) together with its interaction partner SHIP164 (Syntaxin 6 Habc-Interacting Protein Of 164 kDa) caused a relocalization of VPS52 which also resulted in inhibited transferrin receptor recycling [16].

Conversely, we wanted to investigate the effect of the RNF41-VPS52 interaction on the known RNF41-mediated enhanced LR shedding and inhibited LR degradation. Silencing of VPS52 still increased LR shedding upon RNF41 expression and ectopic expression of the L163Q mutant resembled WT RNF41, indicating that VPS52 is not involved in the RNF41-mediated effects on LR rerouting. We can at this point not explain the apparent contradiction between the effect of RNF41 on LR and transferrin recycling where RNF41 enhances LR recycling and subsequent shedding, whereas RNF41, similar to VPS52 depletion, delays transferrin recycling. It is possible that the effect of RNF41 on transferrin recycling is indeed depending on the interaction with VPS52, where RNF41 interferes with EARP function by sequestering VPS52 away, whereas the effects of RNF41 on LR routing are independent of VPS52. This LR rerouting depends on the RNF41-USP8 interaction, where RNF41-mediated loss of USP8 actively stimulates LR recycling [6]. This is coherent with the idea that RNF41 functions at separate stages and possibly at different timepoints during intracellular trafficking, where RNF41-VPS52 functions at the recycling endosomes while RNF41-USP8 operates at the sorting endosome (see Figure 20).

On the other hand, we did notice that silencing of VPS52 decreased basal LR ectodomain shedding, which suggests that VPS52 could be involved in LR recycling. This is in line with the function of the EARP complex in protein recycling, although the LR did not appear to undergo recycling in basal circumstances [6,17]. Also, the LR was not detected in transferrin-positive recycling endosomes after their internalization from the PM, indicating that these two receptors follow different pathways [17]. Transferrin is a CME (clathrin-mediated endocytosis) cargo protein that is known to undergo fast and slow, ERC (endocytic recycling compartment)-dependent recycling via RAB4 and RAB11 respectively. Next to these CME-dependent recycling pathways, another ARF6-, RAB11- and RAB22-dependent slow recycling pathway exists [18,19]. Perhaps the LR recycles via this latter pathway, although this pathway is known to carry clathrin-independent endocytosed cargo back to the PM via recycling endosomes, while LR was reported to undergo CME [20]. It is possible that VPS52 influences basal LR recycling via another unknown mechanism, or that the effect of VPS52 on LR recycling depends on the interaction with other proteins, for instance MAGEL2 (melanoma antigen L2). Indeed, in a recent collaboration with the group of prof. Wevrick (University of Alberta, Canada), we established that VPS52 interacted with MAGEL2, a protein that is known to regulate retromer-mediated recycling both towards the TGN and the PM [21]. MAGEL2 was found to recruit the LR via necdin to the RNF41-USP8-ESCRT-0 ubiquitination complex on the sorting endosomes to regulate its trafficking [22]. MAGEL2 could form a separate complex with VPS52 and function somewhere at the retromer-mediated recycling pathway towards the PM, which could explain the effects of silenced VPS52 on LR shedding.

<u>A high confidence interactome for RNF41 built on multiple orthogonal assays</u>

In the second part of this thesis we expanded the array MAPPIT-derived list of RNF41 interaction partners with data obtained from orthogonal screening methods in order to build an RNF41 interactome network. Mapping and analyzing the RNF41 interactome network will provide useful

information for future studies that further elucidate the role of RNF41 and can reveal how this protein relates to human disease. Virotrap, BioID (proximity-dependent biotin identification) and AP-MS (affinity-purification-mass spectrometry) screens were performed and their resulting datasets were pooled with available data from previously performed microarray MAPPIT and Y2H screens [3,23]. The combined datasets were incorporated in a high-resolution RNF41 interactome map that encompassed all detected interactions. This map includes many known RNF41 interaction partners such as USP8, BRUCE (BIR repeat containing ubiquitin-conjugating enzyme) and KDM3B (lysine-specific demethylase 3B) thereby confirming the efficiency of the screens. In addition, it revealed several functional clusters of proteins involved in ubiquitination and in the insulin receptor signaling pathway. This high-resolution interactome map also resulted in the discovery of new RNF41 interaction partners, such as CCP110 (Centriolar Coiled-Coil Protein of 110 kDa), which was identified with BioID. This protein regulates centrosome duplication and separation, and modulates ciliogenesis. Next to suppressing ciliogenesis, it has recently been found to also promote cilia formation depending on the accessible interacting proteins and the cellular microenvironment [24–27]. The involvement of this candidate protein in ciliogenesis is in line with the function of another well-known RNF41 interaction partner USP8 and thus illustrates the competence of an interactome map to uncover functional links. USP8 deubiquitinates and stabilizes the transcription factor HIF1α (hypoxia-inducible factor α), an essential ciliogenesis factor. In this way, HIF1α suppresses the RAB5 effector Rabaptin5 thereby hindering early endosome fusion and promoting ciliogenesis [28].

Candidate proteins that were identified in two or more of the orthogonal methods were assembled in the high-confidence RNF41 interactome map. This map comprises 19 high-confident RNF41 interaction partners including functionally well-characterized proteins such as BRUCE and USP8, and novel candidate proteins such as KIAA1598, NAV1 (Neuron navigator 1) and AP2S1 (Adaptor related Protein complex 2 sigma 1 subunit). KIAA1598 and NAV1 were both picked up in the BioID and AP-MS screen. Next to this, KIAA1598 also appeared as an RNF41 interaction partner in the microarray MAPPIT screen, while NAV1 interacted with RNF41 in Virotrap. Both proteins are involved in axon outgrowth and guidance [29–31]. PAK1 (p21-activated kinase 1) induces phosphorylation of KIAA1598 thereby enabling the interaction with F-actin. In this way KIAA1598 bridges the interaction between F-actin and neuronal cell adhesion molecule L1-CAM, which further promotes axon outgrowth [29,30]. The recent characterization of RTN4A as a new RNF41 interaction partner further supports a role for RNF41 and candidate interaction partners in neuronal development. This key structural protein of ER tubules was also found to interact with receptors on the axonal growth cone and inhibits axonal regeneration [32,33]. Furthermore, KIAA1598 also regulates neural polarization by accumulating and recruiting PI3K (phosphatidylinositol-3-kinase) activity in the growing axon [34]. Likewise, RNF41 plays a role in planar cell polarity required for neuronal development by downregulating VANGL (Vang-like protein)-dependent non-canonical Wnt signaling. Through interactions with KITENIN (KAI1 C-terminal interacting tetraspanin) and VANGL2, RNF41 mediates the K63-linked polyubiquitination of DVL (Dishevelled), which inhibits its recruitment to activated Frizzled receptors, resulting in suppressed Wnt signaling [35]. In addition, Par-1b mediated phosphorylation of RNF41 targets laminin-111 receptors to the basolateral membrane which establish cell-ECM contacts with laminin-111 required for apical-basal cell polarity in epithelial cells [36]. Although Virotrap, BioID and AP-MS screens were performed in non-polarized HEK293T cells, the identification of RNF41 interaction partners involved in cell polarity is not so surprising as many endocytic traffic proteins appeared to be involved in processes such as epithelial and neuronal planar cell polarity

[37]. Of note, the HEK293 cell line was found to have characteristics of immature neurons, presumably originating from migrating neural crest cells in the kidney [38].

This also further suggests a potential role for RNF41 in intracellular trafficking, which is emphasized by the identification of AP2S1 as another novel RNF41 interaction partner in a Virotrap and microarray MAPPIT screen. AP2S1 represents the σ2 subunit of the clathrin adaptor protein AP-2 which plays a crucial role in CME. This heterotetrameric AP-2 complex further comprises two large subunits, α and β2, and a medium subunit μ2 [39]. Binding of AP-2 to the PM triggers a conformational change, which enables interaction with internalization motifs in the cytoplasmic tail of cargo proteins, followed by clathrin recruitment [40,41]. Further investigation revealed that AP2S1 was not involved in the well-established function of RNF41 in LR shedding, degradation and signaling as silencing of AP2S1 did not hamper the RNF41-mediated enhanced ectodomain shedding, blocked CTS formation or decreased LR signaling. Instead we observed an increase in basal LR and LIFR signaling when cells were depleted of AP2S1, which corresponds to the enhanced signaling observed in RNF41-depleted cells [5]. At this point it is unclear whether AP2S1 and thus AP-2 are involved in LR internalization. We observed enhanced LR signaling upon depletion of AP2S1, suggesting that if AP2S1 is involved in LR internalization, LR signaling would occur at the plasma membrane. However, our observations revealed that LR internalization was necessary for LR signaling, which implies that AP2S1 and AP-2 are not involved in LR endocytosis. This is also supported by the lack of a putative dileucine or tyrosine-based motif in cytoplasmic tail of the LR which could be recognized by the σ2 or μ2 subunit of AP-2 respectively. It is possible that other adaptor proteins regulate LR internalization, as seen for the EGF (Epidermal growth factor) and LDL (low-density lipoprotein) receptors, where AP-2 depletion does not influence EGFR and LDLR CME [42].

Domain mapping showed that the substrate binding domain of RNF41 is responsible for AP2S1 interaction. Surprisingly we did not detect ubiquitination of AP2S1 by RNF41, although interactions with this substrate binding domain are usually conserved for proteins, like BRUCE, USP8 and ERBB3 that undergo RNF41-mediated ubiquitination [43–45]. This can be attributed to the observed indirect interaction between RNF41 and AP2S1. Nonetheless, we did observe a stabilization of AP2S1 upon RNF41 ectopic expression. Moreover, experiments with the proteasomal inhibitor MG132 revealed that RNF41 likely stabilizes AP2S1 by preventing its proteasomal degradation. This RNF41-evoked stabilization of AP2S1 appeared to be independent of its E3 ubiquitin ligase function but relied on its membrane anchoring and oligomerization ability since a RING domain mutant still stabilized AP2S1, while the G2A and ΔCC mutants did not.

This stabilizing effect of RNF41 on AP2S1 is in contrast to its effect on VPS52, where RNF41 directly interacts with and relocates VPS52 depending on its E3 ligase activity [46]. Both effects however, require a proper myristoylation site and a domain for oligomerization, suggesting that membrane anchoring and the ability to homo- or hetero-oligomerize is important for general RNF41 function. It is likely that RNF41 exerts its function on both proteins in a temporal or spatial distinct manner (see Figure 20).

As AP2S1 indirectly interacts with the substrate binding domain of RNF41 and RNF41 prevented AP2S1 from proteasomal degradation it is possible that RNF41 directly interacts, via its substrate binding domain, with another currently unknown E3 ligase, which under normal circumstances ubiquitinates AP2S1 resulting in proteasomal degradation. This resembles a similar situation where

RNF41 degrades the E3 ligase parkin thereby stabilizing parkin substrate CDCrel-1 [47]. Since AP2S1 was identified via Virotrap, we reasoned that this dataset likely contains the potential E3 ubiquitin ligase that mediates this effect. Indeed, the Virotrap list entails three ubiquitin ligases. BRUCE, a well-known E3 ligase, could potentially be involved in this RNF41-AP2S1 interaction since it is an important regulator of cytokinesis, a process implicating both clathrin and AP-2 [48–50]. TTC1 (tetratricopeptide repeat protein 1), an unknown protein that contains a TPR (tetratricopeptide repeat) domain, can potentially function as an E3 ubiquitin ligase since the related E3 ligase, TTC3, contains a TPR motif and a canonical RING finger [51]. And finally, CACYBP (Calcyclin-binding protein), a protein involved in the ubiquitin-mediated degradation of β-catenin [52]. Future experiments using siRNA will determine the involvement of these E3 ligases in the AP2S1-RNF41 interaction.

The high-confidence interactome of RNF41 also identified the E3 ubiquitin ligase ASB6 (ankyrin repeat and SOCS box protein 6), as an RNF41 interaction partner. RNF41 was found to stabilize and relocate ASB6, analogous to our observations for AP2S1. Moreover, ASB6 was implicated in LR signaling and knockdown of ASB6, like knockdown of AP2S1, potentiated LR signaling (De Ceuninck, manuscript in preparation). Although AP2S1 and ASB6 are both stabilized by RNF41 and appear to have similar functions, these proteins were not found to interact with, or influence each other. USP8, which shares the RNF41 interaction interface with ASB6 also failed to interact with AP2S1, despite the fact that RNF41 mutants specifically disrupting this interface resulted in a loss of AP2S1 binding.

The role of RNF41 in selective autophagy

In the third part of this thesis we characterized the RNF41-bodies observed with immunofluorescence. These RNF41-bodies are assumed to be detergent-resistant as ectopically expressed RNF41 resided only in the insoluble fraction of RIPA lysed cells detected by immunoblotting [46]. Due to its oligomerization properties it is easily presumed that these RNF41 bodies represent aggregates. However, DN RNF41 and the RNF41 G2A mutant, both lacking the putative myristoylation site but retaining the coiled-coil domain, were found to have a more homogenous cytosolic distribution, thus arguing against this non-functional aggregation. Moreover, we show that the RNF41-bodies colocalize with the autophagic cargo receptor p62, indicating a role for RNF41 in cargo tagging. RNF41 was found to maintain endogenous p62 and lipidated LC3B-II levels as RNF41 depletion decreased these proteins, independently of increased autolysosomal turnover. Since the RNF41-bodies failed to colocalize with LC3B or LAMP1 (lysosomal-associated membrane protein 1) we presumed that RNF41 exerts its function somewhere in the early stages of autophagy, at the autophagosome formation site. In line with this, it is known that p62 sequesters ubiquitinated cargo into aggregates prior to the recruitment of LC3B. These detergent resistant p62-positive structures did not colocalize with lysosomal markers and represented a stage before the formation of detergent dissolvable autophagosomes [53–55]. Furthermore, binary MAPPIT studies showed that RNF41 interacted with class III PI3K complex I components Beclin1 and ATG14 (autophagy-related protein 14), its effector WIPI2 and with ATG5 of the ubiquitin-like conjugating complex ATG5-ATG12-ATG16. These complexes are required for autophagosome formation through their involvement in the nucleation and elongation of the isolation membrane which further supports a role for RNF41 at the early stage of autophagosome biogenesis (see Figure 20).

The isolation membrane originates from different sources such as the ER, mitochondria, Golgi, endosomes and plasma membrane [56,57]. The small GTPase ARF6 (ADP ribosylation factor 6), a key

regulator of clathrin-independent endocytic trafficking also plays a role in plasma membrane delivery to the isolation membrane via its ability to generate PI(4,5)P2 [58]. This places ARF6 somewhere upstream in autophagosome biogenesis which correlates with our hypothesized role for RNF41 in autophagosome formation since RNF41 depletion lowers the levels of ARF6. Furthermore, ARF6 has also been implicated in CME, another essential mediator in the contribution of plasma membrane to the autophagosomal formation site [59–61]. As AP-2 was found to associate with ARF6 in both CME and CIE, and ARF6 functions cooperatively with PI(4,5)P2 to recruit AP-2 to membranes [59,62], it is possible that AP2S1 also functions in the delivery of membrane to the isolation membrane, connecting yet another RNF41 interaction partner to autophagosome biogenesis.

Next to ARF6, many other proteins involved in intracellular trafficking are known to influence autophagy. This is also true for VPS52, where silencing of VPS52 and other members of the GARP complex resulted in defective autophagy. In this case dysfunctional autophagy was caused by impaired lysosomal turnover, as depleted GARP subunits reduced the amount of acid hydrolases in the lysosomes [10,15]. This is in contrast to our observations of RNF41 in autophagy, although we did observe colocalisation between VPS52 and our p62-positive RNF41 bodies (unpublished observations).

Despite the inability to detect an interaction between TBK1 (TANK-binding kinase 1) and RNF41, although this is described in literature [63], we did observe colocalization between RNF41 and phosphorylated TBK1. TBK1 is activated upon phosphorylation and can in turn phosphorylate the ubiquitin binding domain of p62, thereby increasing binding affinity for ubiquitinated cargo [64–66]. Since K63-linked polyubiquitination of TBK1 is required for TBK1 phosphorylation, and RNF41 is one of the E3 ligases responsible for this ubiquitination [63,67], we presume that RNF41 is required for its activation, which is further corroborated by our finding that silencing of RNF41 decreased phosphorylated and thus activated TBK. Moreover, RNF41 could in this way indirectly regulate p62 recruitment to autophagic cargo. This could also explain the observation that RNF41 silencing decreases p62, as inhibited TBK1 results in unphosphorylated p62 which has a low affinity for ubiquitinated cargo, making it more available to E3 ligases, such as parkin, responsible for its proteasomal degradation [68]. And since RNF41 degrades parkin [47], silencing RNF41 should stabilize parkin, thereby further enabling the proteasomal degradation of p62.

Although several RNF41 interaction partners such as parkin, CLEC16A (C-type lectin domain family 16, member A) and USP8 were found to be involved in mitophagy [69–71], we found no association between the RNF41-bodies and mitochondria, which again highlights the possible temporal and spatial distinct function of many RNF41 interactions. We presume that RNF41 plays a role in aggrephagy, another selective autophagic pathway where misfolded and aggregated proteins are first recognized by HDAC6 (histon deacetylase 6) which results in their delivery to the microtubule organizing center to form aggresomes. This is followed by the recognition of the K63-linked polyubiquitined cargo by p62 resulting in recruitment of the autophagic machinery and eventual autophagic clearance [72]. The identification of HDAC6 as an RNF41 interaction partner in our initial array MAPPIT screen further supports this hypothesis. Moreover, parkin is known to regulate aggrephagy by mediating K63-linked polyubiquitination of misfolded proteins [73]. Our observation that RNF41 sequesters parkin indicates that RNF41 could be involved in the clearance of aggresomes via its interaction with parkin and thereby assists in the further recruitment of the autophagic machinery. On the other hand, it is also possible that RNF41, similarly to parkin, directly ubiquitinates

autophagic cargo and in this way mediates the binding of p62 to these K63-linked polyubiquitinated cargo.
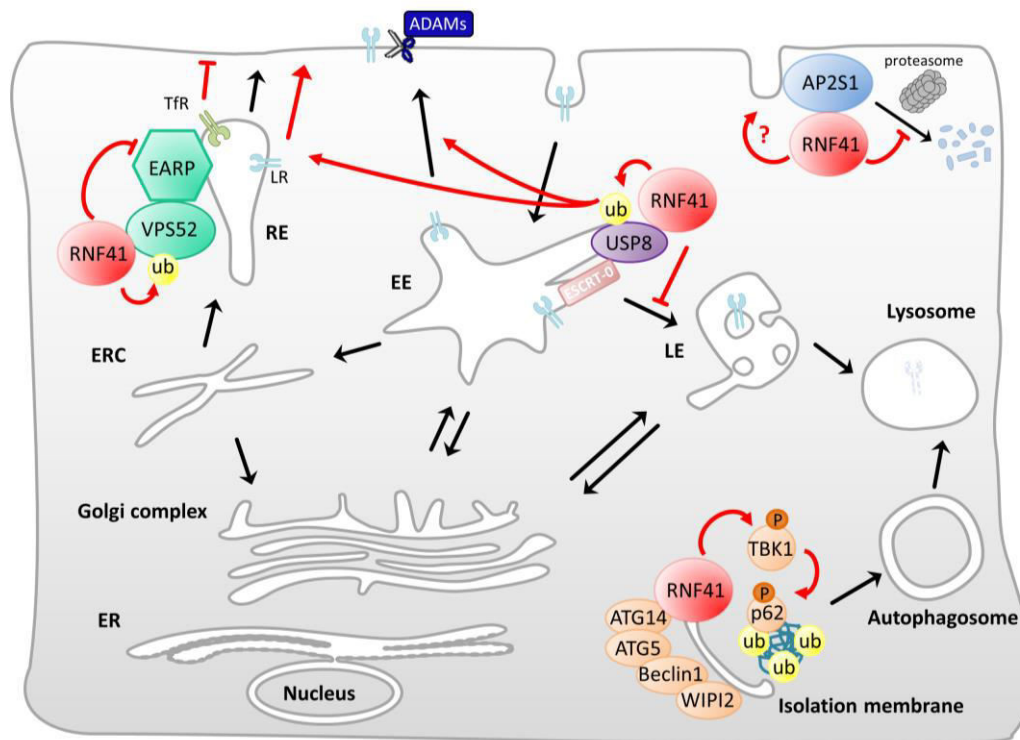
Figure 20. Overview of the spatially distinct functions of RNF41. The RNF41-USP8 interaction determines the fate of JAK2-associated type I cytokine receptors, such as the LR (leptin receptor, blue). At the early endosome, RNF41 ubiquitinates and suppresses USP8 thereby destabilizing the ESCRT-0 complex required for incorporation of these receptors into intraluminal vesicles in the late endosomes, ultimately resulting in inhibited degradation. As a consequence, receptors are rerouted towards the plasma membrane via slow and fast recycling pathways, where they can undergo ectodomain shedding by members of the ADAM (a disintegrin and metalloproteinase) family (note: it is currently unclear where shedding of these receptors occurs, as ADAMs are found at the plasma membrane, endosomes and Golgi). The RNF41-VPS52 interaction likely occurs at the recycling endosomes where RNF41 ubiquitinates and sequesters VPS52 away from the EARP complex thereby inhibiting TfR (transferrin receptor, green) recycling. The stabilizing effect of RNF41 on AP2S1 results in relocalization of AP2S1 from its normal subcellular location at the plasma membrane possibly affecting internalization routes of certain cargo. Finally, RNF41 interaction with ATG-related proteins Beclin1, ATG14, WIPI2 and ATG5 occurs at the isolation membrane. This location of RNF41 possibly enables RNF41 to phosphorylate TBK1 which in turn phosphorylates p62 in this way maintaining p62 levels resulting in sequestering of polyubiquitinated cargo destined for aggrephagy.

Conclusion and future prospects

The study of PPIs can provide valuable insights into the function of a protein as interacting proteins are often involved in the same cellular processes. The function of an unidentified protein can potentially be predicted based on the known function of its binding partner, and detailed analysis of PPIs can in this way reveal the molecular mechanism of cellular processes [74]. By applying this principle throughout this thesis we were able to obtain new insights into RNF41 function. Novel candidates such as VPS52 and AP2S1 indicated additional roles for RNF41 in intracellular transport, more specifically at the level of cargo recycling and internalization, although further investigation is

needed to clarify the functional link between RNF41 and VPS52 or AP2S1 in these processes. Next to this, we also revealed a clear connection between autophagy and RNF41 (see Figure 20 for overview). As the results in this thesis suggest, it is important to keep in mind that RNF41 most likely functions at spatially and temporally distinct stages and is greatly influenced by local interaction partners that regulate its stability. For instance, USP8 stabilizes RNF41 at the level of the sorting endosomes, while Rtn4A at the ER inhibits its E3 ligase activity [6,32]. Furthermore, intracellular trafficking comprises many pathways, some of which appear to be functional redundant or exert compensatory mechanisms when tempered with, which often complicates the study of these processes.

Characterizing the protein interaction network further elucidates the functionality of a certain PPI and can be a valuable tool for drug discovery and development. Specific perturbation of a single PPI (or "edgetic perturbation"), while retaining all others has a more subtle effect on the network and has proven to be more useful than the removal of an entire protein (or "node") which often results in a drastic alteration of the network structure and function [75]. In accordance to this, we applied a strategy that combines random mutagenesis with MAPPIT in order to generate and identify single mutants that specifically disrupt an interaction between RNF41 and a certain interaction partner. A limitation to this method is the need for overexpression, and as WT RNF41 is known to oligomerize, it can easily hetero-oligomerize with these mutants thereby affecting and minimizing the observed phenotypes. A way to circumvent this problem is by first silencing RNF41 followed by ectopic expression of these mutants. However, several attempts by our lab to make a cell line with stable RNF41 knockdown were unsuccessful, as the initial partial knockdown was gradually lost overtime even though the selection pressure was maintained. Although we have proven before that transient knockdown of RNF41 using siRNA has an effect on LR surface expression and signaling [5] and affects endogenous p62 levels (Results section 3), this transient treatment only yields partial knockdown. This is in line with previously published results in literature describing poor RNF41 knockdown efficiencies [36,76] and indicates that RNF41 is essential for cell viability. Consequently, cells with too low RNF41 protein levels will be negatively selected and cells in transient or stable knockdown experiments will always maintain a basal endogenous RNF41 protein pool, which complicates the interpretation of RNF41 knockdown and ectopic expression of RNF41 mutants in functional assays (addendum Results section 1).

Since RNF41 represents a tightly regulated protein where an imbalance caused by excessive or insufficient amounts likely results in its dysfunction, we now aim to circumvent these problems by introducing intrabodies as a new method to selectively modulate RNF41 interactions. These intrabodies represent intracellularly expressed nanobodies that target distinct binding sites in RNF41 and can in this way be used to block specific cellular functions. As intrabodies do not appear to suffer from the reducing environment of the cell, they have been successfully used to target intracellular proteins, such the F-actin capping protein CapG and the actin-binding proteins fascin and cortactin [77,78]. Nanobodies against fascin and cortactin, which respectively inhibit F-actin bundling and perturb WIP (WASP interacting protein) recruitment towards the plasma membrane, revealed their role in invadopodium formation and cancer cell invasion [78]. Moreover, the anti-CapG nanobody prevented the interaction between CapG and actin polymers, thereby reducing cell migration of breast cancer cells and diminishing lung metastasis in xenograft tumor mouse models [77]. RNF41 intrabodies are currently being developed and will first be tested against known interaction partners using MAPPIT. Intrabodies that disrupt the interaction between RNF41 and VPS52 or AP2S1 will help

clarify the role of these interactions in transferrin recycling and CME. Additionally, we could couple intrabodies to GFP, thus creating chromobodies [78,79], which would enable us to visualize the location of endogenous RNF41 since we do not have an anti-RNF41 antibody suitable for immunofluorescent detection of endogenous RNF41. By comparing intrabodies that disrupt the specific interactions between RNF41 and its corresponding partner we could trace the loss-of-interaction effect on the subcellular location of endogenous RNF41.

RNF41 is implicated in various diseases via its interaction with distinct proteins. RNF41 acts as a tumor suppressor through its ability to maintain ERBB3 receptors at modest levels [80–88]. It is also considered to be a pro-apoptotic protein by targeting BRUCE [43,89–91], and could potentially be used as a therapeutic target for Parkinson's disease since it suppresses the levels of parkin [47,92,93]. Characterization of the RNF41 interactome is therefore crucial to determine the interaction partners of RNF41 that function as inhibitors or activators, or vice versa, determine whether RNF41 acts as an inhibitor or activator of a certain interaction partner in order to specifically target and modify the interaction involved in that particular disease. It would be interesting to find an intrabody that targets the interaction between RNF41 and parkin, as RNF41 acts as a culprit in this disease by ubiquitinating and degrading parkin, thereby stabilizing parkin substrates which result in the death of dopaminergic neurons [47,92]. Cell-specific targeting of such intrabodies would require a proper delivery system that can cross the BBB (blood-brain-barrier) such as viral delivery systems with expression under cell type-specific promoters or perhaps intrabody encapsulated immunoliposomes that are decorated with monoclonal antibodies via PEGylation, which target transferrin and in this way mediate their endocytosis across the BBB [94,95]. Additionally, the potential role of RNF41 in autophagy is also of great interest, as autophagy plays a dual role in cancer. On the one hand it acts as a tumor suppressor by preventing accumulation of damaged proteins and organelles, whereas on the other hand it induces tumor growth by its response to cellular stress and increased metabolic demands due to rapid cell proliferation which enables tumor cell survival [96,97]. Since autophagy is emerging as a new target for drug development, our study revealing a function of RNF41 in this process provides a possible new means to modulate autophagy in therapeutic settings.

References

1 Eyckerman S, Verhee A, Van der Heyden J, Lemmens I, Van Ostade X, Vandekerckhove J & Tavernier J (2001) Design and application of a cytokine-receptor-based interaction trap. *Nat. Cell Biol.* **3**, 1114–1119.

2 Lievens S, Vanderroost N, Van der Heyden J, Gesellchen V, Vidal M & Tavernier J (2009) Array MAPPIT: High-Throughput Interactome Analysis in Mammalian Cells. *J. Proteome Res.* **8**, 877–886.

3 Lievens S, Van der Heyden J, Masschaele D, De Ceuninck L, Petta I, Gupta S, De Puysseleyr V, Vauthier V, Lemmens I, De Clercq DJH, Defever D, Vanderroost N, De Smet A-S, Eyckerman S, Van Calenbergh S, Martens L, De Bosscher K, Libert C, Hill DE, Vidal M & Tavernier J (2016) Proteome-scale Binary Interactomics in Human Cells. *Mol. Cell. Proteomics* **15**, 3624–3639.

4 Diamonti AJ, Guy PM, Ivanof C, Wong K, Sweeney C & Carraway KL (2002) An RBCC protein implicated in maintenance of steady-state neuregulin receptor levels. *Proc. Natl. Acad. Sci. U. S. A.* **99**, 2866–71.

5 Wauman J, De Ceuninck L, Vanderroost N, Lievens S & Tavernier J (2011) RNF41 (Nrdp1) controls type 1 cytokine receptor degradation and ectodomain shedding. *J. Cell Sci.* **124**, 921–32.

6 De Ceuninck L, Wauman J, Masschaele D, Peelman F & Tavernier J (2013) Reciprocal cross-regulation between RNF41 and USP8 controls cytokine receptor sorting and processing. *J. Cell Sci.* **126**, 3770–81.

7 Printsev I, Yen L, Sweeney C & Carraway KL (2014) Oligomerization of the Nrdp1 E3 ubiquitin ligase is necessary for efficient autoubiquitination but not ErbB3 ubiquitination. *J. Biol. Chem.* **289**, 8570–8.

8 Fasshauer D (2003) Structural insights into the SNARE mechanism. *Biochim. Biophys. Acta - Mol. Cell Res.* **1641**, 87–97.

9 Parlati F, Varlamov O, Paz K, McNew JA, Hurtado D, Söllner TH & Rothman JE (2002) Distinct SNARE complexes mediating membrane fusion in Golgi transport based on combinatorial specificity. *Proc. Natl. Acad. Sci. U. S. A.* **99**, 5424–9.

10 Schindler C, Chen Y, Pu J, Guo X & Bonifacino JS (2015) EARP is a multisubunit tethering complex involved in endocytic recycling. *Nat. Cell Biol. 17(5), 639–50.* **17**, 639–50.

11 Sönnichsen B, Lowe M, Levine T, Jämsä E, Dirac-Svejstrup B & Warren G (1998) A role for giantin in docking COPI vesicles to Golgi membranes. *J. Cell Biol.* **140**, 1013–21.

12 Folta-Stogniew E (2006) Oligomeric States of Proteins Determined by Size-Exclusion Chromatography Coupled With Light Scattering, Absorbance, and Refractive Index Detectors. In *New and Emerging Proteomic Techniques* pp. 97–112. Humana Press, New Jersey.

13 Komander D & Rape M (2012) The Ubiquitin Code. *Annu. Rev. Biochem.* **81**, 203–229.

14 Pérez-Victoria FJ, Mardones GA & Bonifacino JS (2008) Requirement of the human GARP complex for mannose 6-phosphate-receptor-dependent sorting of cathepsin D to lysosomes. *Mol. Biol. Cell* **19**, 2350–62.

15 Pérez-Victoria FJ, Schindler C, Magadán JG, Mardones GA, Delevoye C, Romao M, Raposo G & Bonifacino JS (2010) Ang2/fat-free is a conserved subunit of the Golgi-associated retrograde protein complex. *Mol. Biol. Cell* **21**, 3386–95.

16 Otto GP, Razi M, Morvan J, Stenner F & Tooze SA (2010) A novel syntaxin 6-interacting protein, SHIP164, regulates syntaxin 6-dependent sorting from early endosomes. *Traffic* **11**, 688–705.

17 Belouzard S & Rouillé Y (2006) Ubiquitylation of leptin receptor OB-Ra regulates its clathrin-mediated endocytosis. *EMBO J.* **25**, 932–42.

18 Weigert R, Yeung AC, Li J & Donaldson JG (2004) Rab22a regulates the recycling of membrane proteins internalized independently of clathrin. *Mol. Biol. Cell* **15**, 3758–70.

19 Grant BD & Donaldson JG (2009) Pathways and mechanisms of endocytic recycling. *Nat. Rev. Mol. Cell Biol.* **10**, 597–608.

20 Tu H, Hsuchou H, Kastin AJ, Wu X & Pan W (2010) Unique leptin trafficking by a tailless receptor. *FASEB J.* **24**, 2281–91.

21 Hao Y-H, Fountain MD, Fon Tacer K, Xia F, Bi W, Kang S-HL, Patel A, Rosenfeld JA, Le Caignec C, Isidor B, Krantz ID, Noon SE, Pfotenhauer JP, Morgan TM, Moran R, Pedersen RC, Saenz MS, Schaaf CP & Potts PR (2015) USP7 Acts as a Molecular Rheostat to Promote WASH-Dependent Endosomal Protein Recycling and Is Mutated in a Human Neurodevelopmental Disorder. *Mol. Cell* **59**, 956–969.

22 Wijesuriya MT, De Ceuninck L, Masschaele D, Sanderson MR, Carias KV, Tavernier J & Wevrick R (2017) The Prader-Willi syndrome proteins MAGEL2 and necdin regulate cell surface abundance of the leptin receptor through ubiquitination pathways involving USP8 and RNF41. *Hum. Mol. Genet.* **26**, 4215–4230.

23 Rolland T, Taşan M, Charloteaux B, Pevzner SJ, Zhong Q, Sahni N, Yi S, Lemmens I, Fontanillo C, Mosca R,

Kamburov A, Ghiassian SD, Yang X, Ghamsari L, Balcha D, Begg BE, Braun P, Brehme M, Broly MP, Carvunis A-R, Convery-Zupan D, Corominas R, Coulombe-Huntington J, Dann E, Dreze M, Dricot A, Fan C, Franzosa E, Gebreab F, Gutierrez BJ, Hardy MF, Jin M, Kang S, Kiros R, Lin GN, Luck K, MacWilliams A, Menche J, Murray RR, Palagi A, Poulin MM, Rambout X, Rasla J, Reichert P, Romero V, Ruyssinck E, Sahalie JM, Scholz A, Shah AA, Sharma A, Shen Y, Spirohn K, Tam S, Tejeda AO, Trigg SA, Twizere J-C, Vega K, Walsh J, Cusick ME, Xia Y, Barabási A-L, Iakoucheva LM, Aloy P, De Las Rivas J, Tavernier J, Calderwood MA, Hill DE, Hao T, Roth FP & Vidal M (2014) A Proteome-Scale Map of the Human Interactome Network. *Cell* **159**, 1212–1226.

24 Chen Z, Indjeian VB, McManus M, Wang L & Dynlacht BD (2002) CP110, a Cell Cycle-Dependent CDK Substrate, Regulates Centrosome Duplication in Human Cells. *Dev. Cell* **3**, 339–350.

25 Spektor A, Tsang WY, Khoo D & Dynlacht BD (2007) Cep97 and CP110 Suppress a Cilia Assembly Program. *Cell* **130**, 678–690.

26 Tsang WY, Bossard C, Khanna H, Peränen J, Swaroop A, Malhotra V & Dynlacht BD (2008) CP110 suppresses primary cilia formation through its interaction with CEP290, a protein deficient in human ciliary disease. *Dev. Cell* **15**, 187–97.

27 Yadav SP, Sharma NK, Liu C, Dong L, Li T & Swaroop A (2016) Centrosomal protein CP110 controls maturation of the mother centriole during cilia biogenesis. *Development* **143**, 1491–501.

28 Troilo A, Alexander I, Muehl S, Jaramillo D, Knobeloch K-P & Krek W (2014) HIF1α deubiquitination by USP8 is essential for ciliogenesis in normoxia. *EMBO Rep.* **15**, 77–85.

29 Toriyama M, Kozawa S, Sakumura Y & Inagaki N (2013) *Conversion of a Signal into Forces for Axon Outgrowth through Pak1-Mediated Shootin1 Phosphorylation*.

30 Shimada T, Toriyama M, Uemura K, Kamiguchi H, Sugiura T, Watanabe N & Inagaki N (2008) Shootin1 interacts with actin retrograde flow and L1-CAM to promote axon outgrowth. *J. Cell Biol.* **181**, 817–29.

31 van Haren J, Boudeau J, Schmidt S, Basu S, Liu Z, Lammers D, Demmers J, Benhari J, Grosveld F, Debant A & Galjart N (2014) *Dynamic Microtubules Catalyze Formation of Navigator-TRIO Complexes to Regulate Neurite Extension*.

32 Hatakeyama J, Wald JH, Rafidi H, Cuevas A, Sweeney C & Carraway KL (2016) The ER structural protein Rtn4A stabilizes and enhances signaling through the receptor tyrosine kinase ErbB3. *Sci. Signal.* **9**.

33 Fournier AE, GrandPre T & Strittmatter SM (2001) Identification of a receptor mediating Nogo-66 inhibition of axonal regeneration. *Nature* **409**, 341–346.

34 Toriyama M, Shimada T, Kim KB, Mitsuba M, Nomura E, Katsuta K, Sakumura Y, Roepstorff P & Inagaki N (2006) Shootin1: A protein involved in the organization of an asymmetric signal for neuronal polarization. *J. Cell Biol.* **175**, 147–57.

35 Wald JH, Hatakeyama J, Printsev I, Cuevas A, Fry WHD, Saldana MJ, VanderVorst K, Rowson-Hodel A, Angelastro JM, Sweeney C & Carraway KL (2017) Suppression of planar cell polarity signaling and migration in glioblastoma by Nrdp1-mediated Dvl polyubiquitination. *Oncogene*.

36 Lewandowski KT & Piwnica-Worms H (2014) Phosphorylation of the E3 ubiquitin ligase RNF41 by the kinase Par-1b is required for epithelial cell polarity. *J. Cell Sci.* **127**, 315–27.

37 Balklava Z, Pant S, Fares H & Grant BD (2007) Genome-wide analysis identifies a general requirement for polarity proteins in endocytic traffic. *Nat. Cell Biol.* **9**, 1066–1073.

38 Shaw G, Morse S, Ararat M & Graham FL (2002) Preferential transformation of human neuronal cells by human adenoviruses and the origin of HEK 293 cells. *FASEB J.* **16**, 869–71.

39 Collins BM, McCoy AJ, Kent HM, Evans PR & Owen DJ (2002) Molecular Architecture and Functional Model of the Endocytic AP2 Complex. *Cell* **109**, 523–535.

40 Jackson LP, Kelly BT, McCoy AJ, Gaffry T, James LC, Collins BM, Höning S, Evans PR & Owen DJ (2010) A large-scale conformational change couples membrane recruitment to cargo binding in the AP2 clathrin adaptor complex. *Cell* **141**, 1220–9.

41 Kelly BT, Graham SC, Liska N, Dannhauser PN, Höning S, Ungewickell EJ & Owen DJ (2014) AP2 controls clathrin polymerization with a membrane-activated switch. *Science (80-.).* **345**, 459–463.

42 Motley A, Bright NA, Seaman MNJ & Robinson MS (2003) Clathrin-mediated endocytosis in AP-2-depleted cells. *J. Cell Biol.* **162**, 909–18.

43 Qiu X-B, Markant SL, Yuan J & Goldberg AL (2004) Nrdp1-mediated degradation of the gigantic IAP, BRUCE, is a novel pathway for triggering apoptosis. *EMBO J.* **23**, 800–10.

44 Avvakumov G V, Walker JR, Xue S, Finerty PJ, Mackenzie F, Newman EM & Dhe-Paganon S (2006) Amino-terminal dimerization, NRDP1-rhodanese interaction, and inhibited catalytic domain conformation of the ubiquitin-specific protease 8 (USP8). *J. Biol. Chem.* **281**, 38061–70.

45 Bouyain S & Leahy DJ (2007) Structure-based mutagenesis of the substrate-recognition domain of

Nrdp1/FLRF identifies the binding site for the receptor tyrosine kinase ErbB3. *Protein Sci.* **16**, 654–61.

46 Masschaele D, De Ceuninck L, Wauman J, Defever D, Stenner F, Lievens S, Peelman F & Tavernier J (2017) RNF41 interacts with the VPS52 subunit of the GARP and EARP complexes. *PLoS One* **12**, e0178132.

47 Zhong L, Tan Y, Zhou A, Yu Q & Zhou J (2005) RING finger ubiquitin-protein isopeptide ligase Nrdp1/FLRF regulates parkin stability and activity. *J. Biol. Chem.* **280**, 9425–30.

48 Pohl C & Jentsch S (2008) Regulation of apoptosis and cytokinesis by the anti-apoptotic E2/E3 ubiquitin-ligase BRUCE. *Ernst Schering Found. Symp. Proc.*, 115–26.

49 Pohl C, Jentsch S, Gould GW, Sweeney C, Carraway KL, Ricci R, Peter M, Sanderson CM, Urbe S, Noda T & al. et (2008) Final stages of cytokinesis and midbody ring formation are controlled by BRUCE. *Cell* **132**, 832–45.

50 O'halloran TJ (2000) Membrane Traffic and Cytokinesis. *Traffic* **1**, 921–926.

51 Suizu F, Hiramuki Y, Okumura F, Matsuda M, Okumura AJ, Hirata N, Narita M, Kohno T, Yokota J, Bohgaki M, Obuse C, Hatakeyama S, Obata T & Noguchi M (2009) The E3 Ligase TTC3 Facilitates Ubiquitination and Degradation of Phosphorylated Akt. *Dev. Cell* **17**, 800–810.

52 Fukushima T, Zapata JM, Singha NC, Thomas M, Kress CL, Krajewska M, Krajewski S, Ronai Z, Reed JC & Matsuzawa S (2006) Critical Function for SIP, a Ubiquitin E3 Ligase Component of the β-Catenin Degradation Pathway, for Thymocyte Development and G1 Checkpoint. *Immunity* **24**, 29–39.

53 Itakura E & Mizushima N (2011) p62 Targeting to the autophagosome formation site requires self-oligomerization but not LC3 binding. *J. Cell Biol.* **192**, 17–27.

54 Wurzer B, Zaffagnini G, Fracchiolla D, Turco E, Abert C, Romanov J & Martens S (2015) Oligomerization of p62 allows for selection of ubiquitinated cargo and isolation membrane during selective autophagy. *Elife* **4**.

55 Bjørkøy G, Lamark T, Brech A, Outzen H, Perander M, Overvatn A, Stenmark H & Johansen T (2005) p62/SQSTM1 forms protein aggregates degraded by autophagy and has a protective effect on huntingtin-induced cell death. *J. Cell Biol.* **171**, 603–14.

56 Lamb CA, Yoshimori T & Tooze SA (2013) The autophagosome: origins unknown, biogenesis complex. *Nat. Rev. Mol. Cell Biol.* **14**, 759–774.

57 Carlsson SR & Simonsen A (2015) Membrane dynamics in autophagosome biogenesis. *J. Cell Sci.* **128**, 193–205.

58 Moreau K, Ravikumar B, Puri C & Rubinsztein DC (2012) Arf6 promotes autophagosome formation via effects on phosphatidylinositol 4,5-bisphosphate and phospholipase D. *J. Cell Biol.* **196**, 483–96.

59 Paleotti O, Macia E, Luton F, Klein S, Partisani M, Chardin P, Kirchhausen T & Franco M (2005) The Small G-protein Arf6 GTP Recruits the AP-2 Adaptor Complex to Membranes. *J. Biol. Chem.* **280**, 21661–21666.

60 Ravikumar B, Moreau K & Rubinsztein DC (2010) Plasma membrane helps autophagosomes grow. *Autophagy* **6**, 1184–6.

61 Ravikumar B, Moreau K, Jahreiss L, Puri C & Rubinsztein DC (2010) Plasma membrane contributes to the formation of pre-autophagosomal structures. *Nat. Cell Biol.* **12**, 1021–1021.

62 Lau AW & Chou MM (2008) The adaptor complex AP-2 regulates post-endocytic trafficking through the non-clathrin Arf6-dependent endocytic pathway. *J. Cell Sci.* **121**.

63 Wang C, Chen T, Zhang J, Yang M, Li N, Xu X & Cao X (2009) The E3 ubiquitin ligase Nrdp1 "preferentially" promotes TLR-mediated production of type I interferon. *Nat. Immunol.* **10**, 744–52.

64 Ma X, Helgason E, Phung QT, Quan CL, Iyer RS, Lee MW, Bowman KK, Starovasnik MA & Dueber EC (2012) Molecular basis of Tank-binding kinase 1 activation by transautophosphorylation. *Proc. Natl. Acad. Sci. U. S. A.* **109**, 9378–83.

65 Matsumoto G, Shimogori T, Hattori N & Nukina N (2015) TBK1 controls autophagosomal engulfment of polyubiquitinated mitochondria through p62/SQSTM1 phosphorylation. *Hum. Mol. Genet.* **24**, 4429–42.

66 Matsumoto G, Wada K, Okuno M, Kurosawa M & Nukina N (2011) Serine 403 phosphorylation of p62/SQSTM1 regulates selective autophagic clearance of ubiquitinated proteins. *Mol. Cell* **44**, 279–89.

67 Tu D, Zhu Z, Zhou AY, Yun C, Lee K-E, Toms A V, Li Y, Dunn GP, Chan E, Thai T, Yang S, Ficarro SB, Marto JA, Jeon H, Hahn WC, Barbie DA & Eck MJ (2013) Structure and ubiquitination-dependent activation of TANK-binding kinase 1. *Cell Rep.* **3**, 747–58.

68 Song P, Li S, Wu H, Gao R, Rao G, Wang D, Chen Z, Ma B, Wang H, Sui N, Deng H, Zhang Z, Tang T, Tan Z, Han Z, Lu T, Zhu Y & Chen Q (2016) Parkin promotes proteasomal degradation of p62: implication of selective vulnerability of neuronal cells in the pathogenesis of Parkinson's disease. *Protein Cell* **7**, 114–29.

69 Narendra D, Tanaka A, Suen D-F & Youle RJ (2008) Parkin is recruited selectively to impaired mitochondria and promotes their autophagy. *J. Cell Biol.* **183**.

70 Soleimanpour SA, Gupta A, Bakay M, Ferrari AM, Groff DN, Fadista J, Spruce LA, Kushner JA, Groop L,

Seeholzer SH, Kaufman BA, Hakonarson H & Stoffers DA (2014) The diabetes susceptibility gene Clec16a regulates mitophagy. *Cell* **157**, 1577–90.

71 Durcan TM, Tang MY, Pérusse JR, Dashti EA, Aguileta MA, McLelland G-L, Gros P, Shaler TA, Faubert D, Coulombe B & Fon EA (2014) USP8 regulates mitophagy by removing K6-linked ubiquitin conjugates from parkin. *EMBO J.* **33**, 2473–91.

72 Lamark T & Johansen T (2012) Aggrephagy: Selective Disposal of Protein Aggregates by Macroautophagy. *Int. J. Cell Biol.* **2012**, 1–21.

73 Chin L-S, Olzmann JA & Li L (2010) Parkin-mediated ubiquitin signalling in aggresome formation and autophagy. *Biochem. Soc. Trans.* **38**, 144–9.

74 Zhang A (2009) *Protein Interaction Networks: computational analysis*, 1st ed. Cambridge University Press, New York, NY, USA.

75 Zhong Q, Simonis N, Li Q-R, Charloteaux B, Heuze F, Klitgord N, Tam S, Yu H, Venkatesan K, Mou D, Swearingen V, Yildirim MA, Yan H, Dricot A, Szeto D, Lin C, Hao T, Fan C, Milstein S, Dupuy D, Brasseur R, Hill DE, Cusick ME, Vidal M, Ball C, Dolinski K, Dwight S, Harris M, Issel-Tarver L, Kasarskis A, Scafe C, Sherlock G, Binkley G, Jin H, Kaloper M, Orr S, Schroeder M, Weng S, Zhu Y, Botstein D, Cherry J, Botstein D, Risch N, Braun P, Tasan M, Dreze M, Barrios-Rodiles M, Lemmens I, Yu H, Sahalie J, Murray R, Roncari L, Smet A de, Venkatesan K, Rual J, Vandenhaute J, Cusick M, Pawson T, Hill D, Tavernier J, Wrana J, Roth F, Vidal M, Chenna R, Sugawara H, Koike T, Lopez R, Gibson T, Higgins D, Thompson J, Chik J, Lindberg U, Schutt C, Day P, Cleasby A, Tickle I, O'Reilly M, Coyle J, Holding F, McMenamin R, Yon J, Chopra R, Lengauer C, Jhoti H, Finn R, Mistry J, Schuster-Bockler B, Griffiths-Jones S, Hollich V, Lassmann T, Moxon S, Marshall M, Khanna A, Durbin R, Eddy S, Sonnhammer E, Bateman A, Goh K, Cusick M, Valle D, Childs B, Vidal M, Barabasi A, Gunsalus K, Yueh W, MacMenamin P, Piano F, Hamosh A, Scott A, Amberger J, Bocchini C, McKusick V, Harris M, Clark J, Ireland A, Lomax J, Ashburner M, Foulger R, Eilbeck K, Lewis S, Marshall B, Mungall C, Richter J, Rubin G, Blake J, Bult C, Dolan M, Drabkin H, Eppig J, Hill D, Ni L, Ringwald M, Hsu W, Pang C, Sheetal J, Wilkins M, Jeffrey P, Tong L, Pavletich N, Lamesch P, Li N, Milstein S, Fan C, Hao T, Szabo G, Hu Z, Venkatesan K, Bethel G, Martin P, Rogers J, Lawlor S, McLaren S, Dricot A, Borick H, Cusick M, Vandenhaute J, Dunham I, Hill D, Vidal M, Lassing I, Schmitzberger F, Bjornstedt M, Holmgren A, Nordlund P, Schutt C, Lindberg U, Maglott D, Ostell J, Pruitt K, Tatusova T, Meier M, Janosik M, Kery V, Kraus J, Burkhard P, Mihel J, Sikic M, Tomic S, Jeren B, Vlahovicek K, Rual J, Venkatesan K, Hao T, Hirozane-Kishikawa T, Dricot A, Li N, Berriz G, Gibbons F, Dreze M, Ayivi-Guedehoussou N, Klitgord N, Simon C, Boxem M, Milstein S, Rosenberg J, Goldberg D, Zhang L, Wong S, Franklin G, Li S, Sammut S, Finn R, Bateman A, Schuster-Böckler B, Bateman A, Schutt C, Myslik J, Rozycki M, Goonesekere N, Lindberg U, Seidman J, Seidman C, Stenson P, Ball E, Mort M, Phillips A, Shiel J, Thomas N, Abeysinghe S, Krawczak M, Cooper D, Subramanian S, Kumar S, Suzuki Y, Kagawa N, Fujino T, Sumiya T, Andoh T, Ishikawa K, Kimura R, Kemmochi K, Ohta T, Tanaka S, Titus G, Mueller H, Burgner J, Cordoba SR De, Penalva M, Timm D, Bokhoven H van, Brunner H, Venkatesan K, Rual J, Vazquez A, Stelzl U, Lemmens I, Hirozane-Kishikawa T, Hao T, Zenkner M, Xin X, Goh K, Yildirim M, Simonis N, Heinzmann K, Gebreab F, Sahalie J, Cevik S, Simon C, Smet A de, Dann E, Smolyar A, Wang G, Dunbrack R, Wang Z, Moult J, Wilkie A, Wilson D, Charoensawan V, Kummerfeld S, Teichmann S, Wilson R, Goodman J, Strelets V, Ye Y, Li Z, Godzik A, Yue P, Li Z & Moult J (2009) Edgetic perturbation models of human inherited disorders. *Mol. Syst. Biol.* **5**, 321.

76 Ye S, Xu H, Jin J, Yang M, Wang C, Yu Y & Cao X (2012) The E3 ubiquitin ligase neuregulin receptor degradation protein 1 (Nrdp1) promotes M2 macrophage polarization by ubiquitinating and activating transcription factor CCAAT/enhancer-binding Protein β (C/EBPβ). *J. Biol. Chem.* **287**, 26740–8.

77 Van Impe K, Bethuyne J, Cool S, Impens F, Ruano-Gallego D, De Wever O, Vanloo B, Van Troys M, Lambein K, Boucherie C, Martens E, Zwaenepoel O, Hassanzadeh-Ghassabeh G, Vandekerckhove J, Gevaert K, Fernández LÁ, Sanders NN & Gettemans J (2013) A nanobody targeting the F-actin capping protein CapG restrains breast cancer metastasis. *Breast Cancer Res.* **15**, R116.

78 Van Audenhove I, Boucherie C, Pieters L, Zwaenepoel O, Vanloo B, Martens E, Verbrugge C, Hassanzadeh-Ghassabeh G, Vandekerckhove J, Cornelissen M, De Ganck A & Gettemans J (2014) Stratifying fascin and cortactin function in invadopodium formation using inhibitory nanobodies and targeted subcellular delocalization. *FASEB J.* **28**, 1805–1818.

79 Kaiser PD, Maier J, Traenkle B, Emele F & Rothbauer U (2014) Recent progress in generating intracellular functional antibody fragments to target and trace cellular components in living cells. *Biochim. Biophys. Acta - Proteins Proteomics* **1844**, 1933–1942.

80 Yen L, Cao Z, Wu X, Ingalla ERQ, Baron C, Young LJT, Gregg JP, Cardiff RD, Borowsky AD, Sweeney C & Carraway KL (2006) Loss of Nrdp1 enhances ErbB2/ErbB3-dependent breast tumor cell growth. *Cancer Res.* **66**, 11279–86.

81 Ingalla EQ, Miller JK, Wald JH, Workman HC, Kaur RP, Yen L, Fry WHD, Borowsky AD, Young LJT, Sweeney C & Carraway KL (2010) Post-transcriptional mechanisms contribute to the suppression of the ErbB3 negative regulator protein Nrdp1 in mammary tumors. *J. Biol. Chem.* **285**, 28691–7.

82 Jiao S, Liu W, Wu M, Peng C, Tang H & Xie X (2015) Nrdp1 expression to predict clinical outcome and efficacy of adjuvant anthracyclines-based chemotherapy in breast cancer: A retrospective study. *Cancer Biomarkers* **15**, 115–123.

83 Chen L, Siddiqui S, Bose S, Mooso B, Asuncion A, Bedolla RG, Vinall R, Tepper CG, Gandour-Edwards R, Shi X, Lu X-H, Siddiqui J, Chinnaiyan AM, Mehra R, Devere White RW, Carraway KL & Ghosh PM (2010) Nrdp1-mediated regulation of ErbB3 expression by the androgen receptor in androgen-dependent but not castrate-resistant prostate cancer cells. *Cancer Res.* **70**, 5994–6003.

84 Savoy RM, Chen L, Siddiqui S, Melgoza FU, Durbin-Johnson B, Drake C, Jathal MK, Bose S, Steele TM, Mooso BA, D'Abronzo LS, Fry WH, Carraway KL, Mudryj M, Ghosh PM & Ghosh PM (2015) Transcription of Nrdp1 by the androgen receptor is regulated by nuclear filamin A in prostate cancer. *Endocr. Relat. Cancer* **22**, 369–386.

85 Brizzolara A, Benelli R, Venè R, Barboro P, Poggi A, Tosetti F & Ferrari N (2017) The ErbB family and androgen receptor signaling are targets of Celecoxib in prostate cancer. *Cancer Lett.* **400**, 9–17.

86 Shi H, Gong H, Cao K, Zou S, Zhu B, Bao H, Wu Y, Gao Y, Tang Y & Yu R (2015) Nrdp1-mediated ErbB3 degradation inhibits glioma cell migration and invasion by reducing cytoplasmic localization of p27Kip1. *J. Neurooncol.* **124**, 357–364.

87 Wu Y, Wang L, Bao H, Zou S, Fu C, Gong H, Gao Y, Tang Y, Yu R & Shi H (2016) Nrdp1S, short variant of Nrdp1, inhibits human glioma progression by increasing Nrdp1-mediated ErbB3 ubiquitination and degradation. *J. Cell. Mol. Med.* **20**, 422–9.

88 Cao K, Gong H, Qiu Z, Wen Q, Zhang B, Tang T, Zhou X, Cao T, Wang B, Shi H & Wang R (2016) Hepatitis B virus X protein reduces the stability of Nrdp1 to up-regulate ErbB3 in hepatocellular carcinoma cells. *Tumor Biol.* **37**, 10375–10382.

89 Shi H, Du J, Wang L, Zheng B, Gong H, Wu Y, Tang Y, Gao Y & Yu R (2014) Lower expression of Nrdp1 in human glioma contributes tumor progression by reducing apoptosis. *IUBMB Life* **66**, 704–710.

90 Byun S, Shin SH, Lee E, Lee J, Lee S-Y, Farrand L, Jung SK, Cho Y-Y, Um S-J, Sin H-S, Kwon Y-J, Zhang C, Tsang BK, Bode AM, Lee HJ, Lee KW & Dong Z (2015) The retinoic acid derivative, ABPN, inhibits pancreatic cancer through induction of Nrdp1. *Carcinogenesis* **36**, 1580–1589.

91 Chen S-J, Lin J-H, Yao X-D, Peng B, Xu Y-F, Liu M & Zheng J-H (2016) Nrdp1-mediated degradation of BRUCE decreases cell viability and induces apoptosis in human 786-O renal cell carcinoma cells. *Exp. Ther. Med.* **12**, 597–602.

92 Yu F & Zhou J (2008) Parkin is ubiquitinated by Nrdp1 and abrogates Nrdp1-induced oxidative stress. *Neurosci. Lett.* **440**, 4–8.

93 Tan Y, Yu F, Pereira A, Morin P & Zhou J (2011) *Suppression of Nrdp1 toxicity by Parkin in Drosophila models*.

94 Bowers WJ, Breakefield XO & Sena-Esteves M (2011) Genetic therapy for the nervous system. *Hum. Mol. Genet.* **20**, R28–R41.

95 Steeland S, Vandenbroucke RE & Libert C (2016) Nanobodies as therapeutics: big opportunities for small antibodies. *Drug Discov. Today* **21**, 1076–1113.

96 Yang ZJ, Chee CE, Huang S & Sinicrope FA (2011) The Role of Autophagy in Cancer: Therapeutic Implications. *Mol. Cancer Ther.* **10**, 1533–1541.

97 Puissant A, Fenouille N & Auberger P (2012) When autophagy meets cancer through p62/SQSTM1. *Am. J. Cancer Res.* **2**, 397–413.

Addendum

KISS, a mammalian two-hybrid method for in situ analysis of protein-protein interactions

This manuscript describes a detailed protocol for KISS (Kinase Substrate Sensor), a MAPPIT (Mammalian Protein-Protein interaction trap) derived two-hybrid technology that allows in situ detection of protein-protein interactions in intact mammalian cells.

Cover page

Author: Delphine Masschaele; Affiliation: VIB-Ugent, Center for Medical Biotechnology

Author: Sarah Gerlo; Affiliation: VIB-Ugent, Center for Medical Biotechnology

Author: Irma Lemmens; Affiliation: VIB-Ugent, Center for Medical Biotechnology

Author: Sam Lievens; Affiliation: VIB-Ugent, Center for Medical Biotechnology

Corresponding author: Jan Tavernier; Affiliation: VIB-Ugent, Center for Medical Biotechnology; email: jan.tavernier@vib-ugent.be

Running Head: KISS, a mammalian protein interaction sensor

KISS, a mammalian two-hybrid method for in situ analysis of protein-protein interactions

Delphine Masschaele, Sarah Gerlo, Irma Lemmens, Sam Lievens and Jan Tavernier

Abstract

KISS (KInase Substrate Sensor) is a recently developed two-hybrid technology that allows in situ analysis of protein-protein interactions in intact mammalian cells. In this method, which is derived from MAPPIT (MAmmalian Protein-Protein Interaction Trap), the bait protein is coupled to the kinase domain of TYK2, while the prey protein is fused to a fragment of the gp130 cytokine receptor chain. Bait and prey interaction leads to phosphorylation of the gp130 anchor by TYK2, followed by recruitment and activation of STAT3, resulting in transcription of a STAT3-dependent luciferase reporter system. This approach enables the identification of interactions between proteins, including transmembrane and cytosolic proteins, and their modulation in response to physiological or pharmacological challenges. Here, we describe a detailed step-by-step protocol for the detection of an interaction between two proteins of interest using KISS.

Key words
KISS, interactomics, protein-protein interaction, MAPPIT, membrane proteins, two-hybrid

1. Introduction

Our lab previously developed the two-hybrid technology MAPPIT (MAmmalian Protein-Protein Interaction Trap) to detect PPIs (protein-protein interactions) in intact mammalian cells *(1)*. MAPPIT is based on the functional complementation of the JAK-STAT (Janus kinases-signal transducers and activators of transcription) signaling pathway of type I cytokine receptors upon bait and prey interaction. In this assay the bait protein is coupled to a signaling-deficient chimeric receptor comprising the extracellular domain of the EpoR (erythropoietin receptor) and the transmembrane domain and cytoplasmic tail of the LepR (leptin receptor). The three conserved tyrosine residues in the cytoplasmic tail of the LepR are mutated to phenylalanine, thereby eliminating STAT3 recruitment (Y1138F) and negative-feedback mechanisms (Y985F and Y1077F). The prey protein is fused to a C-terminal portion of the gp130 (glycoprotein 130) receptor, containing functional STAT3 recruitment sites. Upon ligand binding, bait and prey interaction leads to trans-phosphorylation and activation of the associated JAKs. In turn, JAKs phosphorylate the prey chimera followed by recruitment and activation of STAT3. STAT's dimerize and migrate to the nucleus resulting in transcriptional activation of a luciferase reporter gene (Fig. 1a). An important limitation of MAPPIT is the fact that genetic fusions of full size transmembrane proteins with the cytokine receptor portion of the chimeric bait are mostly dysfunctional. In addition, MAPPIT samples PPIs in the cytoplasm, close to cell membrane, which for many baits is not their native cellular environment. To overcome these shortcomings, KISS (KInase Substrate Sensor), a binary mapping approach enabling *in situ* analysis of PPIs in mammalian cells, was developed *(2)*. In this method, the prey protein is fused to the gp130 anchor, similar to the MAPPIT prey chimera, while the bait protein is coupled to a C-terminal, kinase-containing portion of TYK2 (tyrosine kinase 2). Importantly, the Tyk2 kinase does not provide a subcellular localization signal and hence localization of chimeric KISS baits is strictly determined by sequences present in the specific bait. As the name KISS suggests, upon bait-prey interaction, the TYK2 domain (kinase) phosphorylates both the STAT3 docking sites of the gp130 anchor and STAT3 (substrates). This results in STAT3 dimerization, migration and luciferase reporter gene activation, identical to MAPPIT (Fig. 1b).
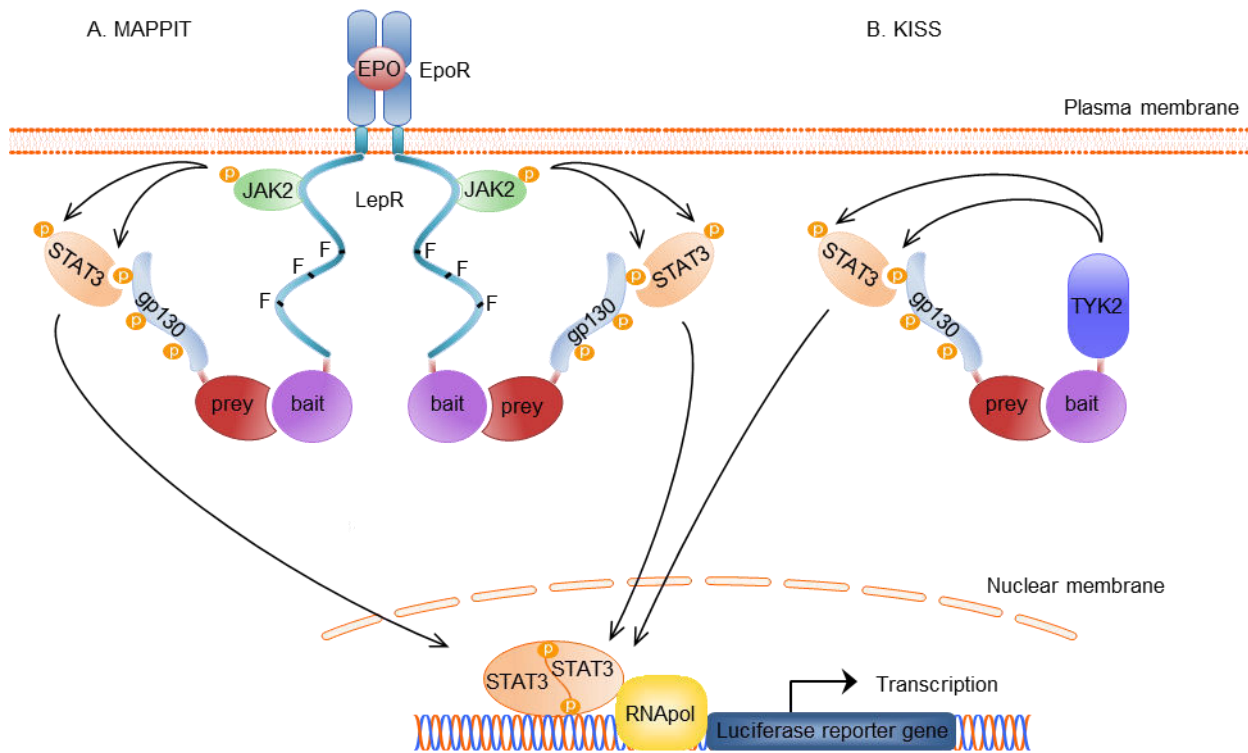
Fig 1. Principle of MAPPIT and KISS. (a) MAPPIT. The MAPPIT bait is coupled to a signaling-deficient chimeric receptor, lacking STAT3 recruitment sites. The prey is fused to the gp130 anchor. Upon ligand stimulation, bait-prey interaction leads to phosphorylation and recruitment of STAT3 to the gp130 anchor, thereby complementing the JAK-STAT signaling pathway, resulting in luciferase reporter gene activation. (b) KISS. The KISS bait is fused to the kinase-containing portion of TYK2, while the prey is coupled to the gp130 anchor, similar to MAPPIT. Bait-prey interaction leads to STAT3 phosphorylation resulting in luciferase reporter gene activation. EpoR, erythropoetin receptor; LepR, leptin receptor; JAK, Janus kinase; gp130, glycoprotein 130; STAT, signal transducer and activator of transcription 3; TYK2, tyrosine kinase 2.

KISS has been shown to detect interactions between p51 and p66, two cytosolic subunits of the HIV-1 RT (human immunodeficiency virus 1 reverse transcriptase), as well as interactions involving transmembrane proteins, like GPCRs (G-protein coupled receptors) and ERN1 (endoplasmic reticulum to nucleus signaling 1). Recruitment of ARRB2 (β-arrestin2) to SSTR2 (somatostatin receptor 2) or AGTR1 (angiotensin receptor 1) upon addition of their respective ligand, combined with specific inhibition of this signal when adding their proper antagonists indicates that KISS can be used to study modulations of ligand-dependent interactions. Next to indirect pharmacological interference, direct PPI disruptors such as Nutlin-3 and ABT-737, which respectively interfered with the KISS interaction between p53 (tumor protein p53) and MDM2 (human homolog of mouse double minute 2), and BCL2 (B-cell lymphoma 2) and BAD (BCL-2-associated agonist of cell death) can also be assayed with this method. In addition, KISS successfully detected enhanced oligomerization of ERN1 upon ER stress induced with tunicamycin, further illustrating the potential of this method to evaluate PPI modulations in complex cellular processes. Moreover, the ERN1 bait and prey fusion proteins correctly localized to the ER, demonstrating the *in situ* behavior of this PPI sensor.

Importantly, not only does KISS extend the repertoire and complexity of PPIs that can be detected with MAPPIT, it still offers the same advantages. The system operates in living mammalian cells,

which allows the detection of interactions relying on PTMs (post-translational modifications). Moreover, signal amplification via the luciferase reporter read-out results in a high signal-to-noise ratio and enables the detection of weak and transient interactions. Benchmarking experiments using the previously established PRS (positive reference set) and RRS (random reference set) *(3)* validated the method's specificity and sensitivity, which was comparable to that of MAPPIT, Y2H (yeast two-hybrid), LUMIER (luminescence-based mammalian interactome mapping), wNAPPA (a variant of nucleic acid programmable protein array) and a YFP (yellow fluorescent)-based PCA (protein fragment complementation assay). These scores could be even higher, if the reference sets, with approximately 35% of membrane proteins, were more enriched for these types of proteins. As reported for other assays *(3, 4)*, KISS also detected a different subset of PPIs.

Since the preys in MAPPIT and KISS are identical, we can adopt the entire prey collection, derived from the huORF (human open reading frame) collection (± 15.000 full size ORFs), which was used for arrayMAPPIT and microarrayMAPPIT *(5, 6)*. This, together with a downscaling of the method with the help of robotics from a 96-well to a 384-well, or even a cell-microarray format, covering 6912 spots per plate, creates the possibility of using KISS as a high-throughput screening method. Furthermore, similar to the three-hybrid MAPPIT setup, MASPIT *(7, 8)*, a three-hybrid variant of KISS was developed that allows screening for interactions between small molecules and integral membrane target proteins in a physiological relevant environment. Here, the small molecule is introduced as a bait inside the cell by means of chemical tethering to MTX (methotrexate) which binds eDHFR (*E. coli* dihydrofolate reductase) fused to the TYK2 kinase domain. This system validated the interaction between the drugs FK506 and simvastatin and their respective protein targets FKBP12 (FK506 binding protein) and HMGCR (3-hydroxy-3-methylglutaryl-CoA reductase), which illustrates its potential as new drug-screening platform *(2)*.

Here, we outline a standard KISS protocol that allows *in situ* detection of both cytosolic and transmembrane protein interactions and their responses to physiological or pharmacological challenges in 96-well plate format. In brief, this protocol describes the cloning of the appropriate KISS bait and prey plasmids, transfection of the necessary constructs in HEK293T cells, an optional stimulation step depending on the interaction of interest followed by luciferase reporter activity measurement. This binary assay can be performed in 4 days from seeding the cells up to the signal readout, using standard molecular and cell biological research equipment.

2. Materials

2.1 Plasmids
1. Bait plasmid:
The KISS bait vector pMT comprises the protein of interest C-terminally fused to a fragment of human TYK2 (AA589-1187) followed by an HA-tag in a pMET7 mammalian expression vector containing the SRα promotor. Alternately, other backbone vectors and configurations, depending on the topology of your protein of interest, can be used for cloning (*see* **Note 1**, *(2)*).
2. Prey plasmid: The pMG1 constructs used for MAPPIT experiments are suitable for KISS. These pMET7 backbone vectors contain the prey protein of interest N-terminally coupled to a FLAG-tagged part of the gp130 (glycoprotein 130; AA 760-918) *(1)*.
3. Luciferase reporter plasmid: the pXP2d2-rPAP1-luci construct, controlled by a STAT3-responsive rPAP1 (rat Pancreatitis Associated Protein 1) promotor *(1)*.
4. Thermal cycler

2.2 Cell culture
1. 96-well black tissue-culture plates. Clear bottom plates can be used for microscopic inspection of cells and transfection precipitate.
2. HEK (human embryonic kidney) 293 T cells.
3. Culture medium: DMEM (Dulbecco's modified Eagle's medium) supplemented with 10% fetal calf serum. Antibiotics (gentamycin or penicillin/streptomycin) can be added to avoid contamination.
4. Agonists or antagonists, for KISS experiments that involve treatment.

2.3 Transfection
The standard calcium phosphate transfection method is applied for transfecting HEK293T cells.
1. $CaCl_2$ buffer: prepare a 2.5 M $CaCl_2$ stock solution in distilled water. Filter-sterilize (0.45 μM nitrocellulose membrane) and store at -20°C.
2. 2x HeBS (Hepes-buffered saline) buffer: prepare 280 mM NaCl, 1.5 mM Na_2HPO_4 and 50 mM Hepes in 90 ml of distilled water. Adjust the pH to 7.05 with 1 M NaOH and adjust the volume to 100 ml. Filter-sterilize (0.45 μM nitrocellulose membrane) and store at -20°C.

2.4 Luciferase assay
1. Lysis buffer: prepare 25 mM Tris-phosphate, pH 7.8, 2 mM DTT, 2 mM CDTA (*trans*-1,2-diaminocyclohexane- *N,N,N',N'*-tetraacetic acid), 10% glycerol and 1% Triton X-100 in 500ml of distilled water. Aliquot into 50-ml volumes and store at -20°C.
2. Luciferase substrate buffer: prepare 40 mM Tricine, 2.14 mM $(MgCO_3)_4Mg(OH)_2.5H_2O$, 5.34 mM $MgSO_4$, 66.6 mM DTT, 0.2 mM EDTA, 509 μM Coenzyme A, 734 μM ATP and 940 μM D-luciferin in 500 ml of distilled water. Aliquot into 50-ml volumes, store at -20°C and protect from light as the reagent is light sensitive.
3. Chemiluminescence meter suitable for 96-well format measurement

3. Methods

3.1 Cloning bait and prey of interest

1. Design primers flanking your gene of interest that contain restriction sites compatible to the sites in the pMT bait or pMG1 prey vector. Cloning of the bait protein in the pMT vector requires the EcoRI and SalI restriction sites, while the prey protein can be cloned in the pMG1 vector using EcoRI and NotI or XbaI (Fig. 2).

2. Carry out a PCR (Polymerase Chain Reaction) using a DNA polymerase with proof-reading activity (Pfu or high-fidelity Q5) in a thermal cycler.

3. Digest your DNA, isolate your vector and insert by gel purification and ligate your insert in the designated vector to obtain the desired bait and prey construct.

4. Transform your ligation product into a bacterial line (e.g. DH10B)

5. Pick single colonies and prepare plasmid DNA of a quality suitable for transfection. Check and verify the plasmids by restriction digest or sequencing (*see* **Note 2**).
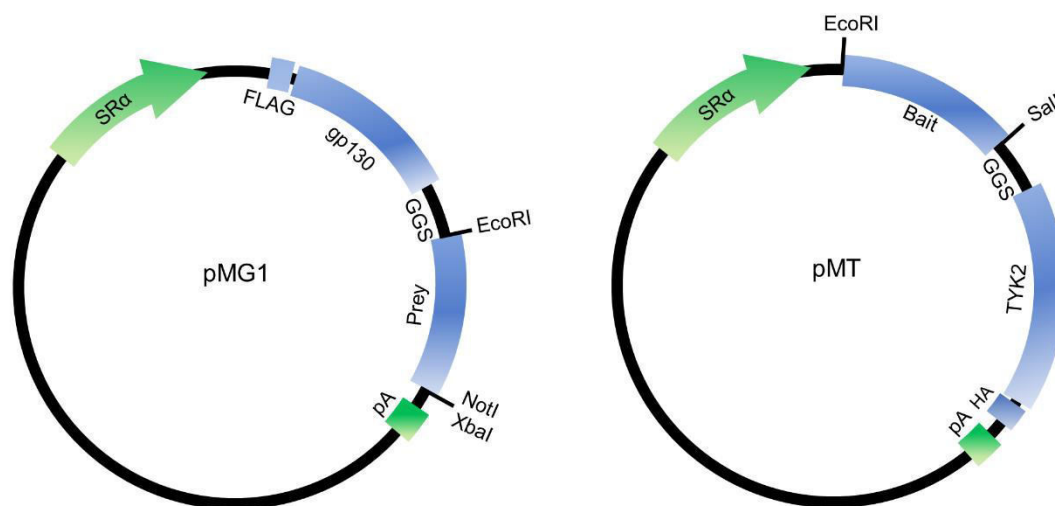
Fig 2. KISS prey and bait plasmid. The pMG1 plasmid is used for cloning of the prey. The prey protein of interest is N-terminally fused to a FLAG-tagged portion of the gp130 cytokine receptor with the help of EcoRI and NotI or XbaI restriction sites. A GGS hinge (glycine-glycine-serine) is placed between the gp130 anchor and the prey for more flexibility. The pMT plasmid is used for bait cloning. The bait protein of interest is C-terminally fused to the kinase containing fragment of TYK2, followed by a HA tag using EcoRI and SalI restriction sites. Also here, the GSS hinge alows for more flexibility. gp130, glycoprotein 130; SRα, promotor consisting of SV40 (simian virus 40 early promotor) and the R-U5 segment of human T-cell leukemia virus type 1 long terminal repeat; pA, SV40 polyadenylation signal.

3.2 Seeding cells (day 1)

1. Seed 5×10^3 HEK293T cells per well in a 96-well plate in 100 µl of culture medium (*see* **Notes 3, 4** and **5**). Each bait-prey interaction is tested in three wells. When using agonists/antagonists or compounds to stimulate or modulate the interaction, use an additional three wells per condition. The relevant controls for possible background include an irrelevant or empty prey for each bait tested and an irrelevant or empty bait for each prey tested.
2. Incubate overnight at 37°C and 5-8% CO_2.

3.3 Transfection of cells (day 2)

1. For each bait-prey interaction, make a mixture of DNA and $CaCl_2$ containing 6,25 ng of the bait plasmid, 12,5 ng of the prey plasmid, and 5 ng of the rPAP1-luci reporter together with 5µl of sterile 2.5M $CaCl_2$ in a total volume of 50µl of distilled water per well in a 96-well plate, the 'mix' plate (*see* **Note 6**).
2. Add 50 µl of 2x HeBS to each well of the mix plate (*see* **Note 7**).
3. Shake the mix plate for 1 min at 800 rpm
4. Resuspend the wells of the mix plate
5. Add 10 µl to the cells in the 96-well plate in triplicate for every bait-prey interaction.
6. In case you used clear bottom-plates, check the precipitates under a conventional light microscope. You should be able to see small speckles surrounding your cells in the plate.
7. Incubate the cells overnight at 37°C and 5-8% CO_2

3.4 Stimulation of cells with agonist/antagonist or compound (optional) (day 3)

1. For bait-prey interactions where agonist/antagonist or treatment is used, stimulate the three extra wells with 50 µl of your agonist/antagonist or compound diluted in culture medium (*see* **Note 8**). Add 50 µl of culture medium in the wells with the same bait-prey interaction that are left unstimulated.
2. Incubate the cells overnight at 37°C and 5-8 % CO_2.

3.5 Luciferase read-out (day 4)

1. Remove culture medium from the 96-well plates.
2. Add 50 µl of lysis buffer to each well and incubate for 10 min at room temperature (*see* **Note 9**).
3. Add 35 µl of luciferase substrate buffer to each well and immediately measure luciferase activity using a chemiluminescence meter.

3.6 Data analysis

1. For every bait-prey interaction, calculate the fold induction value by dividing the average of the triplicate luciferase counts of the specific bait-prey interaction by the average of the triplicate luciferase counts obtained for the interaction of that specific bait with an empty/irrelevant prey. In case you investigate the effect of a treatment on a PPI, you can calculate the fold induction for each bait-prey interaction by dividing the mean value of the stimulated wells by the mean value of the non-stimulated wells. In addition, compare the fold induction for the specific bait-prey interaction to that obtained for the interaction of an empty/irrelevant bait with the specific prey.

2. A bait-prey interaction is considered positive, if the fold induction value is at least three times higher than both the fold induction of the bait-empty/irrelevant prey and the empty/irrelevant bait-prey interactions.

4. Notes

1. Depending on the protein of interest, better fold inductions can be obtained when using an alternative bait backbone vector such as the pSVSport. This carries the weak early SV40 promotor giving rise to low expression levels in cells, which can lead to higher fold inductions. Alternatively the pcDNA5/FRT plasmid can be used. Although this contains the strong CMV promotor, it can be advantageous as it is designed for the use with Flp-in™ systems thereby creating stable cell lines which can be useful for high-throughput screening. To further increase the fold induction signal, a pMG2 prey construct can be used, containing the gp130 anchor in duplicate *(9)*. However, next to an increased fold induction, this can also elevate the background signal. To further optimize your bait and prey interaction, different configurations can be tested to reduce steric hindrance of the tag or to preclude incorrect location of your protein. For this, the bait or prey protein can be N-terminally or C-terminally fused to the TYK2 domain or gp130 anchor respectively. In case of type I, III and IV transmembrane proteins, a C-terminal TYK2 or gp130 fusion should be used, whereas an N-terminal fusion is necessary for type II transmembrane proteins. Furthermore, all bait and prey backbone vectors can be made compatible for Gateway recombination cloning by inserting the Gateway Reading Frame Cassette B from the Gateway Vector Conversion System (Invitrogen) into the vectors. In this way, all ORFs from the huORF collection *(10)* can easily be cloned into the designated bait or prey vectors using an LR clonase reaction, thereby greatly facilitating the cloning process.

2. It is favorable to check the subcellular location of your bait and prey fusion protein with confocal microscopy as tags can sometimes interfere with the native location of proteins. The used bait and prey vectors contain an HA and FLAG-tag respectively, which simplify confocal imaging of the proteins.

3. Like for MAPPIT, the KISS strategy is not restricted to HEK293T cells, other easy transfectable cell lines can be used that contain a sufficient amount of endogenous STAT3 (e.g. erythroleukaemia TF-1 or N38 hypothalamic cell lines *(11, 12)*) which may provide a more physiological setting to study your protein-protein interaction.

4. Make sure your cells are in a logarithmic growth phase and are kept subconfluent at all times (maximum density of 20×10^6 cells per 175-cm^2 flask). 'Unhealthy' cells can greatly affect transfection efficiencies.

5. We tend to not use the outside rows and columns of the 96-well plate. These wells are filled with culture medium as they are prone to evaporation during the incubation process which can possibly skew the results.

6. Depending on your protein-protein interaction, different amounts of bait and prey DNA can lead to a higher fold induction. We have noticed that low amounts of DNA often yield higher signals, usually due to a reduced background.

7. The pH of the 2x HeBS buffer is critical for transfection efficiency (optimal range between 7.05 and 7.12), avoid repeated freeze-thaw cycles to maintain this pH. Also, it is important

not to wait too long before adding the DNA precipitates to the cells after the 1 minute of shaking in the mix plate, as long incubation time can reduce the transfection efficiency.

8. A reduced fold induction can be due to toxicity of the added treatment. Therefore, check the toxicity of your compound and perform a dose-response analysis of the interaction upon treatment. If your compound is dissolved in a reagent such as DMSO, which can be toxic for the cells, then add the same amount of reagent diluted in culture medium to the unstimulated wells. An extra control to check whether your treatment does not affect STAT3 signaling is to additionally stimulate your cells with LIF (leukaemia inhibitory factor) since the LIFR, which is endogenously present in HEK293T cells, also operates via STAT3 signaling.

9. After lysis, plates can be stored at -20°C for a few days before measuring.

5. <u>References</u>

1. S. Eyckerman, A. Verhee, J. Van der Heyden, et al. (2001) Design and application of a cytokine-receptor-based interaction trap, Nature Cell Biology. 3, 1114–1119.
2. S. Lievens, S. Gerlo, I. Lemmens, et al. (2014) Kinase Substrate Sensor (KISS), a mammalian in situ protein interaction sensor., Molecular & cellular proteomics : MCP. 13, 3332–42.
3. P. Braun, M. Tasan, M. Dreze, et al. (2009) An experimentally derived confidence score for binary protein-protein interactions, Nature Methods. 6, 91–97.
4. Y.-C. Chen, S.V. Rajagopala, T. Stellberger, et al. (2010) Exhaustive benchmarking of the yeast two-hybrid system, Nature Methods. 7, 667–668.
5. S. Lievens, N. Vanderroost, J. Van der Heyden, et al. (2009) Array MAPPIT: High-Throughput Interactome Analysis in Mammalian Cells, Journal of Proteome Research. 8, 877–886.
6. S. Lievens, J. Van der Heyden, D. Masschaele, et al. (2016) Proteome-scale Binary Interactomics in Human Cells, Molecular & Cellular Proteomics. 15, 3624–3639.
7. M. Caligiuri, L. Molz, Q. Liu, et al. (2006) MASPIT: Three-hybrid trap for quantitative proteome fingerprinting of small molecule-protein interactions in mammalian cells, Chemistry & Biology. 13, 711–722.
8. M.D.P. Risseeuw, D.J.H. De Clercq, S. Lievens, et al. (2013) A "clickable" MTX reagent as a practical tool for profiling small-molecule-intracellular target interactions via MASPIT., ChemMedChem. 8, 521–6.
9. I. Lemmens (2003) Heteromeric MAPPIT: a novel strategy to study modification-dependent protein-protein interactions in mammalian cells, Nucleic Acids Research. 31, 75e–75.
10. S. Wiemann, C. Pennacchio, Y. Hu, et al. (2016) The ORFeome Collaboration: a genome-scale human ORF-clone resource, Nature Methods. 13, 191–192.
11. T. Montoye, J. Piessevaux, D. Lavens, et al. (2006) Analysis of leptin signalling in hematopoietic cells using an adapted MAPPIT strategy, FEBS Letters. 580, 3301–3307.
12. J. Wauman, A.-S. De Smet, D. Catteeuw, et al. (2008) Insulin receptor substrate 4 couples the leptin receptor to multiple signaling pathways., Molecular endocrinology (Baltimore, Md.). 22, 965–77.

Straightforward protein-protein interaction interface mapping via random mutagenesis and MAPPIT

This manuscript describes the method that combines random mutagenesis with MAPPIT (Mammalian Protein-Protein Interaction trap), a technique that allows extensive mapping of protein-protein interaction interfaces in intact human cells. We have used this method to detect RNF41 mutants that specifically disrupted the interaction between RNF41 and a particular interaction partner (see Results section 1).

The random mutagenesis-MAPPIT method was developed by Frank Peelman and this manuscript was co-written by Delphine Masschaele and Laurens Vyncke.

Biotech Methods

Straightforward protein-protein interaction interface mapping via random mutagenesis and MAPPIT

Laurens Vyncke[1,2]*, Delphine Masschaele[1,2]*, Jan Tavernier [1,2] and Frank Peelman [1,2]

[1]Cytokine Receptor Laboratory, Department of Biochemistry, Faculty of Medicine and Health Sciences, Ghent University, Albert Baertsoenkaai 3, B-9000 Ghent, Belgium
[2]VIB Medical Biotechnology Center, VIB, Albert Baertsoenkaai 3, B-9000 Ghent, Belgium
*These authors contributed equally to this work

Correspondence: Prof. Frank Peelman, VIB Medical Biotechnology Center UGent, Albert Baertsoenkaai 3, 9000 GENT, Belgium
Email: frank.peelman@vib-ugent.be

Keywords: interface mapping, MAPPIT, protein-protein interaction, random mutagenesis

Abstract

The MAPPIT (mammalian protein protein interaction trap) method allows high-throughput detection of protein interactions by very simple co-transfection of three plasmids in HEK293T cells, followed by luciferase readout. MAPPIT detects a large percentage of all protein interactions, including those requiring posttranslational modifications and endogenous or exogenous ligands. Here, we present a straightforward method that allows detailed mapping of interaction interfaces via MAPPIT. By combining error-prone PCR for random mutagenesis, 96-well DNA prepping, Sanger sequencing, and MAPPIT via 384-well transfections, we test the effects of a large number of mutations of a selected protein on its protein interactions. The entire screen takes less than three months and interactions with multiple partners can be studied in parallel. The effect of mutations on the MAPPIT readout is mapped on the protein structure, allowing unbiased identification of all putative interaction sites. We thus far analyzed 6 proteins, and mapped their interfaces for 16 different interaction partners. Our method is broadly applicable as the required tools are simple and widely available.

Abbreviations: Apobec3G, apolipoprotein B messenger RNA-editing catalytic polypeptide-like G; **Epo,** erythropoietin; **gp130,** glycoprotein 130; **JAK,** Janus kinase; **LepR,** leptin receptor; **Mal,** MyD88 adapter-like; **MAPPIT,** mammalian protein-protein interaction trap; **MyD88,** myeloid differentiation primary response gene 88; **NMR,** nuclear magnetic resonance; **PPAR-α**, peroxisome proliferator-activated receptor α; **PPI,** protein-protein interaction; **PTM,** post-translational modification; **RNF41**, ring finger protein 41; **STAT,** signal transducers and activators of transcription; **TIR,** Toll/interleukin-1 receptor; **TRIF**, TIR-domain-containing adapter inducing interferon-β

Introduction

The expansion of the protein interactomics field is driven by a wide variety of techniques for detection of protein-protein interactions (PPIs). Classical techniques such as yeast two-hybrid [1] and affinity-purification coupled to mass spectrometry [2] have been complemented with new and improved approaches. These enable the study of PPIs at their subcellular location [3,4] or in a physiological context between weak and transient interactions [5–7], full-length integral membrane proteins [8] and post-translationally modified proteins [9]. Our laboratory developed the mammalian protein-protein interaction trap (MAPPIT), a method combining many of these traits. MAPPIT is based on the Janus kinases-signal transducers and activators of transcription (JAK-STAT) signaling pathway of type I cytokine receptors upon bait and prey interaction (Fig. 1A). As MAPPIT acts in intact mammalian cells, it allows detection of proteins requiring intracellular cofactors or post-translational modifications (PTMs) [10]. A typical MAPPIT experiment simply involves co-transfection of three plasmids in HEK293T cells: a bait, a prey, and a STAT3-inducible luciferase reporter plasmid (Fig. 1B). Interaction between bait and prey protein is detected by luciferase activity induced after stimulation with erythropoietin (Epo) or leptin, depending on the extracellular domain of the bait. MAPPIT can detect up to one third of all protein interactions in high-throughput screening modus, but this number can probably be increased by switching bait and prey, using different bait constructs or using domains instead of full-length proteins [11–13].
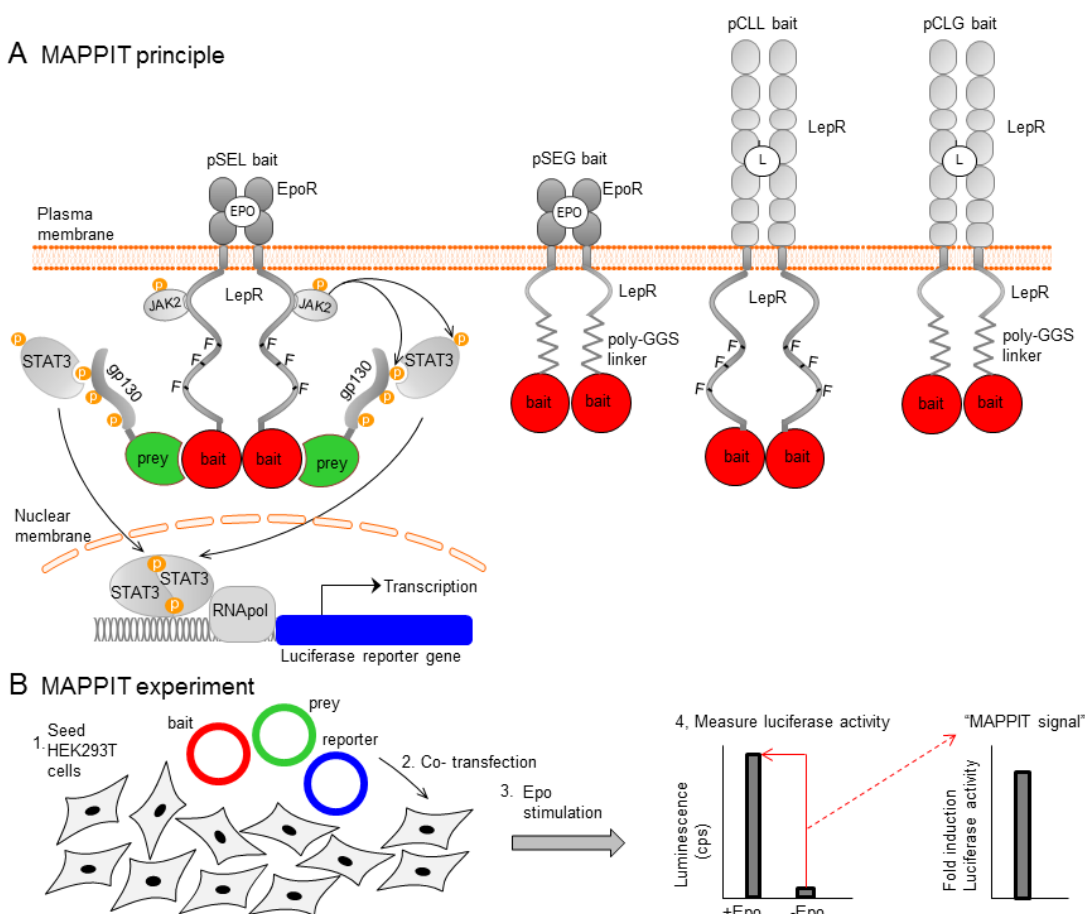
Figure 1. MAPPIT (A) MAPPIT principle. The pSEL MAPPIT bait is fused to a signaling-deficient chimeric receptor comprising the extracellular EpoR and transmembrane and intracellular LepR, lacking STAT3 recruitment sites. The prey is coupled to the gp130 anchor. Upon Epo stimulation, bait-prey interaction leads to phosphorylation

and recruitment of STAT3 to the gp130 anchor, thereby complementing the JAK-STAT signaling pathway, resulting in luciferase reporter gene activation. For the alternative pSEG and pCLG MAPPIT baits, the intracellular LepR domain C-terminal of the JAK2 binding site is replaced by a GGS (glycine-glycine-serine) linker allowing more flexibility. The pCLL and pCLG baits consist of the extracellular LepR domain. (B) MAPPIT outline. HEK293T cells are seeded and transfected the next day with bait, prey and reporter constructs. 24h post-transfection, cells are stimulated with Epo. The next day, luciferase activity (luminescence, in counts per second) is measured. The MAPPIT signal represents the fold induction between stimulated and non-stimulated wells.

High-resolution structure determination of protein complexes via X-ray crystallography, nuclear magnetic resonance (NMR) spectroscopy or cryo-electron microscopy is inherently slow and often remains very challenging. Even with the major advances and speedup in structure determination, these methods cannot keep up with the rapid growth of the interactome [14]. This leads to a huge and growing gap between the number of known protein interactions and the number of structurally characterized complexes.

Alternatively, many approaches can predict protein complex structures based on the separate models or structures of the interacting proteins in the complex [14,15]. Several methods provide experimental insight in the location of the protein interaction interface [15]. Examples include NMR titration/chemical shift perturbation experiments or mass spectrometry combined with limited proteolysis, chemical crosslinking or deuterium exchange. Similarly, mutagenesis combined with a detection method of protein interactions can identify critical interacting residues. Combining experimental insights on the location of the interacting interfaces with homology modeling or *in silico* protein-protein docking, enables building of reliable models for the protein complex [15,16].

In this paper, we describe a straightforward method combining random mutagenesis with MAPPIT that allows extensive mapping of PPI interfaces in intact human cells.

2   Materials and methods

Figure 2 summarizes the 6-step workflow of our method. Below, we describe the six steps in more detail.

2.1 Step 1: Optimization of the MAPPIT readout

We first set up and optimize MAPPIT assays that specifically detect the interaction between the protein of interest and its interaction partners (Fig. 2A). Their cDNA is cloned in both MAPPIT bait and MAPPIT prey plasmid vectors. The MAPPIT assay is optimized by testing the protein of interest both as bait and prey and by varying the concentration of bait and prey plasmids. To ensure the specificity of the assay, baits and preys are also tested versus negative control baits and preys, expressing an irrelevant protein. The induction of luciferase activity upon cytokine stimulation should be at least 10-fold. Both prey and bait can be randomly mutated. Below, we describe the screening process, where the mutation target is cloned as prey.

2.2 Step 2: Random mutagenesis via error-prone PCR

The DNA insert is randomly mutated via error-prone PCR using Mutazyme II DNA polymerase following the guidelines of the Genemorph™ II Random Mutagenesis kit (Agilent Technologies, Santa Clara, CA, USA) (Fig. 2B). This permits a suitable mutation rate and a balanced mutation spectrum [17]. To obtain a maximum number of single missense mutants, the PCR condition is first optimized by varying the concentration of input DNA and number of PCR cycles. The PCR primers contain unique restriction sites allowing in-frame ligation of the linear PCR product into the MAPPIT prey plasmid vector. The ligation product is electroporated into *E. coli* DH10B cells. For each PCR condition, 24 colonies are grown overnight in 2x Yeast Tryptone medium in a 96-deepwell block. DNA is purified via a 96-well miniprep protocol using the Nucleospin™ Robot-96 plasmid kit (Machery Nagel, Easton, PA, USA). Next, the MAPPIT mutants are sequenced on Applied Biosystems 3730XL DNA Analyzers to determine the PCR condition with the highest number of single missense mutations. In our studies, up to one third of the random mutant clones contain single missense mutations [18,19]

2.3 Step 3: Generation of a mutant plasmid library in 96-well format

Mutant *E. coli* colonies of the optimal PCR condition are plated and single colonies are inoculated in 96-deepwell blocks for DNA miniprep purification, as described above (Fig. 2C). In the automated DNA minipreps, DNA is eluted in water into UV-transparent flat-bottom 96-well plates and DNA concentration is measured via the Magellan UV spectrophotometer (Tecan, Männedorf, Switzerland). The OD 260/280 ratio should be above 1.8 for every sample to obtain reliable MAPPIT results. Next, DNA is normalized to the optimized concentration for transfection. The sequences of all randomly mutated plasmids are determined via Sanger sequencing and plasmids with a single missense mutation are transferred into 96-well plates (Fig. 2C). Two individual rows of each 96-well plate contain plasmids with a wildtype and a negative control prey.

2.4 Step 4: MAPPIT in 384-well assay

The normalized 96-well MAPPIT prey plates are co-transfected with the MAPPIT bait and STAT3 luciferase (pXP2d2-rPAPI-luciferase) reporter plasmids, as optimized in step 1 (Fig. 2D). The first day,

3000 HEK293T cells/well are seeded into black 384-well plates. The next day, cells are transfected with the MAPPIT prey together with a mixture of MAPPIT bait and STAT3 luciferase reporter plasmids using a calcium phosphate precipitation method. Each unique prey/bait mixture is transfected in 8 384-wells. One 96-well plate with prey mutant DNA thus requires transfection of two 384-well plates. As the optimized 96-well DNA plates contain 12 wildtype and 12 negative control prey plasmids, each transfected 384-well plate contains 6 different wildtype preys and up to 36 different prey mutants.

On day three, 4 out of 8 wells for each transfection mixture are stimulated with leptin or Epo. The 4 other wells are left unstimulated (Fig. 2D). After 24 hours, cells are lysed in 15µl of Cell Culture Lysis Reagent buffer (25 mM Tris/phosphate (pH 7.8), 2 mM DTT, 2 mM CDTA, 10% glycerol, 1% Triton X-100) followed by the addition of 11 µl of luciferase substrate buffer (40 mM Tricine, 2.14 mM $(MgCO_3)_4Mg(OH)_2.5H2O$, 5.34 mM $MgSO_4.7H_2O$, 66.6 mM DTT, 0.2 mM EDTA, 270 µM coenzyme A (Sigma-Aldrich, St. Louis, MO, USA), 530 µM ATP (Sigma-Aldrich, St. Louis, MO, USA), 470 µM luciferin (Duchefa, Haarlem, The Netherlands)). The luminescence is measured via the EnSpire plate reader (PerkinElmer Life Sciences, Waltham, MA, USA).

2.5 Step 5: Data analysis

First, the "MAPPIT signal" is determined by dividing the average of the luciferase counts of the 4 stimulated wells by the average of the luciferase counts of the 4 unstimulated wells (Fig. 2E). Then, the "normalized MAPPIT signal" of each mutant is calculated by dividing its MAPPIT signal by the median of the MAPPIT signals of the 6 wildtype preys on the same 384-well plate. As each MAPPIT transfection experiment is performed three times, the "relative MAPPIT signal" of each mutant is determined by the average of the normalized MAPPIT signals in these three experiments.

We also calculate the relative MAPPIT signals of the wildtypes, as described above, and plot the variation (Fig. 3A). However, the MAPPIT signal of each wildtype is divided by the median of the MAPPIT signals of the 5 other wildtypes on the same 384-well plate. We consider that a mutant has an effect on the interaction when its relative MAPPIT signal is below the minimum relative MAPPIT signal of all wildtypes (Fig. 3B).

2.6 Step 6: Mapping of relative MAPPIT signals

First, we create an attribute list in a fixed .txt format in which the relative MAPPIT signal is assigned to the corresponding residue number. This attribute list is then loaded in the modelling program University of California San Francisco (UCSF) Chimera [20]. The relative MAPPIT signals of the mutated residues are mapped on the template structure using the "render by attribute" tool (Fig. 3C). Based on the histogram of the relative MAPPIT signals, up to three threshold values with respective colors can be determined. The color intensity of each mutated residue depends on the proximity of its relative MAPPIT signal to the thresholds in the histogram.
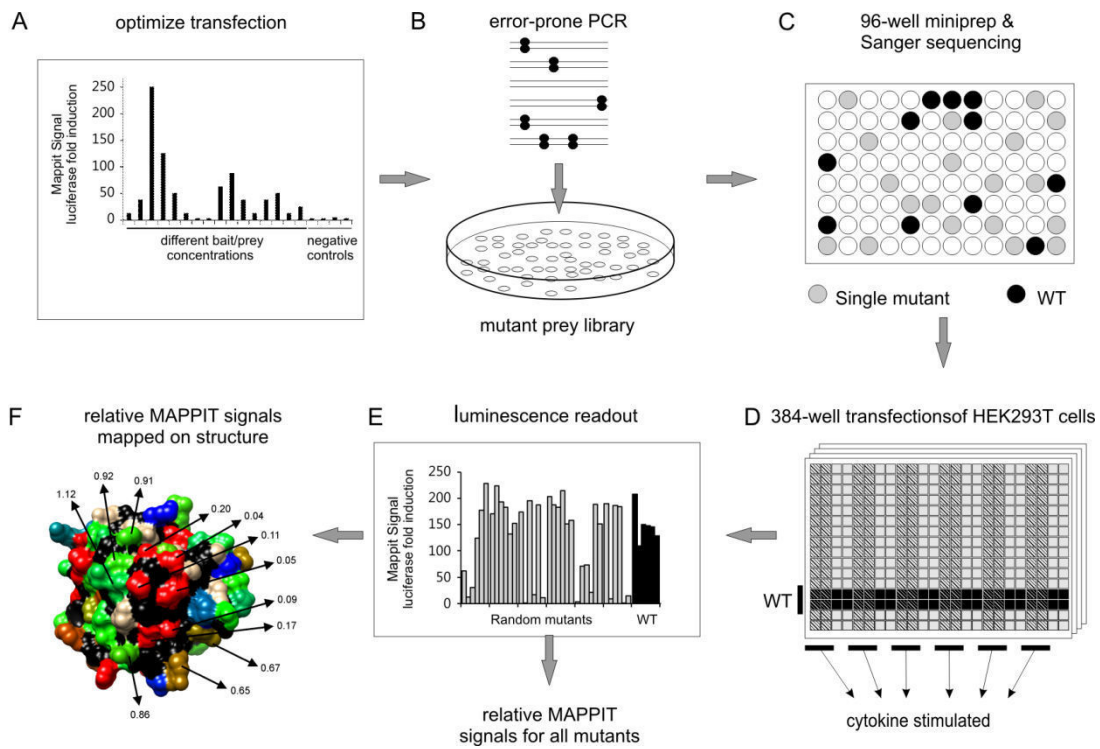
Figure 2. 6-step workflow of the MAPPIT-based interface mapping method. (A) MAPPIT transfection conditions are optimized by varying the concentration of bait and prey plasmids and by reversing the order of bait and prey proteins. (B) The target protein is randomly mutated via error-prone PCR. The linear PCR product is cloned into the MAPPIT prey plasmid vector and electroporated into *E. coli* DH10B cells, resulting in the MAPPIT mutant prey library. (C) Individual *E. coli* colonies are inoculated in 96-deepwell blocks. Mutant prey DNA is isolated via a 96-well DNA miniprep protocol and sequenced by Sanger sequencing. (D) MAPPIT prey mutants harboring a single missense mutation are co-transfected with the MAPPIT bait and STAT3 luciferase reporter plasmids in 384-well plates seeded with HEK293T cells. (E) After cytokine stimulation via Epo or leptin, the luciferase activity is measured and normalized MAPPIT signals are calculated. (F) The relative MAPPIT signal of each mutant is determined and mapped on the protein structure.
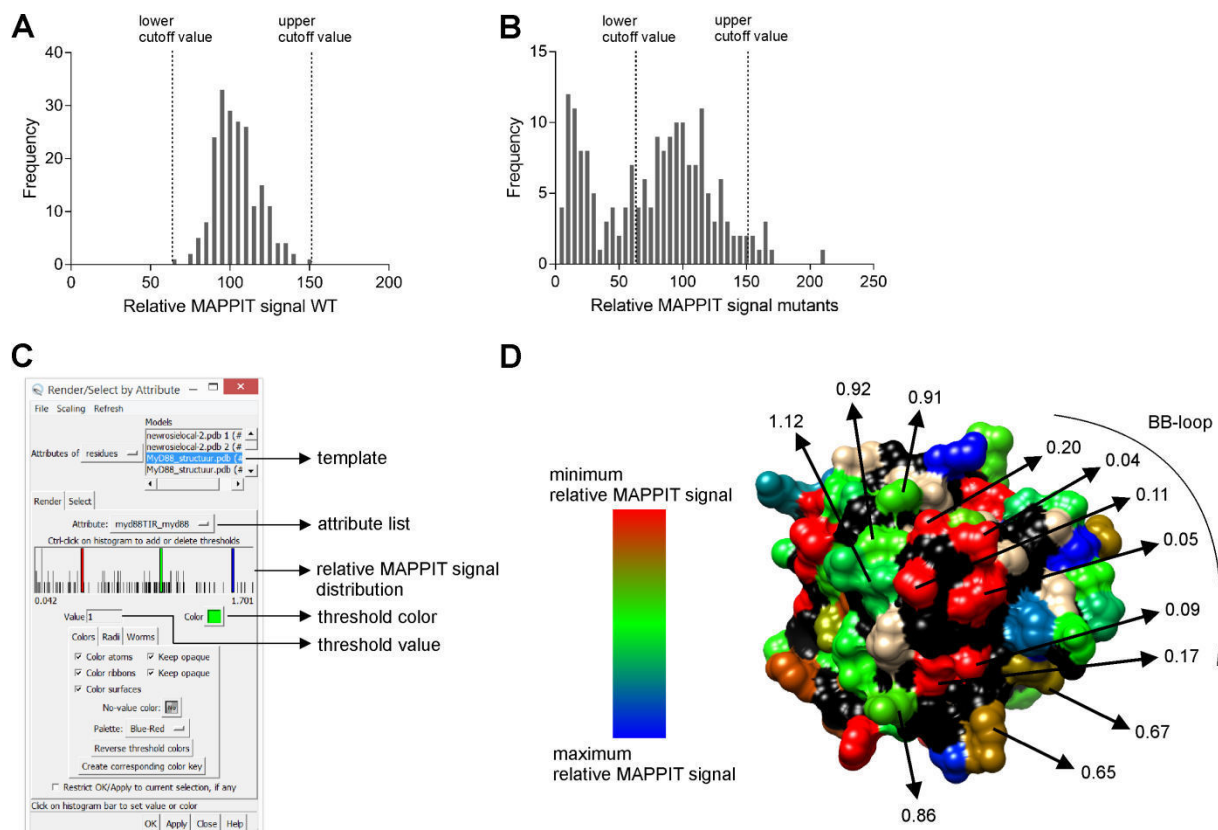
Figure 3. Random mutagenesis and MAPPIT reveal potential binding sites in MyD88 TIR involved in MyD88 TIR prey–MyD88 bait interaction. (A) Relative MAPPIT signal distribution of all MyD88 TIR wildtypes (WTs) for MyD88 TIR prey-MyD88 bait interaction. The lowest and highest wildtype relative MAPPIT signal determine lower and upper cutoff value, respectively. (B) Relative MAPPIT signal distribution of all unique single mutants for MyD88 TIR prey-MyD88 bait interaction. Mutants with a relative MAPPIT signal below the lower cutoff value or above the upper cutoff value are considered having an effect on the interaction. (C) The "render by attribute" tool of Chimera enables mapping of relative MAPPIT signals on the template structure. Entering the attribute list leads to automatic generation of the relative MAPPIT signal distribution. Up to three threshold values with respective colors can be selected. (D) Effect of mutations on the MyD88 TIR prey-MyD88 bait interaction. Residues are colored on the MyD88 TIR crystal structure according to their indicated relative MAPPIT signal [23]. A cluster of red-colored residues forms a potential binding site (BB-loop). Green-colored residues do not alter the interaction compared to the wildtype. Non-mutated residues are gray and backbone atoms are black.

3   Results and Discussion

3.1 MAPPIT detects interfaces in diverse target proteins

We successfully applied random mutagenesis combined with MAPPIT for interaction interface analysis of six targets in four unrelated protein families: the antiviral host restriction factor apolipoprotein B messenger RNA-editing catalytic polypeptide-like G (Apobec3G) [21], the ring finger protein 41 (RNF41), the ligand binding domain of peroxisome proliferator-activated receptor α (PPAR-α), and the Toll/IL-1R (TIR) domains of the Toll-like receptor adapters MyD88 adapter-like (Mal) [18], myeloid differentiation primary response gene 88 (MyD88) [19], and TIR-domain-containing adapter inducing interferon-β (TRIF). For five of these targets, we tested the interaction of the mutant libraries with three or four different interactors in parallel. We thus mapped interaction interfaces for 16 protein-protein interactions. Figure 3 shows an example of a MAPPIT random mutagenesis screen, testing the interaction of MyD88 coupled as bait with random mutants of the prey MyD88 TIR domain. A mutant library of 17 96-well plates led to 185 unique single missense mutants, resulting in a coverage of 78% of the entire MyD88 TIR domain. No MyD88 TIR wildtype has a relative MAPPIT signal below 60% or above 155%, which were used as lower and upper cutoff values, respectively (Fig. 3A). Figure 3B illustrates that 37% of all unique single missense mutants has a relative MAPPIT signal below the lower cutoff value. Figure 3D shows one of the 4 protein interaction interfaces detected in this screen. Residues in the center of this interface have a relative MAPPIT signal well below the 60% cutoff. Typical for all interfaces found in the screens, these residues are surrounded by mutations having a relative MAPPIT signal between the lower cutoff value and the average wildtype relative MAPPIT signal. To confirm these effects, we reisolate DNA of the putative interface mutations and new wildtype clones, and retest these selected samples in triplicate MAPPIT experiments.

3.2 Interfaces detected via MAPPIT are confirmed via other methods and studies

All tested mutants are available as individual clones and easily cloned into other vectors. This permits retesting of a large number of mutations in different assays without the need of extra mutagenesis. The biological importance of new potential interfaces identified via MAPPIT was confirmed via orthogonal assays, such as co-immunoprecipitation and signaling assays [18,19]. Protein interfaces identified via our method are well in line with other studies. We confirmed the well-known importance of the TIR "BB-loop" in TIR interactions of MyD88, Mal, and TRIF (Fig. 3D) [18,19]. In agreement with other studies, MAPPIT analysis demonstrated that one of two crystallographic interfaces in the Mal TIR crystal structures is a Mal homodimerization interface [18]. By mapping our MAPPIT data on a homology model for Apobec3G, we identified an extensive Apobec3G homodimerization site, as found in parallel studies [21]. We demonstrated that this complete area is also critical for the interaction with the viral infectivity factor (Vif)of HIV, later confirmed by the NMR structure of the Apobec3G N-terminal domain.

3.3 Interactions requiring additional ligands or phosphorylation can be studied via MAPPIT

MAPPIT operates in intact mammalian cells, providing a natural environment with endogenous cofactors and regulatory proteins, and is therefore able to detect protein interactions requiring PTMs such as phosphorylation. Via inhibitory and phosphomimetic mutations of phosphorylated residues in the MAPPIT bait or prey, we were able to study the crucial role of phosphorylation on protein

interactions [19,21]. MAPPIT also allowed to study interactions of Apobec3G that required cellular RNA as additional ligand [21], while interactions of PPAR-α could only be studied after adding an exogenous ligand.

3.4 Critical considerations in data interpretation

The MAPPIT signal is also affected by mutations disrupting the structure or proper folding of the protein. For example, most mutations in the core of the protein affect the MAPPIT signal. As mutations at the protein surface can equally disrupt the protein structure, it is mandatory to carefully inspect possible structural effects. As a tool for estimating the mutational effect on the protein structure, we use the FoldX prediction program [22]. However, *in silico* predictions remain quite unreliable. In this context, any mutation of an isolated surface residue should be considered with caution. Potential interface areas rather present themselves as patches of multiple adjacent residues with missense mutations that all affect the interaction (Fig. 3D).

We analyze expression levels of prey or bait mutants to exclude an effect on the MAPPIT interaction due to differential expression. Expression levels of MAPPIT preys can be determined via Western blot, as these contain a Flag-tag. Expression of the MAPPIT baits can be determined in a (parallel) MAPPIT experiment with a MAPPIT prey specifically recognizing the receptor portion or JAK2 portion of the bait. However, expression levels of bait or prey mutants are not a good measure for their proper folding or structural integrity. Very often, mutations that clearly disrupt the structure or folding of the protein hardly affect the expression level.

Our method identifies all regions required for protein interaction, and some of these do not necessarily represent the actual interface between bait and prey. This is relevant for proteins binding their target as a homodimer or requiring a third interaction partner. In MAPPIT, both bait and prey proteins are free to homodimerize or even homo-oligomerize. We do find that mutations in the homodimerization interface of the mutated target affect its heterotypical interaction. Similarly, for interactions that require an extra third protein or other ligand, mutations in the binding site of these ligands also affect the MAPPIT readout [19].

4   Concluding remarks

Our combination of MAPPIT and random mutagenesis allows extensive and unbiased validation of interfaces in high- or low-resolution structures. Interface residues identified via MAPPIT can also guide the docking process in *in silico* data-driven protein-protein docking [19]. A major advantage of our screening method lies in its simplicity and rapid setup. The entire optimization and screening process is performed in three months. We therefore believe that our MAPPIT-based interface mapping method is an excellent tool for detailed study of a large number of PPIs.

Conflict of interest

The authors declare no financial or commercial conflict of interest.

5   References

[1]   Fields, S., Song, O., A novel genetic system to detect protein-protein interactions. *Nature*. 1989, *340*, 245–246.

[2]   Gingras A.-C., Gstaiger, M., Raught, B., Aebersold, R., Analysis of protein complexes using mass spectrometry. *Nat. Rev. Mol. Cell Biol.* 2007, *8*, 645–654.

[3]   Söderberg, O., Gullberg, M., Jarvius, M., Ridderstråle, K. et al., Direct observation of individual endogenous protein complexes in situ by proximity ligation. *Nat. Methods*. 2006, *3*, 995–1000.

[4]   Boute, N., Jockers, R., Issad, T., The use of resonance energy transfer in high-throughput screening: BRET versus FRET. *Trends Pharmacol. Sci.* 2002, *23*, 351–354.

[5]   Barrios-Rodiles, M., Brown, K. R., Ozdamar, B., Bose, R. et al., High-throughput mapping of a dynamic signaling network in mammalian cells. *Science*. 2005, *307*, 1621–1625.

[6]   Roux, K. J., Kim, D. I., Raida, M., Burke, B., A promiscuous biotin ligase fusion protein identifies proximal and interacting proteins in mammalian cells. *J. Cell Biol.* 2012, *196*, 801–810.

[7]   Eyckerman, S., Titeca, K., Van Quickelberghe, E., Cloots, E. et al., Trapping mammalian protein complexes in viral particles. *Nat. Commun.* 2016, *7*, 11416.

[8]   Petschnigg, J., Groisman, B., Kotlyar, M., Taipale, M. et al., The mammalian-membrane two-hybrid assay (MaMTH) for probing membrane-protein interactions in human cells. *Nat. Methods*. 2014, *11*, 585–592.

[9]   Weinrich, D., Jonkheijm, P., Niemeyer, C. M., Waldmann, H., Applications of protein biochips in biomedical and biotechnological research. *Angew. Chem. Int. Ed. Engl.* 2009, *48*, 7744–7751.

[10]   Eyckerman, S., Verhee, A., Van der Heyden, J., Lemmens, I. et al., Design and application of a cytokine-receptor-based interaction trap. *Nat. Cell Biol.* 2001, *3*, 1114–1119.

[11]   Yu, H., Braun, P., Yildirim, M. A., Lemmens, I. et al., High-quality binary protein interaction map of the yeast interactome network. *Science*. 2008, *322*, 104–110.

[12]   Braun, P., Tasan, M., Dreze, M., Barrios-Rodiles, M. et al., An experimentally derived confidence score for binary protein-protein interactions. *Nat. Methods*. 2008, *6*, 91–97.

[13]   Rolland, T., Taşan, M., Charloteaux, B., Pevzner, S. J. et al., A Proteome-Scale Map of the Human Interactome Network. *Cell*. 2014, *159*, 1212–1226.

[14]   Mosca, R., Céol, A., Aloy, P., Interactome3D: adding structural details to protein networks. *Nat. Methods*. 2012, *10*, 47–53.

[15]   Xue, L.C., Dobbs, D., Bonvin, A.M.J.J., Honavar, V., Computational prediction of protein interfaces: A review of data driven methods. *FEBS Lett.* 2015, *589*, 3516–26.

[16]   de Vries, S.J., Melquiond, A.S.J., Kastritis, P.L., Karaca, E. et al., Strengths and weaknesses of data-driven docking in critical assessment of prediction of interactions. *Proteins*, 2010, *78*, 3242–9.

[17]   Rasila, T.S., Pajunen, M. I., Savilahti, H., Critical evaluation of random mutagenesis by error-prone polymerase chain reaction protocols, Escherichia coli mutator strain, and hydroxylamine treatment. *Anal. Biochem.* 2009, *388*, 71–80.

[18]   Bovijn, C., Desmet, A.-S., Uyttendaele, I., Van Acker, T. et al., Identification of Binding Sites for Myeloid Differentiation Primary Response Gene 88 (MyD88) and Toll-like Receptor 4 in MyD88 Adapter-like (Mal). *J. Biol Chem*. 2013, *288*, 12054-12066.

[19]   Vyncke, L., Bovijn, C., Pauwels, E., Van Acker, T. et al., Reconstructing the TIR Side of the Myddosome: a Paradigm for TIR-TIR Interactions. *Structure*. 2016, *24*, 437–447.

[20]   Pettersen, E.F., Goddard, T.D., Huang, C.C., Couch, G.S. et al., UCSF Chimera--a visualization system for exploratory research and analysis. *J. Comput. Chem.* 2004, *25*, 1605–1612.

[21]   Uyttendaele, I., Lavens, D., Catteeuw, D., Lemmens, I. et al., Random mutagenesis MAPPIT analysis identifies binding sites for Vif and Gag in both cytidine deaminase domains of Apobec3G. *PLoS One*. 2012, *7*, e44143.

[22]   Van Durme, J., Delgado, J., Stricher, F., Serrano, L. et al., A graphical interface for the FoldX forcefield. *Bioinformatics*, 2011, *27*, 1711–1712.

[23]   Snyder, G.A., Cirl, C., Jiang, J., Chen, K. et al. Molecular mechanisms for the subversion of MyD88 signaling by TcpC from virulent uropathogenic Escherichia coli. *Proc. Natl. Acad. Sci. U. S. A.*, 2013, *110*, 6985–90.

Personal Details:

Name: Delphine Masschaele

Address: Fluweelstraat 16

                 9000 Gent

                 Belgium

Mobile: +32 499 29 10 47

Email: delphine.masschaele@vib-ugent.be

Date of birth: 14-12-1986 (Oostende, Belgium)

Education and work experience:

Education:

2010-present: PhD in Biomedical Sciences

2008-2010:   Master in Biomedical Sciences

2004-2008:   Bachelor in Biomedical Sciences

1998-2004:   Mathematics-Sciences

                 Sint-Andreasinstituut, Oostende

Professional experience:

October 2010-present:

PhD in biomedical sciences at the cytokine receptor lab (CRL), UGent; Center for Medical Biotechnology, VIB

IWT fellowship

Attended conferences with poster presentations:

-2011-2016: Annual VIB seminar

-2012: BMB meeting: UGent, Belgium

-2013: EMBO meeting: Systems dynamics in endocytosis. Villars, Switzerland

-2014: IUAP meeting, KULeuven, Belgium

-2014: EMBO meeting: Signalling to and from endomembranes , Allensbach-Hegne, Germany

-2015: EMBO meeting: The multidisciplinary era of endocytic mechanics and functions. Mandelieu-la-Napoule, France

Courses:

- 2011: Statistics SPSS (UGent)

- 2011: VRTC Summer School on Advanced Light Microscopy (VIB)

- 2013: Effective scientific communications (Jean-Luc Dumont)

- 2015: Career guidance (Lucia Smit)

Skills:

Technical lab skills: SDS-PAGE, western blotting, Immunoprecipitation, cell culture, ELISA, immunofluorescence, detection of protein-protein interactions, qPCR, cloning

IT skills: Microsoft Windows, MS office (Word, Excel, Powerpoint)

Publications:

De Ceuninck L., Wauman J., <u>Masschaele D</u>., Peelman F., Tavernier J. (2013). Reciprocal cross-regulation between RNF41 and USP8 controls cytokine receptor sorting and processing. Journal of Cell Science, 126, 3370-3381.

Lievens S., Van der Heyden J., <u>Masschaele D</u>., De Ceuninck L., Petta I., Gupta S., De Puysseleyr V., Vauthier V., Lemmens I., De Clercq D.J.H., Defever D., Vanderroost N., De Smet A-S., Eyckerman S., Van Calenbergh S., Martens L., De Bosscher K., Libert C., Hill D.E., Vidal M., Tavernier J. (2016). Proteome-scale binary interactomics in human cells. Molecular & Cellular Proteomics, 15, 3624-3639.

<u>Masschaele D</u>., De Ceuninck, L., Wauman J., Defever D., Stenner F., Lievens, S., Peelman F., Tavernier J. (2017). RNF41 interacts with the VPS52 subunit of the GARP and EARP complexes. Plos One. 12(5): e0178132.

<u>Masschaele D</u>., Gerlo S., Lemmens I., Lievens S., Tavernier J. (2017). KISS, a mammalian two-hybrid method for in situ analysis of protein-protein interactions. Accepted in Methods to Molecular Biology, 2017

Wijesuriya M., De Ceuninck L., <u>Masschaele D</u>., Matthea, Carias V. K., Tavernier J., Wevrick R. The Prader-Willi syndrome proteins MAGEL2 and necdin regulate leptin receptor cell surface abundance through ubiquitination pathways. Accepted in Human Molecular Genetics, 2017

<u>Masschaele D</u>., Vandemoortele G., Desutter D., Wauman J, De Ceuninck L, Eyckerman S, Tavernier J. Building a high-confidence RNF41 interactome. Submitted to Journal of Proteome Research, 2017

Vyncke L.*, <u>Masschaele D.</u>*, Tavernier J., Peelman F. Straightforward protein-protein interaction interface mapping via random mutagenesis and MAPPIT. Submitted to Biotechnology Journal, 2017